Titanite zoning and magma mixing

Graham William McLeod
B.Sc. (Hons.), Glasgow

Thesis presented for the degree of Doctor of Philosophy (Ph.D.)

University of Glasgow

Department of Geographical & Earth Sciences

November 2007

Abstract

Titanite is a calcium titanium silicate accessory mineral that serves as a sink for trace elements, especially the rare-earth elements and the high-field strength elements (Cerny and Rivadisa.L 1972; Groat, Carter et al. 1985; Enami, Suzuki et al. 1993; Perseil and Smith 1995; Della Ventura, Bellatreccia et al. 1999; Piccoli, Candela et al. 2000). It is also characterised by very sluggish diffusion of these elements, and as such it has the ability to resist most sub-solidus alteration. These characteristics make titanite a prime candidate for the ability to preserve a record of the petrogenetic processes which formed the igneous rocks in which it is found.

In order to assess titanite's ability to serve as a petrogenetic tool, a textural and geochemical study of titanite from different igneous environments was undertaken. The Ross of Mull Granite is an igneous complex located on the south west coast of the Isle of Mull, Scotland. It is a Caledonian age pluton that displays evidence of magma-mixing processes at depth and also contains notable amounts of titanite. Samples of different host granite and diorite enclave lithologies and relationships were documented and collected in order to asses the ability of titanite to retain evidence of magma-mixing processes within its compositional zoning.

Titanite from the Ross of Mull Granite displays a large variety of textural features, both with respect to crystal shape and compositional zoning. The variation of the trace elements observed in titanite is a direct reflection of the compositional zoning pattern. Melts that are enriched in particular trace elements pass on that signature to the titanites. If melts of significantly contrasting chemistries mix or mingle, then titanite may record any significant instance of trace element diffusion between the melts. More importantly, there doesn't need to be a transfer of trace elements between mingling/mixing melts for titanite to record evidence of the interaction. If the melts are of significantly different oxygen fugacities, then titanite may become destabilised and partially dissolve. This dissolution may only be temporary, but it may be difficult to tell if it was a product of increasing heat of the melt of if it was due to a change in oxygen fugacity. Titanite however, may record evidence of the cause of dissolution based on the nature of re-growth. As shown by some of the titanites within the Ross of Mull Granite, re-growth following a period of dissolution may be attributed to a change in oxygen fugacity if the new titanite growth is characterised by unusually low REE content. This is related to the nature of trace element incorporation in the titanite structure; REE are taken up due to coupled substitution mechanisms involving

tetravalant Al and Fe. If a melt becomes reduced then the activity of ferric Fe will also be reduced, thus inhibiting the ability of titanite to take up REE by affecting the activity of the coupled substitution (Wones 1989; Piccoli, Candela et al. 2000).

Titanite from the ROMG is largely characterised by compositional zoning that reflects the trace element chemistry of one of the end-member lithologies (host granite or dioritic enclaves), or has compositional zoning that reflects the changing conditions of the magmatic environment, namely: changes in melt composition, changes in temperature and pressure and changes in oxidation of the magma. In the case of the ROMG, all of these changes were wholly, or in part, brought about by magma mixing processes. Another way in which titanite reflects processes of petrogenesis is that it has been found to reflect the degree of homogenisation of the melt from which it has crystallised.

To further asses the ability of titanite serve as a petrogenetic tool, a study was made of the characteristics of titanite from the volcanic environment. The Fish Canyon Tuff, from the San Juan volcanic field, Colorado, USA, was chosen as a suitable candidate for study due to its well documented nature; it is the largest known pyroclastic eruption to be documented. The Fish Canyon tuff also contains numerous phenocrysts of titanite.

Eruption of the Fish Canyon Tuff is thought to have been brought about by the thermal rejuvenation of a batholith-sized magma chamber which had previously cooled to a rigid crystal mush (Bachmann and Bergantz 2003). The main conclusion from the study of titanites from the Fish Canyon Tuff and is that evidence for the thermal rejuvenation of the magma chamber by a mafic melt prior to eruption is preserved in the textural and chemical signature preserved in the compositional zoning of the titanites as dissolution and re-growth textures.

This study illustrates that titanite is able to not only preserve evidence of magma mixing processes occurring at depth, but it is also able to preserve evidence of similar processes all the way through to the volcanic environment.

Table of Contents

List of Figures

List of Tables

Acknowledgments

Firstly, I would like to extend my gratitude to the organisations that have made this research possible. This study was funded by a scholarship from the Carnegie Trust for the Universities of Scotland, with additional financial support from the University of Glasgow. I would like to give thanks to Dr Brian Bell for nominating me for the Carnegie Scholarship and for all the kindness he has shown me. I would like to thank Dr Chris Burton for being so instrumental in my decision to pursue postgraduate research. My sincerest gratitude goes to all of the staff, past and present, within the Department of Geographical and Earth Sciences at Glasgow. I would especially like to thank Dr Martin Lee for his never-ending good humour and pretend contempt for accessory mineral research; Dr Jeff Harris for taking me along to Ardnamurchan with him and joining in a few libations with me. Thanks to Robert Macdonald for his help and break-time chats about existentialism. Thanks to John Gileece; Maggie Cusack; Alan Owen; Colin Braithwaite; Gordon Curry; and Zoe Shipton. Special thanks go to Peter Chung for all his invaluable help in acquiring EMPA analyses, and for having good chat on those long drives in the Kangoo out to Edinburgh.

Love goes out to all my friends who have given me support over the past four years. Things haven't been easy and when I have been down and nearly thrown in the towel, you have all helped me to keep going. Thanks to all my friends from Optimo, good times were always had there -Gemma, Jill, Euan, Dave, Teamy, and our beloved hosts Jonnie and Keith, I thanks you for the mirth and magic. Extra special love and thanks go to my boys: James, Ben, Adam, Gee, Colin, Duncan, and John -you are the best friends a guy could have! I want to give my love and thanks to Amy for being there for me and never giving up on me, you're super special, girl, don't you ever forget it.

My eternal gratitude goes to my mum, Irene and dad Hugh, for their unwavering support and love; I would also like to thank Elena and Kevin and Les for helping to keep me grounded. Much love to you all.

Finally, I would like to give very special thanks to one of the nicest and cleverest people I have ever met, my supervisor, Dr Tim Dempster. I owe you more gratitude than I can ever possibly express in words. You kept me going when I felt like I couldn't anymore and I thank you for that. Your kindness and patience is very humbling.

Declaration

The material presented in this thesis is the result of the independent research undertaken by myself between October 2003 and August 2007. This work was supervised by Dr Tim Dempster. All work by other researchers that is quoted in this thesis is given full acknowledgement in the text.

Graham W. McLeod

November 2007

1

Introduction

Accessory minerals can play a very significant role in the control of trace elements during petrogenetic processes (Gromet and Silver, 1983), thus, a better understanding of the nature of accessory minerals with respect to their ability to sequester trace-elements is desirable, since the igneous petrologist is distinctly unable to get inside a magma chamber and witness petrogenesis in action.

Titanite is an accessory mineral that is characterised by slow diffusion of trace elements (Gromet and Silver 1983; Della Ventura, Bellatreccia et al. 1999; Piccoli, Candela et al. 2000; Tiepolo, Oberti et al. 2002; Prowatke and Klemme 2003). This refractory nature means that it is able to preserve compositional zoning of a primary magmatic origin. Titanite naturally serves as a sink for numerous chemical elements of geological interest, including, the rare-earth elements (REE) and high-field-strength elements. The slow diffusion of trace elements within the titanite structure, coupled with its natural predisposition in being able to preferentially sequester key trace elements of petrogenetic significance, makes titanite ripe for assessment as a tool for modelling petrogenetic processes.

In order to assess the ability of titanite to record evidence of magmatic processes, an investigation into the textural and geochemical characteristics of titanite from both the plutonic and volcanic environments is desirable. In the plutonic environment, the slow rate of cooling helps minerals to achieve chemical equilibrium through diffusion driven processes. If titanite can withstand these post-magmatic, sub-solidus processes then it may have potential to preserve a geochemical fingerprint of its genesis. An assessment of the ability to preserve primary magmatic textural features and compositional zoning from the plutonic environment would be complimented by an assessment of titanite textural characteristics from volcanic rocks.

The Ross of Mull Granite is a plutonic igneous complex that displays a variety of magma-mixing phenomena at depth and also contains significant amounts of titanite in both the dioritic and granodioritic lithologies which form the majority of the representative lithologies in the complex. A comprehensive study of the textural characteristics and geochemical signatures of the titanite within the granite and associated mafic enclaves will allow direct assessment of titanite's ability to record geochemical evidence of magma-mixing.

Titanite behaviour from the volcanic environment will assessed by investigation of its textural and geochemical characteristics as preserved in the Fish Canyon Tuff, part of the San Juan volcanic field, Colorado, USA. The Fish Canyon Tuff is significant in that it is the world's largest ever documented pyroclastic eruption. There is debate over the exact nature of the processes which led to such a voluminous eruption, and magma-mixing is thought to play a significant role. If the assessment of titanite's ability to preserve evidence of magma mixing at depth in the Ross of Mull Granite is successful, then it is possible that similar textural features and characteristics of compositional zoning may be recognised in titanite from the Fish Canyon Tuff.

The aims of the project may be simply stated as follows:

- To conduct a coupled micro-textural and geochemical analysis of the chemical zoning in titanite found within mixed-magma/hybrid rocks, from the plutonic and volcanic environments.

- To assess the ability of titanite to retain a record of mixing processes, at depth and through to the emplacement and eruption of the hypabyssal and volcanic products.

2

Titanite

2.1 Introduction

Titanite is a calcium-titanium-silicate accessory mineral that has a large stability field and is found in a wide variety of igneous and metamorphic rocks. In intermediate and silicic igneous rocks it tends to be the dominant titanium-bearing phase (Deer W.A. 1992). Despite its relatively simple chemical formula, $CaTi(SiO_4)(O, OH, F)$, titanite has the ability to incorporate a large number of different elements as substitutes into its crystal lattice, including a variety of trace-elements, rare-earth elements (REE) and high-field-strength elements (HFSE) (Panov and Tarnovsk.An 1973; Staatz, Conklin et al. 1977; Paul, Cerny et al. 1981; Sawka, Chappell et al. 1984; Green and Pearson 1986; Bernau and Franz 1987; Wones 1989; Nakada 1991; Piccoli, Candela et al. 2000; Tiepolo, Oberti et al. 2002; Prowatke and Klemme 2003; Seifert and Kramer 2003; Seifert 2005; Vuorinen and Halenius 2005; Prowatke and Klemme 2006). Titanite is a relatively refractory mineral and tends to resist alteration and diffusive modification, allowing it to retain it's primary chemistry of crystallisation (Piccoli, Candela et al. 2000; Tiepolo, Oberti et al. 2002; Prowatke and Klemme 2003; Seifert and Kramer 2003).

Due to titanite's robust and stable nature in magmatic systems, the sluggish diffusion of trace elements, and its role as a mineral species that can sequester geochemically important trace elements, titanite is a potentially powerful tool for modelling of petrogenetic processes (Piccoli, Candela et al. 2000; Tiepolo, Oberti et al. 2002; Vuorinen and Halenius 2005; Cherniak 2006). This study aims to evaluate the potential of titanite to preserve a record of magma-mixing processes in its chemical zoning.

This chapter introduces the mineralogy of titanite: its structure, chemistry, optical and physical properties, mode of occurrence and paragenesis, and briefly documents the history of research into the mineral. Previous work undertaken that relates to the present study will

also be investigated. The focus of the chapter will be on the properties of titanite that relate to its crystallisation and role as a carrier of important trace-elements.

2.2 Mineralogy

This section will briefly cover the mineralogical basics of titanite. Certain aspects of the mineralogy will be covered in more detail in further sections where relevant.

2.2.1 General information

Titanite is named for its titanium content. It is also known by the name *sphene*, so named for its characteristic sphenoid shape, but modern practice is for the use of the name titanite. It is an orthosilicate. Under the Dana mineral classification scheme it is a nesosilictate (with insular SiO_4 Groups and O,OH,F,H_2O) specifically part of the humite group. In the Strunz mineral classification scheme it is considered a nesosubsilicate (with anions unfamiliar to tetrahedrons and cations of octahedral and tetrahedral orientation) (Speer and Gibbs 1974; Deer W.A. 1992).

TITANITE   **CaTiSiO$_5$**   (basic chemical formula)

Also reported as: CaTiO(SiO4) (Deer W.A. 1992) and CaTi(SiO4)(O,OH,F) (Della Ventura, Bellatreccia et al. 1999). It has a molecular weight of 197.76 g/mol based on its basic chemical formula. It is known to decompose with H2SO4 There are several different varieties and analogues of titanite: grothite is the Al rich variety; yttrotitanite is the Y rich variety; malayite, is the Sn analogue; keilhauite is the REE-rich variety; and greenovite is the Mn analogue (Deer W.A. 1992; Barthelmy 2005).

2.2.2 Crystallography

Crystal system: monoclinic (+) prismatic; 2/m. **Space Group**: *P2$_1$/a*. Usually occurs as wedge shaped crystals which result from the combination of {001}, {110} and {111}, may be lamellar or massive in habit as well. **Unit cell parameters**: *C2/c*a = 7.057-7.088, b = 8.643-8.740, c = 6.572-6.584 Å, β = 113.74-114.15°; Z = 4; **Axial ratios:** a : b : c = 0.7522 : 1 : 0.8532**. Unit cell volume:** 367.55 Å³**.** (Higgins and Ribbe 1976; Deer W.A. 1992)

2.2.3 Physical properties

Colour: gray, brown, green, yellow, black, orange, colourless; yellow or light brown in thin section. **Streak**: reddish-white. **Lustre**: resinous to adamantine. **Transparency**:

transparent to translucent. **Hardness:** 5-5.5. **Habit**: usually small sphenoid/wedge shaped crystals, sometimes massive or lamellar. **Specific Gravity** (G): 3.4-3.55. **Luminescence**: non-fluorescent or very weak brown. **Cleavage**: {110} distinct, good {100} imperfect, {112} imperfect. **Twinning**: single twins with twin plane {100} and very occasional lamellar twining on {221}.**Density:** calculated density based on basic chemical formula is 3.52g/c2, however, it ranges slightly higher or lower depending on the impurities within the lattice and the metamict state.

2.2.4 Optical properties

Biaxial (+); 2V: 17-40°; Refractive index values: n_α = 1.840 - 1.950; n_β = 1.870 - 2.034; n_γ = 1.943 - 2.110; Max birefringence: δ = 0.100 - 0.192; Very high surface relief; Dispersion: r > v strong/extreme; Orientation: y : z ~ 51° , O.A.P. {010}; Pleochroism: α - pale yellow; β - brownish yellow; γ - orangey brown

2.2.5 Crystal structure

The simplicity of the major element chemistry of titanite belies the complexity of substitutions that can occur within its crystal lattice. The impurities taken up by natural titanite is a direct result of the unique crystal chemistry of this mineral.

Zachariasen (1930) was the first to solve the structure of titanite by studying a natural crystal for which and he reported a large range of Si-O bond distances (1.54-1.75 Å), thus proposing the space group *C2/c.* The structure was then refined by Mongiori and Riva di Sanseverino, in 1968, by looking at another titanite in the transformed space group *A2/a*, where they reported bond lengths that were far more reasonable for the silica tetrahedron (Ribbe 1982).

Speer and Gibbs (1974) examined a synthetic titanite and elucidated the crystallographic details as accepted today. They deduced that the common structural units in titanite are kinked chains of corner-sharing TiO_6 octahedra. These chains run parallel to the unit cell edge x axis, with the repeat unit in the chain defined by two tilted TiO_6 octahedra that share a common oxygen atom. This shared oxygen atom is defined as O(1). The oxygen atoms that surround the Ti atoms form almost perfect octahedra. The Ti atoms themselves are not at the geometrical centre of the octahedra.(see Figure 1**)** This results in alternating short and long Ti-O(1) bonds with the remaining four Ti-O bonds in the octahedra longer than either of the Ti-O(1) bonds. The octahedra chains are cross-linked with silica tetrahedra that share the remaining four oxygens. In turn each silica tetrahedra shares

oxygen atoms with four different TiO_6 octahedral groups from three separate chains. The O(2) and O(2A) oxygens are shared by two separate chains while the O(3) and O(3A) oxygens are belong to the same chain (Speer and Gibbs 1974). The result is a $[TiOSiO_4]^{-2}$ framework with large cavities enclosing calcium atoms in irregular seven-fold coordination polyhedra. Since the O(1) oxygen is the only oxygen from the TiO_6 octahedra not bound to a silica tetrahedra , it is considered "underbonded" and can be replaced by (OH) or (F) (Deer W.A. 1992).
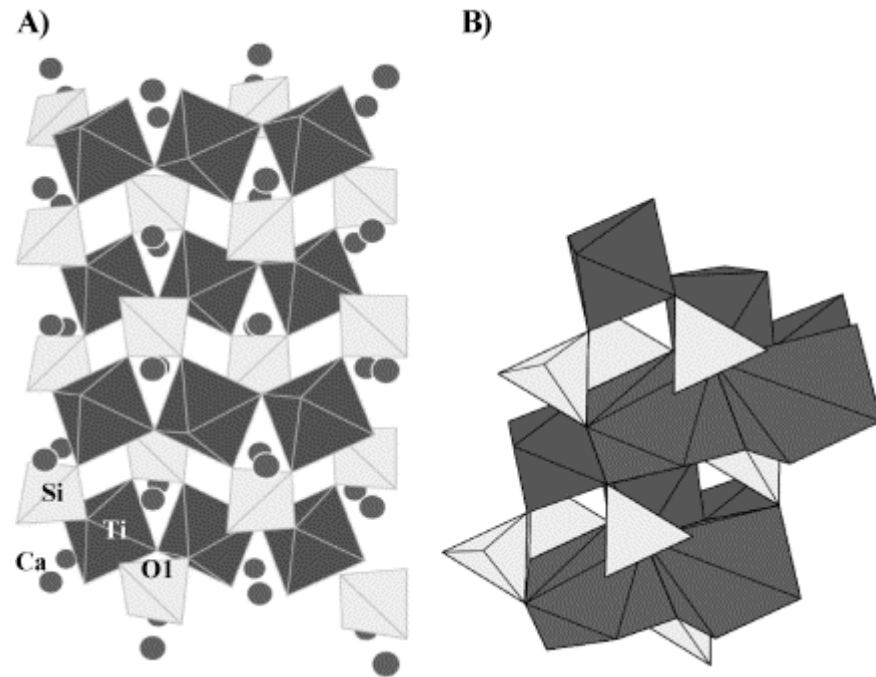
Figure 1: The structure of titanite. (A) Corner-sharing chains of octahedra parallel to {100}; (B) edge-sharing chains of (7)-fold-coordinated sites running parallel to {101}. From Tiepolo et al. (2002).

At a temperature of 220°C there is a transformation from space group *P2₁/a* to *A2/a*. This was discovered by Taylor and Brown(1976) when they examined X-ray diffraction photographs of synthetic *P2₁/a* titanite. They noticed a class of reflections (*k + ℓ odd*), violating the A-centring condition, which were systematically weak but sharp. These reflections were found to become weaker, but not diffuse, as the temperature of the crystal was raised gradually, finally disappearing altogether at roughly 220°C. A second order "distortional transformation" involving the displacement of the Ti atom closer towards the centre of the octahedron as well as a displacement of the O(2), O(2A), and O(3), O(3A) oxygen pairs which then become related by a centre of symmetry at the titanium site (Ribbe 1982). Further work concerning this phase transition, and isomorphism of phase transitions seen in other minerals, has been done by Malherbe (1999; Malcherek, Paulmann et al. 2001; Malcherek, Bosenick et al. 2004).

Hughes et al (1997) have written about the stabilisation of the *A2/a* dimorph by the creation of antiphase boundaries through incorporation of REEs in titanite. Investigations into domain textures in titanite started with Robbins in 1968, however, the bulk of the theory and evidence for domain textures seen in natural titanites was provided by Speer and Gibbs (1974), Taylor and Brown (1976)**,** Higgins and Ribbe (1976). Ribbe (1982) also notes that impure titanites show an increase in the frequency of linear anti-phase domains with an increase in the activity of the substitution: (Al + Fe) + (OH, F) for Ti + O.

Minerals (including non-silicates) isostructural with titanite include Malayite $CaSnO(SiO_4)$, the tin analogue of titanite; the synthetic germanium analogue $CaTiO(GeO_4)$; isokite, $CaMgFPO_4$ and tilasite $CaMgFAsO_4$ (Ribbe 1982).

2.2.6 Crystal Chemistry

The subject of elemental substitution in titanite has received much attention. This is due to the fact that there are many ways in which nature attempts to balance the inherent electrostatic charge imbalance of pure titanite. In addition, titanite is known to be stable in a wide variety of geological environments and is therefore also likely to incorporate different trace elements (as well as major elements) which may be characteristic of the system in which it is crystallising. For example, it has been reported that titanite is key carrier of zirconium in rocks of lamprophyric affinity such as kersantites, minettes, and spessartites (Seifert and Kramer 2003), whereas, Perseil and Smith(1995) report unique Sb-rich titanite from an ophiolite that has witnessed polyphase-metamorphism (prograde from blueschist to eclogite, then retrograde to greenschist facies). Chakhmouradian (2004) has reported high levels of Al, Fe, Nb and Zr in titanite from silicocarbonatite in the Afrikanda alkaline-ultramafic complex. Thus, titanite has a significant tolerance for a wide variety of atomic substitutions at each of the cation and bridging-anion positions in its lattice, making it an ideal sink for trace elements which carry a fingerprint of the petrological and geochemical processes which formed the host rock.

The first major review of the chemistry and classification of titanite, including a summary of known substituents, was provided by Sahama in 1946 (Ribbe 1982). Staatz et al (1977) have also provided a review of the literature dealing with rare-earth element substitution in titanite. These reviews provide information about the variety of substitution mechanisms, coupled and un-coupled, which occur in titanite as well as giving details about the crystal chemistry of titanite that make these reactions possible.

There are three positions, or sites, within the titanite structure (see Figure 2) that can participate in isomorphous substitution in natural titanites:

- Underbonded oxygen O(1) site

- (7)-coordinated Ca polyhedron site

- Ti octahedron site

Although the position of Si in the silica tetrahedra may technically be considered as a possible site for substitution to occur, it has been shown that this is not true for natural systems (Frost, Chamberlain et al. 2001). Al is sometimes assigned to tetrahedral coordination by some workers in order to balance the structural formula, however, Ribbe (1982) claims that this practice is largely unjustified, citing the fact that careful microprobe analyses result in values for Si stoichiometry within a percent or two of what is expected. Oberti et al (1991)state that in synthetic titanites some Ti may occur at the tetrahedral site, and that this has significant effects on tetrahedral and unit cell dimensions.

2.2.6.1 Underbonded O(1) oxygen site

In pure titanite, $CaTiO(SiO_4)$, the oxygen atoms are either under- or over-bonded resulting in a net imbalance in the electrostatic charge of the unit cell (Higgins and Ribbe 1977). The O(1) oxygen is the under-bonded oxygen as it is the only one in the Ti octahedra that is not shared with a silica tetrahedron, and it participates in substitution reactions with monovalent OH and F (Enami, Suzuki et al. 1993). The substitution is thought to be part of a coupled substation mechanism whereby Ti^{4+} from the octahedron is substituted by trivalent cations (especially Fe^{3+} and Al^{3+}), thus helping to balance the electrostatic charge of the unit cell. Ribbe (1982) notes that this most likely accounts for the extensive substitution (up to 30 mol%) of $(Al, Fe)^{3+} + (OH, F)$ that is observed in natural titanites.

2.2.6.2 (7)-coordinated Ca polyhedron site

Tiepolo et al (2002) point out that although the structure of titanite is often simply described as chains of corner-sharing octahedra running parallel to the crystallographic axis {100}and cross-linked by isolated tetrahedra, it is important to consider that the 7-fold coordinated polyhedron sites also form edge-sharing chains. These are due to the O(5) oxygens being shared, and the resulting chains of polyhedra run parallel to the {101} face. Tiepolo et al (2002) state that since these chains of octahedra and polyhedra are mutually

connected by shared edges, the crystal-chemical mechanisms responsible for charge balancing at the shared oxygen atoms must therefore be able to involve any combination of the structural sites. This point illustrates the way in which the substitutions that occur at the octahedral and polyhedral site are often coupled with those occurring at the underbonded O(1) shared oxygens.
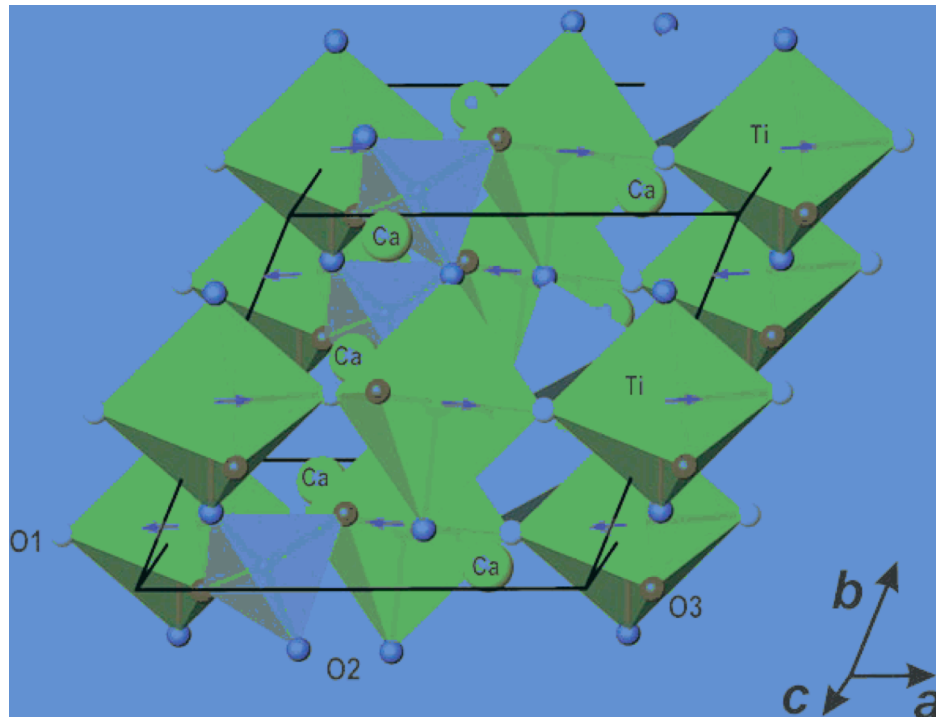
Figure 2:Crystal structure of titanite showing locations of under-bonded O(1) site, (7)-coordinated Ca polyhedron site and Ti octahedral site. From (Liferovich and Mitchell 2006).

The seven-fold coordinated polyhedron is the structural site that Ca dominates in almost all natural titanites. In terms of substitutions, it tends to be the site that takes up ions such as the REEs, Mn, U, Th, Pb, Sr, Ba and sometimes Na and K. (Russell, Groat et al. 1994; Lloyd, Edgar et al. 1996; Della Ventura, Bellatreccia et al. 1999; Frost, Chamberlain et al. 2001; Tiepolo, Oberti et al. 2002; Liferovich and Mitchell 2005; Vuorinen and Halenius 2005).

Perseil and Smith (1995) have reported Sr and Ba substitution in this site, with upper limits of 0.009 apfu (atoms per formula unit) for Sr and 0.006 apfu for Ba. Rare-earth element content tends not to exceed 5wt% oxide, but has been reported by Exley (1980) to exceed 80% replacement of Ca in granites from Skye. Ribbe (1982) states that in most natural titanite specimens the REE which dominate are Ce and Nd and La (Ce>>La>>>Nd) with Y occasionally ranging as high as the total lanthanide content.

Uranium and thorium have been reported to occupy the Ca site by many workers (Reiners and Farley 1999; Aleinikoff, Wintsch et al. 2002; Seifert 2005; Lehmann, Storey et al. 2007), with Th dominant over U but usually at concentration less than 3000ppm, even in completely metamict titanite (Cerny and Rivadisa.L 1972; Ribbe 1982) Due to this substitution, titanite has been used as a geochronometer both with respect to the U-Pb system and fission-track age determinations (Naeser 1967; Lehmann, Storey et al. 2007).

2.2.6.3 Ti octahedral site

The Ti-octahedral site is the final location where charge-balancing substitutions can occur. The site is normally occupied by Ti^{4+} cations but the two main species that are known to substitute for titanium are Fe^{3+} and Al^3 (Deer W.A. 1992). The following is a list of elements known to substitute into the Ti octahedral site with values for upper limits reported in literature:

Al -up to 14 wt% oxide (Franz and Spear 1985)

Fe (normally trivalent) up to 3 wt% oxide (Deer W.A. 1982)

Zr -up to 15.3 wt% oxide (Chakhmouradian 2004)

Ta -up to 20 wt% oxide (Cerny, Novak et al. 1995)

Sb -up to 11 wt% oxide (Perseil and Smith 1995)

Nb -up to 5 wt% oxide (Cerny, Novak et al. 1995)

Other elements reported to substitute in this site in very small amounts include Cr, Cu and Mg (Ribbe, 1982).

Substitution sometimes does occur as a straight swap -direct isovalent substitution, as in the case of tetravalent Zr for tetravalent Ti (Della Ventura, Bellatreccia et al. 1999), however, most workers agree that replacement of Ti from the octahedral site occurs due to some form of coupled substitution involving exchange taking place at either the under-bonded O(1) oxygen site or the 7-coordinated Ca site (Piccoli, Candela et al. 2000; Frost, Chamberlain et al. 2001; Tiepolo, Oberti et al. 2002; Liferovich and Mitchell 2005). Trivalent or pentavalent cations substituting for tetravalent Ti must be balanced by additional substitutions involving the other sites.

2.2.6.4 Chemical substitutions summary

It is clear that there are three sites in the titanite structure that can participate in chemical substitution and that due to under-bonding and over-bonding of structural oxygen, as well as non-isovalent substitution of cations, that charge balancing is often achieved through coupled substitutions involving more than one site. Some exchange mechanisms are more widely accepted than others, and not all workers agree about which coupled substitutions are the most common. Indeed, depending on the bulk chemistry of the rocks or the nature of the processes (magmatic, metasomatic, etc) the main substitution mechanisms may differ as there will be different abundances of elements involved.

To simplify, we can think of the titanite formula as such: $^7\mathbf{X}^6\mathbf{YOSiO_4}$, whereby the $^7\mathbf{X}$ represents the cation residing in the 7-fold coordinated Ca site, and $^6\mathbf{Y}$ represents the cation residing in the6-fold coordinated Ti octahedral site. The most common cations are as follows:

$^7\mathbf{X} = \mathbf{Ca^{2+}}$ (principle cation), REE^{3+}, Fe^{2+}, Y^{3+}, Sr^{2+}, Mn^{2+}, Na^+, K^+, U^{3+}, Th^{3+}, Pb^{2+}

$^6\mathbf{Y} = \mathbf{Ti^{4+}}$ (principle cation), Al^{3+}, Fe^{3+}, Zr^{4+}, Ta^{5+}, Nb^{5+}, Sb^{5+}, Cr^{3+}

It is easy to see why coupled substitutions occur as the main cations replacing Ca and Ti are often not the same valancy. The charge balancing is achieved by other concomitant reactions. Reactions involving substitutions can be heterovalent, usually involving a coupled charge-balancing agent, or homovalent where there is no charge balancing needed.

If we designate the substituents as R, designate the site of reaction by noting the coordination number (i.e.: ^7R for 7-coordinated Ca site; ^6R for octahedral site), and if we consider the charge balancing reaction occurring at the O(1) site ($^{O1}O^{2-} \leftrightarrow {}^{O1}[OH, F]^- + e^-$) the same as adding or removing an electron (e^-), we can summarise the types of substitutions that can occur as follows:

$^{O1}R^{2-} \leftrightarrow {}^{O1}R^- + e^-$ this is essentially: $^{O1}O^{2-} \leftrightarrow {}^{O1}[OH, F]^- + e^-$

$^7R^{2+} \leftrightarrow {}^7R^{2+}$

$^7R^{2+} \leftrightarrow {}^7R^{3+} + e^-$

$^7R^{2+} \leftrightarrow {}^7R^{4+} + 2e^-$

$$^7R^{2+} \leftrightarrow {}^7R^+ - e^-$$

$$^6R^{4+} \leftrightarrow {}^6R^{4+}$$

$$^6R^{4+} \leftrightarrow {}^6R^{3+} - e^-$$

$$^6R^{4+} \leftrightarrow {}^6R^{5+} + e^-$$

$$^6R^{4+} \leftrightarrow {}^6R^{2+} - 2e^-$$

$$2{}^6R^{4+} \leftrightarrow {}^6R^{3+} + {}^6R^{5+}$$
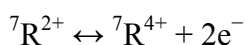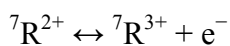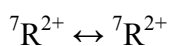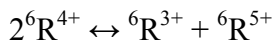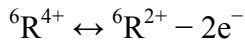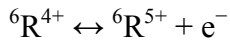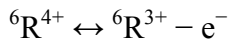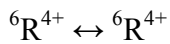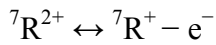
Of course, there can be combinations of portions of these equations to form coupled substitutions whereby the octahedral and 7-coordinated polyhedral sites exchange concomitantly to balance the charge (Perseil and Smith 1995). An example would be:

$$^6R^{4+} + {}^7R^{2+} \leftrightarrow {}^6R^{3+} + {}^7R^{3+} \quad \text{i.e.:} \quad {}^6Ti^{4+} + {}^7Ca^{2+} \leftrightarrow {}^6(Al, Fe)^{3+} + {}^7REE^{3+}$$
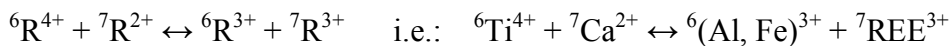
The following is a list of the main chemical substitutions, coupled and uncoupled, that have been suggested.

$$Ca^{2+} + Ti^{4+} \leftrightarrow REE^{3+} + (Al, Fe)^{3+} \quad \text{(Green and Pearson 1986; Enami, Suzuki et al. 1993)}$$

$$Ca^{2+} + Th^{4+} \leftrightarrow 2REE^{3+} \quad \text{(Gromet and Silver 1983)}$$

$$(Al, Fe)^{3+} \leftrightarrow Ti^{4+} + (OH, F)^- \quad \text{(Franz and Spear 1985)}$$

$$2Ti^{4+} \leftrightarrow (Nb, Ta)^{5+} + (Al, Fe)^{3+} \quad \text{(Cerny, Novak et al. 1995; Vuorinen and Halenius 2005)}$$

$$Ti^{4+} + Al^{3+} \leftrightarrow Zr^{4+} + Fe^{3+} \quad \text{(Seifert and Kramer 2003)}$$

$$Ti^{4+} + Ca^{2+} + Th^{4+} \leftrightarrow REE^{3+} + Zr^{4+} + Al^{3+} \quad \text{(Seifert 2005)}$$

$$Ti^{4+} \leftrightarrow Zr^{4+} \quad \text{(Della Ventura, Bellatreccia et al. 1999)}$$

$$2\,Ti^{4+} \leftrightarrow (Al, Cr, Mn, Fe)^{3+} + Sb^{5+} \quad \text{(Perseil and Smith 1995)}$$

$$2Ca^{2+} \leftrightarrow 2REE^{3+} + Na^+ \quad \text{(Tiepolo, Oberti et al. 2002)}$$

$$Ti^{4+} + Ca^{2+} \leftrightarrow (U, Th)^{4+} + Mg^{2+} \qquad \text{(Tiepolo, Oberti et al. 2002)}$$

This list probably does not include all of the possible substitutions that operate in nature, but it does cover the main substitutions reported in literature.

2.3 Magmatic titanite

Titanite is known to occur as a primary igneous mineral, as a mineral formed during sub-solidus cooling of igneous rocks, and also as a metasomatic and metamorphic mineral in many rock types (Franz and Spear 1985; Frost, Chamberlain et al. 2001; Broska, Harlov et al. 2007). This study is concerned primarily with the behaviour of titanite formed in magmatic environments both plutonic and volcanic, and in particular titanite that is crystallised from intermediate to acidic magmas. Since the study is aimed at examining whether the mineral is capable of retaining a chemical signature of magma-mixing processes from both plutonic and volcanic rocks, a review of the literature on titanite behaviour from said environments and rock types is necessary.

The majority of mineralogical and petrological-related work on titanite has focused on peculiar compositional varieties that have unusually high amounts of trace and rare-earth elements and which come from unusual rock types (Paul, Cerny et al. 1981; Franz and Spear 1985; Groat, Carter et al. 1985; Bernau and Franz 1987; Woolley, Platt et al. 1992; Janeczek 1996; Della Ventura, Bellatreccia et al. 1999; Seifert 2005; Vuorinen and Halenius 2005; Liferovich and Mitchell 2006). Focus is often placed on unusual varieties or occurrences of minerals and rocks simply because of their novelty. However, there is a lack of focus on titanite behaviour from the more common intermediate and acidic igneous rocks (granites, granodiorites, and diorites), where the trace-element and REE contents are generally low (less than 2-3 wt % of the mineral) compared to titanite from alkaline silicate and carbonatitic igneous complexes where they can total as much as 15 wt% or more of the mineral (Chakhmouradian 2004; Vuorinen and Halenius 2005). It is easy to understand why less attention is paid to the more common occurrences of titanite since they contain less variety and quantity of impurities, however, this does not mean that the more ubiquitous and compositionally discreet titanite from intermediate and acidic rocks is neither interesting nor useful to the petrologist. The behaviour of titanite in the magmatic environment need not rely on high numbers of impurities alone to be indicative of petrological processes as titanite behaviour has been shown to indicate changes in oxygen fugacity (hereafter referred to as fO_2) and also is known to be useful in reflecting the temperature and pressure of formation as well as the bulk chemistry of the source (Gromet

and Silver 1983; Wones 1989; Nakada 1991; Piccoli, Candela et al. 2000; Frost, Chamberlain et al. 2001; Tiepolo, Oberti et al. 2002).

The fact that compositional zoning is visible by method of atomic number contrast imaging techniques (like backscattered electron (BSE) imaging), and that the differences in the key trace-elements and REE are measurable above detection limits, means that titanite may prove very useful as a small-scale recorder of potentially very large scale petrogenetic processes (Piccoli, Candela et al. 2000).

2.3.1 Compositional zoning

There are some key issues about titanite growth in the magmatic environment that need to be understood in order to unlock the potential information encoded in its chemical zoning. Firstly, the nature of the zoning must be magmatic and not metasomatic or metamorphic. Distinguishing this may not be as easy as it seems, as some varieties of titanite may not contain obvious compositional zoning at all and may therefore have re-crystallised entirely or been subject to metamictisation (destruction of the ordered crystalline structure to an amorphous one due to radiation damage). Furthermore, magmatic zoning itself may be normal (expected chemical trends based on fractional crystallisation or down-temperature trends), reversed (opposite of normal zoning), or simple oscillatory zoning (due to boundary-layer diffusion dynamics), or may occur as sector zoning caused by differences in the lateral-layer spreading rates of different crystal faces during growth. Since the latter is related to disequilibrium partitioning of elements between morphologically (and crystallographically) important crystal faces it may not reliably be used to model the changes in composition of an evolving magma (Paterson and Stephens 1992). Understanding the differences between the main types of compositional zoning (normal zoning, oscillatory zoning, and sector zoning), especially those which indicate growth in a magmatic environment, and their causes is very important to being able to utilise the information stored within the mineral chemistry.

2.3.1.1 Absence of zoning

The absence of oscillatory zoning or the presence of only limited sector zoning does not preclude titanite from being of primary igneous origin. However, it may inform about the temperature of the melt at the time of crystallisation and the rate of effective diffusion of the trace and rare-earth elements within the melt that are so indicative of sector and magmatic zoning.

2.3.1.2 Oscillatory zoning in titanite

This is compositional zoning that is due to small-scale fluctuations in the crystallising environment that are related to factors such as: pressure, temperature and melt composition; however, the biggest factor may be the process of crystallisation itself affecting the local environment of crystallisation: namely, the depletion and subsequent replenishment of elements by diffusion through the melt (Clarke 1992).

This type of zoning is on a very small scale in titanite, usually the order of 10 microns per zone; the small-scale of the zoning is in large part related to the speed of diffusion versus crystallisation. It is wholly magmatic but since it is on such a fine scale, it can be regarded as being of secondary importance to the overall aim of the study. It is not the fine scale oscillatory zoning that will record wholesale changes in the melt composition brought about events such as the mixing of magmas, but rather the larger features of compositional zoning such as core to rim profiles, normal zoning, discontinuous zoning, reverse zoning, in conjunction with features like solution surfaces that truncate zoning, these are the features that will be indicative of large scale magmatic processes. If it comes down to semantics, then it is a question of scale when considering the main differences between oscillatory zoning and larger scale zoning (simple, normal, reverse etc), because the physical, chemical and mineralogical processes are similar. Oscillatory zoning, however, is a very useful compositional texture that may be used to positively identify magmatic growth and differentiate between it and post-magmatic sub-solidus alteration/zoning.

2.3.1.3 Sector zoning

The most thorough investigation into sector zoning in titanite was carried out by Paterson and Stephens (1992) who deduced that the main causes of sector zoning lay in kinetically induced disequilibrium partitioning of REE and trace elements between different crystal faces. They deduced that most compositional zoning is titanite is defined by variations in REE and trace elements and these are usually only visible when employing atomic number contrast imaging methods, of which backscattered-electron imaging is the best method.

When analysing compositional zoning in titanites from monzonitic and granitic Caledonian intrusions, Paterson and Stephens (1992) noticed that the patterns of sector zoning (see Figure 3) were defined by the morphologically less important {111} crystal faces, which seemed to be richer in elements with equilibrium coefficients greater than one (the REE, Y and Nb). The morphologically dominant {100} crystal faces, which have faster lateral-

layer spreading rates compared to the {111} faces, preferentially take up certain elements that have an equilibrium partition coefficient of less than one (mainly Al and Fe).
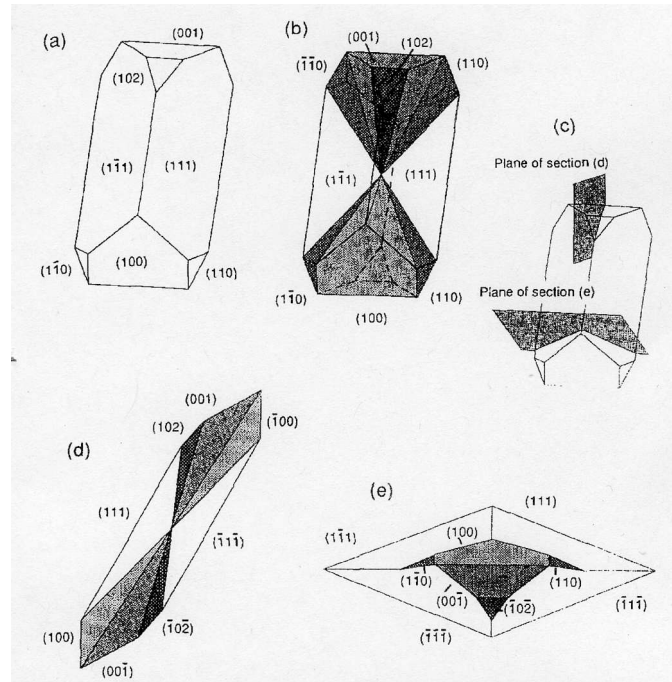
Figure 3: Titanite crystal faces and sector zoning patterns; a) orthographic projections of a typical titanite crystal in which the habit is dominated by the {111} form; b) similar crystal forms showing the different sectors arising from the different crystal forms (faces); c) cross-section reference for d) and e); d) internal pattern of sector zoning cut parallel to a and c axes; e) section cut perpendicular to the {111} crystal face. From Paterson and Stephens (1992)

Patterns of sector zoning, of which the most common is a type of stylised fir-tree pattern, are the product of the crystal habit of titanite and the changes of the crystal habit during growth of the titanite (Figure 4). Extreme fluctuations in the relative normal growth rates of the different crystal faces, namely {111} and {102} faces, are the key causes of fir tree zoning according to Paterson and Stephens (1992). They also attribute these fluctuations of relative growth rates to changes in temperature, pressure or composition of the melt and state that these changes could occur immediately adjacent to the crystals or throughout the melt. The existence of sector zoning in titanites from metaluminous granitoid melts demonstrates that kinetics play an important role in the processes of element partitioning as well as crystal growth and that this kinetically-induced compositional zoning is a result of the growth outstripping the onset of processes at the crystal/melt interface that induce equilibrium (Paterson and Stephens 1992). If this is true, then it holds major implications for the conventional method of centre-rim or whole grain traverse microanalytical techniques and analyses strategies unless the texture of the crystal is well understood and the sector zoning is avoided or taken into account (Paterson and Stephens 1992). For these

reasons, sector zoning is not going to be heavily involved in the analyses of titanites in this study, as they will not be indicative of large scale magmatic processes.
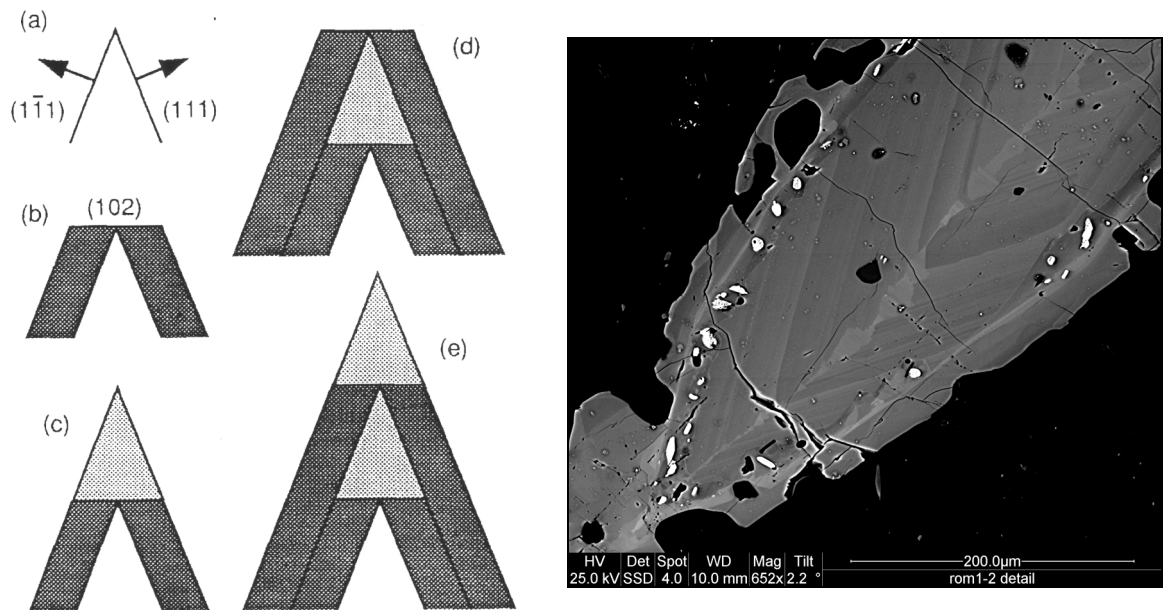
Figure 4: Schematic illustration of fir-tree sector zoning developments in titanite (on the left). a) two initial faces of the {111} form exist; b) preferential and progressive growth of the {111} form allows the {102} face to become stable; c) growth only occurs on the {102} face until it is no longer stable, resulting in renewed growth on the {111} face. The pattern repeats as per d) and e). From Paterson and Stephens (1992). On the right is a BSE image of fir-tree sector zoning form the ROM1 sample of the Ross of Mull Granite.

2.3.2 Trace element partitioning

Factors controlling the solid/melt partitioning of trace elements include: pressure, temperature, oxygen fugacity, crystal composition and melt composition. Because titanite can incorporate large amounts of REE and HFSE into its crystal lattice it can exert a significant control on the distribution of these trace elements during petrological processes such as late-stage fractional crystallisation of melts and partial melting events (Prowatke and Klemme 2005). In order to model geochemical processes which occur during petrogenesis, it is desirable to understand the behaviour of trace elements with respect to titanite and the melt it is crystallising in. (Green and Pearson 1986; Paterson and Stephens 1992; Prowatke and Klemme 2003; Prowatke and Klemme 2005).

Investigations of the trace element partitioning between titanite and silicate melts began with Green and Pearson (1986) who studied the effects of pressure, temperature for several different melt compositions. They experimentally determined partition coefficients for seven elements (La, Sr, Dy, Lu, Nb, Ta, and Sm) that were added in concentrations exceeding 1wt%.

Work carried out by Tiepolo *et al* (2002) on trace element partitioning between titanite and melt focused on a fixed bulk melt starting composition but did so for a large range of elements (in the mass range form Li to U). The experiments to determined solid/liquid partition coefficients were carried out on synthesised lamproite that is based on the bulk chemistry of a lamproite found in West Kimberley, Australia and described by Arima and Edgar (1983). They cite the reasons for using such a starting material as being because the natural lamproite contains abundant titanite and therefore the run products did not have to be enriched with titanite components. Run products included amphibole, titanite, subordinate clinopyroxene, rare-ilmenite and glass. The degree of crystallisation was cited as being lower than 50%. Figure 5 (below) shows a spider diagram of the titanite/melt partition coefficients ($^{Ttn/melt}D$) as reported by Tiepolo et al (2002).
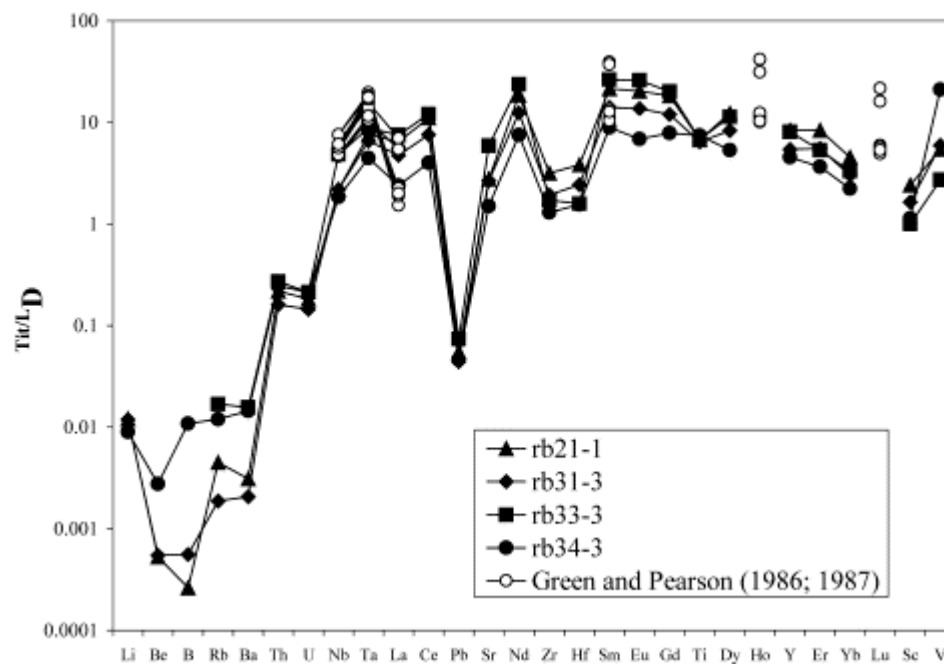
Figure 5: Spider diagram of experimentally determined solid-liquid partition coefficients for titanite from Tiepolo et al (2002).

Results show most elements (except Li, Be, B, Rb, Ba, U, Th and Pb) to be compatible to various extents in titanite, REE and Y are highly compatible, Pb is highly incompatible, Ta is by far the most compatible HFSE and is strongly fractionated from Nb. Zr and Hf are less compatible than Ta and Nb, and one would expect the rims of titanite to be more enriched in Zr compared to cores. Due to the significant differences in compatibility, the

crystallisation of titanite in lamproitic systems increases the LREE/HREE and Nb/Ta ratios in residual liquids. U and Th are incompatible and the reasons for this are thought to be due to the extra two positive charges that require balancing when U or Th substitutes for Ca, and although Tiepolo et al. state that this substitution is scarce, they interpret that the charge balancing is achieved by simultaneous substitution of Mg at the Ti site, citing as evidence that titanite which shows the highest compatibility for U and Th also shows the highest Mg contents.

Tiepolo et al (2002) state that their results follow the general trend reported by Green and Pearson (1986) although their values for partition coefficients ($^{Ttn/melt}D$) are lower and their results are characterised by higher LREE/HREE ratios than Green and Pearson's. They suggest that the likely reasons for the lower $^{Ttn/melt}D$ are due to the different system compositions (lamproite vs. intermediate-acid silicic melts), but cite the differing REE fractionation to be a result of crystal chemical constraints because melt does not discriminate between elements with similar ionic radius and charge (Tiepolo, Oberti et al. 2002). Since the effect of pressure, temperature and melt composition was fixed for this experiment, the interpretation of the results regarding solid-liquid partition coefficient values, as well as the fractionation between different elements, should be based on and related to crystal chemical variations only (Tiepolo et al 2002). In effect, this explains the observed compatibility or incompatibility of trace elements in the titanite structure in terms of crystal chemical controls only, which although helpful for the elucidation of possible substitution mechanism, is not so useful in predicting the partitioning of trace elements in natural systems since the effects of pressure, temperature, oxygen fugacity, volatile content, and changes in melt composition are not taken into account.

Prowatke and Klemme (2005) conducted isobaric and isothermic experiments to investigate the effect of melt composition on the partitioning of trace elements between titanite crystals and different silicate melts systems. They synthesised a range of melt compositions with varying alumina saturation index values (ASI: molar $Al_2O_3/(Na_2O + K_2O + CaO)$; commonly used to quantify the degree of melt polymerisation).In terms of the degree of polymerisation, the bulk compositions represented a range of melts which occur naturally -from basalt to rhyolite (Prowatke and Klemme (2005). The melts were doped with a trace element cocktail consisting of 18 components (Sr, Rb, Y, Zr, Nb, Cs, Ba, La, Ce, Pr, Sm, Gd, Lu, Hf, Ta, Pb, Th, and U). A range of compositions with a similar ASI but without the added trace-elements were also prepared, to carry out experiments aimed at determining the solubility of Al in titanite as a function of Al in the system.

Additionally, two bulk melts of dacitic and rhyolitic compositions were prepared in the same fashion as the doped ASI series. All synthetic rock compositions were doped with 33 wt% synthetic titanite glass.

Prowatke and Klemme (2005) state that because titanite has a major element composition that is stable and virtually constant over a wide range of temperatures, pressures and melt compositions, the effect of titanite composition (i.e.: crystal chemical controls) on the changes in trace element partitioning may be neglected. This is somewhat at odds with the findings of Tiepolo et al (2002) who state that it is the crystal chemical controls that exert the biggest influence on the partitioning of trace elements between titanite and melt, however, this may be due to the work by Tiepolo et al concerning a fixed melt composition. Prowatke and Klemme are primarily concerned with the general effect of melt composition on solid/liquid partitioning of trace elements, and therefore have chosen titanite due to their stated reason of its supposed stability negating the crystal chemical controls. However, this approach may be flawed when one considers the obvious control that crystal chemical factors have on the partitioning of trace elements between titanite and melt, as illustrated by Tiepolo et al (2002). Results from both studies may need to be regarded with caution as it is obvious that crystal chemical effects on partitioning of trace elements are hard (if impossible) to control in experiments, whereas other factors such as pressure, temperature and melt composition may be more readily controlled. Therefore, it is perhaps more difficult to neglect the effect of crystal chemical controls, and indeed the crystal chemistry may be affected by factors like melt composition (different coupled substitutions will be prevalent depending on the different elements in the melts), and pressure (phase changes have direct effects on what elements can substitute into the crystal lattice due to ionic radii and site coordination considerations).

Caveats notwithstanding, the results of the experiments are interesting. The morphology of titanite crystals seems to be linked to the ASI of the run products, with the size of the titanite decreasing with increasing ASI. The largest (up to 400 μm) were from a run with ASI200, and the smallest crystals (less than 30 μm) were from a run with ASI280. Melt composition seemed to also affect the shape of the titanites; with the lower ASI runs containing euhedral crystals and the higher ASI runs containing subhedral to anhedral titanites with increasing numbers of melt inclusions. The runs corresponding to dacitic and rhyolitic bulk compositions contained nearly euhedral titanites that were very similar in characteristics of shape and melt inclusions (Prowatke and Klemme 2005).

Figure 6 (below) shows a table of the trace element partition coefficients as reported by Prowatke and Klemme (2005). Figure 7 shows a spider diagram of the same data.

Sample	ASI200	ASI220	ASI240	ASI250	ASI260	ASI280	DAC	RHY
Rb	0.00034 (4)	0.00043 (11)	0.00025 (7)	0.00022 (8)	0.00019 (3)	0.00043 (−)	0.00026 (4)	0.00033 (3)
Sr	0.54 (3)	0.61 (4)	0.51 (2)	0.45 (2)	0.44 (1)	0.48 (1)	0.62 (3)	0.44 (1)
Y	0.73 (2)	1.53 (9)	4.39 (24)	18.5 (12)	126 (11)	246 (39)	14.3 (17)	8.69 (48)
Zr	2.65 (10)	2.57 (18)	3.32 (38)	2.53 (30)	2.46 (26)	2.72 (39)	3.78 (57)	3.48 (47)
Nb	1.3 (1)	2.81 (26)	2.97 (17)	4.42 (37)	6.22 (53)	6.5 (37)	7.26 (73)	5.44 (10)
Cs	0.0024 (2)	0.0024 (4)	0.0018 (2)	0.0017 (3)	0.0017 (1)	0.0032 (−)	0.0023 (5)	0.0022 (1)
Ba	0.0019 (3)	0.0021 (3)	0.0023 (1)	0.0022 (1)	0.0029 (1)	0.0055 (−)	0.0025 (2)	0.0029 (1)
La	0.40 (2)	0.81 (5)	1.38 (13)	2.76 (21)	5.17 (59)	8.2 (22)	2.17 (38)	1.88 (8)
Ce	0.55 (2)	1.21 (7)	2.35 (18)	6.09 (37)	16.8 (18)	28.4 (33)	4.60 (72)	3.61 (19)
Pr	0.83 (2)	2.07 (13)	4.55 (25)	15.38 (97)	58.3 (59)	77 (11)	9.7 (12)	7.39 (45)
Sm	1.23 (4)	3.44 (24)	10.46 (63)	59.0 (44)	383 (46)	364 (85)	31.2 (40)	20.4 (14)
Gd	1.09 (4)	2.83 (24)	9.06 (67)	53.4 (48)	416 (51)	368 (58)	30.5 (39)	18.2 (15)
Lu	0.31 (2)	0.55 (3)	1.33 (9)	3.56 (26)	13.2 (13)	50 (6)	3.65 (51)	2.38 (8)
Hf	3.07 (10)	2.64 (28)	4.71 (39)	4.50 (57)	4.84 (62)	4.74 (52)	6.9 (14)	4.90 (71)
Ta	4.94 (22)	9.9 (11)	25.1 (33)	63.5 (86)	88 (17)	41 (19)	84 (14)	54.8 (72)
Pb[a]	0.25 (5)	0.23 (5)	0.40 (8)	0.57 (13)	0.88 (23)	0.61 (16)	0.87 (17)	0.75 (16)
Th	0.025 (3)	0.045 (6)	0.11 (1)	0.23 (3)	0.48 (9)	3.55 (30)	0.28 (8)	0.15 (1)
U	0.07 (1)	0.091 (31)	0.10 (2)	0.093 (10)	0.104 (6)	0.39 (4)	0.14 (2)	0.101 (8)

Figure 6: Titanite liquid-solid partitions coefficients for trace elements as experimentally determined by Prowatke and Klemme (2005). 1 σ uncertainty quoted in terms of last significant digits - 1 σ uncertainty by normal error propagation.

Trace element analyses of the titanites show a variation of less than 10% and they report no zoning of trace elements. Partition coefficients between titanite and melt show a very large range and magnitude, with Rb being the lowest at 0.0002 and Sm having the highest value at more than 350 (Prowatke and Klemme 2005).Large ion lithophile elements (LILE), including Rb, Cs and Ba, are known to be incompatible with respect to titanite and exhibit the lowest $Ttn/meltD$ values. There is no significant systematic variation in partition coefficients for the monovalent and divalent elements (K, Na, Cs, Ba, Rb and Sr) with respect to melt composition. Prowatke and Klemme (2005) also report that there is no great

variation in Ttn/meltD values with respect to bulk melt composition for Zr, Hf and U in addition to the monovalent and divalent elements already mentioned.
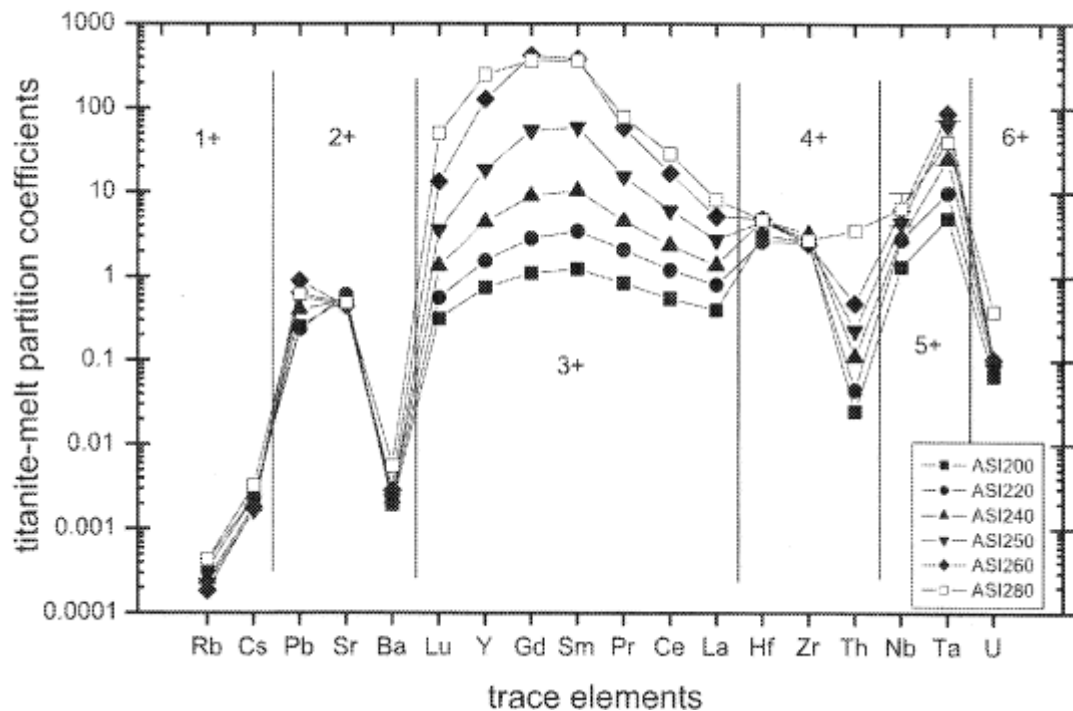
Figure 7: Spider diagram of trace element liquid-solid partition coefficients for titanite as determined experimentally. From Prowatke and Klemme (2002).

Overall, the results indicate a large influence of bulk melt composition on certain partition coefficients. Particularly, the REE, Th, Nb, and Ta show significant variation in partition coefficients, where increasing ASI is followed by orders of magnitude increases in the Ttn/meltD values. Furthermore, Prowatke and Klemme conclude that due to this information they argue that crystal structure factors cannot be responsible for the large variation in REE, Th, Nb and Ta partition coefficients. Instead they offer two explanations for the observed variations in partitioning of these elements with respect to increasing ASI. Firstly, they state that the increasing Al content plays a role in influencing the coupled substitutions that occur, and these seem to favour the elements stated. Secondly, they cite the change of coordination and the regularity of the coordination space of trace elements in the melt structure as being able to significantly affect partition coefficients in their experiments, arguing that a change in cation coordination with changing melt composition could be responsible for an increase of the partition coefficients observed for the REE, Nb, and Ta (Prowatke and Klemme 2005). They predict fairly constant coordination for Sr, and other monovalent, divalent and quadrivalent trace elements regardless of melt composition, however, they do admit that there is limited in the literature to back this up. An important outcome of this paper is the need for better and more valid descriptions of melt structure,

and its influence on the coordination of cation species, if predictive trace element partitioning models are to be coherent and useful (Prowatke and Klemme 2005).

2.3.3 Titanite and oxygen fugacity

Wones (1989) studied the assemblage titanite + magnetite + quartz in granitic rocks and concluded that the assemblage was indicative of a relatively high oxygen fugacity (fO_2), most relevant to melts above 800ºC. He examined a series of equilibria involving the phases magnetite, quartz and titanite, and in particular a buffer involving titanite, quartz, magnetite, clinopyroxene and ilmenite. The buffer behaves thus:

$$3CaTiSiO_5 + 2Fe_3O_4 + 3SiO_2 \leftrightarrow 3CaFeSi_2O_6 + 3FeTiO_3 + O_2$$

titanite + magnetite + quartz ↔ hedenbergite + ilmenite + oxygen
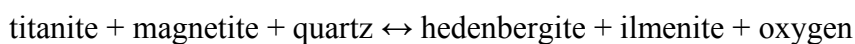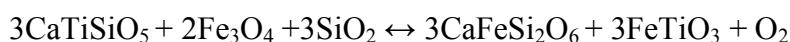
The buffer/equilibrium shows that in a magma saturated with respect to titanite, quartz and magnetite, if the oxygen fugacity decreases, ilmenite may become stabilised (Wones 1989). Many workers have reported titanite with ilmenite inclusions, whereas the predominant Fe-Ti oxide outside the grains is magnetite (Wones 1989; Nakada 1991; Piccoli, Candela et al. 2000). These ilmenite inclusion zones tend to follow solution horizons within the titanite crystals or they tend to be restricted to a particular portion of the compositional zoning, and Piccolo, Candela et al (2000) state that they are probably associated with episodes of reduction in the magma chamber. The proximity of the ilmenite inclusions to solution horizons or anhedral cores of titanite grains also points to the resorption of titanite immediately prior to the precipitation of ilmenite, and is also indicative of a change in oxygen fugacity or reduction event in the melt (Nakada 1991; Piccoli, Candela et al. 2000). Piccoli, Candela et al (2000) also state that the REE concentration of the zoning in titanite associated with ilmenite inclusions is somewhat reduced when compared to the rest of the crystal, which is logical when considering that ilmenite nucleation is stabilised by a reduction event. A period of lowered fO_2 in a dominantly granitic magma chamber, which could be brought about by the addition of a mafic magma, would promote the resorption of titanite, allow the stabilisation and subsequent nucleation of ilmenite, followed by the re-growth of titanite at lower fO_2 (Piccoli, Candela et al. 2000). The lower oxygen fugacity would affect the activity of the coupled substitution involving REE and ferric iron:

$$Ca^{2+} + Ti^{4+} \leftrightarrow REE^{3+} + Fe^{3+}$$
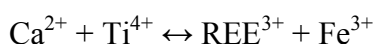
The reduction of ferric iron to ferrous iron would reduce the activity of the above reaction and limit the incorporation of REE. Thus, oxygen fugacity, and factors affecting it such as the mixing of magmas, can affect the stability of titanite and ilmenite as well as have an effect on the REE intake via control of the Fe species available for participation in coupled substitutions. Therefore, the presence of ilmenite inclusions in titanite and associated dissolution/re-growth textures may be textural features that record evidence of magma chamber processes (Nakada 1991; Xirouchakis and Lindsley 1998; Della Ventura, Bellatreccia et al. 1999; Piccoli, Candela et al. 2000; Tiepolo, Oberti et al. 2002; Harlov, Tropper et al. 2006).

2.3.4 Titanite in volcanic rocks

Titanite, although a common accessory mineral in plutonic rocks of intermediate and acidic composition, is relatively rare in volcanic rocks (Nakada 1991; Deer W.A. 1992; Della Ventura, Bellatreccia et al. 1999; Kowallis, Christiansen et al. 2005). Volcanic titanite has been reported mainly from calc-alkaline dacitic to rhyolitic rocks, but may also occur in alkalic rocks from a wide range of silica concentrations (Kowallis, Christiansen et al. 2005). Kowallis (2005) has reported that there is a systematic variation in the contents of certain elements in titanite with respect to the rock type, citing as an example the decrease in Ca from 1 apfu in andesite to nearly 0.9 apfu in rhyolite, while Ti decreases from about 0.95 apfu in andesite to 0.85 apfu in rhyolite. Conversely, he reports an increase in LREE concentration in rhyolitic titanites compared with dacitic titanites. It is clear that the variations in titanite composition mimic the chemical variations of the host rocks, and are preserved in the quenched volcanic state. Titanite from alkalic volcanic rocks tends to be higher in Fe and Nb, but lower in Y, Al and LREE when compared to calc-alkaline volcanic rock titanites (Kowallis, Christiansen et al. 2005).

Nakada (1991) analysed titanites from dacites in the Central Andes, and reports that volcanic titanite is able to record evidence of oxygen fugacity changes brought about by reduction events in the magma chamber, through textural features such as ilmenite inclusions and solution horizons. He states that the fO_2 change was most likely brought about by devolatilisation of the magma at the upper reaches of the magma chamber, and that subsequent heating of the titanites during mixing caused vesiculation of their melt inclusions which lead to fragmenting of the phenocrysts.

It is clear from these studies that volcanic titanite may be able to record evidence of magma chamber processes that may affect the oxygen fugacity of the melts involved. Such

a process would include the mixing of magmas of contrasted oxidation state and/or bulk composition.

2.4 Other work

One of the most prominent uses of titanite has been that as a geochronometer. Due to its inclusion of U and Th, and Pb and because it has such a high closure temperature (roughly 500˚C), it has been successfully used to date rocks (Reiners and Farley 1999; Frost, Chamberlain et al. 2001; Aleinikoff, Wintsch et al. 2002; Davis and McNicoll 2005; Imonetti, Heaman et al. 2007).

In metamorphic rocks titanite is stable in mafic and calc-silicate rocks and is predominantly found in greenschist, blueschist, and amphibolite facies rocks, although in calcic rocks its stability may extend into granulite facies. However, some studies have shown titanite closure temperatures to lie at the upper limit of the amphibolite facies (Reiners and Farley 1999; Frost, Chamberlain et al. 2001; Aleinikoff, Wintsch et al. 2002; Davis and McNicoll 2005; Imonetti, Heaman et al. 2007).

3

The Ross of Mull Granite

3.1 Introduction

The Ross of Mull Granite is an igneous complex consisting of a series of late Caledonian, syntectonic and post-tectonic, plutonic bodies ranging in composition from granite through granodiorite to microdiorite and diorite (Zaniewski, Reavy et al. 2006). For ease, the term **ROMG** is proposed for use when referring to the intrusive igneous complex as a whole. The complex lies at the extreme south-western edge of the Isle of Mull, western Scotland, and occupies the largest area of the pre-Tertiary inlier found on the Ross of Mull peninsula. The pluton has long been of interest to geologists, owing much to the fact that there is excellent exposure all along the coast of the promontory, and the granite has been extensively quarried.

Evidence of magma-mixing at depth is ubiquitous and well exposed along the south-western margin of the peninsula, especially on bare wave-washed coastal rock in the Sound of Erraid (Rock and Hunter 1987; Piper 1998; Zaniewski, Reavy et al. 2006). A range of magma-mixing textures, from simple mingling through to thorough mixing between the granite and diorite end-members, is well displayed. Titanite is also present in abundance within all of the facies of the complex. These two facts combined make the ROMG an ideal area for the study of titanite's potential to preserve a record of magma-mixing at the mesozone level.

This chapter will review the extent of research into the ROMG, both historical and modern. The evidence for magma-mixing at depth will be explored in detail. Fieldwork undertaken and sampling methods will be outlined with subsequent rock descriptions and petrographical work. The bulk of the chapter will deal with the characterisation of the chemical zoning of titanite observed using Backscattered Electron analysis (BSE) on a Scanning Electron Micrsocope (SEM), this textural characterisation will then be interpreted in relation to the process of magma-mixing at depth

3.2 Previous work

Macculloch gave the very first account of the geology of the area with a published map in 1819, and commented briefly on the character and relationship of the granite in relation to the country rocks, paying particular attention to the presence of Moine xenoliths therein (Cunningham-Craig 1911; Bailey 1925). Judd and Goodchild both published short papers (in 1874 and 1892, respectively) dealing with the granite-country rock relationships, espousing the views that age of the granite was later than that of the "primary strata"(Moine lithologies) but earlier that the "secondary" (Mesozoic) and Tertiary rocks, placing the age of the pluton as later Palaeozoic (Cunningham-Craig 1911; Bailey 1925). Cunningham-Craig's classic Geological Survey Memoir for the 1 inch map, sheet 35, (1911) gave the first thorough account of the geology of the Ross of Mull igneous complex (ROMIC) Similarly, Bailey and Anderson's (1925) Geology of Staffa, Iona, & Western Mull (description of Sheet 43), is a classic memoir of the Geological Survey that contains a description of the ROMG and its relation to the country rocks. It would be close to fifty years before any further significant research was carried out on the area.

Halliday et al (1979) have performed radiometric dating on the ROMIC using the Rb-Sr and U-Pb isotopic systems, giving an age of 414 ± 3 Ma for the complex.. The current British Geological Survey map of the area, Sheet 43S, was compiled by Harris and Highton using various maps from unpublished sources (Zaniewski, Reavy et al. 2006). Rock and Hunter (1987) discuss the spatial and temporal links between the late-Caledonian dyke swarms and the pluton, paying particular attention to the lamprophyric minor intrusions.

As part of the Geological Conservation Review series (GCR), Highton (2001) provides a thorough account of the form and nature of the eastern contact of the pluton with the Moine country rocks found along the Ardalanish peninsula. The same publication contains an account of the Knockvologan to Eilean A'Chalmain GCR site which focuses on the magma-mixing phenomena displayed within the central part of pluton, and with which the content of this chapter is primarily concerned Other research related to the mixing of magmas has been carried out by Petford, et al. (1996) and Pugliese and Petford (2001), where they attempt to model the mechanisms by which microdioritic enclaves become infiltrated by granitic material, producing a net-veined texture in many of the hybrid rocks found in the pluton.

The most up to date and comprehensive account of the field relationships and emplacement of the ROMG has been given by Zaniewski, Reavy et al. (2006). The paper is the result of work carried out for a PhD thesis by Zaniewski (2006) and stems from detailed re-mapping of the entire area. The result has been a reclassification of the all the components of the pluton along with a proposed model of emplacement within the given regional tectonic framework.

3.3 Regional geology and context

The Isle of Mull, (see Figure 8 below) located off the western coast of Scotland is famed for its igneous Tertiary geology. The island is dominated by the exposed, central subvolcanic complex and its extensive plateau lavas which it intrudes. The Tertiary rocks lie on a basement of older lithologies which include metasediments of Moine and Dalradian age, as well as younger sedimentary rocks of Late Paleozoic and Mesozoic age (Cunningham-Craig 1911; Bailey 1925; Preston, Bell et al. 1998; Bluck 2001; Zaniewski, Reavy et al. 2006).
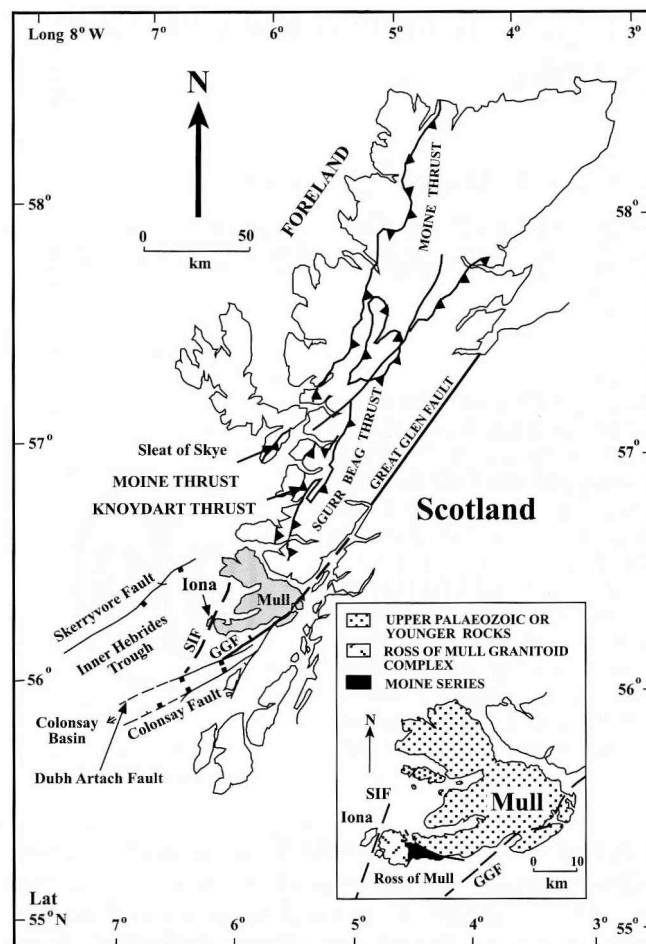
Figure 8: Location map for Isle of Mull and Ross of Mull. From Zaniewski, Reavy et al. (2006).

3.3.1 Ross of Mull and Iona pre-Tertiary inlier

The Ross of Mull and Iona pre-Tertiary inlier is separated to the east from the rocks of the Palaoecene age plateau lavas and the Mull igneous central complex by the NW trending Assapol Fault (see Figure 9 below).
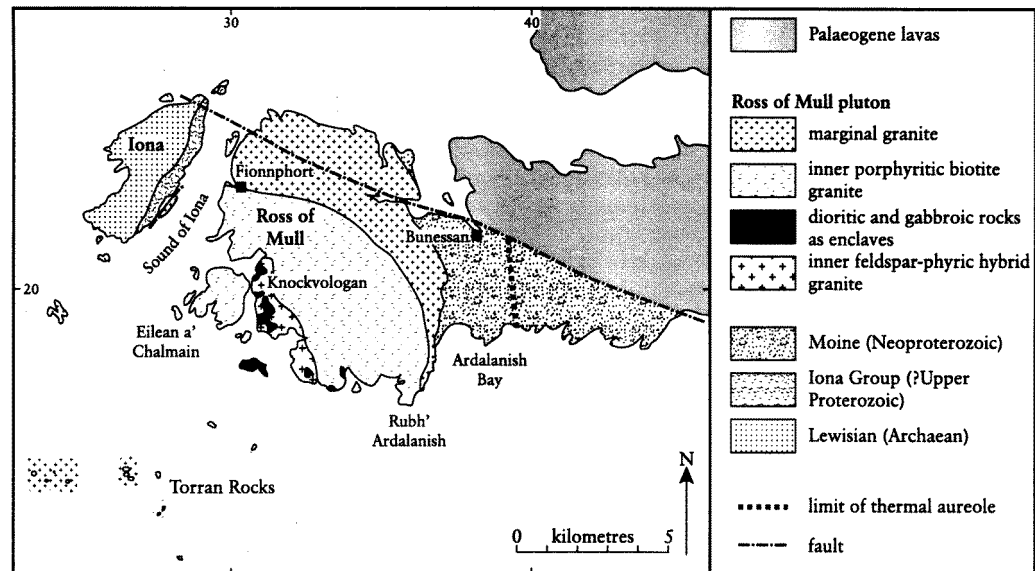
Figure 9: Geological map of Ross of Mull Pre-Tertiary Inlier. From Highton (2001).

The inlier itself is comprised of the late Caledonian age ROMG which is mostly hosted by metasedimentary rocks of the Moine Supergroup, namely the Assapol and Shiaba groups, which are thought to the be equivalents of the Glenfinnan and Morar groups (respectively) of the mainland Moine succession; (Holdsworth, Harris et al. 1987; Highton 2001; Zaniewski, Reavy et al. 2006). The lithostratigraphy and structural geology of the Ross of Mull Moine rocks have been described by Holdsworth, Harris et al. (1987).

The western margin of the inlier comprises the Island of Iona and is made up of the Iona Group (thought to be Torridonian age metasediments) which lie unconformably, albeit tectonically modified, on the older, late Archean, Lewisian gneisses (Bailey 1925; Potts, Hunter et al. 1995; Highton 2001; Zaniewski, Reavy et al. 2006)

3.3.2 Structural geology and emplacement

Caledonian age granitoid plutons have been recently studied by Jacques & Reavy (1994)and Reavy (2001)with a view to determining the relationship between the siting, ascent and subsequent emplacement of the plutons, and the possible controls exerted on these by major tectonic structures.

Two of Scotland's largest faults are thought to intersect some 30km to the SSW of the Ross of Mull (see Figure for structural features). Work carried out by Potts, Hunter et al. (1995) and Zanieweski, Reavy et al.(2006), suggest that it is the intersection of the Dubh Artach Fault (a splay of the Great Glen Fault) and the Sound of Iona Fault (a structure related to, or replacing the Moine Thrust), which may be the cause of the siting and ascent of the magmas that have formed the ROMG. Zaniewski, Reavy et al. (2006) envisage that "the ROMG was constructed from pulses magma rising in the conduit provided by the fault intersection....magma passing up this ascent zone was then emplaced north-eastward as flattish sheets in the late-orogenic extensional environment produced by the collapse of Scandian nappes". Figure 10, below, is a block diagram from Zaniewski, Reavy et al. (2006), illustrating the proposed emplacement geometry of the ROMG pluton.
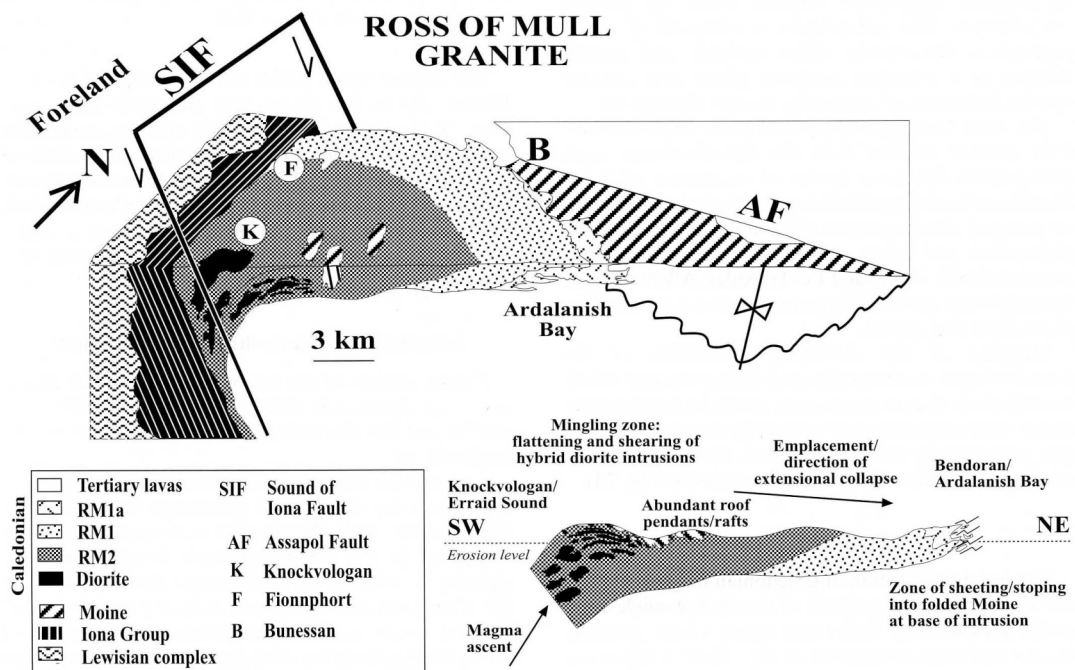
Figure 10: Block diagram depiction of ROMG pluton emplacement, as proposed by Zaniewski and Reavy. Diagram from Zaniewski et al (2006)

3.3.3 Field relationships of the ROMG and country rocks

The western end of the Ross of Mull peninsula is where the onshore portion of the ROMG outcrops, covering an area nearly 80 km², however, the complex extends offshore, forming skerries along the eastern shore of Iona and even extends to the Torran Rocks; occupying an estimated total area of close to 140 km² (Cunningham-Craig 1911; Bailey 1925; Highton 2001; Zaniewski, Reavy et al. 2006)

The western portion of the complex is in contact with the Iona Group metasediments, thought to be Torridonian in age (Highton, 2001). The contacts are visible on the skerries

of Eilean Carrach and Sgeir Ruadh [277 224] just off the east coast of Iona (Cunningham-Craig et al. 1911; Zaniewski et al 2006).

The eastern margin of the complex is in contact with Moine Supergroup metasediments (the Shiaba and Assapol groups) and essentially represents the base of the ROMG intrusion with a stoped floor zone which in places grades into a gently inclined sheeted complex of granite inter-fingering with the country rocks (Highton, 2001). Where the country rocks are psammitic, the contact zone is gradational from in-situ country rocks sheeted with granite, to granite containing many rafts of minimally digested psammites, to the ubiquitous presence of partially oriented, tabular xenoliths found some tens of metres into the granite envelope (Highton 2001). Where the country rocks are more pelitic in character, instances of anatexis occur whereby the complete digestion of suitable country rock has created a zone of contact migmatites as well as contributing to a band of leucocratic granite (RM1a of Zaniewki) thought to entirely represent melted Moine protolith (Highton 2001; Zaniewski et al 2006).

The present level of erosion of the complex is thought to have preserved, in places, the actual roof of the intrusion, as many workers have noted the presence of many large xenoliths which contain tectonic structures and fabrics that correspond well with the country rocks -essentially preserving a "ghost stratigraphy" which is coherent with the adjacent Moine lithologies (Highton, 2001; Zaniewski 2006; Holdsworth 1987).

The thermal metamorphic aureole of the ROMG extends up to 3km away from the contact of the eastern margin. However, significant alteration of the Moine rocks to a high metamorphic grade is first found 500m from the contact, where the baked Moine rocks are found to contain andalusite. Closer to the contact, sillimanite and cordierite can be found (Bailey and Anderson 1925, Highton 2001).

3.4 The pluton

The ROMG pluton, although mainly granitic, is highly heterogeneous in character with most recent workers recognizing at least three distinct facies of granitoid in addition to a synplutonic diorite component and hybrid variants thereof (Cunningham-Craig, 1911; Bailey et al. 1925; Harris & Highton 1999; Highton 2001; Zaniewski et al 2006).

Overall, the pluton displays a very crude reverse zonation, (diorites in the centre more evolved granitoids towards the rim.) and is centred offshore to the southwest of the

peninsula. It is broadly elliptical in shape with the long axis trending NE to SW. Based on a gravity survey, Beckinsale and Obradovich (1973) interpret the pluton as being a wedge-shaped sheet in 3D, with a maximum thickness of 3.5 km and a general dip of 30° to the west for the wedge bottom (Pugliese 2001).

There is gradation between the contacts of the granitoids that make up the facies, and some of the facies themselves are significantly heterogeneous. Due to the synplutonic nature of the different intrusive bodies (granitoids and diorites) that comprise the pluton, extensive mingling and mixing phenomena is ubiquitous

3.4.1 Granitoids

The granitoids are readily distinguished in the field on the basis of variations in biotite content, the presence or lack of alkali feldspar megacrysts, and the concentration of mafic enclaves. Highton (2001) describes the granitoids as having a potassium-rich, calc-alkaline affinity; being mostly metaluminous to weakly peraluminous, and with compositions of the silica content ranging from 67-68%. Pugliese and Petford (2001) refer to the granitoids as being monzogranite and subdivide the facies based on texture and minor differences in mineralogy

Work done by Zaniewski et al (2006) uses a classification scheme (albeit with some minor differences) which is similar to that of the British Geological Survey , Ross of Mull (43S) Sheet, compiled by Harris and Highton (1999) and is the classification used herein (see Figure 11 for Zaniewski et al's (2006) map as published in the Scottish Journal of Geology).

3.4.1.1 RM1: equigranular biotite monzogranite

This rock forms the outer facies of the complex and equates to G_{RM1} on the BGS Sheet 43S. It is an equigranular (0.3-10mm), quartz-rich, biotite granite. Petrography shows that biotite and plagioclase are subhedral, the quartz is interstitial, and the alkali feldspar is often poikilitic and perthitic. Zaniewski et al (2006) state that the plagioclase is not readily distinguishable in the field due to it's reddened appearance, and thus field petrography alone can suggest the facies is modally an alkali feldspar granite. Thin section petrography reveals the plagioclase component to be roughly 25-30% of the felsic minerals. Euhedral hornblende is rare and the main accessory phases are titanite and allanite.

FORELAND SEQUENCE

Iona Group
Lewisian Complex

MOINE SUPERGROUP

Assapol Group
Shiaba Group

ROCKS OF THE MULL IGNEOUS
COMPLEX (PALAEOCENE)

Tertiary lavas cut
by dolerite intrusions

ROCKS OF THE CALEDONIAN
ROSS OF MULL GRANITE

RM1: Equigranular biotite granite

**RM1a: Leucocratic marginal
muscovite-biotite granite**

**RM2: Alkali feldspar-megacrystic
granite/granodiorite**

Diorite

Symbols

— ┼ —   Fault, crossmark on downthrow side

**Figure 11: Geological map of the Ross of Mull Granite (from Zaniewski et al.
2006).**

3.4.1.2 RM1a: leucocratic muscovite-biotite granite

This is essentially a two mica contaminated variant of the RM1 facies, produced from local interaction with the Moine lithologies of the pluton's envelope. Essentially a contact facies, up to 800m wide, it is found at the western margin of the pluton (Zaniewski, Reavy et al. 2006). This is equivalent to G_{RM1a} on BGS Sheet 43S. It is an equigranular rock with equal proportions of plagioclase and white perthitic microcline, and contains more quartz that RM1 (up to 30%). Biotite is abundant and of a dark red colour, containing many inclusions of zircon and apatite, and often occurs in clusters with muscovite. (Zaniewski, Reavy et al.

2006). Where Moine xenoliths are present in other parts of the pluton a similar white granitoid is often locally developed around their margins.

3.4.1.3 RM2: alkali feldspar-phyric granite/granodiorite

Over roughly 1km, RM1 grades into RM2 which occupies the central portion of the complex. RM2 is equivalent to both G_{RM2} G_{RM3} on BGS Sheet 43S, although G_{RM3} is now not recognized as an independent facies (Zaniewski, Reavy et al. 2006). It contains more plagioclase and biotite than RM1 and also less quartz, while hornblende is rare. The facies is readily identifiable by the presence of alkali feldspar megacrysts (orthoclase perthite) which range from 8-15 mm in size. According to Zaniewki *et al*. (2006), biotite is dispersed throughout the rock. It occurs as aggregates with Fe-Ti oxides and is occasionally seen to replace primary hornblende. Thin section work shows the presence of both acicular, euhedral as well as anhedral apatite. Other accessory minerals include: ilmentite, rutile, magnetite, zircon (often found as inclusions in biotites). Titanite is often euhedral, sphenoid in shape and ranges in size from 0.5 to 2.5 mm.

3.4.2 Diorites

Within the RM2 facies in the very central portion of the ROMG are a complex suite of dioritic and microdioritc bodies, of various sizes, the largest discreet diorites being up to 250m in width. These diorites outcrop in the western and southern portion of the Ross of Mull as well as on the Torran rocks offshore to the southwest (see Figure 9, Figure 11, and Figure 12 for location of diorite bodies within the ROMG).
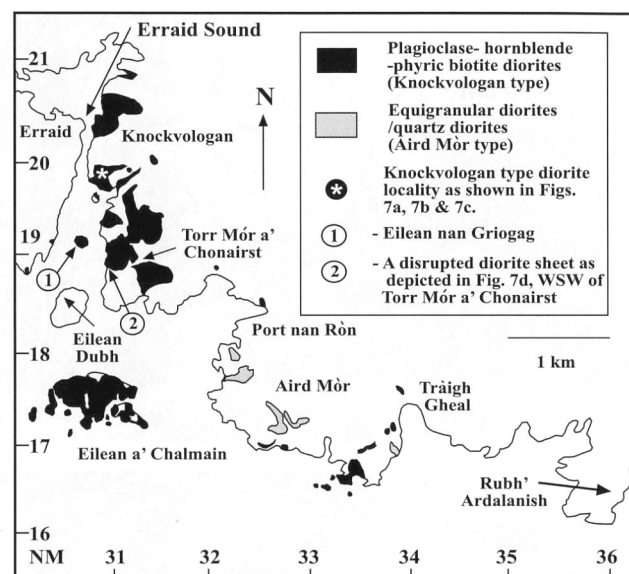
Figure 12: Location of diorite bodies within the ROMG. (from Zaniewski et el 2006)

The diorite bodies display evidence of magma mixing with the host granitoids, with the largest bodies interpreted as representing sites of injection of diorite into partially crystallized host rocks. Synplutonic diorite dykes are observed near to these sites, and smaller bodies of diorite, which have spalled or pillowed off of the intrusions, can be seen dispersed within the feldspar-phyric granite of RM2 as microgranular mafic enclaves (**MME**) The evidence of acid-basic interaction is ubiquitous, displaying a great amount of petrological variety of both MME and host granitoids. These rock types will be dealt with in detail as they form an important part of this investigation into the ability of titanite to preserve a record of magma-mixing at depth.

Coastal exposure of the facies is excellent, especially along the east coast of the Sound of Erraid and on the tidal island within the sound, Eilean nan Griogag, and the small skerries to its south. Zaniewski (2006) reports that the islands of Eilean Dubh, and Eilean a'Chalmain also lie within the diorite/hybrid facies. There is debate about the timing of emplacement of the diorites. Pugliese and Petford (2001) claim that the field relations suggest both the equigranular biotite granite (RM1) of the outer facies and the diorite bodies the first magma pulses to be emplaced, and that mechanical and chemical mixing subsequently produced the feldspar-phyric granite (RM2). Zaniewski Reavy *et al.*(2006), postulate that the feldspar-phyric biotite granite (RM2) already existed before the intrusion of synplutonic diorites. They state that the diorites were emplaced into the cooler, partially crystallized RM2 facies, and this represents the last major intrusive phase of the ROMG complex. They also claim that despite there being abundant evidence at the present level for mixing *in situ*, the overall impression is that the diorite hybrids were produced by mixing at depth prior to synplutonic intrusion into their host granitoids.**.**

3.4.3 Enclave types and evidence for magma-mixing processes

Diorite enclaves within the area display a range of textures and mineralogy that reflect the stage of mingling or mixing with the host granitoids. Pugliese and Petford (2001) and Zaniewski, Reavy et al (2006), have described the large diorite bodies in detail; their associated mafic microgranular enclaves, their states of mingling and mixing with the host granitoids, and the resulting hybrid varieties. As the subject of this chapter deals particularly with the titanites found within the mixed-magma rocks of the ROMG, the detailed descriptions of the diorites and associated hybrid rocks, as well as their field relations, will be independent observations.

3.4.3.1 Discrete MMEs

Discreet enclaves are the most common type found. They can be found close to or at a distance from the large diorite bodies and synplutonic dykes; however the former instance is more common. They have discrete margins that are well defined and slightly chilled against the host granitoid. There is little observable interaction with the host and these enclaves represent a state of simple mingling. This type may be further subdivided based on grain size, where there are microdiorite and diorite examples (see Figure 13 below).

Figure 13: Discrete diorite enclave types from the ROMG, foreshore of southern end of Eilean nan Griogag, Erraid Sound. Head of hammer is ~17cm

3.4.3.2 Partially digested MMEs

These enclaves are ubiquitous, but tend to occur at a further distance from the larger diorite bodies, or are associated with swarms of diorite enclaves that have apparently spalled or pillowed off the larger diorite bodies or feeder dykes. The defining feature of this enclave type is the advanced stage of mingling with the host granitoid, which is often seen to grade into the initial stages of physical and chemical mixing with the host material at their margins (see Figure 14 below).

Figure 14: Partially digested enclave, near foreshore of southern end of Eilean nan Griogag, Erraid Sound. Head of hammer is ~17cm long.

3.4.3.3 Network-veined MMEs

Certain enclaves, whether partially digested or discrete, contain a pervasive network veining of granitic material (see Figure 15 below). These enclaves are often found proximal to pillow-trains of partially digested MMEs, near to the margins of larger diorite bodies whose edges show an advanced stage of mingling/mixing with the host granitoids, producing lithologies of a hybrid nature. It is inferred that the veining must be partly due to the temperature differences between the enclaves and host, such that the granitic material is sufficiently hot enough to infiltrate the enclaves. The degree of crystallinity of the enclaves must similarly play a significant role in the development of this texture. Pugliese and Petford (2001) describe such network-veined MMEs and theorise about the processes leading to their formation.

Figure 15: Network-veined MME from the ROMG. Note the weathering-in of the diorite to show the degree of interconnectedness of the veins.

3.4.3.4 Megacrystic MMEs

These are mafic enclaves, of any of the type described above, that also contain alkali feldspar megacrysts. These megacrysts are the same as those found in the RM2 facies of the ROMG (Zaniewski, Reavy et al. 2006), and may best be described as xenocrysts. These enclaves indicate physical mixing of diorite with the RM2 facies where crystal scavenging has been an important process (see Figure 16).

3.4.3.5 Vesicular MMEs

These enclaves may be of any of the type described above, with the added defining feature being the presence of glomerocrysts of hornblende mantled by both alkali and plagioclase feldspar. The centres of these glomerocrysts often have voids and hence are likely to have formed through the filling of vesicles by a late stage, supra-solidus liquid fraction. Feldspar

xenocrysts are particularly common in the enclave type although not always present. (see Figure 16 below

Figure 16: Vesicular and feldspar megacrystic enclave. Note the rounded dark spots mantled with light coloured material, these are the vesicle; there is a prominent megacryst of feldspar just left of centre.

3.4.4 Minor intrusions

The final episode of Caledonian igneous activity for the ROMG was emplacement of westward dipping, cross-cutting shallow angle sills and dykes, often composite in nature. (Rock and Hunter 1987; Zaniewski, Reavy et al. 2006). Two main types exist: (1) composite porphyritic microgranodiorites and (2) non-composite, porphyritic microdiorites. Zaniewski et al (2006) postulate that the composition and hybrid nature of these minor intrusions reflects, in a general sense, the plutonic components of the ROMG, stating that this shows the continued interaction of acid and basic magmas in the waning stages of emplacement

3.5 Fieldwork

Fieldwork was focused on the excellent exposures found on the coastal areas in the west of the Ross of Mull, especially in and around the Sound of Erraid and the tidal islands immediately to the south, especially Eilean nan Griogag. The wave-washed rocks on the coast provide spectacular access to a huge textural variety of magma mixing phenomena.

3.5.1 Field evidence for magma mixing and sampling

The range of lithologies, from diorite through to feldspar-phyric granite, and the textural suite of hybrid varieties, is extremely diverse, and whilst an extensive account would be ideal, the aim of the project precludes such a necessity. Evidence of the main varieties of

textual relationships between the lithologies represented, and an account of the types of MMEs and hybrid lithologies are deemed sufficient in the context of this study since the focus is on the titanite within the rocks and the record of magma mixing the mineral may preserve.

3.5.1.1 Sample ESd1: synplutonic diorite sheet

Several diorite dykes/sheets (most 1-2 wide) occur in the area, and represent synplutonic intrusions of the most mafic material found in the complex. These are assumed to be similar in composition to the main mafic source of the within the depths of the pluton, and many of the sheets and dykes can be seen in close proximity to, and connected to the larger diorite bodies as well as cross-cutting hybrid rocks and their host granites. This sample is the most mafic of all samples collected and since it is from a synplutonic sheet and not an MME, it is regarded as the mafic end member of the suite of rocks collected from the pluton.

Figure 17: Photo of synplutonic diorite sheet (ESd1) from the Sound of Erraid (grid reference 30912 18910). Sheet is 134cm wide. Photo is west facing.

The above photo shows the microdioritic synplutonic sheet found on the east coast of the Sound of Erraid (grid reference 30912 18910). The sheet is chilled against the country rocks, is 1.34m in width and has an overall dip of 35 degrees and an east-south-east strike. Sample **ESd1** was taken from this sheet.

The groundmass exhibits a weak foliation, especially of the plagioclase laths. The grain size is fine (mostly less than 1 mm), and the main minerals are plagioclase (45%), biotite (25%), hornblende (15 %), orthoclase (5%). The remaining 10 % is composed of accessory

phases and quartz. The quartz occurs as small ocelli (1-2mm) mantled by biotite and hornblende. The titanite crystals are mostly interstitial, with very few euhedral examples. The overall shape of the groundmass crystals are subhedral, with the plagioclase crystals often being the largest and poikilitically enclosing the hornblende and biotite.

3.5.1.2 Sample RM1-granitoid end member

RM1 is the outer facies of the ROMG, an equigranular biotite monzogranite. This facies represents the most evolved rocks of the entire pluton (Zaniewski, Reavy et al. 2006) and is thus considered as the granitic end-member for this study. The sample used was collected by Zaniewski who kindly provided an off-cut.

Thin section analysis shows the rock to consist of 20% plagioclase, 35% alkali feldspar, 25% quartz, 15% biotite crystals. The remaining 5% is composed of euhedral hornblende and titanite, some zircon, apatite and rare opaques. Grain size varies from 0.5mm to 1cm. The titanites are typically euhedral and vary in size from 50μm to 150μm.

3.5.1.3 Sample ES5 -simple mingling

The evidence for a whole range of textures of acid-basic interaction is ubiquitous around the east coast of the Sound of Erraid. The simplest being liquid-liquid interaction, representing the earliest stages of host granite-enclave mingling. Such textural relationships are characterised by sharp contacts, where the margins of rounded to sub-rounded mafic enclaves are slightly chilled against the host granite, or apparently display limited interaction with the host (for an example refer to Figure 13).

These simple mingling textures are mostly found close to mafic synplutonic dykes or massive (over 200m long) diorite bodies within the RM2 granite facies, and are often characterised by large numbers of MMEs of various sizes clustered as swarms. However, simple mingling textures may also be observed in close proximity to areas where granite-enclave textures display more advanced states of mingling.

Sample ES5 was obtained from the rocks exposed on the foreshore roughly 25m southwest of the path leading from Knockvologan farm to Laimhrig nan Draoidhean (30915 19665). The diorite enclave within the sample was round in shape and 14cm wide. The sample displays a fairly sharp contact with the host granite in hand specimen, however, in thin section some inter-fingering of the enclave with the host is obvious, albeit on the scale of < 250 μm (see Figure 18 below). There is a lack of an active zone of mixing between the

host and enclave, and sample ES5 is regarded as a host-enclave texture representative of simple mingling
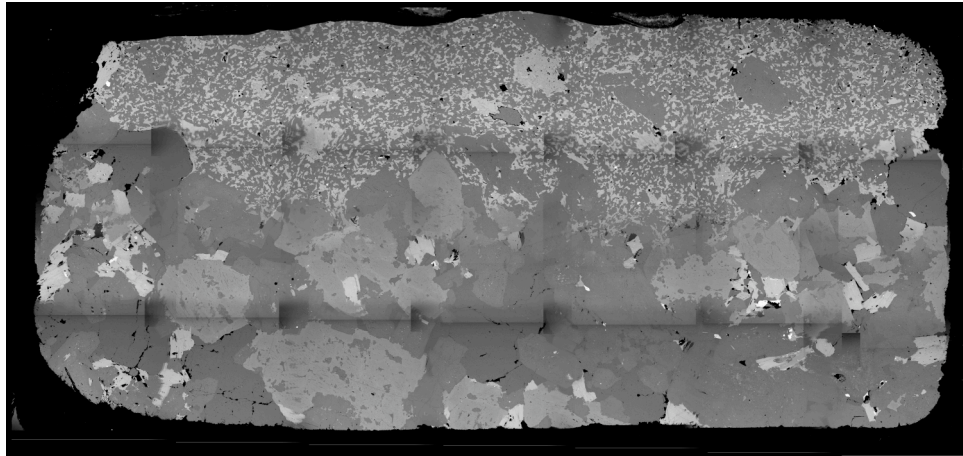
Figure 18: BSE photomicrograph of sample ES5. Sample is just over 2.5cm long. Note the fine-scale inter-fingering between diorite and host.

Thin section work shows that the contact between enclave and granite displays some inter-fingering. This is mostly represented by small biotite, amphibole and feldspar minerals from the enclave growing along the boundaries of the large feldspar crystals in the granite (see above photo). However, this is on a very small scale. In this case, biotite and hornblende dominate, and tend to be slightly finer grained that the groundmass of the enclave.

3.5.1.4 Sample A -active mixing margin

This sample was collected by Dr Tim Dempster from the eastern foreshore of Erraid Sound immediately east of Eilean nan Griogag. The sample displays a state of active mixing between the RM2 granite facies and a vesicular mafic enclave. This mixing zone is up to 1.5cm wide and is characterised by a grain size intermediate between the host granite and dioritic vesicular enclave (average grain size is 0.3cm), as well as the presence off an increased amount of mafic minerals than observed in the granite (see Figure 19).

This sample displays an initial state of active mixing on both a physical and chemical level, as evidenced by the development of a mixing zone of grain size intermediate between the host and enclave. Comparing the textural and chemical aspects of titanite from the mixing zone with those found in the granite and enclave respectively, will be essential to evaluating the record of mixing possibly preserved within the titanite.

Figure 19: Polished section of sample A used for microanalysis. Note the thin zone of mixing between the granite on the right and vesicular diorite enclave on the left. Section is 4 cm long

3.5.1.5 Sample ES3A -mechanical mixing/streaking

There are numerous examples of advanced stages of mechanical mixing between diorite MMEs and the host granite RM2 all around the east side of Erraid Sound. Fine examples can be seen on the wave-washed rocks exposed along the coast immediately east and southeast of Eilean nan Griogag. The textural relationship between the host granite and diorite enclaves is one of liquid-liquid character. The enclaves are stretched and streaked out within the granite, indicating that both the granite and enclaves were hot and lacked a significant viscosity contrast. This allowed a greater degree of physical mixing compared to that of sample ES5 (simple mingling).

A greater degree of physical mixing may allow for increased exchange of minerals (phenocryst scavenging) between the commingled magmas as well as increase the likelihood of bulk chemical exchange and localised homogenisation.

Sample ES3, a large block (30cm long) displaying streaking/mingling of granite and microdiorite, was obtained from the foreshore of Erraid Sound, just southwest of Eilean nan Griogag, (30921 18864). The locality is just 15m south of the synplutonic dyke from which sample ESd1 was obtained. The area is dominated by a large diorite body (over 10m long) that is highly disrupted and invaded by the RM2 granite. The margin of the large diorite body is where the most notable evidence for mechanical mixing and streaking is found.

The enclaves, mostly lenticular in shape, range in size from several meters in length to as small as 10cm. The smaller enclaves often have wispy margins and interfinger with the granite on a centimetre scale. The large enclaves have more cuspate margins. The overall orientation of the streaking is similar to that of the synplutonic dyke, with a dip of roughly 25-35 degrees in an east-south-east direction. The enclaves contain feldspar xenocrysts and vesicles filled with hornblende, indicating they are likely the product of a previous episode of mixing between the RM2 facies and diorite at depth.

Figure 20: ES3A sample location photograph. Note the degree of streaking between granite and diorite. GPS is 12cm long Photo is facing due east with a grid reference of (30921 18864).

3.5.1.6 Sample ES16-diorite/RM2 hybrid

Where commingled diorite and granite magmas have experienced a huge amount of mechanical mixing, a state is reached where the resultant rock may be considered to be of a hybrid nature. Hybridization is a process which depends primarily upon two very important factors: the stage of crystallization of the host; and the relative volumes of the two liquids (Sparks and Marshall 1986; Pugliese 2001). As noted by Pitcher (1993), one cannot expect mixing to occur between a granitic crystal mush and mafic enclaves unless there is a sufficient quantity of mafic material and heat provided to reverse the process of crystallization.

The input of mafic magma, via synplutonic dykes, into the granite has been significant in terms of both volume and heat, resulting in a spectrum of petrological variety that

encompasses mingling through mixing to hybridization. It is clear that some of the diorite bodies have experienced mixing at depth prior to high level emplacement, as evidenced by the scavenging of alkali feldspar megacrysts from the RM2 facies. These xenocrystic diorite enclaves also sometimes contain more mafic microgranular enclaves, and are referred to as double enclaves.
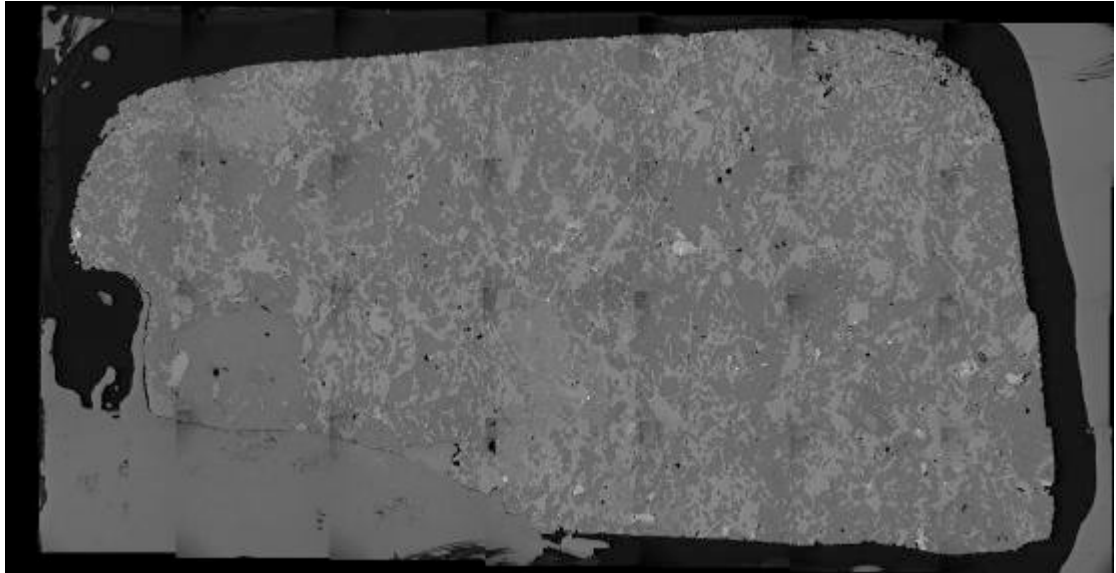
Figure 21 BSE map of ES16, hybridised rock, from the ROMG; section in 4cm long.

Field evidence shows that double enclaves and enclaves rich in alkali feldspar xenocrysts are often juxtaposed with, or grade into, enclaves containing granitic veining. Alternatively, where mechanical mixing with the host has been significant, enclaves may grade into hybrid rocks, intermediate in grain size and colour between the RM2 facies and diorite MMEs. An area displaying such field relationships is found on the southern part of Eilean nan Griogag, Erraid Sound. Sample ES16 (a hybrid rock fragment 17 cm long) was collected from this locality at (30642 19135).

The density of enclaves in the southern portion of this tidal island is significantly higher than 50% and it is clear that immediately to the south of this island there is a large body of diorite which is possibly a point of source or point of emplacement of the diorite. The concentration of diorite emplaced in the granite would have provided sufficient heat to allow for mixing and hybridization to occur.

Thin section work reveals a texture that hints at mechanical mixing, with localised flow and swirl textures on the cm scale. The range of crystal sizes reflects both the diorite enclave and the granite. There are large alkali feldspars that are partially resorbed. The matrix is dominated by hornblende crystals (25%), biotite (20%), both of which vary in

size from 1mm to 5mm and can be seen to form glomerocrysts. Plagioclase (20%) and alkali feldspar (20%) range in size from 2 to 10mm and can be seen to poikilitcally enclose smaller biotites and amphiboles (1mm and less). Roughly 10 % is quartz, which is always interstitial with few inclusions. The remaining 5 % is accessory minerals, including apatite, zircon, titanite and Fe Ti oxides. The titanite s crystals are mostly interstitial and subhedral to anhedral.

3.5.1.7 Sample ROM1-vesicular mafic enclave

Dioritic enclaves of this type are conspicuous due to the presence of micropegmatitic amphibole rich clots. They are found only around the Knockvologan area of the ROMG, and have no discernable preferred distribution with respect to other enclave types or host/enclave associations. Enclaves of this type have also been found to contain alkali feldspar xenocrysts and/or granitic veining. The matrix of the enclaves is composed primarily of equigranular amphibole + plagioclase + biotite + small amounts of orthoclase, quartz and accessories such as titanite, and apatite.

A   **B**
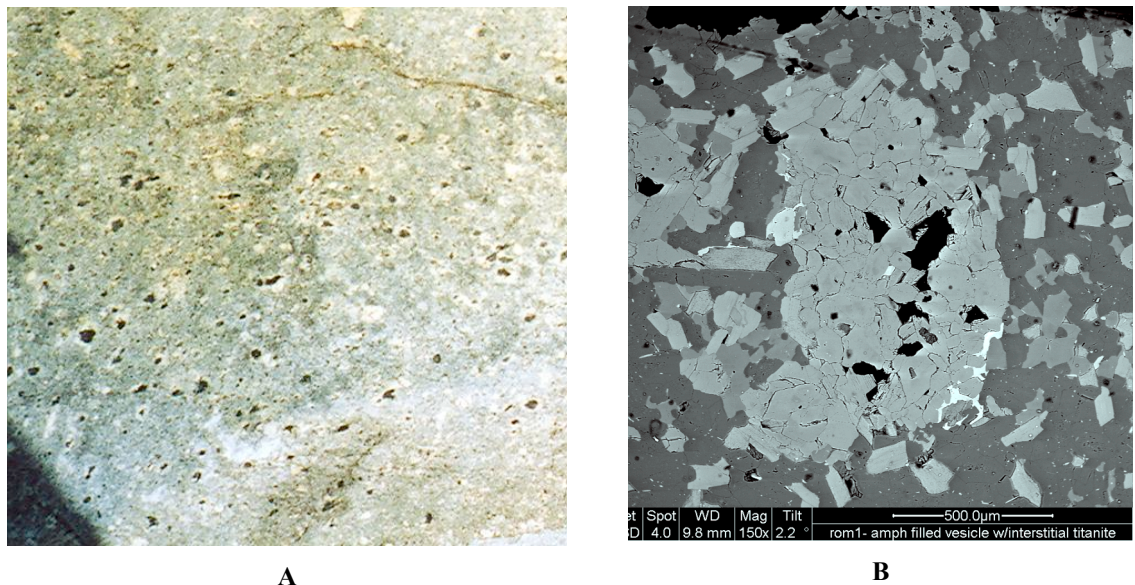
Figure 22: Photos of ROM1, a vesicular diorite MME. A. Sample location of ROM1, Erraid Sound, Ross of Mull; note the small, round black clots of amphibole surrounded by creamy white feldspar. The field of view is 50cm wide. B. BSE image of one of the clots from sample ROM1; note the black voids in the middle (indicating a vesicle origin) and the bright interstitial titanite near the bottom right margin. Scale bar is 0.5cm long.

The majority of such enclaves are medium to fine grained and are best described as microdioritic. The clots range in size from 3 to 10mm and are best described as glomerocrysts of hornblende mantled by highly altered alkali feldspar. The hornblende crystals are euhedral to subhedral, and sometimes have inclusions of euhedral titanite. Titanite may also be found as part of the glomerocrysts and not as inclusions within the

hornblende. The centres of the glomerocrysts sometimes contain a pore space or void, up to 3mm in some clots. This is taken as possible evidence that these micropegmatitic clots may have resulted from the filling of vesicles. See Figure 22, above, for images of ROM1 and amphibole clots.

Work carried out at the University of Glasgow by Nick Shaw (2003), shows that the Fe-oxide and Al-oxide compositional variations of matrix versus clot titanites suggests that they grew in separate environments. This would suggest that they did not form by mutual adhesion of like crystals in a melt, as normal glomerocrysts do. He also shows CL and BSE evidence of zoning within titanites and apatites in the clots that suggest they grew in situ, and therefore can be discounted as having originated as xenolithic material. Shaw's chemical analysis of the amphibole in the clots shows no variation between those at the margins of the clots and those at the centre, suggesting that they did not originate from additional growth on restite, as is the model suggested for the origin of amphibole clots in the Strontian Granite by Stephens (2001)

The sample (ROM1) was collected by Tim Dempster from Erraid Sound.

3.5.1.8 M2 net-veined enclave

In some cases there is a pervasive veining of the microdioritic enclaves by granitic material. These net-veined enclaves are very conspicuous in the field as the leucocratic, pink or milky coloured veining not only stands from the melanocrantic groundmass of the enclaves, in terms of colour, but also is more resistant to weathering and on wave-washed rock surfaces can be seen weathering out from the enclaves (see Figure 15).

Pugliese and Petford (2001)and Petford et al (1996) have written about the possible modes of formation of these net-veined microdiorites, citing melt-infiltration and advection as major processes. They infer that selective partial fusion of granitic magma, brought about by the superheat of the mafic enclaves, has been mechanically incorporated into the microdioritic. They state that as melting of the granitic material ensued, a monzonitic melt formed and exfiltrated from the surrounding microdioritc magma resulting the viscous inter-fingering

The presence of network veining in the enclaves does not seem to follow any discernable pattern with respect to other enclave types mentioned, however, veining seems to be most prevalent where there is an advanced stage of mingling and mixing between the host granite and the diorite enclaves. Veining is also well developed where there are large

swarms of the enclaves, possibly indicating the importance of heat provided by the mafic magma in their formation.

The veining has decussate, as well as radiating and dendritic, geometries, the main feature being their interconnection in three dimensions. These polyhedral veins vary in size from 1 to 5mm wide (Petford, Paterson et al. 1996). The veins are predominantly made up of monzonitic to monzodioritic material (70% albite-oligooclase, 30% orthoclase, with varying amounts of granophyric intergrowths and hornblende). The groundmass of the diorite that is in contact with the veins is often finer grained than the matrix hosting the veins. The matrix also contains alkali feldspar xenocrysts which have embayed margins, in addition to the glomerocrysts of hornblende which are characteristic of the vesicular enclave type.

The veins also occasionally contain titanites. These titanites are usually anhedral to subhedral in shape, contain numerous inclusions of Fe Ti oxides, apatite and zircon, and can be as large as 300 microns. As with all microdioritic enclaves in the ROMG, titanite can be found within the groundmass. The presence of titanites within both the groundmass and vein networks will allow comparison of the chemistry unique to late stage granitic fluids with the chemistry of MME titanites.

3.6 Sample selection

Selection of samples was based around a simple principle: to have as complete a spectrum of the lithologies represented in the ROMG. In addition to this, it was vital to include samples where there was evidence of acid-basic interaction, in order to analyse the behaviour of titanites at interface of interacting magmas.

3.6.1 Sample preparation

Samples were prepared as thin sections suitable for analysis on an SEM and on an electron-microprobe analyser (EMPA). As such, the samples were restricted to the upper limit of the size suitable for loading into an EMPA cartridge: 4.7cm by 2.5cm.

Specimens were cut and mounted as standard polished thin sections on 3100μm-thick fused quartz using araldite epoxy and subsequently ground down to a thickness of 30μm. The samples were polished to the highest degree possible using colloidal silica as the final polishing medium, with the finished polish being suitable for SEM and EMPA analyses.

As such, the samples were suitable for petrographic analysis using a transmitted light polarising microscope. For SEM and EMPA analyses, the samples were carbon coated and mounted on stubs using silver DAG to ensure contact between stubs and sample in order to prevent electric charging of the sample during analysis.

3.6.2 Transmitted-light petrography

Each sample was primarily analysed by method of transmitted-light petrography. This allowed characterisation of the textures and mineralogy of the rocks and identification of which samples had suitable titanite.

3.6.3 Scanning-electron microscopy

The principle tool used in this study was the scanning-electron microscope. This device employs an electron optical column in which a very finely focused beam of electrons is scanned over a small area of the specimen. When the primary electron beam reaches the sample and dwells at any given spot for a few milliseconds, interactions occur inside the sample as the incidents electrons lose energy due to repeated scattering and absorption within a semi-circular shaped volume of the sample known as the interaction volume.

The size of this interaction volume is dependant on the mean atomic number of the specimen, the density of the specimen and on the accelerating voltage of the electron beam. The interaction and energy exchange between the electron beam and the sample produces an emission of electromagnetic radiation and electrons, which can be detected and electronically interpreted to produce different images that convey information about the sample such as: topography, morphology, composition and crystallography. The main types of electromagnetic radiation and electron phenomena emitted when the incident beam strike the sample are illustrated by the diagram below:
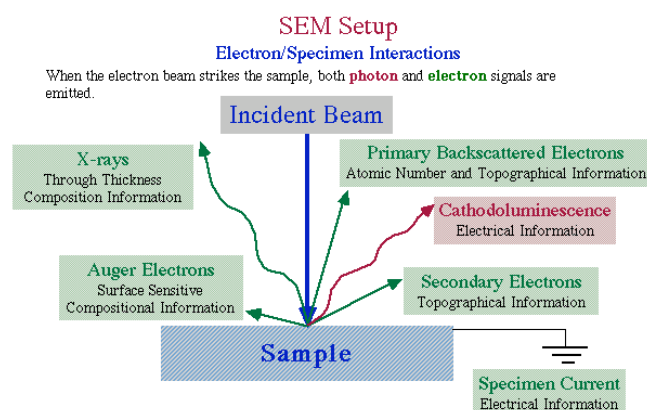
Figure 23: Schematic of SEM setup and electron/specimen interaction...

3.6.3.1 Secondary electron imaging (SEI)

There are several imaging modes that use specific emission phenomena to convey information about the sample. The most common imaging uses the emission of secondary electrons. As the incident electrons enter the sample, they may pass near enough to some of the atoms to impart some of their energy to lower-energy electrons within the atoms, essentially ionizing them. These ionized electrons can then leave the atom as secondary electrons. Due to the low energy (about 5 eV), that accompanies these secondary electrons, it is only those that are very near the surface of the sample that have enough energy to exit the specimen as secondary electrons. Differences in the angle between the incident electron beam and the sample surface (due to sample topography) will cause differing intensities in emission of secondary electrons. The differences in emissions can be electronically detected and enhanced with a scintillator-photomultiplier (Everhart-Thornley detector) and converted into well defined three-dimensional images.

3.6.3.2 Energy dispersive X-ray analysis (EDX)

A by-product of the emission of secondary electrons is the emission of X-rays. This occurs because high-energy electrons from outer valancy shells will fall to lower valancy shells where emitted secondary electrons have left a vacancy. The energy difference between the higher energy electron and the lower energy valancy shell it falls to occupy is balanced by the emission of X-rays. The X-rays emitted are unique to the element that they emanate from and can be spectrally analysed with an energy-dispersive X-ray detector system (EDX). The information derived from X-rays is that of a compositional nature.

3.6.3.3 Backscattered-electron imaging (BSE)

The main type of imaging used in this study relies on the detection of backscattered electrons. These are high energy electrons from the incident beam that are elastically reflected/scattered back from the interaction volume of the specimen. This scattering is caused due to the difference in polarity between the electrons of the incident beam and the protons in the nuclei of the sample; hence, the higher the mean atomic number of the sample, the higher the number of backscattered electrons. These are measured with backscatter electron detectors and an image is formed that that correlates in brightness with mean atomic number; areas of the sample higher in mean atomic number will show up as brighter areas in the image.

This is very useful when searching for rare, and usually small, accessory minerals that contain heavy elements, such as titanite. Titanite contains on average 28wt% Ti-oxide, as

well as a significant amount of rare-earth elements and HFSE and trace elements that contribute towards a high mean atomic mass when compared to the major rock-forming silicates. When viewed in backscattered electrons (BSE) the titanite crystals are significantly brighter than the majority of the minerals found in the rocks in this study (see Figure 24). If the contrast of the image is increased and the brightness is decreased to the point where the majority of the rock forming-minerals are shades of dark grey, the titanites will appear as bright spots in the groundmass. There are other minerals that have similarly bright BSE signatures (Fe/Ti oxides, zircon, monazite, apatite, to name a few) but crystal shape, texture and spot analysis using EDX, are sufficient tools to be able to distinguish them from titanite.

More important than simply picking out the titanites due to their brightness, BSE imaging can reveal the chemical zoning of the titanite crystals. Zoning is developed during the process of crystallisation, whereby due to fluctuating physico-chemical conditions of the magma there occurs a preferential uptake of chemical species by the mineral
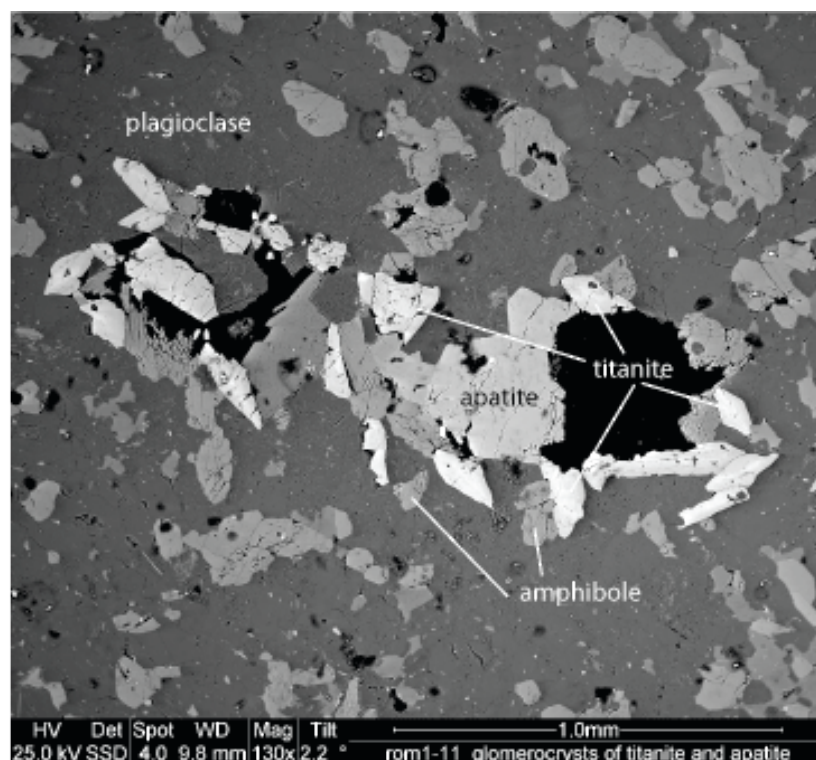
Figure 24: BSE image illustrating brightness/contrast of minerals (in sample ROM1) based on their mean atomic weight. Titanite is very bright and easy to find when viewing in BSE due to its brightness and distinct wedge shape.
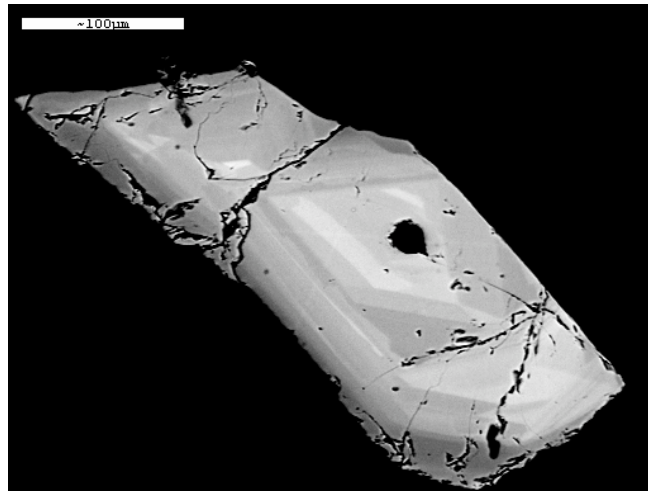
Figure 25: BSE image of compositional zoning in titanite ES5-15. Brightness is a function of mean atomic weight and brighter zones in titanite will have a higher concentration of trace elements which are heavy, such as Fe, the REE, and the HFSE.

The majority of zoning observed in titanite in BSE imaging is due to differing concentrations of heavy elements, such as Fe, the REE and certain trace elements, which can isomorphically substitute into the titanite lattice in place of Ca, Ti and rarely, Si. See Figure 25 for a BSE image of titanite displaying compositional zoning as a function of mean atomic weight

3.6.3.4 SEM specifications

The SEM used in this study was an FEI Quanta 200F Environmental SEM fitted with a Schottky field-emission source gun that enables this microscope to acquire very high-resolution (<2 nm) secondary and backscattered electron images. Individual images can be stored digitally, at resolutions of 512 x 442 to 3584 x 3094 pixels. It is equipped with an array of electron and X-ray detectors that enable comprehensive characterisation of chemical, microstructural, crystallographic and morphological properties of minerals.

Figure 26: Photo of FEI Quanta 200F environmental SEM. A. SEM set-up at the Department of Geographical and Earth Sciences, University of Glasgow. B. Sample chamber and detectors on the FEI Quanta.

For X-ray microanalysis, the Quanta is equipped with an EDAX Pegasus 2000 Energy Dispersive X-ray microanalysis (EDX) system, which can be used to obtain quantitative or qualitative spot analyses and quantitative or qualitative elemental maps and line-scans. It also has a number of secondary electron detectors for high-resolution topographic imaging and a backscattered electron detector for high-resolution atomic number contrast imaging.

3.6.3.5 SEM operating conditions

The SEM is designed to operate under variety of conditions to allow for the best possible imaging and data gathering. Different materials will respond better under different operating conditions. Also, different operating conditions are more desirable depending on the on the aims of the user. For example, if you require high resolution, images or good depth of field you may want to have a small spot size, whereas for collection of X-rays for EDX your main concern would be a higher accelerating voltage to maximise sample excitation and X-ray emission, and a larger spot size to cover a larger area.

The main variables all affect the incident electron beam by focusing the beam, condensing the beam or by or altering the beam current or accelerating voltage. The main variable are: spot size, aperture, accelerating voltage, and beam current.

This study required high resolution imaging of the titanite crystals and their environment of crystallisation, hence spot size and aperture were important. However, to achieve good images of the chemical zoning in the titanites, the samples required a significant amount of excitation (i.e.: sufficient accelerating voltage) in order to maximise the backscatter of electrons and thus produce the best imaging possible with respect to differences in mean atomic number. Therefore the most important variables in this study were spot size, aperture and accelerating voltage.

The set of operating conditions found to best reveal the chemical zoning of titanite are as follows:

- Spot size: 3 - 4 microns

- Aperture: 3 (sometimes 4) on FEI Quanta 200F

- Accelerating voltage: 20 -25 kV

It is worth noting that by varying the conditions above slightly the zoning visible in BSE could be improved, but for most samples the best results were obtained with spot size 4, aperture 3 and kV of 25. The FEI Quanta 200F also has very good capabilities of altering the brightness and contract of BSE images. Zoning in titanite is best revealed by lowering the brightness more than raising the contrast, however, it is always useful to "play" with these variables to achieve the best image possible.

3.7 Textural characterisation and process identification

Identification of petrogenetic processes, or indeed of specific events associated with the interaction of these processes, may be achieved through the detailed analysis of the textural information provided by titanite. In referring to mineral texture, the features of interest are chiefly:

- **Mineral habit** (euhedral/subhedral, anhedral, interstitial).
- **Compositional zoning** (oscillatory, sector, patchy, solution front, inclusion zone, unzoned).

These textural features are the result of the changing physical and chemical characteristics of the environment in which the mineral grew, characteristics which in turn are governed by the processes operating during formation of the rock.

Petrogenesis is controlled by processes that are multifactorial, where the factors governing the different processes are often in state of flux or in direct competition. For example, a magma chamber may start out with fractional crystallisation being the dominant process, but a later introduction of a hotter magma with a contrasting composition may induce fractional melting and facilitate the mingling and mixing of the two magmas and their crystal components (Didier and Barbarin 1991; Nakada 1991; Pitcher 1995; Lipman, Dungan et al. 1997). The result may be that temporarily the new dominant process is magma mixing, with a return to fractional crystallisation when the temperature and viscosity differences between the magmas abate.

In natural environments, the system being dealt with is invariably an open system, and therefore there are many factors to deal with when considering which processes are at work and which ones are dominant and at which times. A closed system will tend to be easier to model since the factors may be limited and it may be assumed that equilibrium may be more easily achieved. In the case of the ROMG, where there is ample field evidence to suggest the mingling and mixing of contrasted magmas has occurred, it is clear that the

type of system being dealt with is an open system (at least periodically), where at different times there will be different petrogenetic processes dominating.

Nature is always aiming to achieve a state of equilibrium, and the components of any given system will be subject to changes in their physical and chemical characteristics in order to achieve equilibrium. Certain petrological processes and events may serve to disrupt or enhance the equilibrium of a system. For example, magma-mixing may serve to fully hybridise two magmas and produce a physically and chemically homogeneous magma, which will enable equilibrium to be achieved faster than if the magmas were simply mingled instead of thoroughly mixed. During fractional crystallisation, if there isn't an effective means of differentiating the crystals from the liquid, then there may be minerals that fully or partially melt in order to equilibrate with a newly crystallising mineral phase.

The continual, natural drive towards chemical and physical equilibrium, and the multifactorial petrological processes at work that enhance or disrupt it, can be inferred from the mineralogical characteristics of the resultant rocks. If equilibrium is reached, then there may be little or no record of the processes that formed the rock, since there will be little or no mineralogical features to indicate which processes were at work. Compositional zoning and disequilibrium textures of minerals are destroyed if equilibrium is achieved. Fortunately, some minerals are less prone to physical and chemical alteration, and thus are more likely to preserve evidence of the processes that formed them. This ability to resist equilibrium, to a certain degree, is what makes titanite a good candidate for preserving evidence for the petrogenesis of its host rock. Diffusion is very sluggish in titanite, especially under sub-solidus conditions, and therefore there is great potential to preserve features like compositional zoning and disequilibrium textures such as: overgrowths, solution fronts, and inclusion zones (Sawka, Chappell et al. 1984; Groat, Carter et al. 1985; Green and Pearson 1986; Wones 1989; Oberti, Smith et al. 1991; Clarke 1992; Perseil and Smith 1995; Della Ventura, Bellatreccia et al. 1999; Piccoli, Candela et al. 2000; Tiepolo, Oberti et al. 2002; Seifert and Kramer 2003; Kowallis, Christiansen et al. 2005).

The linking of mineral textures to petrogenetic processes and events is a crucial aspect of this investigation. The following deals firstly with the textural classification of titanite, and secondly, with the rationale of coupling the mineralogical information recorded by titanite growth to processes and events of formation.

3.8 Titanite characterisation rationale

Characterisation of the titanite crystals will focus on several key aspects:

- Rock context; i.e., enclave type, host granite, enclave/granite association

- Variability in crystal shape and texture;

- Variability in the nature/texture of chemical zoning

- Micro-environment of crystallisation

In each sample thin section, up to 70 titanites were analysed, however, some samples had as little as 25 titanites.

The titanites must be carefully analysed with respect to their micro-environment of crystallisation, as this will hold clues to the timing of growth, because of this they must be analysed within context and not analysed as a mineral separate. The process of rock crushing and mineral separation, while time effective in collecting large numbers of a given mineral, often results in loss of information via the loss of mineral context as well as possible loss of smaller overgrowths which may break off during crushing. These small overgrowths may contain vital clues to the last episodes of growth of such minerals. This was demonstrated with respect to very small overgrowths on zircon by Dempster and Hay (2004)

Furthermore, small interstitial crystals or highly altered and partially recrystallised titanites may be susceptible to breaking during crushing due to their weakened structural state, and may be lost in the process. If indeed they are recovered, they may not provide the vital textural and contextual information they would if analysed in-situ. For these reasons, the analysis of titanites has been carried in-situ within thin section slides that may be analysed with the petrographical microscope, scanning-electron microscope (SEM), and electron microprobe (EMPA).

Titanites were classified into populations based on provenance, crystal shape, and most importantly zoning features. This last criterion being of vital importance because the chemical zoning within the crystals is a direct reflection of the magmatic conditions under which it grew, where it is not a result of metasomatic processes.

3.9 Classification and description of textural features

As previously stated, the shape, and the compositional zoning of titanite will be a product of the processes in operation during the formation of the rock. This section will deal with the criteria by which titanite textures are classified. The exercise of classifying titanites is by and large descriptive in nature and care will be taken to avoid using genetic terms that bear interpretative connotations, and thus the terms for textural classification will remain descriptive; however, where descriptive terms have genetic connotations, these will be explained.

The main textural features that will be focused on are crystal shape (habit) and nature of compositional zoning.

3.9.1 Crystal habit

The shape and size of a crystal are the main features used to describe a crystal's appearance, or habit. The nature of this is related to the timing and rate of growth of the mineral relative to the other minerals in the paragenesis. When dealing with size, the main controlling factor is the rate of nucleation versus rate of growth of the crystal, and care must be taken when interpreting the timing of crystal growth based solely on size. It is more reliable to use the overall shape of the crystal in order to determine the timing of growth. There are four main types of crystal habit to consider: euhedral, subhedral, anhedral and interstitial.

3.9.1.1 Euhedral/subhedral titanite

A crystal that displays well developed crystal faces is termed euhedral. The presence of a regular crystallographic shape suggests that crystal growth was unimpeded by other crystals growing from the melt, and may indicate growth at an early stage of crystallisation of a melt (Shelley 1993). While there are several polymorphs of titanite, the classic euhedral crystal form of titanite is that of a lozenge or wedge shape and the alternate name of **sphene** is derived from the Greek word "sphenos" meaning wedge (see Figure 27A).

Subhedral crystals are those which partly display regular, well-developed crystal faces as well as some crystal faces that are not so regular. The inference is that parts of the crystal have been corroded or growth has been inhibited due to the proximity of another crystal (see Figure 27B). It is likely that subhedral crystals do not form nearly as early as fully euhedral crystals.
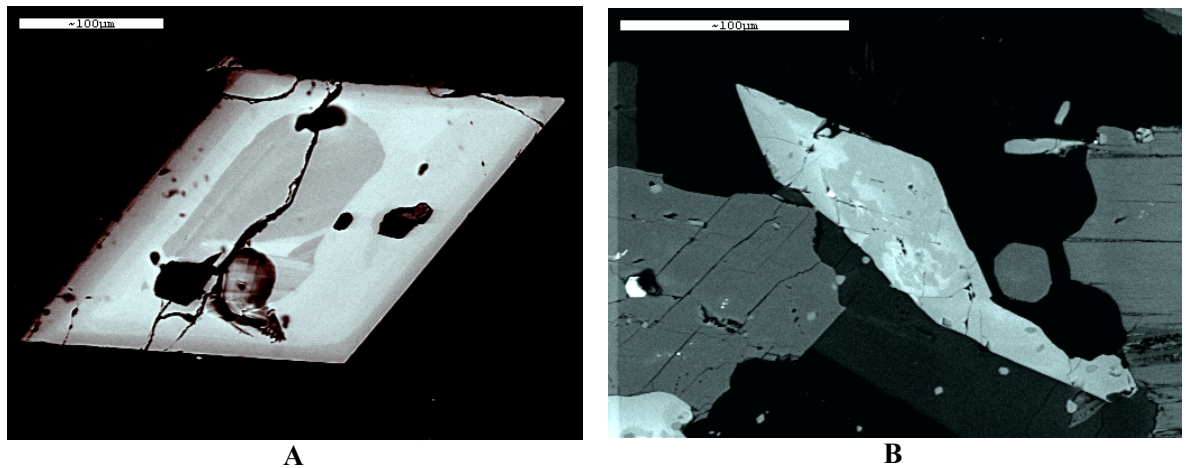
Figure 27: A: BSE image of sample A-13 (granite), a typical wedge-shaped euhedral titanite; B: BSE image of sample M2-4, a typical subhedral titanite. Scale bars are 100 μm in length.

3.9.1.2 Anhedral/interstitial titanite

When a crystal shape does not display well-developed crystal forms, it is termed anhedral. This is often the result of growth in the magma being inhibited by other adjacent crystal in the melt. Thus, the overall shape is mostly controlled by the orientation and arrangement of the surrounding crystals, with crystal edges defined by where they meet other crystals and not by the free growing crystal face (Shelley 1993).

This type of habit generally indicates growth in the latter stages of crystallisation of a melt, where there is not much room for a crystal to grow freely and display its own form, however, anhedral crystals may also form due to corrosion or partial dissolution of crystals in a melt due to changes in the physical or chemical conditions of the melt (Shelley 1993). Thus, a problem may arise in interpreting which process has led to the formation of an anhedral titanite crystal.

If the crystal has grown in the letter stages of the melt's crystallisation history, and has a shape that is controlled by impingement of surrounding crystals due to competition for space, then it is better to apply the term **interstitial** rather than anhedral. The term **anhedral** will be applied to crystals which do not display well-developed crystal forms due to partial dissolution. In order to elucidate whether a crystal is anhedral due to dissolution or whether it is truly interstitial, the compositional zoning of the crystal must be closely examined along with the habit of the surrounding crystals. If a crystal has been partially dissolved, then there may be evidence of compositional zoning being truncated at the margins (see Figure 28A). A truly interstitial crystal will not display truncations of compositional zoning, but will have interstitial margins that are uniform in character (see Figure 28B).
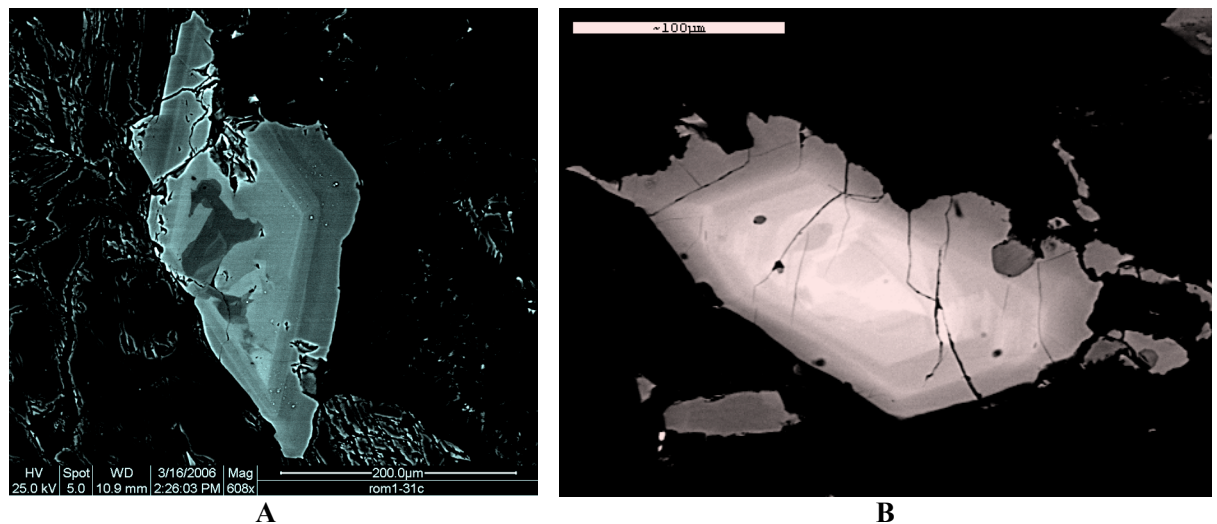
Figure 28: A: BSE image of partially dissolved, anhedral titanite, sample ROM1-31c, scale bar is 200 μm; B: BSE image of a titanite with interstitial margins, sample A-14, scale bar is 100 μm.

3.9.2 Compositional zoning textures

Different types of compositional zoning textures are the products of differing petrogenetic processes. Some of the textures may be used to identify specific processes and/or petrogenetic events; however, the linking of textures to process identification will be dealt with in a subsequent section. The following will deal with descriptions of the key characteristics of the main types of compositional zoning observed, which are: oscillatory, sector, patchy, solution front, inclusion zone, and unzoned.

3.9.2.1 Oscillatory and concentric compositional zoning

Oscillatory zoning is usually of a fine scale, with individual zones normally 1-5μm wide, which are essentially compositional zones that have developed parallel to the main crystallographic faces. In titanite, this type of zoning is usually reflected by differing concentrations of trace elements (especially the REE) and is very visible in BSE imaging (see Figure 29).

Oscillatory zoning may be the dominant type of zoning seen in a titanite crystal, but many titanites may show other types of compositional zoning in tandem with oscillatory zoning. Sector zoning is commonly seen with oscillatory zoning, whereas some titanites display areas with prominent oscillatory zoning and other areas with a distinct absence of zoning.
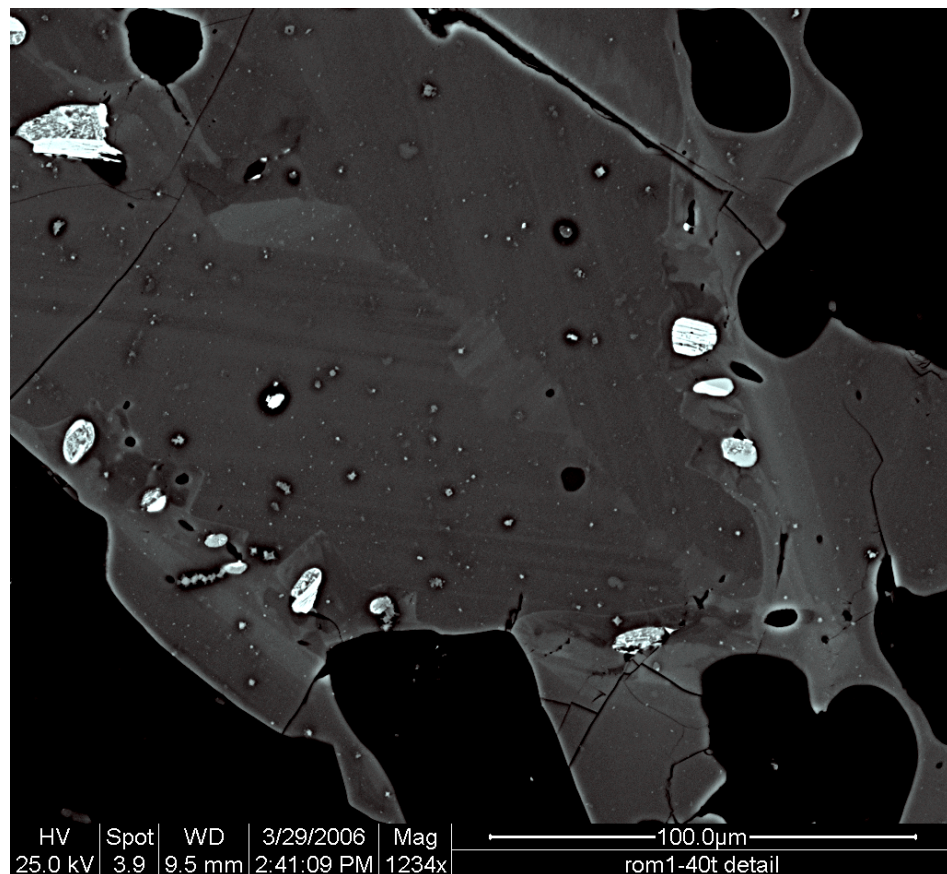
Figure 29: BSE image of sample rom1-40t; the majority o the central portion of the titanite displays very fine-scale oscillatory zoning, whereas the larger scale zoning at the margins of the titanite is more of the concentric compositional type.

Oscillatory zoning is characteristic of growth in a magmatic environment, and is considered to be related to local effects of disequilibrium crystallisation, and/or crystal-liquid interface kinetics coupled with the diffusion of particular chemical species in the melt (Gupta and Marwaha 1989; Paterson and Stephens 1992; Holten, Jamtveit et al. 2000; Kalischewski, Lubashevsky et al. 2007). The inference is that at the boundary layer, incorporation of certain chemical species into the growing crystal face (in the case of titanite, this is usually trace elements, especially the REE) occurs faster than the re-equilibration of the boundary layer chemistry with the rest of the melt; in essence it's a result of a lag time of diffusion of the species being taken up (Nakada 1991; Lheureux 1993; Shelley 1993; Piccoli, Candela et al. 2000; Tiepolo, Oberti et al. 2002).

Oscillatory zoning is generally a local effect of the microenvironment of crystallisation, and such small-scale compositional changes are generally not attributable to large scale changes to the chemical or physical conditions of the entire magma chamber (such as those changes that may be brought about by magma-mixing events).

It may be argued that any concentric compositional zoning that displays episodic repetitions of high and low contents of particular chemical species, regardless of the scale of the zoning, or the regularity, can be referred to as oscillatory zoning, and may be the result of processes operating at magma chamber-wide scale. However, it is important to be able to distinguish between small-scale zoning that is a result of local growth-kinetics related to the crystal alone, and larger-scale zoning that is a result of chamber-wide processes, since this study in concerned primarily with the latter. Thus, in order to avoid the semantics of arguing that both of these instances of concentric compositional zoning are members of a continuum, for the purposes of this study, oscillatory zoning will only be used to refer to the very fine-scale, concentric, face-parallel zoning that is likely to not be a result of larger scale changes in melt conditions. Concentric compositional zoning that is on a larger scale, with individual zones generally upwards of 10µm in width (see Figure 29), and which are less rhythmic in character and less regular, will be considered to be a result of larger scale changes to the magma chamber.

In theory, growth controlled or kinetically-induced oscillatory zoning in titanite should be characterized by chemical changes in the zoning that are very regular and related to titanite chemistry. For example, the main chemical species that cause oscillatory zoning in titanite are the REE, so if the zoning is related to local growth kinetics, then there will be a regular uptake and exclusion of all of the REE, depending on diffusional lag time. However, if the zoning is due to larger-scale changes in the magma chamber, for example a magma-mixing event, then the changes in zoning character will be more random, related less to titanite-related boundary layer depletion, and more related to the changes in the relative concentrations of different REE or trace elements induced by input of a new magma.

It is desirable to be able to use descriptive terminology that is free of genetic connotation, but it is deemed necessary in this instance to differentiate between oscillatory zoning and other concentric compositional zoning, since they are quite similar in character but produced by different processes.

In general, concentric compositional zoning will be differentiated from oscillatory zoning by the scale, size and regularity of the physical and chemical changes between compositional zones. Concentric compositional zones are generally large enough to chemically analyse individually with confidence of no contamination form adjacent zones (being large than 10µm in width on average), whereas oscillatory zoning is generally too small to analyse the individual zones reliable (being on average less than 3µm). Concentric

compositional zones are often wide enough to be considered as specific areas of a crystal (e.g.: core, mantle, rim).

3.9.2.2 Sector zoning

Sector zoning is thought to be related to preferential incorporation of specific elements occurring at specific crystal faces due to kinetically-induced lateral-layer-spreading rates of crystal faces (Paterson and Stephens 1991). Since there are compositional differences between the different crystal faces of titanite (for example the (100) and (111) faces), if the sectors grow simultaneously there will exist a difference in partition coefficients across the interfaces between the crystal faces during growth. This difference results in the preferential uptake/exclusion of certain elements (mostly the REE, Y, Nb, Al and Fe) by certain crystal faces.

Sector zoning is not the best indicator of changing melt conditions brought about by processes such as magma-mixing, as it is compositional zoning controlled by kinetics of growth and crystal-chemical factors (Paterson and Stephens 1992).

Sector zoning does not look like oscillatory zoning or concentric compositional zoning since it is not a concentric type of pattern at all, but rather, it appears as angular geometric patterns since it develops due to differential growth of (and incorporation of elements by) different, and sometimes competing, crystal faces. Furthermore, titanite sector zoning patterns may also look highly different depending on the polymorph of titanite it develops from and depending on the orientation of the mineral in thin section (Paterson and Stephens 1992).

When viewed in BSE, each sector displays uniform gray-scale zoning, with different sectors having different intensities of gray-scale, and each pertaining to different crystal faces. Sector zoning often develops in tandem with other types of zoning. Sometimes sector zoning is referred to as "hour-glass" zoning due to the shapes in produces when not accompanied by oscillatory or concentric compositional zoning (see Figure 30A). When it develops in tandem with oscillatory or concentric compositional zoning, the patterns produced are more complicated. The most prominent type is a "fir-tree" style pattern that develops along the central axis of the crystal, which occurs due to fluctuations in the relative growth rates of the different faces (see Figure 30B below).
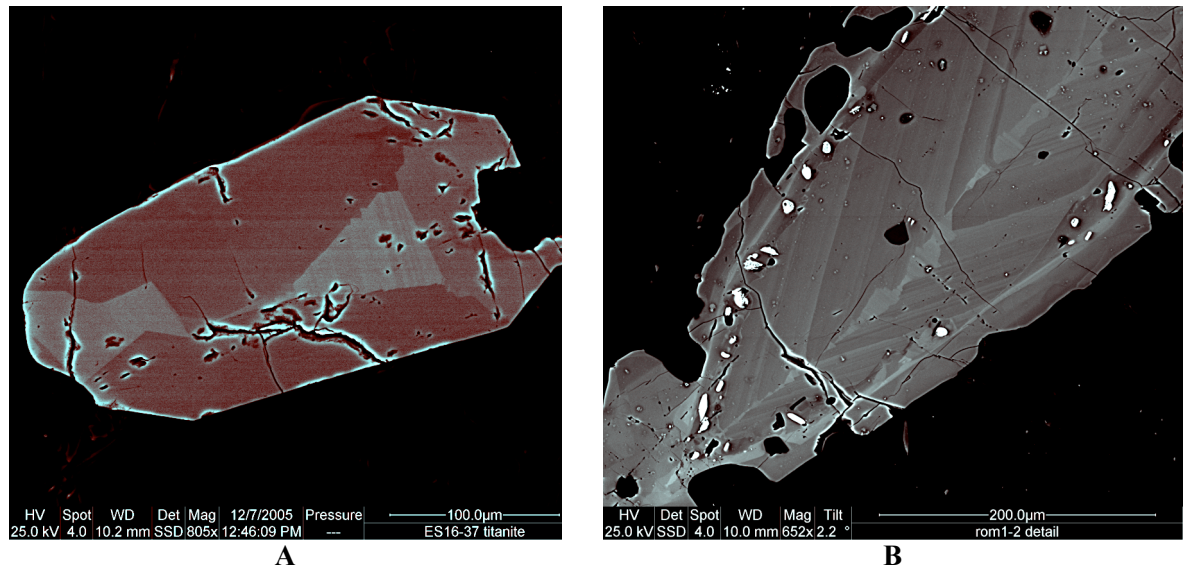
Figure 30: A: BSE image of titanite ES16-37, displaying "hour-glass" style sector zoning; note absence of other zoning. B: BSE image of titanite rom1-2, displaying "fir-tree" style sector zoning along the central long axis of the crystal; note how the oscillatory zoning corresponds with the sector zoning.

3.9.2.3 Patchy zoning

Some titanites display zoning that is not obviously related to the growing crystal faces or the small scale fluctuations in the chemistry of the melt as exemplified by oscillatory and sector zoning, but rather, are characterised by a chaotic, patchy compositional zoning that has little or no discernable geometric pattern. This type of zoning may be accompanied by oscillatory and/or sector zoning, with the core, mantle or rim of the titanite displaying different textures.

It is not clear exactly what type of processes may be responsible for this type of zoning pattern and there has been no literature that has theorised about such zoning. It is possible that such zoning may be a product of sub-solidus alteration of titanite or it may be a result of partial dissolution producing a sieve-texture and subsequent re-growth with the patches being filled with titanite of a different trace-element signature.

It is also possible that complex patterns of sector-zoning in certain titanite polymorphs resemble chaotic patchy zoning in particular cross-sections. These ideas will be explored further when individual titanites analyses are discussed.
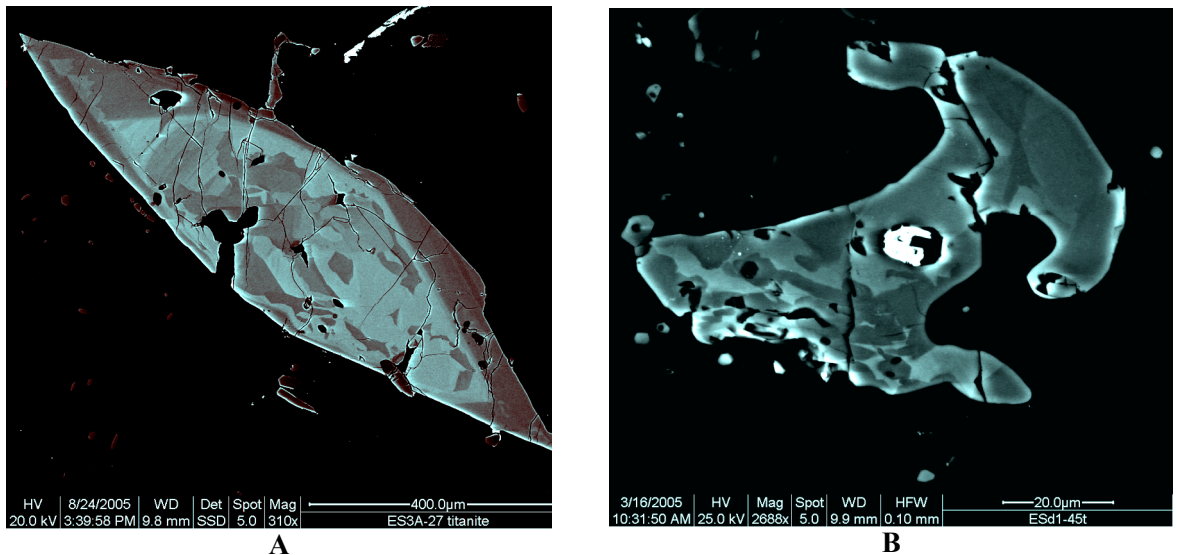
Figure 31: A: BSE image of titanite ES3A-27 displaying patchy zoning in the centre. B: BSE image of titanite ESd1-45 displaying patchy zoning in the lower left hand portion of the crystal.

3.9.2.4 Discontinuous zoning and solution fronts/horizons

The record of compositional zoning is not always a complete record, since crystals may corrode or dissolve as well as grow. The textural evidence for partial melting or corrosion of titanite is represented by discontinuities in the compositional zoning or by undulose and embayed margins of crystals. The most obvious discontinuities are solution fronts that truncate other types of compositional zoning; these discontinuities are often non-planar themselves (see Figure 32 A and B).
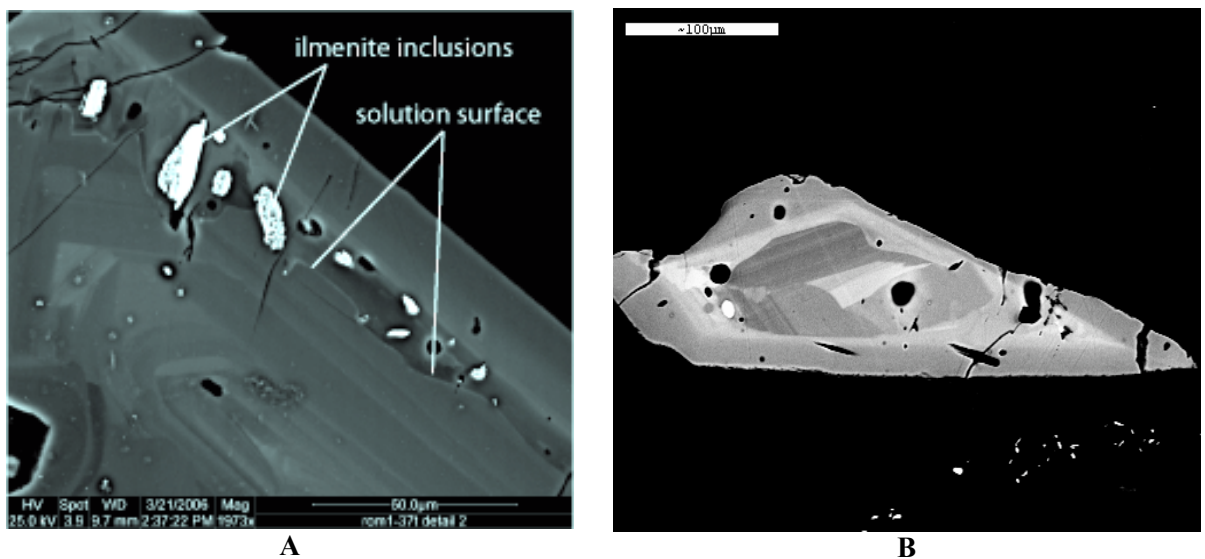
Figure 32: A: BSE image of titanite rom1-37, displaying a solution front mantled by later new growth and with associated ilmenite inclusions; B: BSE image of titanite A-57, displaying a partially dissolved core mantled by new growth; note the truncation of oscillatory zoning of the core by the solution front.

A solution surface may or may not be accompanied by new growth mantling the solution surface. New crystal growth that succeeds a period of dissolution is often characterised by compositional zoning that may differ in intensity of gray-scale, when viewed in BSE, and this is usually a result of trace-element different chemistry.

This type of textural feature indicates a significant change in the nature of the magma, whereby growth of titanite was halted and it became unstable and experienced a period of dissolution. Any new growth indicates a return to conditions favourable to titanite stability. Fe-Ti-oxides inclusions are often associated with a solution front (see Figure 32A).

3.9.2.5 Fe-Ti-oxide inclusion zones

When present, ilmenite and magnetite inclusions tend to be found at the margins of solution fronts and in zones of new growth that mantle the solution fronts and discontinuities. The inclusions are usually concordant with the edge of the crystal where dissolution has occurred, but sometimes they occur in random orientations (see Figure 32A and Figure 33 A and B).

A

B
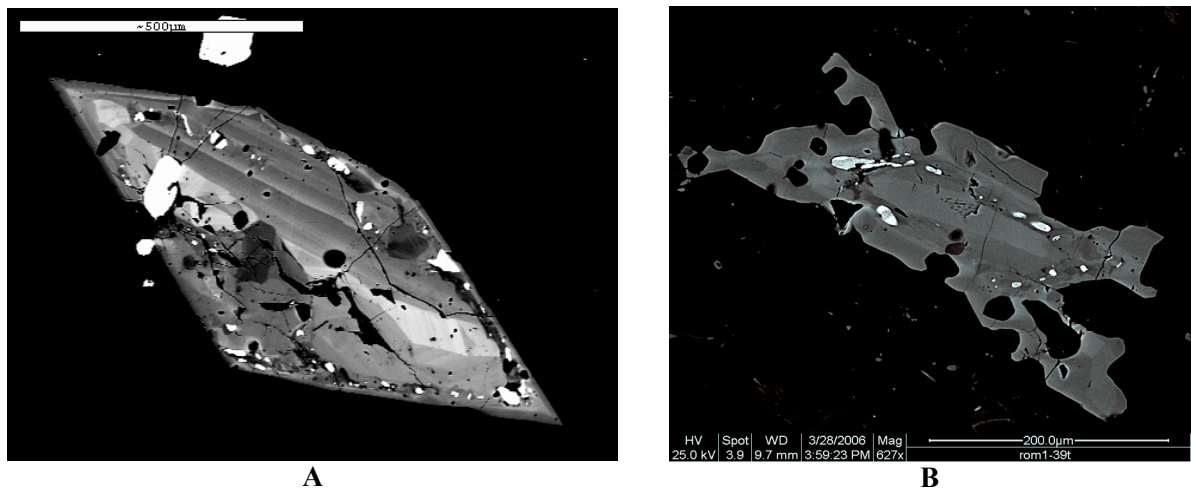
Figure 33: A: BSE image of titanite A-63 displaying an ilmenite rich inclusion zone corresponding to a solution front; B: BSE image of titanite rom1-39, also displaying a solution front that is bordered by an ilmenite rich inclusion zone.

Piccoli et al (2000) note that decreasing oxygen fugacity associated with a transient reduction event (such as input of mafic magma into a granitic magma, lowering the oxygen fugacity) can stabilise ilmenite at the expense of titanite, magnetite and quartz. As such, it is very important to note the exact nature of the Fe-Ti oxides present within samples of titanite and to note whether they are associated with a dissolution event or not. The presence of magnetite or ilmenite can reveal information regarding the stability of titanite.

3.10 Magmatic processes

Any physical or chemical process that operates during the formation of a rock can be regarded as petrogenetic. In the case of igneous rocks, the processes may be broadly divided into two categories: magmatic or post-magmatic (metasomatic). From the generation of magma to the point of critical remaining melt, the processes operating to form an igneous rock are regarded as magmatic. It must be noted, however, that while a rock forms over a range of physical conditions, the particular minerals that make up the rock also form over a range of their own specific physical conditions. It may be important to consider the fact that temperatures considered to be subsolidus with regards to titanite, may not necessarily be considered as post-magmatic since there still may be a proportion of melt that persists.

Magmatic processes are the focus of this study since the aim is to investigate whether titanite records evidence of magma-mixing. The main processes operating in the magmatic environment may be listed as follows:

- Fractional crystallisation
- Fractional melting
- Assimilation
- Replenishment
- Magma mingling/mixing
- Liquid immiscibility
- Volatile mass transfer/degassing
- Magma differentiation (physical processes of segregation)

Most, if not all, of these processes will have been in operation during the history of the ROMG pluton, although some of them will have been more petrogenetically dominant than others. Considering the mafic-microgranular-enclave rich characteristics of many of the ROMG lithologies, it is clear that the dominant processes, at least on a large scale, have been fractional crystallisation and magma-mixing, the latter being a key focus of this investigation.

These processes will have had an effect on the manner in which titanite has formed, leaving a genetic fingerprint in the form of textural features like habit and compositional zoning. It is important to have an understanding of how textural and geochemical features of titanite may indicate which processes were in operation and how specific textural features may indicate specific petrogenetic events. The two key magmatic processes to be

discussed are: fractional crystallisation and magma-mixing; fractional melting will be touched upon in the context of magma mixing.

3.10.1 Fractional crystallisation

The dominant process operating in a magma chamber that is experiencing an overall cooling trend tends to be fractional crystallisation. It is a very important process that often leads to magmatic differentiation through mechanisms that segregate and potentially isolate precipitated crystals from melt, in effect changing the composition of the melt. This process can be used to explain how a silicic magma may be produced from a more mafic magma, through the precipitation of a sequence of minerals, as denoted by Bowen's reaction series, and the concomitant segregation of the precipitated minerals and melt (Didier and Barbarin 1991; Nakada 1991; Pitcher 1995; Lipman, Dungan et al. 1997).

Although it is not always an entirely closed system process, fractional crystallisation can be considered to be a relatively closed system process when compared to magma mixing processes. If a magma chamber doesn't experience episodes of replenishment with new batches of magma, then the process of fractional crystallisation will produce a fairly predictable assemblage of minerals, with the key differences depending on the degree to which the melt and crystals are separated during the cooling of the magma (Clarke 1992). If there is little separation, and if the system is in equilibrium, then the crystals will continually react with the melt so that the resulting assemblage is one that contains crystals that exhibit no compositional zoning. Equilibrium is most likely outstripped by the rate of crystallisation, and the result is that minerals often contain compositional zoning that reflects the melt's inability to equilibrate with the changing conditions (Shelley 1993). If the melt and crystals are segregated by processes such as crystal settling or filter pressing, then the remaining melt will not be free to react with the crystals and the magma chamber may produce compositionally zoned rocks.

It is not necessarily the aim of this study to prove whether the mafic and silicic components of the ROMG were ultimately produced from the same source magma, and represent products of fractional crystallisation that have been later co-mingled, or whether they represent magmas from different sources that have subsequently been co-mingled and mixed. The aim of this study is to consider if titanite can reflect processes of petrogenetic significance in its compositional zoning and its mineral habit. In the case of the ROMG, fractional crystallisation will be considered primarily in the context of the behaviour of the trace elements and how they are concentrated in the titanites growing in the magma; as

such, the process will not be considered as much as a magmatic differentiation process as it will be considered a local crystallisation process dominating a given composition of magma and the paragenesis of minerals that it produces as it cools. In this respect, end-member compositions of magmas form the ROMG will be investigated with a view to understanding how fractional crystallisation processes operating during the cooling of the melts may be recorded by the trace element zoning in titanite.

During fractional crystallisation, the precipitating crystals will be relatively rich in compatible elements and the melt will become relatively enriched in incompatible elements. Among the incompatible elements are trace elements (such as the REE, La, Y, Nb and Zr) that titanite readily incorporates into its crystal lattice due to isomorphous substitution (Gromet and Silver 1983; Sawka, Chappell et al. 1984; Groat, Carter et al. 1985; Green and Pearson 1986; Deer W.A. 1992; Cerny, Novak et al. 1995; Perseil and Smith 1995; Prowatke and Klemme 2003; Cherniak 2006; Broska, Harlov et al. 2007). Once crystallised, titanite can resist diffusion-controlled destruction of its compositional zoning, and hence is able to record changes in the characteristics of the melt. If closed system fractional crystallisation is considered, the melt should progressively become enriched in incompatible elements, and since these are readily incorporated in titanite, then titanite may effectively reflect this enrichment, displaying compositional zoning that reflects a gradual enrichment in trace elements (Gromet and Silver 1983). Conversely, it is also possible that during its first stages of formation, titanite may effectively deplete a magma which is relatively poor in certain trace elements (such as the REE) since they are compatible with respect to titanite, and the latter stages of crystallisation, titanite be contain less trace elements, reflecting its initial depletion of the REE stock in the magma. The patterns of compositional zoning may be used to model the behaviour of the trace elements in the magma, and hence help to model the processes at work.

Magmas of different compositions will have different concentrations of trace elements. For example, in a basic magma, the overall concentration of the REE and ratio of the LREE to HREE will be different to that of a more silicic magma. So, if we are dealing with a single batch of cooling magma of a certain composition (for example a diorite), and the dominant process is fractional crystallisation (as a closed system), then the slope of the LREE vs HREE will be constant amongst the titanites from that system, and indeed different parts of the same titanite crystal should have REE ratios that plot on the same overall slope. In this regard, the slope of the LREE vs the HREE is a key proxy for determining the degree to

which fractional crystallisation (closed system) is, or is not, the controlling the petrogenetic process at work (Tindle 1991).

3.10.1.1 Titanite textures produced by fractional crystallisation

Since we are considering fractional crystallisation processes operating in given melt compositions, and primarily as a crystallisation process instead of a magma differentiation process, then we are dealing with fairly closed systems. Thus, the textures produced will primarily be a reflection of the changing melt composition (especially the trace element) as it cools, and should be free of obvious disequilibrium textures such as solution surfaces, ilmenite inclusion horizons or discontinuities in zoning. As already discussed, the small scale oscillatory zoning disequilibrium textures, which are produced by growth kinetics and controlled by diffusion, will not be considered to be a contraindication of fractional crystallisation

It must be considered that crystals that have experienced significant disequilibrium events (like magma-mixing), may also have parts of their whole that have only experienced fractional crystallisation, and thus may contain a record of that. For example a crystal may have core that has experienced only fractional crystallisation processes, but may also have a solution horizon brought about by heating and melting due to mixing with a hotter magma. In turn, if there is renewed growth, the solution horizon can represent a period of disequilibrium in the melt which separates the core from a rim that also has experienced only fractional crystallisation. So, when considering a crystal's history, the crystal must be considered to possibly contain evidence of more than one system or process at work.

Textural features that may indicate fractional crystallisation include: oscillatory zoning, absence of zoning (if true equilibrium conditions are achieved), and sector zoning. When considering concentric compositional zoning, it is the variation in trace elements (especially the REE) which cause the zoning itself, and hence, if we are dealing with fractional crystallisation, then the patterns of variation should be regular and not random and the overall slope of the LREE vs the HREE should remain constant between different titanites from the same rock (Tindle 1991). There should be steady increases or decreases in particular trace elements from core to rim of the crystals, which depend on the crystal-melt partitioning behaviour of the given elements in question. Random fluctuations in core to rim trace element profiles of titanites would not be reflective of closed system fractional crystallisation.

When considering the shape and habit of titanite, fractional crystallisation can produce euhedral, subhedral or interstitial crystals of titanite; with the key factor being timing of growth relative to the other crystals. The timing of titanite growth has been linked to the magma composition and Prince (1943) has shown that titanite crystallising from more mafic magmas tends to form late and is often subhedral to interstitial in character. He notes that in more felsic systems, the crystals tend to form earlier and are more euhedral. Since partially dissolved or corroded anhedral titanite is formed due to changes in melt conditions and is thus a disequilibrium texture, this habit is not considered as a feature produced from simple closed system fractional crystallisation processes.

3.10.2 Magma mixing

In the ROMG, there is extensive field evidence to suggest that magma mixing has been a very dominant process in the formation of the lithologies that make up the pluton. The presence of mafic microgranular enclaves (**MME**) of different shapes, sizes and internal features, is ubiquitous. Titanite has been analysed from a spectrum of lithologies, including mafic and granitic end-members as well as a range of enclave and host relationships that represent various stages of mingling and mixing of the end members. The compositional zoning textural features of the titanites should, to a certain degree, represent growth in melts that have been subject to significant changes in one or more of the following: temperature, oxygen fugacity, pressure, water content, and composition (Barbarin 1990).

Magma mixing is not a simple process that results in predictable assemblages of granitic host and mafic enclaves. Indeed, the complexity of interaction and the degree of interaction between host rock and enclaves can be quite problematic to the petrologist who wishes to unravel the petrogenesis of the mixed-magma system (Pitcher 1995). There are many classes of enclaves within granites, which may be a result of different processes at work which allow for the physical interaction of magmas of contrasted composition. Five of the main enclave/xenolith types are: (1) restite; a residue produced from partial melting processes of source rocks; (2) enclaves which are liquid or semi-liquid, and are a product of co-magmatic mafic intrusions in the host granite; (3) early consolidated cognate material, essentially a variant of the host; (4) fragments of country rock collected during magma ascent; and (5) accretions of intratelluric crystals (Pitcher 1995). Both Pitcher (1995) and Didier and Barbarin (1991) provide a full discussion of the spectrum of enclave and host relationships and their respective processes of formation. The main enclaves to be found in the ROMG, and indeed the enclaves that are the basis of this study are type number 2 -enclaves that are derived from mingling and mixing of synchronous, co-

magmatic mafic intrusions with the host granite (Harris 1999; Highton 2001; Reavy 2001; Zaniewski, Reavy et al. 2006), and as such, will be the type of magma-mixing process that will be explored.

It has been postulated that some of the lithologies in the ROMG (for example, RM2 of Zaniewski) represent mixing between an initial granitic host and co-magmatic mafic material at depth, and subsequently emplaced at higher levels (Harris 1999; Highton 2001; Reavy 2001; Zaniewski, Reavy et al. 2006). This initial hybridized magma (RM2) has been also later injected with synplutonic mafic intrusions to generate further lithologies of a co-magmatic, mixed and mingled nature. The nature of the processes at work, are such that the different melts and their component enclaves are continually being subject to changes in physical and chemical conditions. As such, the compositional zoning textures in titanite that indicate magma-mixing best are those that are a result of forced disequilibrium.

The temperature, viscosity, and degree of crystallinity of the magmas are the key factors that will dictate the degree of physical and chemical interaction that occurs (Dickin and Exley 1981; Didier and Barbarin 1991; Pitcher 1995; Piccoli, Candela et al. 2000; Kuscu and Floyd 2001; Karsli, Aydin et al. 2004). If the temperature and viscosity difference are too great, then it less likely that the two magmas will be able to physically and chemically interact enough to allow for complete hybridisation. It is not possible for mixing to occur to a high degree between a granitic crystal mush and enclaves suspended within it, unless new heat is added to the system in sufficient quantities to reverse the process of crystallisation. This degree of chemical and physical interaction will control the degree to which he host and enclaves will retain a chemical fingerprint of their origins. It stands to reason that simple physical mingling will allow enclaves and host granitoids to better retain a signature of their original chemical makeup. If there is a greater degree of mingling, possibly progressing to actual physical mixing, then there is less chance of the enclaves and host retaining their original chemical characteristics. If there is sufficient heat and the viscosity difference between the magmas is small enough, then complete hybridisation may occur, essentially resulting in physical and chemical homogenisation of the melts. Such homogenisation will result in a rock that may have no minerals that contain a compositional zoning record of the initial magmatic components.

Furthermore, attempts at chemical homogenisation doesn't need to be a product of actual hybridisation, as it has been noted that diffusion controlled chemical transfer between host rocks and enclaves can result in a closer degree of chemical similarity between the two

even if they remain quite physically independent (Orsini, Cocirta et al. 1991). If this is the case, then it may be difficult to geochemically model magma-mixing unless there is a method to do which that involves minerals that can resist alteration of their compositional zoning due to diffusion. Fortunately, titanite can do this to a certain degree, and as such, can provide a lasting geochemical fingerprint of the magmatic conditions during its crystallisation.

The main characteristics of magma mixing processes are the changes in physical and chemical conditions to the entire system or parts of it. These changes will upset the equilibrium of the system and hence also have significant effects on the minerals in the melt as well as on the melt itself. The main factors associated with magma-mixing that can affect the textural characteristics of titanite are changes in the following:

- Melt composition
- Temperature
- Oxidation state
- Pressure
- Volatile content

The first three are the most important and the possible effects they have on the textural and chemical signature of titanite will be discussed in order to link the textural features to magma-mixing processes.

3.10.2.1 Textural record of changes in melt composition

By and large, the biggest factor affecting any crystal in a system experiencing magma mixing is the change to the melt composition. How effective this is, is obviously dependant on the degree of physical and chemical mixing that has taken place between the host magma and the enclaves. The other controlling factor to consider is the efficacy of diffusion and whether the temperature contrast between the components of the system in likely to enhance of impede diffusion (Orsini, Cocirta et al. 1991; Pitcher 1995; Piccoli, Candela et al. 2000). The compositional zoning preserved within titanite can resist later alteration due to diffusion, and so man very effectively record as well as retain a chemical signature of the magmas which have had an influence upon its crystallisation.

The geochemical characteristic of the end-member magmas are very likely to be different, especially with respect to their trace elements. Thus, end-member lithologies should be characterised with respect to their geochemical signatures in order to allow effective

comparison. In this case, it is the geochemical character of titanites within the end-members that we are interested in, especially the trace elements. Mafic and silicic magmas generally have different trace-element concentrations, and they also generally have different ratios of light to heavy REE, and these ratios can be used to model the changing melt conditions experienced by titanite in mixed-magma systems (Gromet and Silver 1983; Sawka, Chappell et al. 1984; Green and Pearson 1986; Barbarin 1990; Didier and Barbarin 1991; Perseil and Smith 1995; Piccoli, Candela et al. 2000; Tiepolo, Oberti et al. 2002; Prowatke and Klemme 2003; Liferovich and Mitchell 2005; Seifert 2005; Browne, Eichelberger et al. 2006).

In considering the ratio of LREE to HREE, one is essentially modelling the slope pattern of the REE. If the system is operating as a closed system that is not experiencing any overall changes in the composition of the melt, except the changes in melt due to crystallisation, then the overall ratio of LREE to HREE should remain constant in all of the titanites in that system. However, if a new melt is introduced to a system, then it is possible that this new melt will have a different REE signature and any new titanite growth may reflect this. A result would be a potential change in the slope of the REE, reflecting an open system process whereby contamination of existing melts occurs due to mingling and mixing with new melt. This change may be recorded by titanite as changes in the nature of compositional zoning. Different portions of the same titanite crystals may have different REE slopes if new growth has taken place after mixing has occurred, and it is important to consider how the ratios may change from core to rim, and if this is reflected by other titanites in the system.

Figure 34 displays light versus heavy REE variation for titanites from a hypothetical situation where magma-mixing has occurred between enclaves that are relatively HREE enriched compared to their host granitoid. In this case, the overall concentration of the REE for both enclaves and host is increasing during crystallisation, hypothetically indicating an increase in their concentration of REE in the residual liquid, which could be attributable to the REE being incompatible with most mineral phases in the melt. The cores of both the host and enclave titanites display REE slopes which are linear, and since both of these slopes are different, they could represent a geochemical fingerprint of the two different magmas that the cores formed in. However, if the two magmas mix, then there may be a degree of chemical transfer between the resulting host and enclaves, changing the LREE vs HREE ratio of both liquids. This subsequent change in chemistry is reflected in the rim growth of the titanites, where the slope of the REE has changed, reflecting

diffusion controlled chemical transfer between the two melts. The rims of the enclave titanites record a relative enrichment in LREE compared to the cores, whereas the rims of the host titanites record a relative increase in HREE compared to the cores.
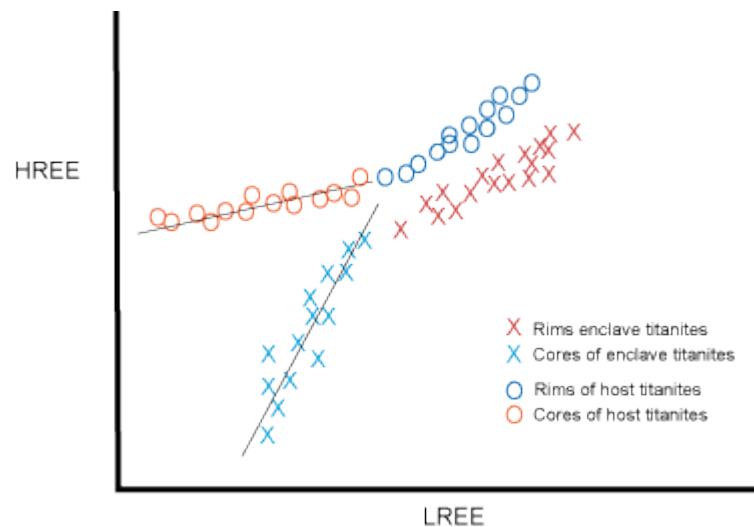
Figure 34: Titanite LREE vs HREE variation diagram for a hypothetical granitoid host- mafic enclave suite of rocks. Scales on axes are equal.

Changes in melt composition may also be highlighted by random and marked changes in the nature of the compositional zoning of titanite. Concentric compositional zoning that is caused by abrupt and significant changes in concentrations of trace elements may hint that the processes at work are very much open system processes like magma-mixing, where the core to rim trend in trace elements across the crystal is not a uniform decrease or increase, as one would expect from a closed system where mineral-melt partitioning behaviour controls the trace element distribution.

Changes to the composition of the magma may also result in physical changes to the titanites that already have been growing. Melt composition will control which crystals are stable and a significant shift in composition can render titanite instable with the result being dissolution at the expense of growth of a competing mineral phase (Sawka, Chappell et al. 1984; Green and Pearson 1986; Wones 1989; Clarke 1992; Pitcher 1995; Della Ventura, Bellatreccia et al. 1999; Piccoli, Candela et al. 2000; Tiepolo, Oberti et al. 2002; Prowatke and Klemme 2003; Broska, Harlov et al. 2007). This type of alteration is an equilibrium controlled event and a direct response to the changes that can be induced by magma mixing, and the resulting disequilibrium textures that can be found in titanite that reflect this kind of process are exemplified by:

- Anhedral habit resulting form dissolution, where the margins of the titanite show truncation of compositional zoning.
- Solution fronts and horizons within the titanite that are mantled by new growth; these solution horizons also usually truncate older compositional zoning.

Please see Figure 32A and B for examples of these textural features.

3.10.2.2 Textural record of changes in temperature

During magma-mixing processes, it is far more likely that heat introduced to a system will have a more significant effect on the textural character of growing titanites than if heat were removed from the system, so up-temperature changes will be focused on here.

Superheat from a mafic magma that is injected into a cooler and partially crystallised granitic magma can easily cause partial melting of the crystal component of the granite magma. Once the system has re-equilibrated, then crystallisation of titanite may resume, therefore, it is likely that magma-mixing can produce titanites that have textures representative of periodic dissolution and re-growth, especially if the magma chamber experiences multiple recharge events. Such textures would include discontinuous zoning in the form of solution fronts or horizons, which may or may not be mantled with new growth. If there is no new growth, then the margins of the titanite may be embayed and the overall shape anhedral in character. For examples of such textures, please see Figure 28A; Figure 30B; and Figure 32A and B for examples of these textural features.

3.10.2.3 Changes in oxygen fugacity (fO_2)

The oxygen fugacity (fO_2) of a magma is a key controlling factor to the formation and stability of titanite, and significant change in oxygen fugacities may be brought about by the injection of reduced mafic magmas into an oxidised granitoid magma(Wones 1989; Piccoli, Candela et al. 2000; Tiepolo, Oberti et al. 2002; Vuorinen and Halenius 2005). As already described in the previous sections, one of the most characteristic textural features that indicate magma-mixing playing a part in the crystallisation of titanite is the presence of a dissolution horizon that truncates magmatic zoning (oscillatory zoning, sector zoning) and new growth that mantles the dissolution horizon. The presence of this type of reaction texture may be accompanied by the growth of specific inclusions. For example, in relatively reducing conditions, the formation of titano-magnetite and ilmenite is favoured as the Ti-bearing phase in intermediate-silicic systems, whereas titanite normally forms under relatively oxidized conditions (Wones 1989; Piccoli, Candela et al. 2000; Tiepolo, Oberti et al. 2002)**.** If a reduction event destabilises titanite, then titanite may start to

dissolve and ilmenite may start to nucleate at its margins. Once oxidation conditions favourable to titanite return, ilmenite may become destabilised and the ilmenite mantling the titanite may begin to partially dissolve and in turn remnants may become mantled by new growth of titanite.

Oxygen fugacity can also play a role in the uptake of rare-earth elements in titanite, as it is thought to affect the coupled substitution mechanisms involving ferric iron which partially control the uptake of REE (Piccoli, Candela et al. 2000). If titanite is destabilised due to a reduction event, it is possible that ferric iron activity may remain temporarily restricted once titanite stability has returned. This may affect the uptake of REE into the titanite structure, causing any new titanite growth mantling the solution horizon to be relatively poor in REE, which will be directly reflected in the

3.11 Textural characterisation of ROMG titanite

Since the sample context of the titanite is paramount to gaining an understanding of how it may record evidence of magma-mixing processes, each sample from the ROMG will be looked at in turn, and a full account of the main varieties of titanite therein will be given. An overview of the nature and occurrence of titanite from the ROMG will be then given.

3.11.1.1 ESd1 synplutonic diorite sheet

This sample is the most mafic of all samples collected from the ROMG and as such is considered to most closely represent the mafic end-member in this study. Overall the titanites are subhedral/anhedral and interstitial in texture, range in size from 25 to 200μm and are scattered throughout the groundmass without any particular association with other minerals. Few have inclusions of Fe-Ti oxides.

With respect to the texture of compositional zoning viewed in BSE imaging, the titanites from this diorite dyke can be divided into three main categories of growth:

1- **Concentric compositional zoning**. Characterised by zoning in the core of the crystals where there are straight edges to the zoning, either oscillatory zoning or sector zoning (see Figure 35A). This is often truncated at the margins by later sub-solidus reactions which are indicative of possible dissolution occurring during a phase of instability within the melt.

2 -**Patchy zoning.** This is the most prevalent type of zoning observed in sample ESd1. Titanites with this type of zoning are characterised by patchy lighter and darker zones with

semi-cuspate margins. Titanites fall within the size range of 25-150µm. The lighter zones look like they are linked to areas of cracks within the crystals. The lighter areas dominate the margins of the crystal and can also be seen where there are cracks. This could be related to late stage sub-solidus alteration (see Figure 35B).

Some of the patchy zoning seems to have a localised fabric to it, although it has no overall pattern that can be linked to magmatic zoning. In Figure 35C, the large titanite is anhedral and has margins that are interstitial. These finger-like protrusions are the last part of the crystal to solidify and are of a brighter nature than the majority of the crystal; this is most-likely an edge effect of the BSE imaging process. The bright patchy zoning observed parallel to the large crack running down the left hand portion of the crystal has a crude fabric that seems to run away from the crack.
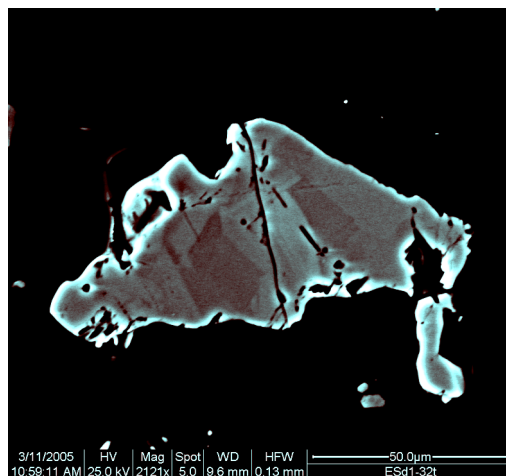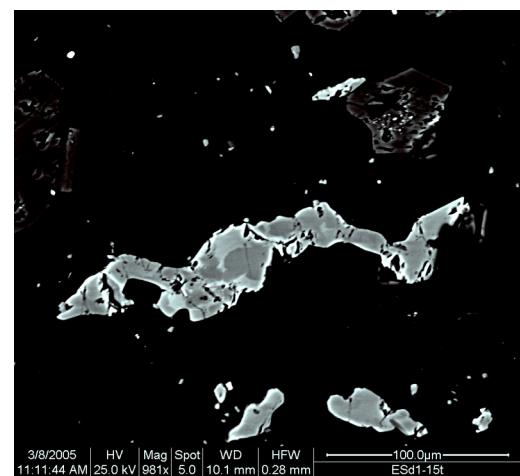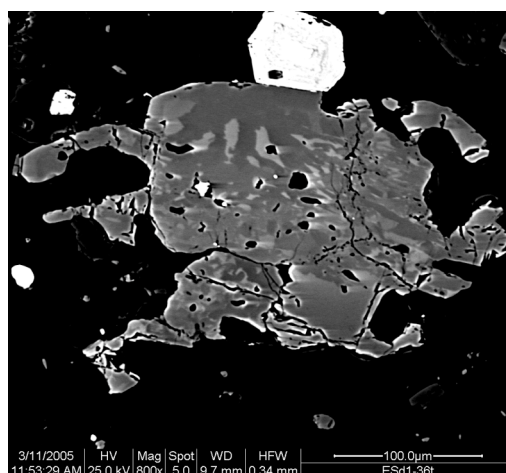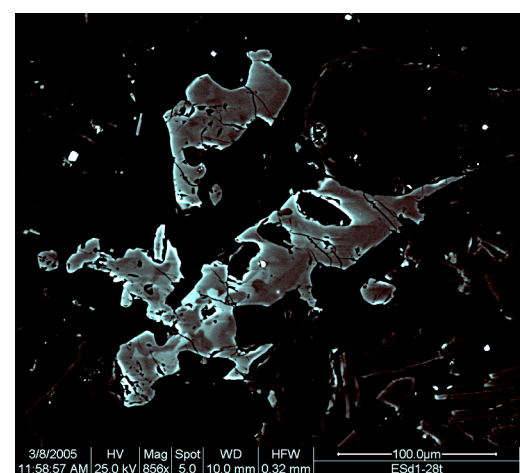
Figure 35: ESd1 titanite textural groups. A. Magmatic zoning, typified by straight zoning. B Patchy zoning/alteration. C. Patchy zoning related to cracks in the titanite. D. Interstitial texture, with protrusions representative of the final stages of magmatic crystallisation.

3-**Interstitial protrusions.** The crystal shape of nearly all of the titanites in the sample is anhedral with finger-like protrusions at the margins (see Figure 35D). This interstitial texture suggests that the majority of the titanites formed late on in the crystallisation of the rock and the finger-like margins of the titanites represent the very last stages of supra-solidus growth. The margins of most of the titanites seem to have a slightly brighter aspect in BSE compared with the interiors. This last stage of growth may retain a chemical signature that can tell us something about the waning stages of crystallisation. Prince (1943) studied crystallisation of the system $CaTiSiO_5$-$NaAlSi_3O_8$-$CaAl_2Si_2O_8$ and found that the solubility of titanite decreases as melts become enriched in albite down temperature. Piccoli et al (2000) have made the observation that titanite growing in a natural system tends to form early in granodiorites with a euhedral shape, and tends to form late and in more mafic magmas with a broadly interstitial texture. These results are consistent with the observation of titanite crystal habit in ESd1

3.11.1.2 RM1 equigranular biotite granite

At the present level of erosion of the complex, RM1 is the earliest and most evolved igneous rock facies of the ROMG, and shows little of no evidence of mixing with diorite magmas. The titanite in this rock very well may contain a chemical fingerprint of one of the earliest pulses of magmatic activity before any significant mingling or mixing occurred between RM1 and synplutonic diorite dykes to create the RM2 facies.

The titanites in this biotite granite are mostly euhedral to subhedral in crystal shape and range in size from 100 to 1000 μm. The smaller grains show very simple compositional zoning, where there are broad, uniform zones and sector zoning. This sector zoning is generally of a two-tone nature when viewed in BSE, and light zones dominate the long axis of the crystal as well as the very centre. There is no complex or fine scale oscillatory zoning visible in these smaller titanite crystals at all (see Figure 36A).

The larger titanites, on average 700μm in length, are more euhedral than the smaller ones and also have slightly more complex zoning. The zoning pattern observed is the same for all large titanites: euhedral, bright central area with equally bright sector zoning emanating from the core and following the long axis of the crystal; the bright core is mantled by a darker zone which then gives way to a rim dominated by a bright zone with some fine scale oscillatory zoning turning darker towards the edge. Simply put, the pattern from core to rim is bright-dark-bright-dark (see Figure 36B and Figure 36C).

The smaller titanites have the same overall pattern of zoning but do not have all of the zone characteristic of the largest titanites. Most of the small to medium sized titanites only show a bright central area, with associated sector zoning, and an outer zone which is darker. They do not have the additional bright zone and fine scale oscillatory zoning on the rim as observed in titanite RM1-7. For an example see RM1-3 in Figure 36D.

There is some evidence for the alteration of amphibole to titanite; however this was limited to one occurrence in the sample. The amphibole, surrounded by large plagioclase and alkali feldspars in a state of un-mixing, shows a very patchy form of replacement, with a main central area and several small areas not connected to the main replacement. The replacement seems to propagate along the axis of the main visible cleavage (see Figure 36E). Inside the largest part of the titanite are small slivers of a material significantly brighter than the titanite in BSE. This has been identified with EDX as allanite, an Al, Fe, Ca, REE-rich silicate (see. Figure 36F). EDX analysis of the titanite also showed it to be relatively enriched in Al and reduced in Ti compared to standard titanite. This alteration is most likely a sub-solidus reaction, based on the texture, with late stage fluids being driven out causing dehydration of the amphibole.
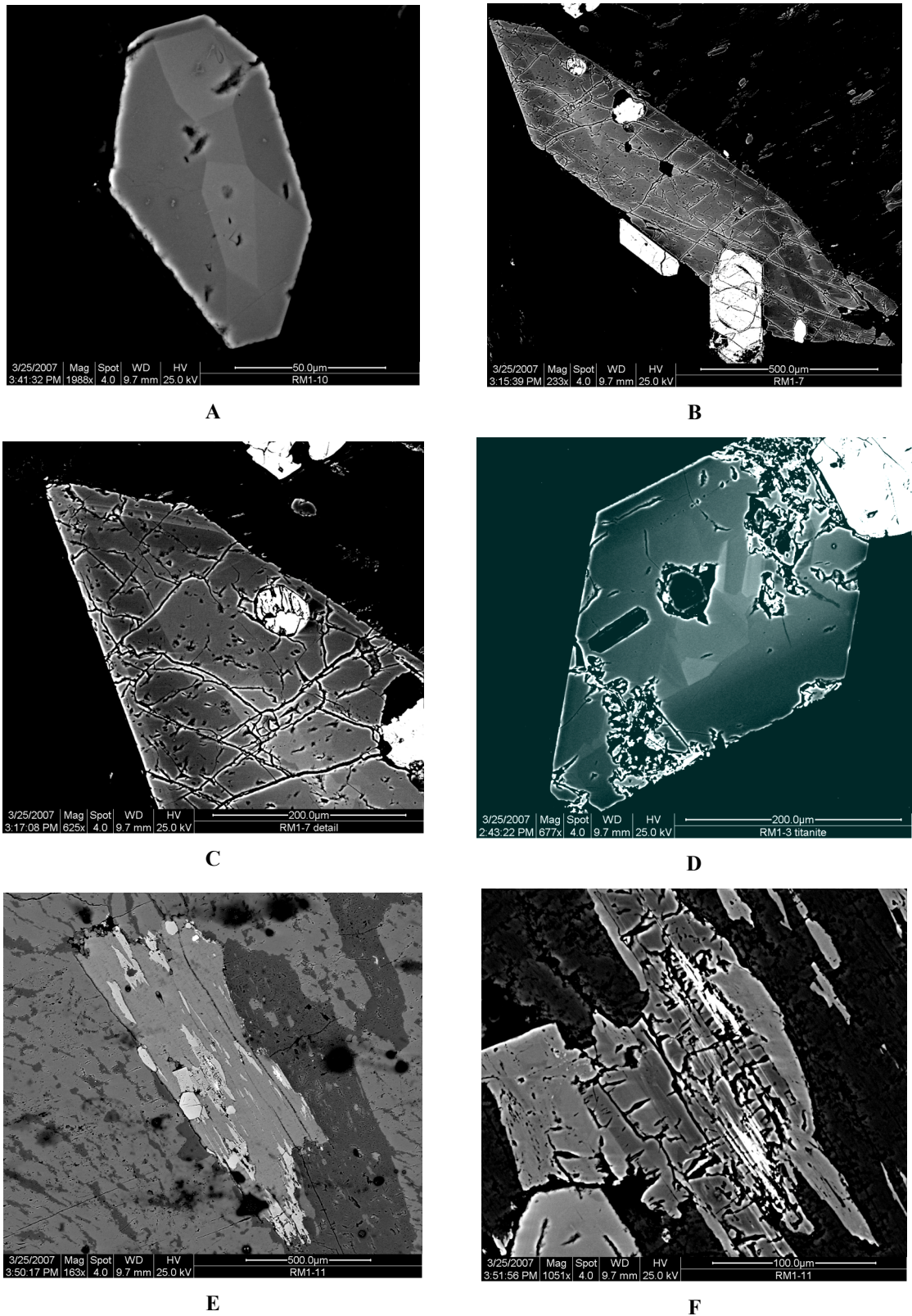
Figure 36: RM1 titanite textural groups. A. Small (50µm) titanite with simple sector zoning. B. Large (1mm) euhedral titanite displaying bright-dark-bright-dark core to rim zoning; also contains sector zoning along the long axis of the crystal. C. Detail of B, showing thins oscillatory zoning near the rim and sector zoning along the c-axis. D. Small (200µm) titanite dominated by sector zoning. E. Amphibole with altering to titanite along cleavage zones. F. Detail of E, showing titanite with brighter patches where it is altering to allanite.

3.11.1.3 ROM1 vesicular mafic enclave

Sample ROM1 is of a vesicular mafic enclave. The groundmass is composed predominantly of plagioclase, biotite, amphibole, alkali feldspar with titanite as the main accessory phase. The groundmass contains clots of amphibole. Which range in size from 3 to 10mm and are glomerocrysts of hornblende mantled by highly altered alkali feldspar.

Titanites from this sample are diverse and complex with respect to their compositional zoning. Titanites range in size from 50μm to the largest being nearly 1.5mm in length. The average size is about 200μm. The majority of the titanites are subhedral to euhedral. However some euhedral titanites have margins that are interstitial with respect to the surrounding crystals while the overall shape and zoning is euhedral. There are some titanites that are anhedral/interstitial. Some titanites contain dissolution horizons, easily spotted due the manner in which the horizons truncate earlier zoning. These solution surfaces are also associated Fe-Ti oxide inclusions. The largest titanite in the sample, ROM1-40, contains a continuous suite of textural features that are representative of every stage of growth present in the titanites within the groundmass (see Figure 37A).

Titanite RM1-40 is 1.5mm in length and 250μm at its widest. Overall, it has good crystal shape; however, the last period of crystal growth seen at the very rim of the crystal is interstitial. The central portion is dominated by the presence of Fe-Ti oxides and a patchy zoning (see Figure 37B). The central portion of the crystal is bounded by a dissolution horizon that forms a clearly defined boundary between the inner patchy zoning with Fe-Ti oxide inclusions and an outer mantle of titanite with fine scale magmatic zoning and a lack of inclusions. The zoning in the mantle is fine-scale oscillatory zoning with sector zoning along the man axis of the crystal. The oscillatory zoning alternates between light and dark with the average zone size being less than 10μm in width. (see Figure 37C). This mantle is separated from the rim of the crystal by a horizon that can be seen to truncate the zoning of the mantle. This horizon is not uniform around the crystal; it does not form a straight line but is very crenulated. This is a solution surface, representing a period of titanite instability and concomitant dissolution. Associated with this boundary, and seen all around the dissolution horizon, are Fe-Ti oxides set in the rim side of the mantle/rim solution surface. The initial portion of the rim is characterised by a very patchy zoning that surrounds the inclusions. This is identical to the type of zoning (and inclusions) observed in the central portion of the crystal. (see Figure 37D). The rim is characterised by a simpler and coarser zoning with light and dark areas, compared to the mantle. The outer rim of the crystal is

also interstitial with respect to the surrounding groundmass. This would suggest very late growth (see Figure 37E).

There are several crystals within the sample that show similar compositional and crystal shape textures, especially titanites associated with the amphibole vesicles fillings (see Figure 37F for an example). However, RM1-40 is the only crystal to show evidence of three main episodes of growth and two separate dissolution events. Most of the other groundmass titanites show the mantle phase of growth with fine scale oscillatory zoning, which is separated from the simpler, coarser zoned rim by a dissolution horizon with associated Fe-Ti inclusions.

ROM1 Textural interpretation:

1- Early magmatic phase of growth. This period of growth is characterized by good oscillatory zoning and sector zoning, both on a very fine scale. Possibly linked to variations in the availability of trace elements in the magma early on.

2- Oxygen fugacity changes. There are two events of this represented by the zoning in the largest of the groundmass crystals. Best example is ROM1-40, where the core has many inclusions of Fe Ti oxides and has a patchy pattern of zoning, with relics of oscillatory zoning (O.Z.) on a coarse scale.

- There has been an early period of magmatic growth.

- This has been subsequently partially dissolved (1st change of Oxygen fugacity) with titanite alteration and growth of the inclusions.

- Renewed magmatic growth, fine scale O.Z.

- 2nd oxygen fugacity change; dissolution of O.Z, growth of Fe Ti Oxide inclusions.

3- Final late stage of growth; interstitial texture if rims. A final period of magmatic growth characterized by coarser zoning, both oscillatory and sector zoning, and most of this final stage of growth looks to be interstitial and hence very late.
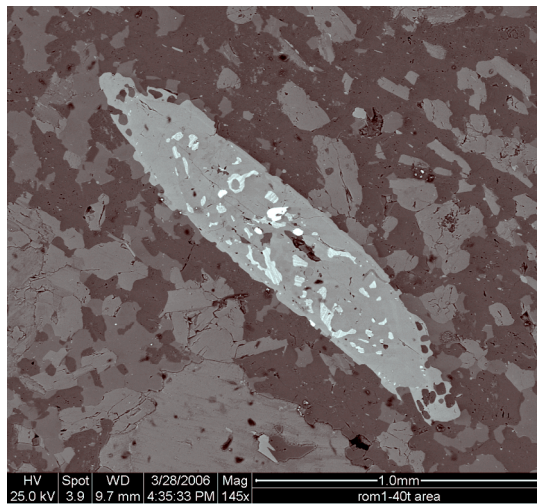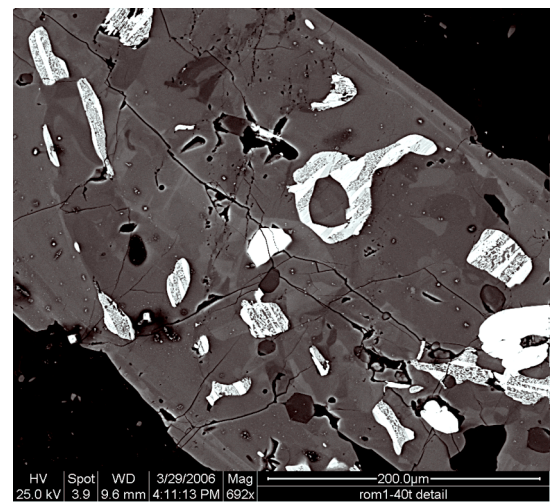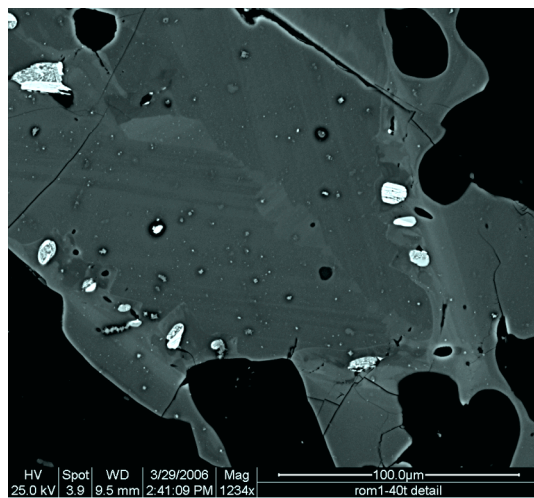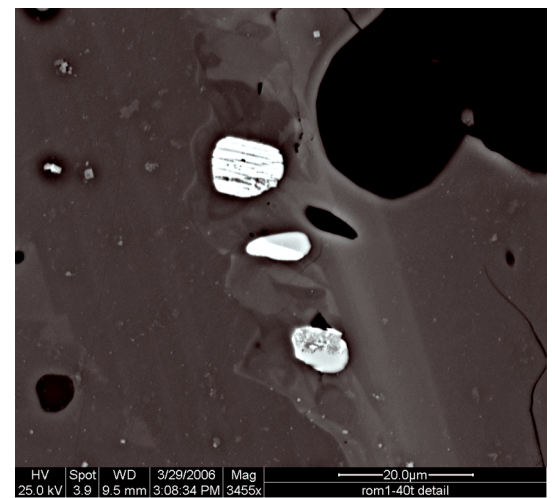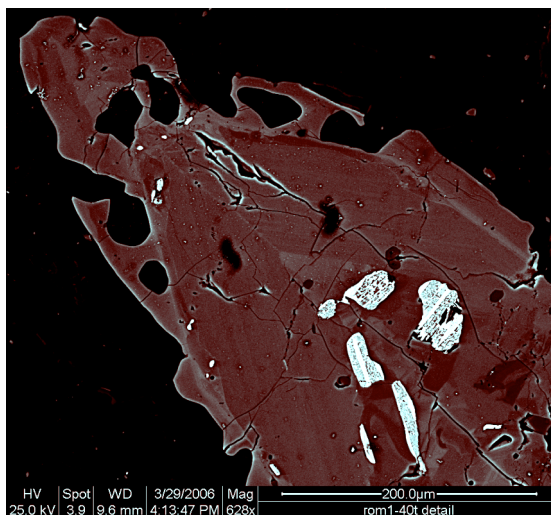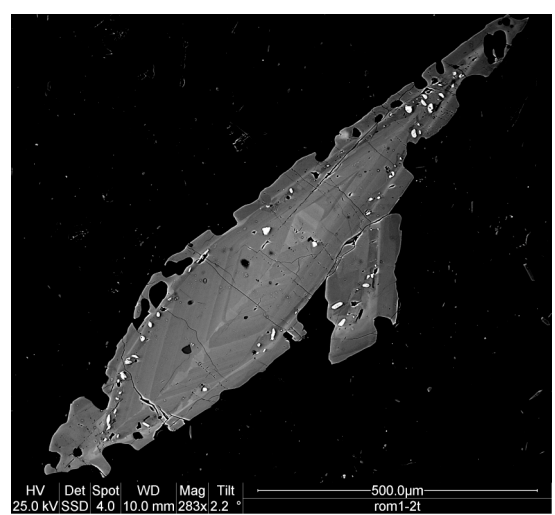
Figure 37: ROM1 titanite textural groups. A. ROM1-40, a large titanite that displays 3 separate episodes of growth punctuated by two episode of dissolution. B. Core of ROM1-40, displaying patchy zoning and ilmenite inclusions. C. Fine-scale oscillatory zoned mantle of ROM1-40. D. Detail of mantle-rim boundary zone as seen in C; note the patchy zoning and associated ilmenite inclusions of the dissolution horizon that represents the boundary. E. ROM1-40, showing detail of all three phases of growth. F. Titanite ROM1-3, showing similar textural features to ROM1-40; however, it lacks the patchy zoned core of ROM1-40.

3- Final late stage of growth -interstitial texture if rims. A final period of magmatic growth characterized by coarser zoning, both oscillatory and sector zoning, and most of this final stage of growth looks to be interstitial and hence very late.

4- Vesicle titanites vs. matrix titanites: Vesicle fill titanites look similar in zoning to the coarse scale zoning of the final period of growth seen in the matrix titanites that exhibit the fine scale oscillatory zoning and oxygen fugacity changes -whereas the vesicle fill titanites do not generally exhibit the periods of early growth or record the o fugacity changes. Some vesicle fill titanites show evidence of sub-solidus alteration of the coarse scale magmatic zoning. Some also show some evidence of the oxygen fugacity change. However, these are not in the centres of the vesicles, they are at the margins where there is more alkali feldspar, and are often associated with the alkali feldspar and not the amphibole of the vesicles. See Figure 38 for examples of vesicle-fill titanites.
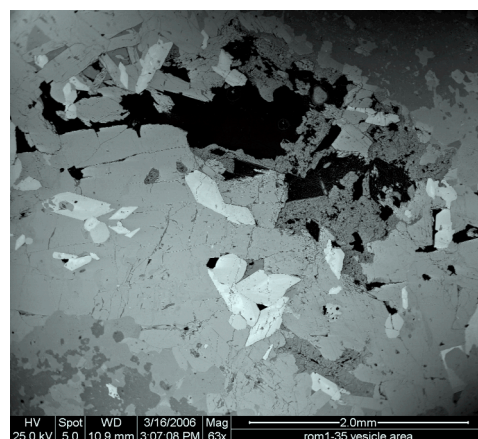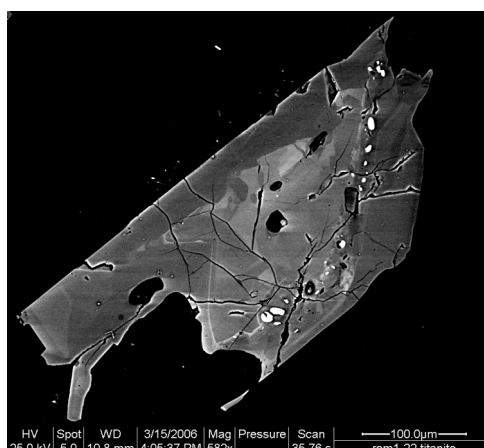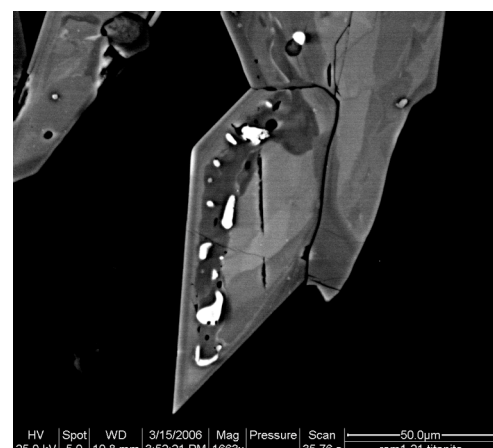
Figure 38: ROM1-40 vesicle fill titanites. A. The very bright, euhedral wedge-shaped titanites are set in the amphibole which makes up the majority of the vesicle fill. B. ROM1-31; detail of titanites from A, displaying alteration of magmatic zoning visible as dark veins. C. and D. Vesicle fill titanites displaying dissolution features and ilmenite inclusions.

3.11.1.4 ES5 (simple mingling)

The host granite-enclave relationship displayed in sample ES5 is one of simple mingling. There is little evidence of significant physical interaction between the diorite enclave and the granite.

Titanites from the enclave are all interstitial in texture with little or no zoning that is concordant with the margins of the crystals. There is a general pattern of brightening from core to rim in the enclave titanites when viewed in BSE. This would suggest that the melt was becoming richer in trace elements towards the final stages of crystallisation, or that the behaviour of the trace elements were large incompatible with respect to the titanite crystal structure. However, some titanites show no zoning at all and are uniform in brightness. Interstitial textures indicate late crystallisation. See Figure 39, below for examples.

<div align="center">A   B</div>
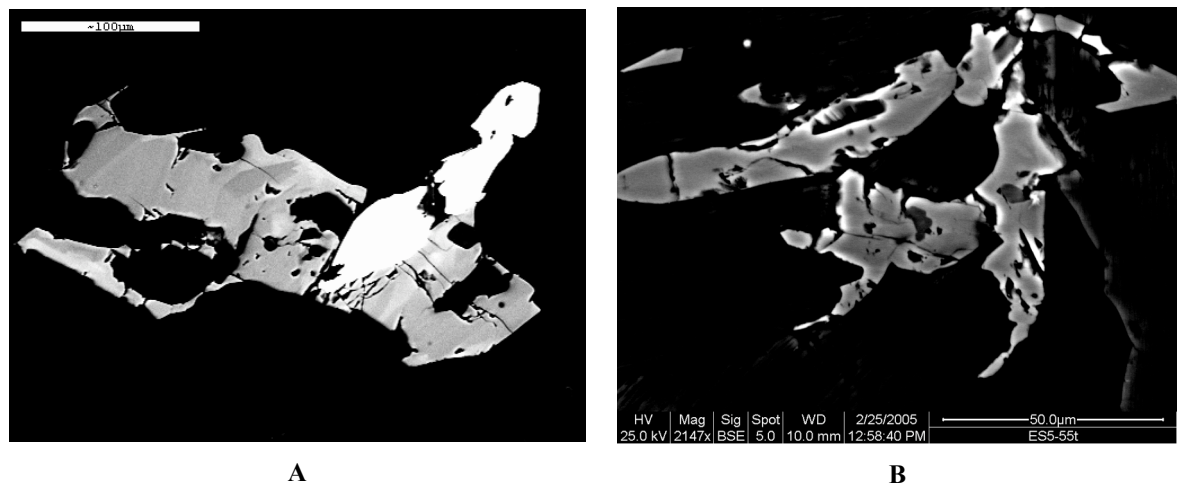
Figure 39: ES5 titanite textural groups from the enclave portion of the sample. A. Interstitial titanite displaying no discernable pattern of zoning; not the bright zoning of the rims compared to the core. There is an elongate zircon (very bright) inter-grown with this titanite. B. Interstitial titanite with little to no zoning at all.

The granite portion of sample ES5 is characterised by titanites that both display euhedral and interstitial features (see Figure 40). Some titanites show both characteristics, as they have a good titanite shape but also have rims with interstitial protrusions. The zoning of these titanites is fairly simple, displaying an overall brightening from core to rim with evidence of both sector zoning and oscillatory zoning. Some titanites display a thin (5-10μm) bright zone immediately before the rim/interstitial area. The combined euhedral shape and interstitial rims suggest that the titanite from the granite had a reasonably long lived period of crystallisation; one period of unimpeded crystal growth early on and a very late period of growth whereby the titanite was filling in the spaces left in the melt and possible competing for space with adjacent minerals.
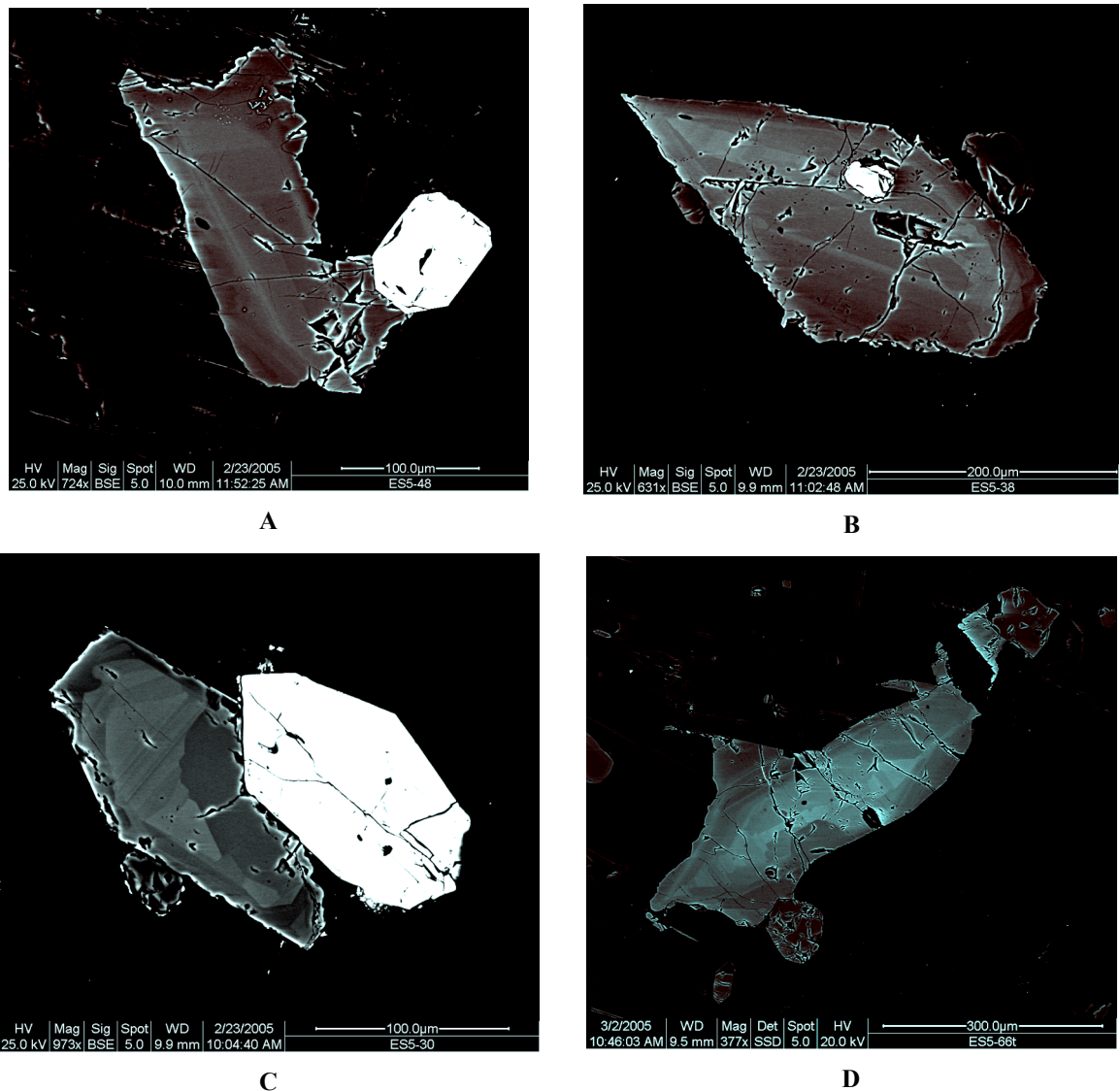
Figure 40: ES5 titanite textural groups from the host granite part of the sample. A. Subhedral titanite with simple zoning and slightly interstitial rim. B. Euhedral titanite displaying well-developed oscillatory and sector zoning. C. Euhedral titanite growing next to a bright zircon. The texture is dominated by sector zoning. D. Euhedral titanite with interstitial rims. Zoning becomes darker towards the rim, with one bright zone just before the rim.

3.11.1.5 ES3A (advanced mechanical mixing)

In parts of the ROMG pluton, the character of the granite and diorite interaction is one of intimate physical mingling and mixing on a very fine-scale; as fine as 1-2cm wide streaks of the inter-fingering lithologies (see Figure 41). This is representative of an advanced stage of interaction of the two liquids which has been frozen in place before complete hybridisation has occurred. Titanite from ES3A that originate from the enclave portion of the sample are characterised by subhedral crystal shapes and interstitial rims and range in size from 50µm to 700µm. The compositional zoning is dominated by either simple zoning, with broad zones that become darker towards the rim,
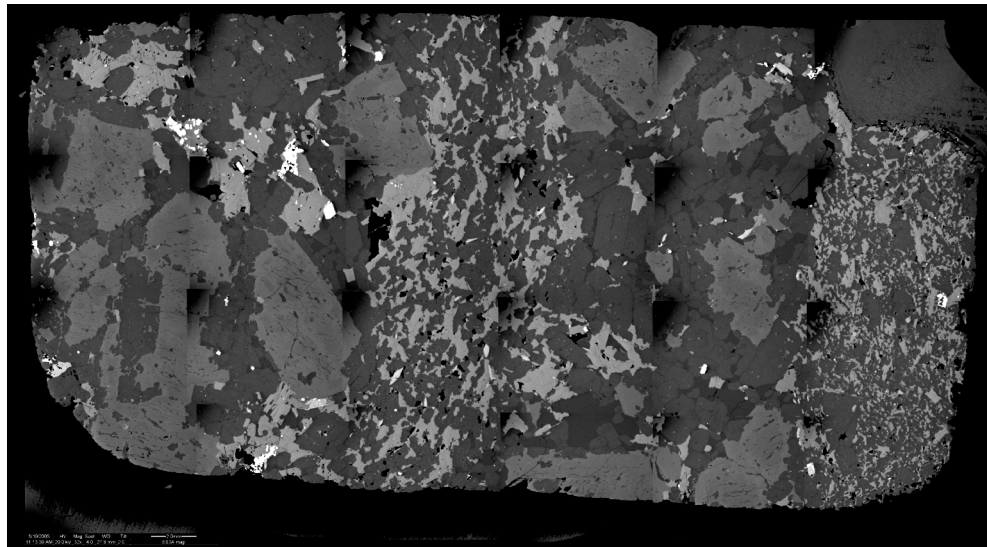
Figure 41: BSE composite image of ES3A displaying inter-fingering of diorite enclave and host granite on the cm-scale. Field of view is 4cm wide.

or by a patchy zoning pattern. Where the zoning is patchy there are occasionally associated inclusions of ilmenite. This patchy zoning is comprised of darker, irregularly shaped patches set in a brighter zoned background which shows vestiges of oscillatory and sector zoning (see Figure 42A). This patchy zoning is inferred to have been produced from partial dissolution of primary magmatic zoning during a transient period of titanite instability.

Titanite from the granite is characterised by euhedral shapes and well developed sector and oscillatory zoning (see Figure 42B). These range in size from 70 to 900μm. The well-developed magmatic zoning indicated fairly early growth that was unimpeded by other crystals.
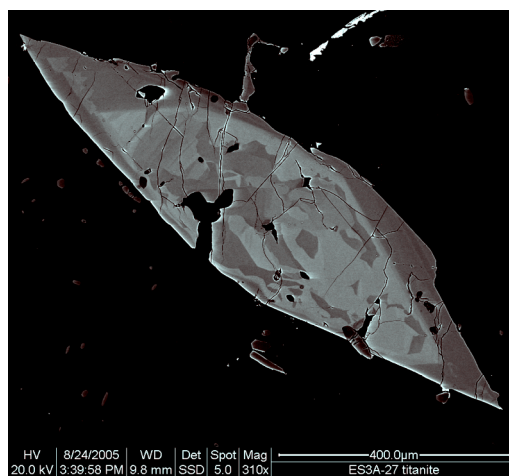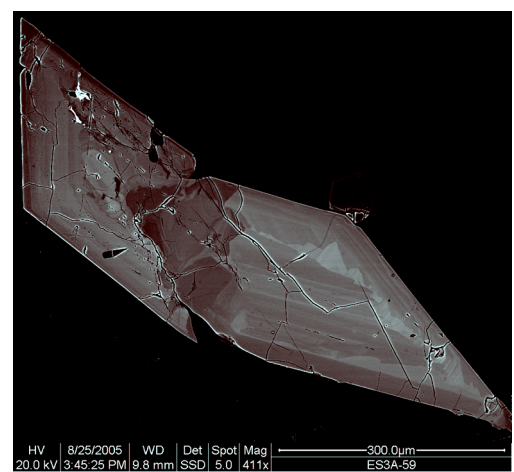
A   B

Figure 42: ES3A titanite textural groups, viewed in BSE. A. Enclave titanite patchy zoned core and interstitial margins. B. Euhedral granite titanite with well developed zoning and evidence of crack-related alteration.

3.11.1.6 ES16 (hybridised rock)

Out of all the rocks sampled, ES16 is the most hybrid in nature. It is a medium-grained rock and has a texture which shows evidence of mechanical mixing of an advanced stage, with localised flow and swirl textures in addition to large partially resorbed megacrystic feldspars. The mineralogy is intermediate between the monzogranite of RM2 and the diorite of the synplutonic dykes (ESd1) and mafic microgranular enclaves (MMEs).

Titanites from ES16 are mostly subhedral to anhedral and some have interstitial margins and the average size is 300µm. Zoning is very weakly developed and is usually restricted to sector zoning only. Sector zoning is developed along the long axis of the crystals and where it occurs it is not significantly different in brightness compared to the rest of the titanite (see Figure 43A). The zoning, overall, does vary greatly in brightness. There are some titanites that contain patchy zoning with inclusions of ilmenite (see Figure 43B).

The absence of well-developed magmatic zoning, other than oscillatory zoning (which is developed due to crystal chemical factors) and the low contrast in brightness of the zoning that does exist, would indicate crystallisation from a fairly homogenous magma. Titanite with patchy zoning and ilmenite inclusions in the core are likely to be the result of partial dissolution and re-growth of titanites that have grown in one of the melts that contributed to the formation of the ES16 hybrid. These titanites have subsequently grown and developed simple zoning that reflects the other titanites in ES16.

| A | B |
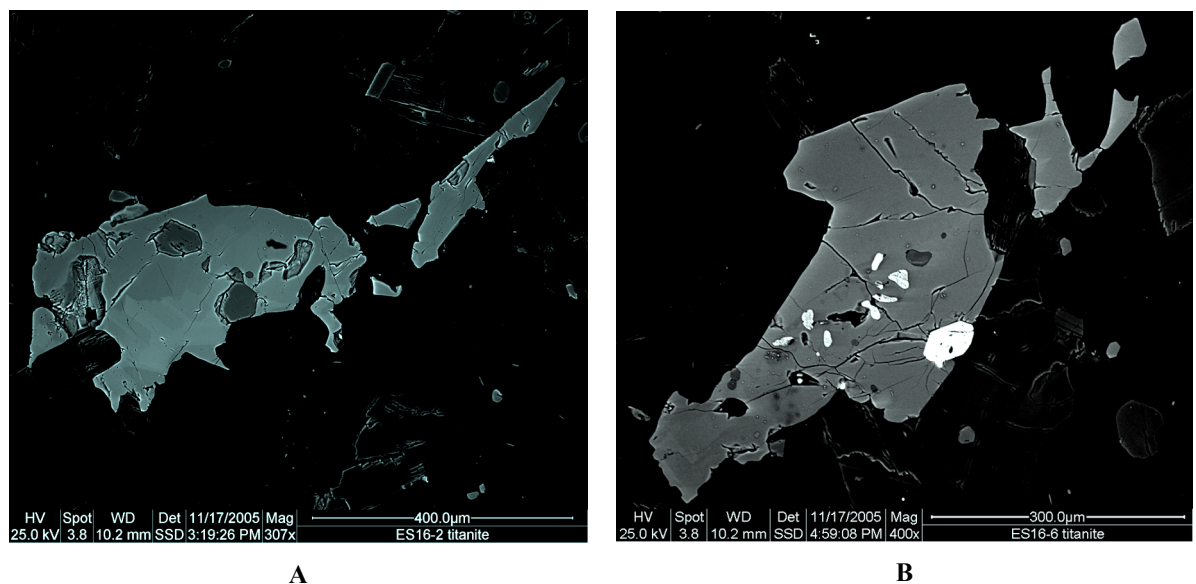
Figure 43: ES16 (hybrid) titanite textural groups viewed in BSE. A. Anhedral titanite with interstitial margins. Only weakly developed sector zoning is visible along the long axis. B. Subhedral titanite with no visible zoning apart from slightly patchy core. Note the bright, anhedral ilmenite inclusions in the core.

3.11.1.7 A (well developed mixing margin)

Sample A displays a mixing margin between the host granite and diorite enclave which suggests that there has been significant chemical interaction between the contrasted melts. The zone of mixing is roughly 1.5cm wide and displays a grain-size intermediate between the granite and diorite (roughly 0.2mm). The fact that the two melts were of sufficiently similar temperature and rheology to mechanically and chemically mix, means that the titanites within the mixing zone (as well as within the granite and enclave) of the sample may hold a record of the mixing.

Titanites from the granite portion of the slide are euhedral and generally have well developed, fine-scale (1-10μm) oscillatory zoning and some development of sector zoning along the long axis of the crystal. Titanites range in size from 50 to 1400 μm. Most have discontinuous zoning, characterised by solution surfaces that truncate earlier formed magmatic zoning (see Figure 44A). This indicates that there has been a period of titanite instability at some point. Some of these solution horizons are characterised by the presence of ilmenite inclusions. In nearly all instances the renewed growth in characterised by a thin bright mantle and less bright but wider rim.

Titanites from the mixing zone and the enclave part of the sample generally show all the same textural variety as the titanites from the granite part of sample A. However, there are some instances of anhedral and subhedral titanite within the mixing zone and the diorite. These titanites sometimes display embayed margins, suggesting possible dissolution towards the end of the crystallisation history (see Figure 44B).

A   B
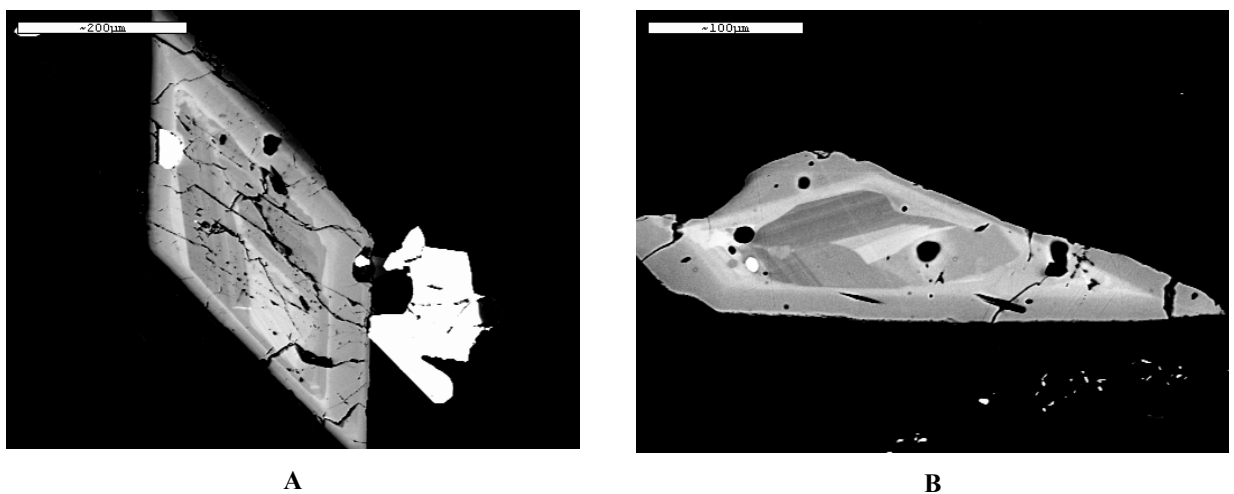
Figure 44: Titanite textural varieties from sample A (mixing margin). A. Euhedral titanite from granite part of the sample, displaying well-developed zoning in the core and a solution surface separating the core from the bright mantle and rim. B. Titanite from enclave displaying similar textural features as A, but with a margin that looks slightly embayed, indicating possible late dissolution.

3.11.2 Interpretation of textures

Titanite from the ROMG displays a large variety of textural features. These textural varieties are often linked to specific rock types within the ROMG co-genetic suite that the titanites are derived from. Certain textures are clearly representative of specific lithologies. For example, subhedral to anhedral titanite with interstitial rims tends to form in the synplutonic diorite dykes and diorite enclaves that have not seen much interaction with the granitic rocks. Also, euhedral titanites with well-developed sector zoning and oscillatory zoning tend to come from granitic rocks. However, there are no textural types that are entirely unique to just one rock type, as some titanite textural features are shared between rock types. This may be a result of crystal scavenging. The titanite shape and pattern of compositional zoning is a product of the processes that govern the crystallisation of the rocks in which they have formed. As such, it is not surprising that a huge range of textural varieties of titanite is found in the ROMG, since the ROMG represents a suite of co-genetic lithologies that display a huge range of textures themselves.

An initial assessment of the textural character of the ROMG titanites would suggest that titanite can record evidence of the petrogenetic processes that played a part in the formation of their host rocks. In the instance of the ROMG, where magma-mixing has played a large role in the formation of the rocks, it would seem that titanite can record evidence of these mixing processes, especially with respect to the dissolution and re-growth textures that are so ubiquitous within the ROMG titanite. In order to confirm the inference that the textural characteristics of the titanites are a reflection of the petrogenetic processes which formed their host rocks, it is necessary to geochemically analyse the compositional zoning and asses whether the chemical signature of the titanites corroborates with the textural signature.

4

Ross of Mull Granite titanite geochemistry

4.1 Introduction

The textural characterisation of titanites from the ROMG may allow an initial assessment of the titanite compositional zoning from this varied co-genetic suite of plutonic rocks; however, in order to assess the ability of titanite to record petrogenetic processes at depth, a detailed geochemical investigation is required in order to understand which elements are causing the patterns recorded in the compositional zoning. An assessment of the petrogenetic significance of the elemental variation may then be done. This chapter deals with the assessment and interpretation of the geochemistry of the ROMG titanites. Titanites from each of the main textural enclave/host groups will be assessed in turn. The focus will be on those elements within titanite that are considered relatively immobile with respect to post-magmatic processes, namely the REE and HFSE.

4.1.1 Analytical methods

Geochemical analysis of titanites was undertaken by electron microprobe analysis (EMPA), a highly precise method of quantitative elemental analysis that employs a focused incident beam of electrons in order to generate X-rays with energies and wavelengths specific to each element within the sample.

The analytical work was carried out at The Electron Microprobe Unit at the Grant Institute for Earth Sciences at the University of Edinburgh and was achieved with great technical support from Dr David Steele. The EMPA unit employs a Cameca SX100 equipped with 5 vertical crystal spectrometers and a PGT Spirit energy dispersive analyser. The instrument operates under Windows 2000 and uses Cameca's PeakSight software.

Element analysis focused on the major constituents of titanite plus trace elements, especially rare-earths and high-field-strength elements. For details of elements analysed, calibration standards, operating conditions, detection limits and errors see Appendix C.

Calibration of the machine was checked using synthetic titanite standards provided by Dr Magne Odegard of the Geological Survey of Norway (Odegard, Skar et al. 2005). Two synthetic titanite standards were provided, one pure standard and one standard doped with trace elements in concentrations of 200ppm.

4.1.2 Titanite selection and spot analysis rationale

The rationale for crystal selection focused on making sure that at least one of every type of textural variation of titanite was included, and that titanite from each of the granite/enclave relationships was represented in the analyses. The idea was to cover as much of the crystallisation history of titanite from the ROMG as possible, with enough textural overlap to make connections between the record of compositional zoning preserved amongst all the crystals across all of the sample types.

The initial assay of the textural character of the titanites was done using backscattered-electron (BSE) image analysis of the titanites from the ROMG. This method allows compositional zoning based on atomic number to be viewed as grey-scale contrast images where areas with higher mean atomic number will appear brighter than areas with low mean atomic number. Since the compositional zoning in viewed in BSE image analysis is a direct reflection of the mean atomic number, the brighter zoning in titanite is inferred to have a higher concentration of heavy elements. Titanite has the ability to incorporate large amounts of trace elements in its crystal structure, especially the rare-earth elements (REE) and high-field-strength elements (HFSE) which all have very high atomic numbers compared to the major elements of titanite (Ca, Ti, Si).

The working assumption with respect to compositional zoning of titanite, when seen in backscattered electrons, is that the differences in contrast intensity are a direct correlation of concentration of trace elements with a high atomic number. The differences in brightness of the zoning relates to differences in trace element concentration, which in turn is a function of melt characteristics, petrogenetic processes, partitioning behaviour of the elements between crystal and melt, and post-magmatic processes. Correlation of the geochemical trends to the variety of textural zoning should help to identify the significance of the processes, magmatic or otherwise, that operated during genesis of the titanite. As such, selection of areas for EMPA analysis was focused on choosing specific compositional zones across each titanite to be analysed. The strategy employed a much focused approach to zone sampling rather than simply performing traverses across the

grains. By choosing each compositional zone to spot analyse, the major differences between the different types of zoning could then be assayed.

Initially, two spot analyses were performed per compositional zone. This was done in order to make sure that the geochemical results were consistent within zones that appeared to be homogenous. It was quickly ascertained that the results were consistent and this double spot analysis approach was abandoned. Where there are two spots analyses per zone, it means that those titanites were analysed early on.

The spot analyses were all done using a focused beam with a diameter of 1μm. This ensured a very high degree of resolution, which is desirable as some of the compositional zoning is very fine in scale. Where the compositional zoning was too fine to be resolved accurately with a 1μm beam, a larger defocused beam of either 10 or 20μm was employed. The instances where a larger defocused beam was used generally relate to analysis of magmatic oscillatory zoning, which can be extremely fine-scale and rhythmic. A defocused beam of a large diameter can produce an average of the fine-scale zoning geochemistry, so that the overall character of the oscillatory zoning can be made when the differences between oscillations are too fine to resolve analytically. It is clearly noted when larger spot sizes are employed.

Zoning that is related to crystal chemical effects which deviate from mineral-melt partitioning behaviour, such as sector zoning, has been largely ignored in order to make sure the chemical variation being scrutinised is related to titanite partitioning behaviour and petrogenetic processes. Where sector zoning has been sampled, it is assayed in terms of the findings of Paterson and Stephens (1995) who have studied sector zoning in titanite and its origins.

Titanite is considered a refractory mineral which resists diffusion of trace element within its lattice (Cerny and Rivadisa.L 1972; Oberti, Smith et al. 1991; Clarke 1992; Deer W.A. 1992; Paterson and Stephens 1992; Enami, Suzuki et al. 1993; Cherniak 1995; Piccoli, Candela et al. 2000; Tiepolo, Oberti et al. 2002; Prowatke and Klemme 2003). The zoning preserved in titanite which is demonstrably magmatic should therefore represent the changing melt conditions during crystallisation. Where there has been sub-solidus alteration, the textural character of the titanite zoning is different to magmatic zoning, and it is treated as such.

4.1.3 Displaying geochemical information

The method for displaying geochemical information focuses on the elements that play the largest role in producing the zoning visible in BSE: the trace elements, particularly the REE and HFSE. Initial assessments confirmed the importance of the REE and HFSE in producing the zoning in BSE, and the focus was firmly placed on these elements and their variation across zoning within crystals and between samples.

Titanite geochemical data is presented mainly by construction of multivariate element graphs showing the variation in different elements across the sample points for each titanite. The position of each spot analysis is displayed on a BSE image of each titanite, and these spot numbers correlate to the numbers on the X axis of the graph (X axis is named: point of analysis). All graphed data is displayed as cations per formula (cpfu) unit of titanite, based on a unit containing 24 cations, 39 oxygen anions and 1 OH molecule per unit. This method of calculating cpfu for titanite (based on 38 oxygens and 2 OH/F), was proposed by Dr David Steele (University of Edinburgh EMPA unit) as it takes into account the presence of volatiles (water, OH and F) in titanite, which can occur in total concentrations up to 2%, since water is impossible to quantify (Groat, Carter et al. 1985; Perseil and Smith 1995).

Another method of presenting data includes construction of bivariate plots of (Ce+Nd) against Y. This plots creates an approximation of the slope of the REE and uses Y in place of the HREE, knowing that its behaviour can proxy for Ho in a number of geological environments (Della Ventura, Bellatreccia et al. 1999). Changes in REE slope may be detected from these graphs reflecting relative depletion or enrichment of the LREE versus the HREE. Such changes generally occur due to open system processes whereby melt composition can be affected by outside sources; examples of such processes include magma-mixing and partial melting of crust. Similar REE slopes between textural zones in titanites or between rock samples would indicate a closed system process in dominant, such as fractional crystallisation (Sawka, Chappell et al. 1984; Lloyd, Edgar et al. 1996; Kuscu and Floyd 2001; Tiepolo, Oberti et al. 2002; Prowatke and Klemme 2003). These plots should help to differentiate between the main end-members of the ROMG rock suite, as the REE signature and slope of the granitoids should be different from the mafic enclaves (Didier and Barbarin 1991).

Table 1 below, shows the main trace elements which were employed to geochemically characterise the ROMG titanites. This list is not exclusive of the elements analysed,

although it contains the elements that display the most significant concentration and/or variation linked to compositional zoning across all samples. All values are in cations per formula unit (cpfu) based on a titanite formula with 24 cations and 40 anions (38 oxygen and 2 OH/F).

Element	Average	Max	Min
Al	0.356	0.895	0.233
Fe	0.359	1.187	0.098
Nb	0.035	0.448	0.003
Zr	0.019	0.498	0.006
La	0.028	0.068	0.003
Y	0.051	0.298	0.011
Ce	0.099	0.230	0.003
Pr	0.015	0.041	0.008
Nd	0.055	0.173	0.022
Sm	0.010	0.040	0.004
Gd	0.009	0.049	0.004
ΣREE	0.188	0.493	0.006

Table 1: Minor and trace elements from the ROMG titanites which are most useful for interpreting compositional zoning, with minimum, maximum and mean values. Values are in cpfu.

4.2 Caveats

The interpretation of the geochemical signature retained by compositional zoning of titanite may be straightforward enough if it is used to say something about the crystallisation history of titanite itself, however, it may be more difficult to ascertain whether or not the record of compositional zoning in the titanite is an absolute direct reflection of the changing melt characteristics, or whether there are other factors at work that have contributed to the chemical signature of the crystal.

Partitioning of trace elements between titanite and melt is a very important factor in the nature of compositional zoning that will develop in titanite. The partitioning behaviour of the trace elements with respect to titanite and melt should be well constrained in order to interpret the compositional zoning. This study relies on partition coefficients for titanite as reported by other workers in the literature, since it was not possible to work out titanite-melt partition coefficients for the ROMG (there was no whole rock geochemical information, nor was there geochemical information for the paragenetic suite of minerals in the ROMG rocks). Therefore, the following assumptions have been made in order to interpret the geochemical signature of the compositional zoning in titanite:

- The paragenetic suite of minerals in the rocks is assumed to have had a negligible effect on the partitioning behaviour of the trace elements with respect to titanite. Where there is crystallisation of REE rich minerals, such as allanite, proximal to titanite, these titanites will not be used for geochemical analysis.

- The geochemical signature of the compositional zoning of titanite is assumed to partly be a direct reflection of the melt chemistry and processes governing the melt, and partly a reflection of the titanite-melt partitioning behaviour of the trace elements with respect to titanite alone.

4.3 ROMG geochemistry overview

Before looking at detailed geochemical results for each of the titanites selected for analysis, it is worth exploring the general geochemical variations that exists in the ROMG titanites. The approach will be a very broad overview of the geochemical variation of titanite in the context of the rock type that the titanites came from. Titanite will be related to one of three main members of the ROMG suite of rocks: granitic host rocks, dioritic enclaves, or mixed/hybridised rocks, based directly upon which rock type the titanite was found in. Some graphs will display information garnered from the whole dataset, with titanite analyses from different rock samples being placed into one of the three main categories of rock type (granitic, dioritic, mixed/hybridised), while other graphs will only consider titanite analyses from particular rock samples that best represent the end-member and mixed lithologies. This will allow both a broad, whole dataset overview as well as a more focused look at titanite from the best sample representative of each rock type.

It is unfortunate that there are no accompanying whole rock analyses for the different lithologies sampled from the ROMG. Thus, it makes it difficult to graphically analyse the general trace element variation across rock type, as can be done with Harker plots. This is why the titanites have been assigned to lithological groups which will be colour differentiated on bivariate or multivariate element diagrams. Trace element variation across the dataset will also be displayed on histograms showing maximum, minimum and average values for each lithological group

The bulk of the data will be presented in the form of bivariate plots of key trace element pairs, or key major and trace element pairs. The behaviour of the REE will be the main focus; however, there will be some exploration of variation of La with respect to the other rare-earths, and some exploration of Zr, Fe and Al behaviour. Some graphs will be comprised of summed data from a group of elements plotted against summed data from another group of elements; this will be done when investigating coupled substitution mechanisms. Most data will be displayed as weight-percent oxides; however, some data will also be displayed as cations per formula unit (cpfu) especially the plots investigating substitution mechanisms.

4.3.1 Trace element histograms

The average, maximum and minimum trace element contents for each of the three main lithological groups have been worked out and displayed on histograms in order for simple visual comparison and overview.

What is immediately apparent is there isn't a great deal of variation between the main rock types with respect individual average trace element contents (see Figure 45A). One may assume that since trace elements generally tend to behave incompatibly with respect to minerals and melt, that the granitic rocks should have much higher average contents, but titanite is a mineral that readily accepts trace elements into its lattice and therefore no matter what the melt composition, it will tend to incorporate a high proportion of traces into its structure, unless there is another mineral co-crystallising and competing for the trace elements.

Eight out of the eleven trace elements displayed are present in slightly higher average concentrations in the granitic rocks compared to the dioritic rocks. Only Zr, P, and La exist in higher average concentration in dioritic rocks. Zirconium exists in very high concentration in diorite compared to both hybrid and granitic rocks, but this may be due to a small number of individual titanites (ESd1-36 in particular) having an unusually high concentration of Zr; however, this will be covered in detail later when individual titanites are looked at.

It is also apparent that the hybrid rocks do contain a high average trace element concentration, and with respect to La, Ce and Pr, display a higher average than that found in the granitic rocks. This is possibly due to the smaller number of titanites analysed for this rock type compared to the granitic and dioritic end members, but as will be shown later on in relevant plots, it is also a result of a smaller range of values than those found in either of the other rocks types.

The trace elements displaying the highest average concentration, across the board, in descending order are: Ce, Nd, Y, La and Nb. This prevalence of Ce and Nd and Y are used later to model the REE slope in plots of (Ce+Nd) vs Y, where Y is used as a proxy for the HREE.

Figure 45: Average (A), maximum (B) and minimum (C) titanite trace element contents for the main rock type samples from the ROMG. For graph C, the hybrid group values off the scale are: Y 0.346 wt% oxide; Nd 0.530 wt% oxide; and Ce 0.936 wt% oxide.
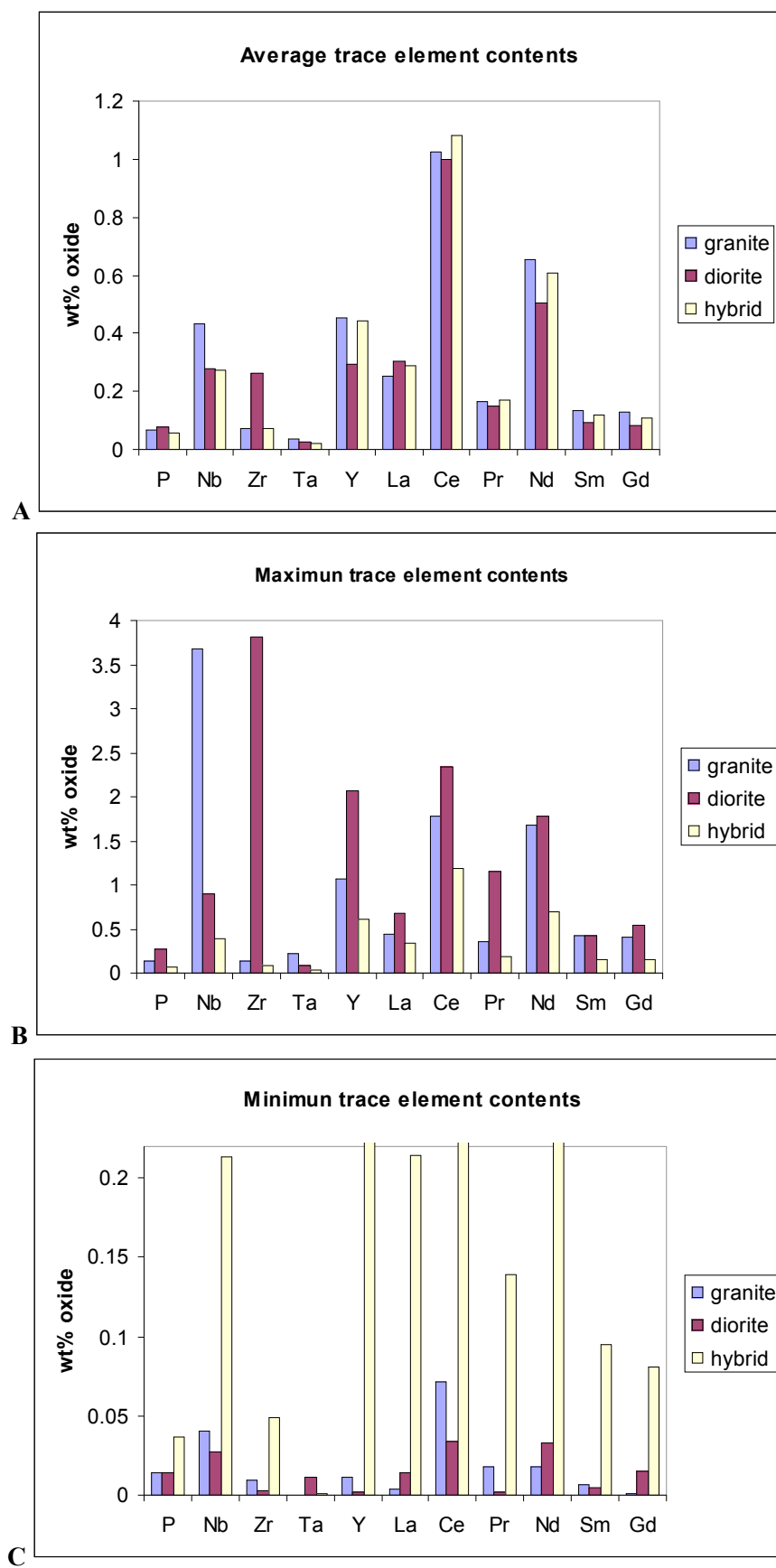
When looking at the maximum trace element contents (see Figure 45B) the very high values for Nb and Zr are immediately noticeable and one can see how these high values have had an influence on the average values in graph A. As mentioned with Zr, these anomalously high values will be addressed late in the chapter when individual titanites are looked at.

While nine out of the eleven average trace element concentrations have higher values in the granite group, eight out of the eleven maximum trace element concentrations belong to the diorite group (see Figure 45B). It would appear as though titanite from dioritic rocks have recorded a larger range of trace element concentrations; this is also obvious when taking into consideration the minimum versus maximum values for dioritic and granitic rocks, especially the values for Ce, Y, Pr and Nd. The highest overall minimum values reported are from the hybridised rocks, with some values orders of magnitude higher and indeed off the graph. These very high minimum values are also a reason why the hybrid rock group seems to have such high average trace element values in comparison to the others.

Since the hybridised rocks are formed from the near complete chemical and physical mixing of granitic and dioritic end-members, it is not surprising that there is a smaller range of trace-element values (compare graphs B and C). The thorough mixing and hybridisation of two contrasted magmas will enhance the likelihood that a homogenised liquid will result, and as such, equilibrium crystallisation is far more likely to occur. If there was little or no titanite growth in the respective granitic and dioritic end members prior to hybridisation, then the crystals growing in the homogenised melt will be more likely to have grown under equilibrium conditions and produce crystals that are less chemically zoned. This will be touched upon in later sections of this chapter when titanites from the hybrid rocks are analysed in detail.

When considering the high values for average and max trace element content of the diorite group, a possible explanation for the high values may come from considering the nature of trace element transfer that may result from mingled rocks. Diorite group analyses are from rocks which are either enclaves in granitic host rocks or they are from a synplutonic dyke. The majority of the analyses come from enclaves and hence, it is entirely possible that these enclaves have had their trace original element signature enhanced due to diffusion of elements from their granitic host rocks. Granitic rocks tend to be enriched in trace elements, especially the REE, as these elements are largely incompatible in behaviour, so it

stands to reason that a concentration gradient may exists between the enclaves and their host rocks, promoting diffusion from the granite to the enclaves. Furthermore, these same elements are compatible with titanite, so any titanite crystallising in the enclaves will be readily taking in trace elements from the enclaves melt pockets during early growth, with later growth possibly benefiting from host rock contamination. Such contamination may be able to be detected if the cores and early zoning in the enclave titanites have different trace element signatures to their rims and later growth. These factors will be explored later during individual titanite analyses.

4.3.2 Bivariate and multivariate element plots

The key major and trace elements in titanite display variation that is related to coupled-substitution mechanisms by which they are incorporated into titanite, however, there may be other co-variation patterns that are not expected. Thus, a range of bivariate and multivariate plots have been constructed for key pairs of elements to assay potential co-variation across the lithologies.

4.3.2.1 Fe and Al variation

Due to their key role in coupled substitutions, and also because they are generally the constituents in titanite which usually are highest in concentration after Ti, Ca and Si, the behaviour of Al and Fe will be explored first.

Fe and Al are both known to participate in coupled substitutions in titanite and they predominantly replace Ti at the octahedral site. Ferrous iron tends to substitute at the sevenfold-coordinated site normally occupied by Ca. (Gromet and Silver 1983; Green and Pearson 1986; Oberti, Smith et al. 1991; Deer W.A. 1992; Cerny, Novak et al. 1995; Piccoli, Candela et al. 2000). Figure 46 displays bivariate plots for Fe^{3+} and Al with respect to Ti (graphs A and B), and also with respect to each other (graph C). As can be seen from graphs A and B, there is generally a good correlation between Ti and Fe and Ti and Al. The relationship is of an inverse nature, which is to be expected since the elements replace each other in the titanite structure. There isn't much differentiation between the granitic titanite and the dioritic titanite with respect to Fe and Al's co-variation with Ti. There is a slight clustering of both Fe and Al values for dioritic titanite at the lower left hand side of the slopes in Figure 46A and B, suggesting that slightly less incorporation of the two elements into the enclaves than the granite host rocks. The hybrid rock titanites show a smaller range of Fe and Al variation with respect to Ti, although the points plotted seem to suggest a similar inverse correlation.
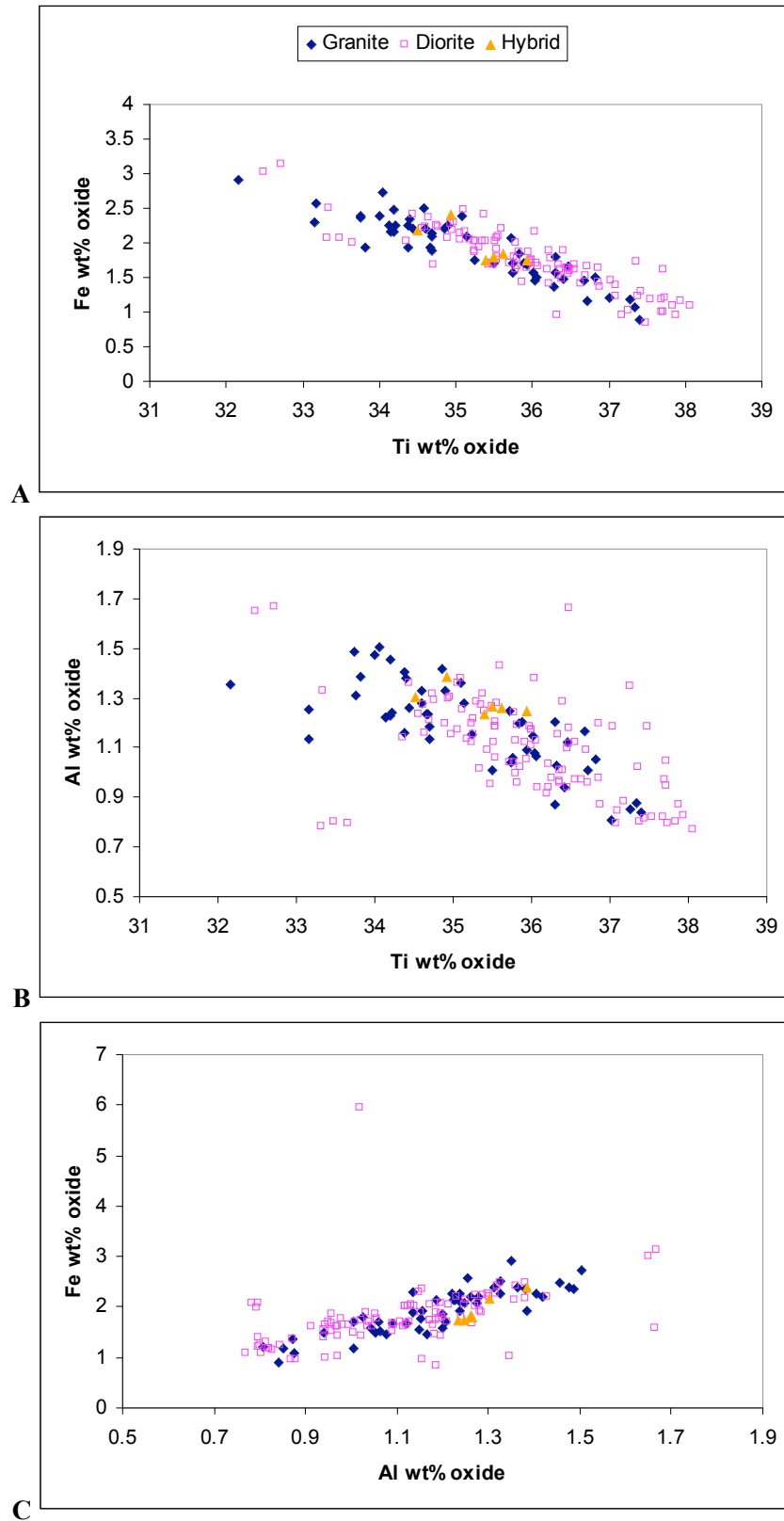
Figure 46: Bivariate plots of (A) Ti vs Fe; (B) Ti vs Al; and (C) Al vs Fe, for titanites from the main ROMG lithological groups.

Figure 46C shows the co-variation of Fe and Al, and it is clear that these two elements behave similarly in the ROMG titanite population. The roughly linear trend indicates that these elements do participate in similar substitution reactions, of which the most common are:

$$Ca^{2+} + Ti^{4+} \leftrightarrow REE^{3+} + (Al, Fe)^{3+} \quad \text{(Green and Pearson 1986; Enami, Suzuki et al. 1993)}$$

$$(Al, Fe)^{3+} \leftrightarrow Ti^{4+} + (OH, F)^- \quad \text{(Franz and Spear 1985)}$$

$$2Ti^{4+} \leftrightarrow (Nb, Ta)^{5+} + (Al, Fe)^{3+} \quad \text{(Cerny, Novak et al. 1995; Vuorinen and Halenius 2005)}$$

$$2\,Ti^{4+} \leftrightarrow (Al, Cr, Mn, Fe)^{3+} + Sb^{5+} \quad \text{(Perseil and Smith 1995)}$$
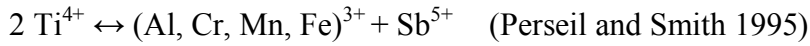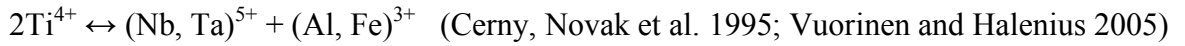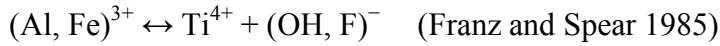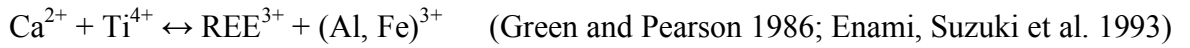
4.3.2.2 Zr and Y variation

These two trace elements participate in coupled substitutions, with Y replacing Ca and Zr usually replacing Ti. Below are some examples of the main substitution schemes known.

$$Ti^{4+} + Al^{3+} \leftrightarrow Zr^{4+} + Fe^{3+} \quad \text{(Seifert and Kramer 2003)}$$

$$Ti^{4+} \leftrightarrow Zr^{4+} \quad \text{(Della Ventura, Bellatreccia et al. 1999)}$$

$$Ca^{2+} + Ti^{4+} \leftrightarrow Y^{3+} + (Al, Fe)^{3+} \quad \text{(Green and Pearson 1986; Enami, Suzuki et al. 1993)}$$
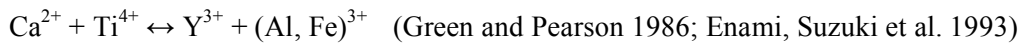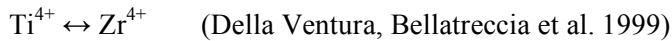
Below is a bivariate plot of Ti and Zr.
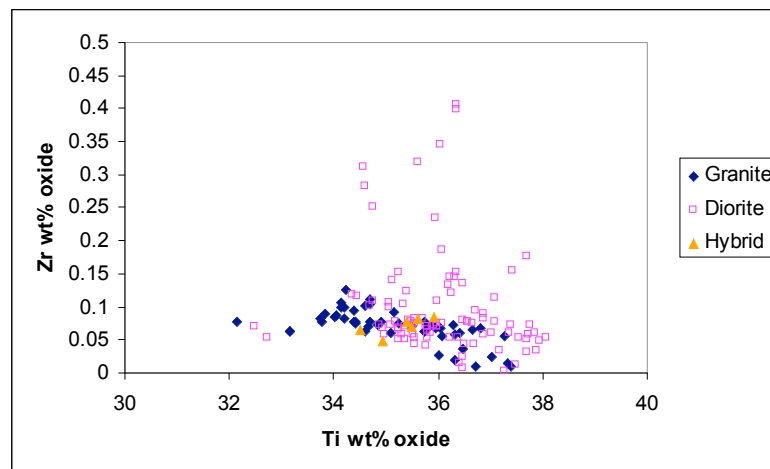
Figure 47: Bivariate plots of Ti vs Zr for main ROMG lithologies.

Figure 47 shows a very rough correlation between Ti and Zr, with the relationship being an inverse one, as expected from two elements that substitute for each other in titanite. The correlation isn't as good as expected, and there is considerable spread with respect to analyses from dioritic titanite. Some of the titanites from samples of diorite synplutonic sheets have extremely high concentrations of Zr. The nature of the compositional zoning that is associated with the Zr looks like it may be produced by late stage magmatic fluids. It is known that F forms complex ligands with REE and Zr, and late stage fluids enriched with these elements may readily react with titanite since titanite can accommodate them in

its structure (Della Ventura, Bellatreccia et al. 1999; Seifert and Kramer 2003; Seifert 2005; Cherniak 2006). This could explain the unusual spread in values associated with the dioritic rocks. More evidence for this will be looked at when individual titanite analyses are looked at.

Y is a high-field-strength (HFSE) trace element that mirrors the behaviour of the heavy rare-earth elements (HREE) in titanite. It has the third highest average concentration of all the trace elements in titanite from the ROMG, with only Ce and Nd in higher average concentration (see Figure 45A). This element replaces Ca and one would expect a fairly decent correlation between the two elements. Figure 48 sows that there is a roughly linear trend, with the Ca and Y showing an inverse relationship, however, there appears to be some flattening, and perhaps curving, of the dataset where Ca values are high.
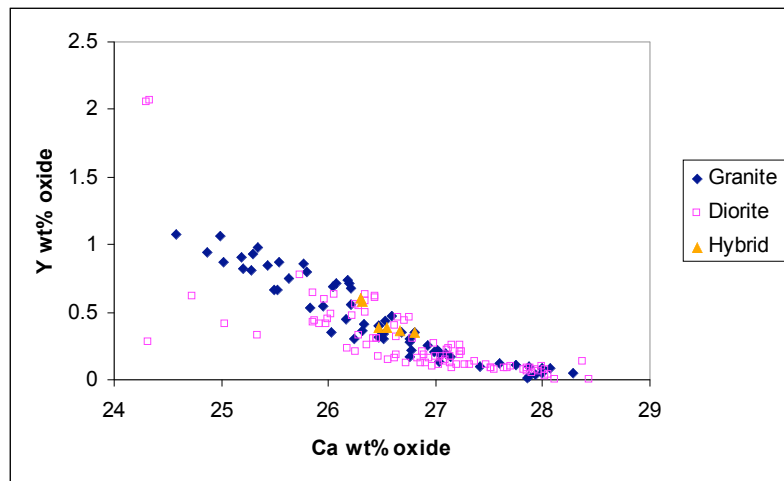
Figure 48: Bivariate plot of Ca vs Y for main ROMG lithologies.

The diorite titanites, for the most part, tend to form a cluster at the lower end of the curve, relating to lower values of Y and higher values of Ca. There are some erratic data points for diorite titanite that do not display a linear co-variation. The granite titanites show a range that is more consistent than the diorite titanites and with a significant group of points that correlate to higher values of Y and lower values of Ca. This could be due to a higher proportion of trace elements being concentrated in the granitic magmas compared to the dioritic magmas. The hybrid rock titanite plots in the middle of all the data, which is unsurprising considering it is a mixture of the granitic and dioritic Y signatures.

Since Y is known to behave in a fashion similar to the HREE, it is worth noting how this high-field strength element varies with respect to the light and medium rare-earth elements, especially since none of the heavy rare-earths were measured in this study. Below are two

diagrams that show the co-variation of Y and a range of rare-earths, one representing granitic rocks and the other representing dioritic rocks.
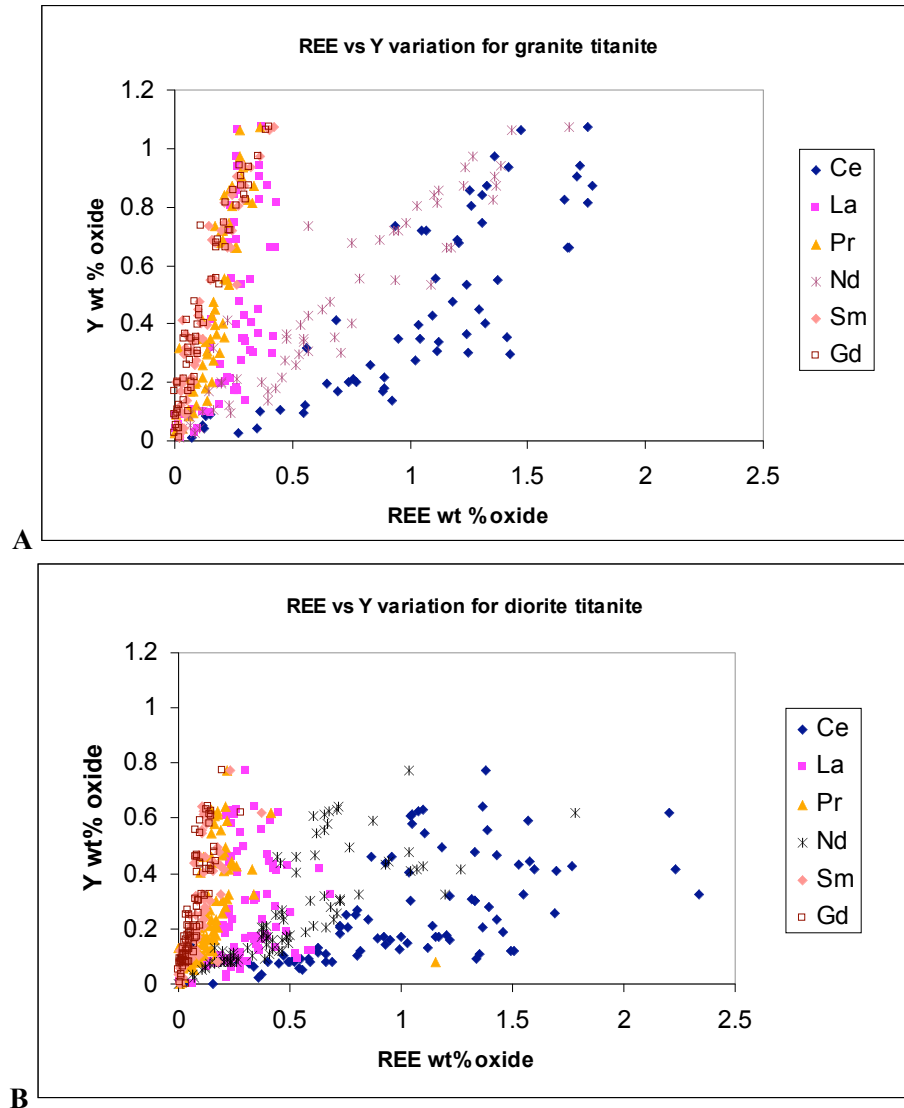
Figure 49: Multivariate plots of various REE vs Y for the ROMG end-member lithologies; granite titanite (A) and diorite titanite (B).

The medium rare-earths (Gd, Sm) and Pr seem to show a more linear correlation with Y than do La, Nd and Ce, and this may be related to the fact that Y is more similar in size and charge to the medium than the light rare-earths.

There is considerable spread with respect to Ce and Nd. Ratios of Y/Nd and Y/Ce tend to be greater than 1, whereas ratios of Y to the other rare-earths tend to be less than 1. The diorite titanites show a larger spread of data for each REE/Y dataset, whereas for granite titanite there seems to be less spread for each REE/Y dataset.

4.3.2.3 Rare-earth element variation

The trace elements that exist in the highest average concentrations in titanite form the ROMG are the rare-earth elements (REE), especially the light rare-earths La, Ce and Nd. Ce is especially prevalent in the ROMG, and has an average concentration that is nearly twice the average of the next most concentrated rare-earth element (Nd) in the ROMG (see Figure 45A). These elements play key roles in this study, since they are the elements that are incorporated into the titanite lattice as substituents that may record changing magmatic conditions. Different magmas may have different REE compositions and titanites readily accept these elements into their lattice during crystallisation. Titanite resists diffusion of these elements out of its lattice, and so it can possibly retain a record of the REE signature of the magma it crystallised in. In order to get an overview of the behaviour of the REE across the different rock types in the ROMG, some bivariate and multivariate plots have been constructed. The REE substitute into the sevenfold-coordinated Ca site in the titanite lattice, and therefore the first plot explores the correlation between Ca and the sum of all the REE for the ROMG dataset.
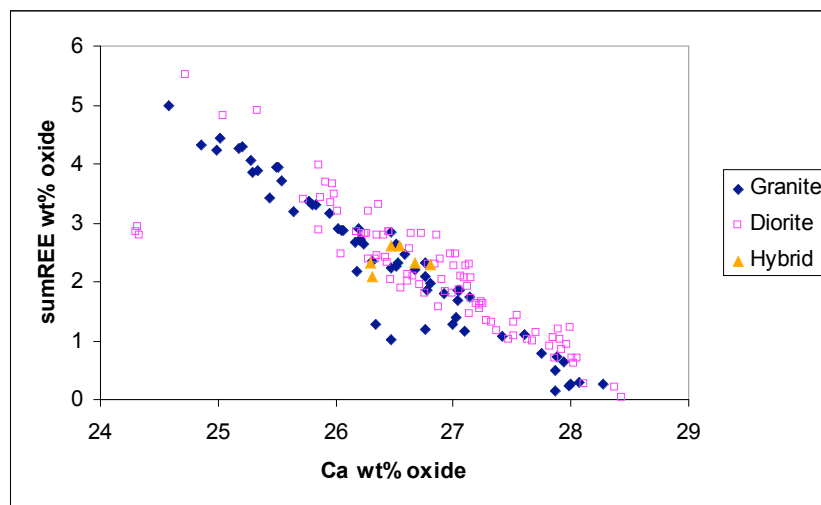
Figure 50: Bivariate plot of Ca vs sumREE for the main ROMG lithologies.

Figure 50 displays a very convincing linear correlation between Ca and the sum of the REE. Both the granite titanite and the diorite titanite display a large range in variation with a similarly small spread. Although there are some outlying points, the general trend for both groups of titanite is broadly similar; the only main differences being that the diorite titanite seems slightly more clustered in the middle and lower left of the diagram, and overall the granite titanite exhibits a less spread along the line. The hybrid titanite, as expected, plots right in the middle of the trend, showing very little variation; this indicates that the titanites were likely growing in a homogenised magma under near equilibrium conditions.

Overall, the broadly inverse relationship is typical of a substitution relationship. The substitutions that incorporate REE into titanite tend to occur as coupled substitutions, and therefore a multivariate plot of all the substituents involved would be ideal to validate the linear correlation even further.

The plot below displays the main REE coupled substitution, $Ca^{2+} + Ti^{4+} \leftrightarrow REE^{3+} + (Al, Fe)^{3+}$ (Green and Pearson 1986; Enami, Suzuki et al. 1993), as a bivariate plot of the two groups of substituents. To garner a more focused insight into how the variation differs with respect to magma mixing, instead of plotting all titanite data grouped by source rock type, only data from the main end-member rock samples and the main mixed rock and hybrid rock will be used. The data is displayed as cations per formula unit instead of wt% oxides, as this allows for better modelling of the substitution scheme.
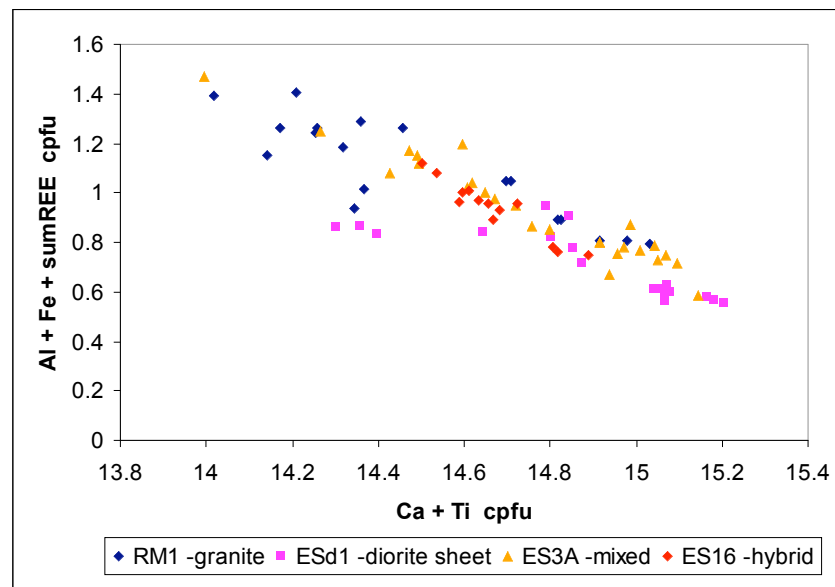
Figure 51: Bivariate plot of groups of substituents involved in the REE

The correlation between the two main groups of the reaction ($Ca^{2+} + Ti^{4+} \leftrightarrow REE^{3+} + (Al, Fe)^{3+}$) seems to be very good despite a few outlying points (see Figure 51). This plot show better differentiation between the main rock types than Figure 50 does. This is perhaps because there is a smaller amount of data used, and it is thus more focused, as it only contains the end-member rock types and the best sample of each of the mixed and hybrid rock types. The granitic titanite has higher concentrations of REE and Fe and Al than the diorite titanite does; both groups overlap but mostly occupy different parts of the trend-line. The mixed rock titanite covers the whole trend-line, which is expected since it is a combination of the chemical makeup of the granitic and dioritic rocks. The hybrid rock titanite occupies the middle of the trend-line, and this smaller range in plotted points is attributable to the fact that it is a homogenised rock that likely crystallised out titanite under near-equilibrium conditions.

If a plot is made of the Ca vs sumREE again (see Figure 52), but unlike in Figure 50, where the whole dataset from the ROMG is used, just the data from the two main end-member samples (RM1 -granitic; ESd1 -dioritic), and the main mixed/hybridised rock sample (ES3A and ES16) is used, then there is better differentiation of the data with respect to the provenance of the titanite. In this plot, the diorite titanite forms a smaller and tighter cluster on the trend-line. Again, there is overlap between the groups; the mixed rock titanite spans the whole range and the hybrid titanite occupies a tighter cluster in the middle of the trend-line, both as expected.
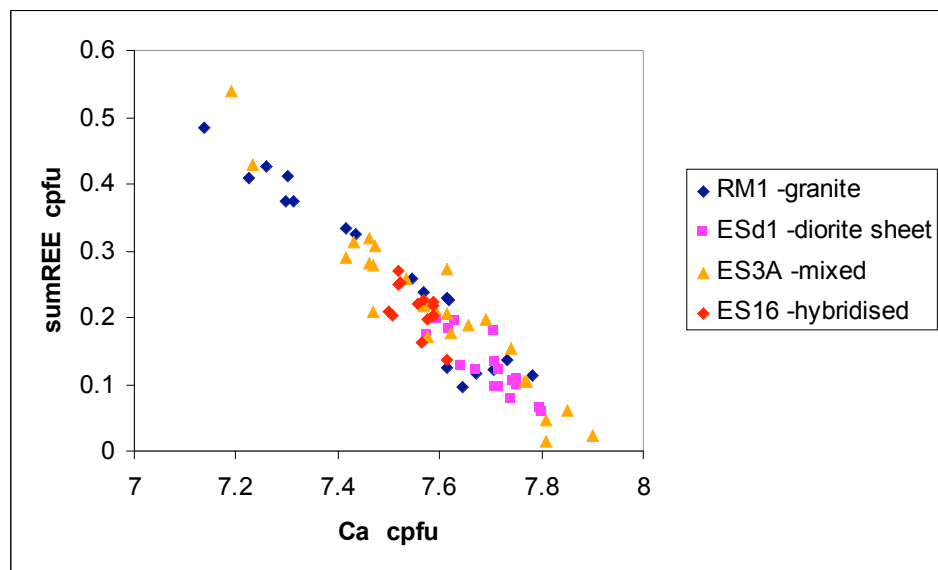
Figure 52: Bivariate plot for Ca vs sumREE for the main ROMG end-member lithologies.

4.3.2.4 La behaviour

Some initial assays of the geochemical data for individual titanites seemed to suggest that the behaviour of La was somewhat odd; it would be assumed that it should mirror the LREE in terms of incorporation into titanite, but it appears to be decoupled from the REE in general. Although this will be dealt with in more detail in the sections to come where individual titanites are analysed, it is worth initially investigating, and graphically displaying here, information from the main ROMG lithologies regarding the co-variation of La and the other REE.

The plots on Figure 53 show that there is no clear linear trend in co-variation between La and the other REE; only Ce shows a vaguely linear correlation (graph A). With respect to the different lithologies, there is some differentiation, although the patterns aren't very clear. The La/REE ratios would appear to be slightly higher for the dioritic rocks, which is.
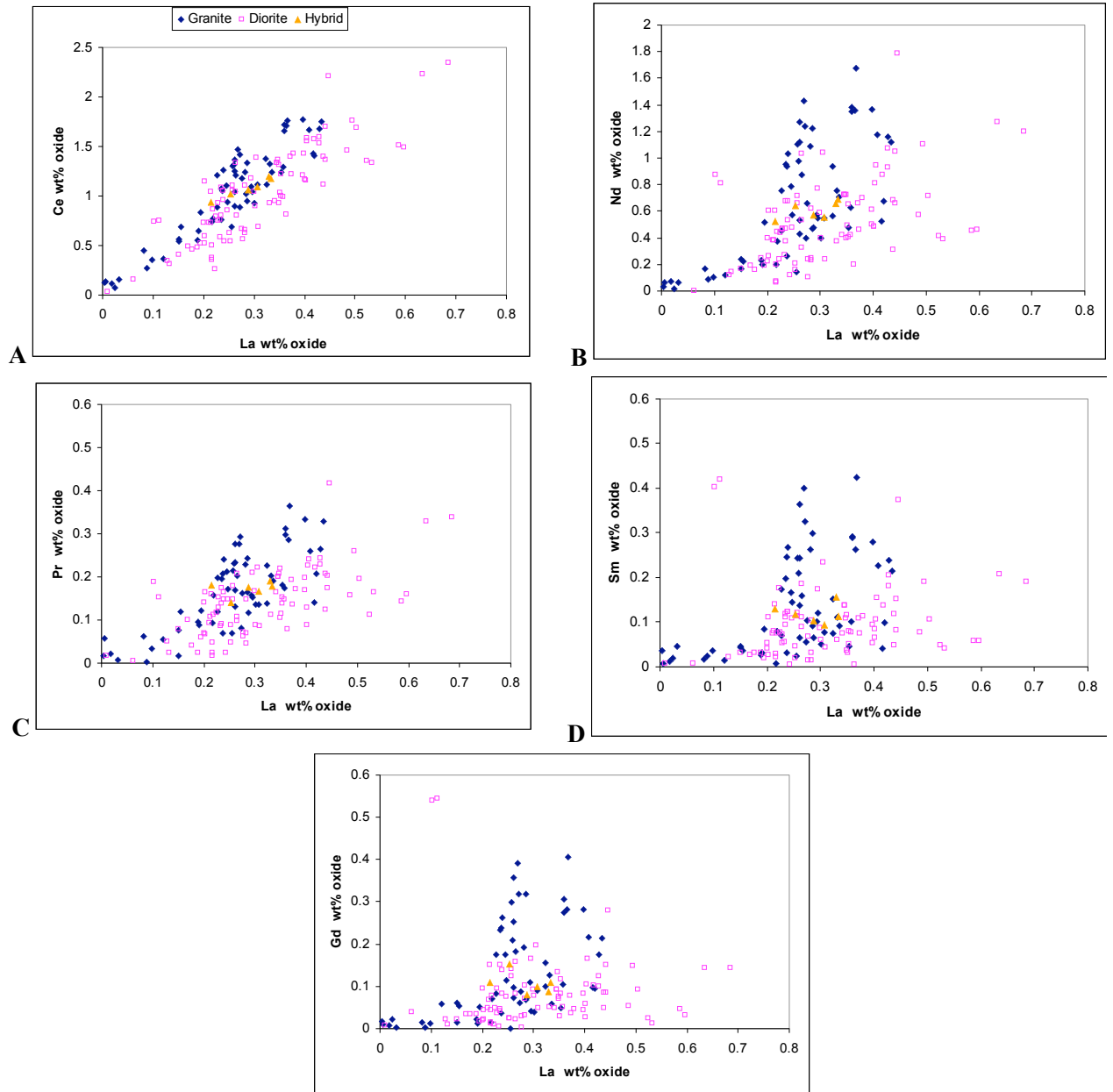
Figure 53: Bivariate plots of La vs other REE for the main ROMG lithologies. (A) La vs Ce; (B) La vs Nd; (C) La vs Pr; (D) La vs Sm; and (E) La vs Gd.

also correlated by the data given in Figure 45 for average trace element concentrations across the main lithologies.

The La/REE co-variation shown for the granitic titanite data is most similar between La/Sm, La/Nd and La/Gd; these all show a spread of data in the middle of the graph that lie away from the majority of the dioritic titanite data. As expected, and which has been a constant similarity amongst all of the data presented so far, the hybrid titanite data plots in a very small range that occupies an area overlapped with both granitic and dioritic titanite data points. Again, the chemical homogeneity of the hybridised rock, and the likelihood of near-equilibrium crystallisation conditions, has produced titanite with a small range of REE variation.

A more focused look at the co-variation of La and Ce, is shown below by Figure 54, a bivariate plot using only data from the four rock samples that best represent the lithologies typified by the ROMG suite: the end-members, RM1 (granite) and ESd1 (synplutonic diorite dyke), and ES3A (mingled/mixed rock) and ES16 (fully hybridised rock).
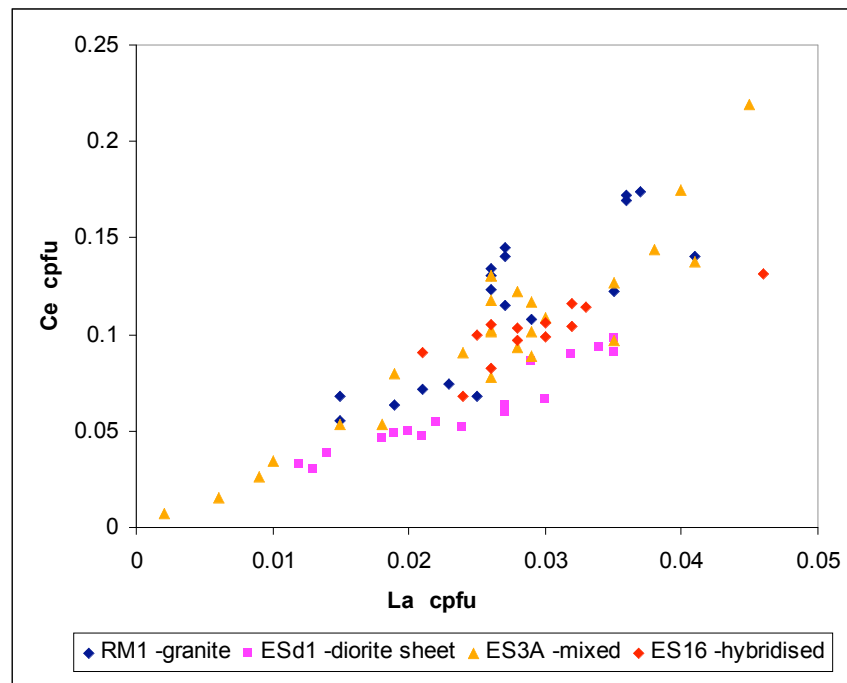
Figure 54: Bivariate plot of La vs Ce for the main end-member (RM1 and ESd1), mixed (ES3A), and hybrid (ES16) rock samples from the ROMG. All data is in cpfu.

The plot shows clearly the chemical differentiation between the main rock types with respect to La/Ce. The data points for the two end-members (RM1 and ESd1) are clearly differentiated and the mixed rock (ES3A) data plots mainly between the other two, albeit with a larger range in values along the vaguely linear trend-line. ES16, as always, has data that plots over a smaller range and sits within and between the ranges of the other 3 samples. Again, as shown by data on Figure 45A and Figure 53A, La is relatively enriched in the dioritic rocks with respect to Ce compared to the other main lithologies.

4.3.3 Summary

The main points derived from this initial overview of the geochemical variation displayed by titanite from the ROMG are:

- Average trace element contents are very similar for the three main lithologies (granitic host rocks, diorite enclaves, mixed-magma/hybrid rocks), with granitic titanite displaying slightly higher values compared to dioritic titanite for all elements except P, Zr and La.

- The trace elements with the highest average content in titanite, in descending order, are: Ce, Nd, Y, La, and Nb.

- The highest maximum trace element values reported are predominantly from dioritic titanite, with only Nb and Ta being reported as higher in granitic titanite.

- Hybrid rock titanite displays the smallest overall variation in trace-element concentration, and as such displays unusually high average concentration values when compared to granitic and dioritic titanite. Hybrid titanite also displays the highest values for minimum trace element concentration.

- Al vs Fe plots display good correlation, which indicates participation in similar coupled substitution reactions. These two elements replace Ti in titanite and when plotted against Ti, also display good correlation.

- Zr vs Ti plots display limited correlation, which is surprising since Zr replaces Ti in titanite. Zr vs Ti behaviour is most erratic in dioritic titanite.

- Y displays generally good correlation when plotted again Ca, as it substitutes for Ca in titanite. Ca vs Y plots show good differentiation between the main lithological groups, with Y being generally more concentrated in granitic rocks.

- Y vs REE multivariate plots show that there is good linear correlation with the MREE (Pr Sm and Gd), compared to the other REE. Most likely due to better similarity in size and charge.

- La displays behaviour that is relatively decoupled from the other REE; however, it displays some correlation with Ce behaviour. La tends to be more concentrated in dioritic titanite.

- Overall, trace element behaviour seems to be relatively differentiated between titanite from different lithologies, with bivariate plots of elements often displaying datasets from different rock types occupying shared and differentiated areas on the graph.

- Hybrid titanite, overall, displays a very limited range of trace element concentration and variability in the ROMG. The data for hybrid titanite often plots in the middle

of trend-lines defined by the two end-member lithologies, but is always within clusters of data points from the other two lithologies. This behaviour is attributed to the chemically homogenised nature of the rock, which is made up from the hybridisation of granitic and dioritic magmas, and also is attributed to crystallisation of titanite likely to be occurring under near equilibrium conditions.

4.4 ROMG titanite analyses and geochemistry

The following sections will deal with the analysis and geochemistry of titanites that best exemplify the textural populations found within each of the major sampled rock types from the ROMG pluton.

4.5 ESd1 (dioritic end-member)

The most mafic component of the ROMG is represented by the synplutonic dykes that cross-cut the other facies (see Figure 55). These are the points of visible input of mafic material and also are seen feeding zones of intense mingling and mixing between the various granites and mafic enclaves. This sample represents the mafic "end-member" and as such should have a geochemical signature that is sufficiently different to make it distinguishable from the rest of the co-genetic suite of ROMG rocks. The titanites within this rock are characterised by their anhedral/subhedral shape, most having crystal margins that are distinctly interstitial, indicating fairly late crystallisation.

**Figure 55: Synplutonic diorite sheet (sample ESd1) Erraid Sound Ross of Mull
(grid reference 30912 18910). Sheet is 134cm wide. Photo is west facing.**

4.5.1 ESd1-32

This titanite is the most euhedral example within ESd1, a microdiorite synplutonic dyke. It is just over 100μm long and has an irregular interstitial crystal margin despite displaying an overall good crystal shape. The zoning (viewed in backscattered electrons, BSE) is fairly simple; a bright core succeeded by a darker mantle and finally a bright rim. The margins of the zones are very straight and as such are indicative of magmatic zoning (see Figure 56**).**

The bright zones are richer in REE and the dark zones are more enriched in Fe and Al than they are in REE (see Figure 57A and 2B). Zr becomes steadily depleted towards the rims, as is expected due to its fairly compatible behaviour with respect to titanite in intermediate rocks (Prowatke and Klemme 2005). Nb and Ta follow the same pattern as the REE and in this case show the same type of compatible partitioning behaviour as the REE, being concentrated more in the core than in the rim (see Figure 57C). However, the pattern is not consistent from core to rim as the mantle portion (analysis points 3 and 4) of the crystal is dark and shows a lower concentration in both the REE and Nb and Ta compared to the rim (points 1 and 2).

(Ce+Nd) plotted against Y displays the approximated slope of the REE, with a fairly small spread in the overall change of slope (see Figure 57D). The textural groups of the titanite correspond to the pattern of core enrichment, mantle depletion and rim enrichment in traces. It is possible that the difference between the rim and mantle is indication of a change in melt late in the crystallisation history. Titanite ESd1-32 is interpreted as having a magmatic origin.

4.5.2 ESd1-15

ESd1-15 is over 200μm in length and is subhedral in shape with margins that are interstitial in character. The nature of the zoning seen is BSE is best described as patchy; none of the zoning boundaries display straight lines that would equate to crystal faces, but are rather very cuspate or irregular. The brighter zones tend to occur near the crystal margins and the darker zones dominate the interior. The overall texture suggests that the brighter outer margins are due to late (perhaps subsolidus) alteration (see Figure 58).

The central dark portion of this crystal has nearly three times higher concentration of Nb than does the lighter outer zone (see Figure 59A-C). The brighter zones have just less than twice the REE content than the darker zones. Nb is thought to be fairly incompatible with respect to titanite when compared with the REE (especially Gd, Ce and Pr) in dacitic and rhyolitic liquids, according to the liquid-solid partition coefficients worked out by Prowatke and Klemme (2005) and Nb should concentrate in the rims under normal crystallisation.. Zr is fairly incompatible and follows the trend of being about twice as
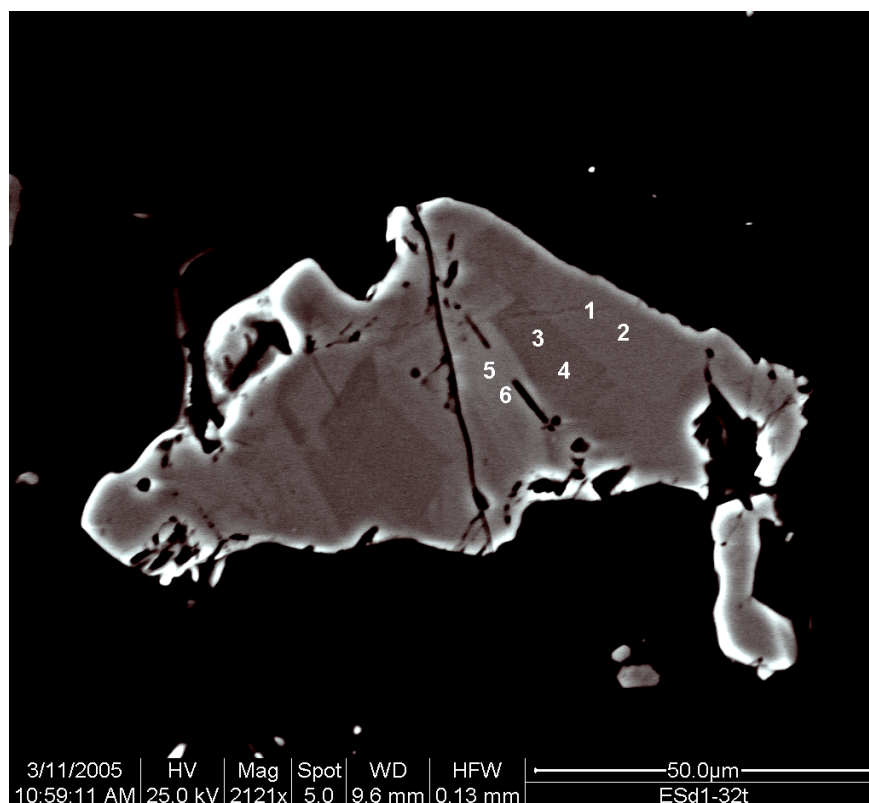
Figure 56: BSE image of ESd1-32 and sample point location
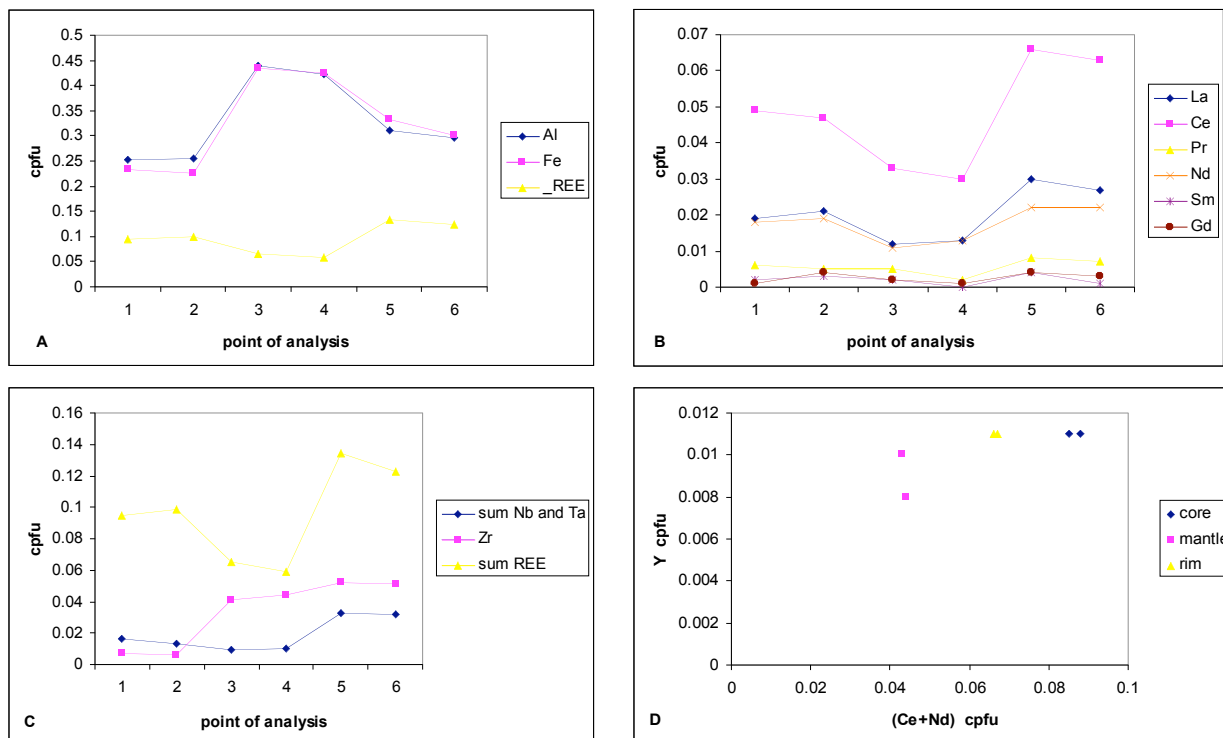
Figure 57: Geochemistry of ESd1-32. A. shows the variation of ΣREE, Al and Fe; B. displays the variation in individual REE and La; C. compares ΣREE to the HFSE; D. plots (Ce+Nd) again Y for the main textual groups of ESd1-32, the plot represents the approximated slope of the REE.
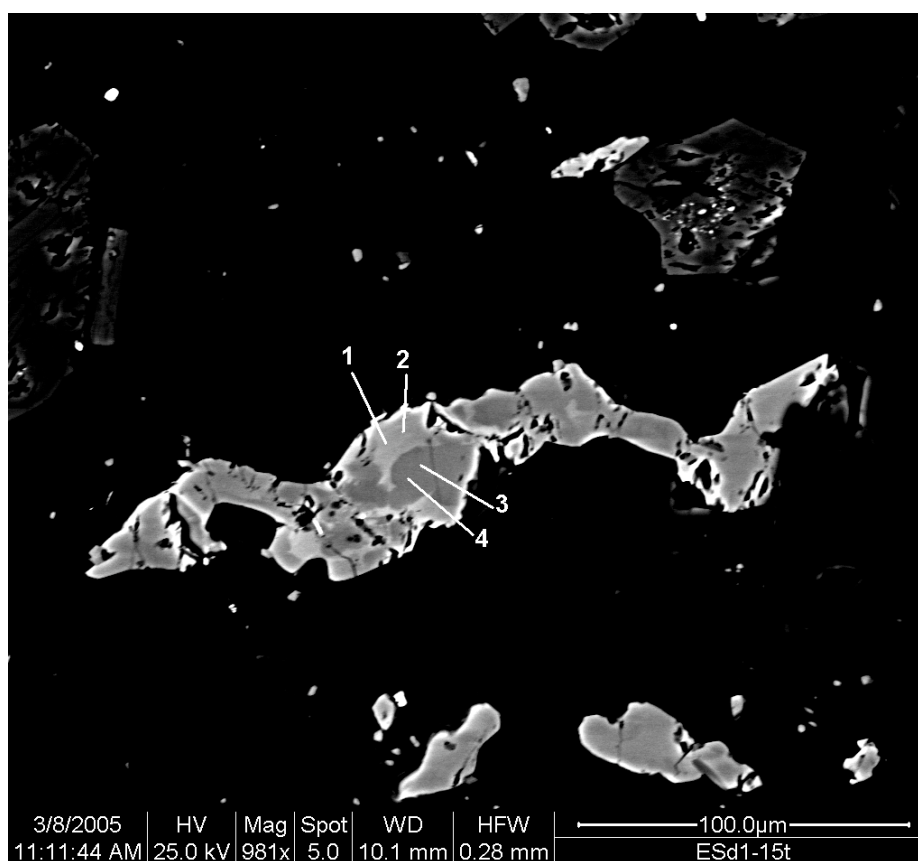
Figure 58: BSE image of titanite ESd1-15 and location of sample points
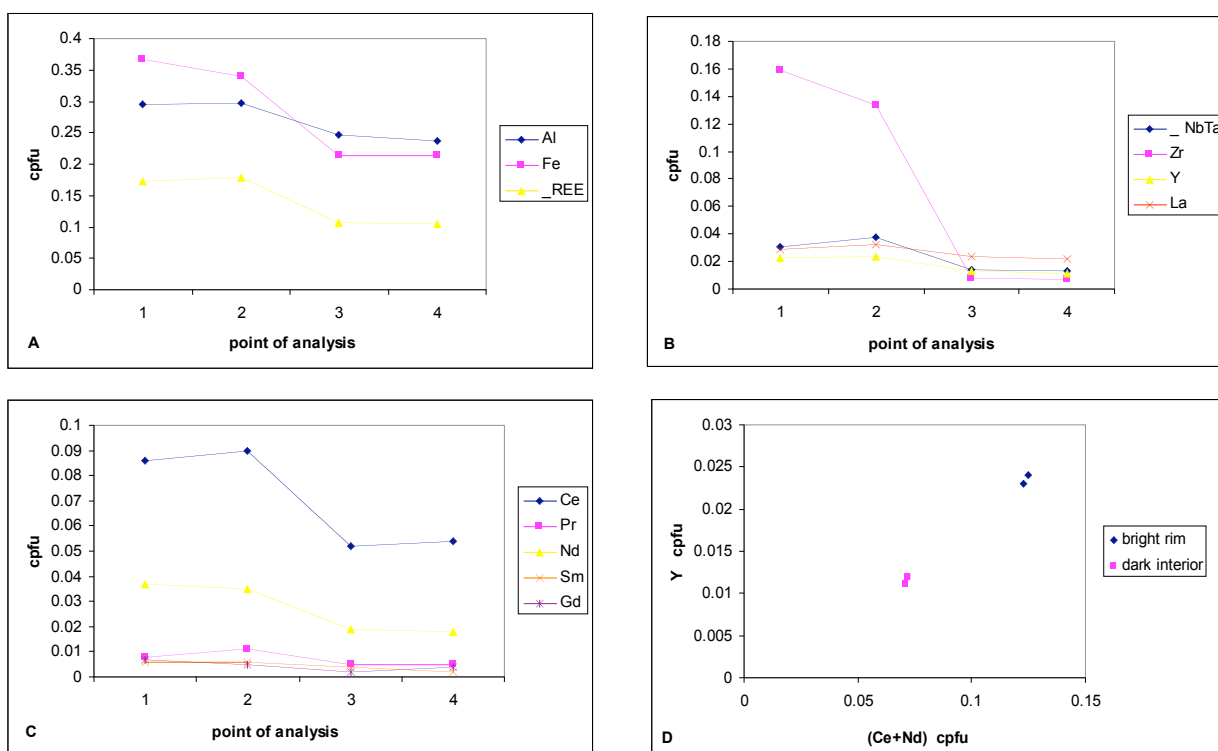
Figure 59: Geochemistry of ESd1-15. A. displays ΣREE, Al and Fe variation; B. displays the variation of HFSE; C. displays individual REE variation; D. plots Ce+Nd against Y (approximating the REE slope) for textural zones of the crystal.

concentrated in the rims/brighter zones, just like the REE. According to Prowatke and Klemme (2005), Zr partitioning is not affected by melt composition and in intermediate rocks should be slightly more compatible that the REE and in basic rocks should be more compatible. If the highest concentration of Zr in this crystal is compared with the highest concentration observed in ESd1-32 (which displays magmatic zoning) it is clear that the brighter outer margins of ESd1-15 has almost twice as much Zr, with 0.16 cpfu in ESd-15 vs. 0.057 in ESd-32.

The elevated concentration REE and HFSE, especially Zr, related to the bright patchy rims of this crystal would indicate a late alteration involving a trace element rich fluid has taken place. A plot of (Ce+Nd) against Y approximates to the overall slope of the REE for ESd1-15 and the difference in concentration of trace elements between the bright and dark zones of the crystal is clearly visible (see Figure 59D). The difference between the bright rim and darker core is perhaps related to contamination of fluids from the host granite brought about by the heat of the diorite synplutonic intrusion itself.

4.5.3 ESd1-36

Of the three titanites analysed from the diorite dyke, ESd1-36, is the largest (over 300μm) and has the most peculiar textural features relating to compositional zoning. It is best described as anhedral with protrusions from the rim; very is interstitial in texture. The crystal centre is fairly equant although there is no zoning that relates to the margins. Texturally, the compositional zoning observed in BSE is very patchy, with numerous bright patches, of no particular shape, seen in the darker more uniform zoning of the rest of the crystal. The bright patches are concentrated around, and seem to originate from cracks running through the crystal (see Figure 60).

Geochemically, this titanite is also very unique as it has the highest concentrations of Zr of any of the titanites analysed in the entire ROMG suite (see Figure 61B). The high Zr titanite is concentrated in the bright patchy zones in the centre of the crystal. Zr should not be affected by melt composition with respect to it's partitioning between solid and liquid (Prowatke and Klemme, 2005). Hence, its incompatible behaviour should indicate that these patchy zones are related to late stage alteration, where any remaining fluids are likely to be enriched in Zr. The only other fairly bright zone analysed is the interstitial protrusion of the rim (analysis points 6 and 7), where the ΣREE are in higher concentration than Zr
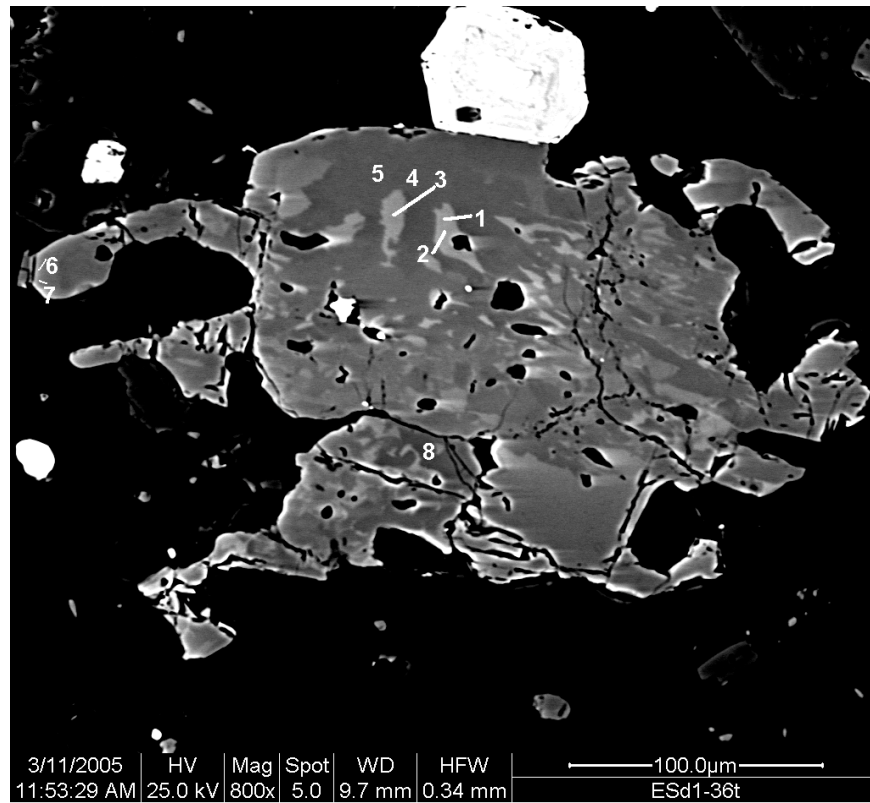
Figure 60: BSE image of ESd1-36 and location of sample points
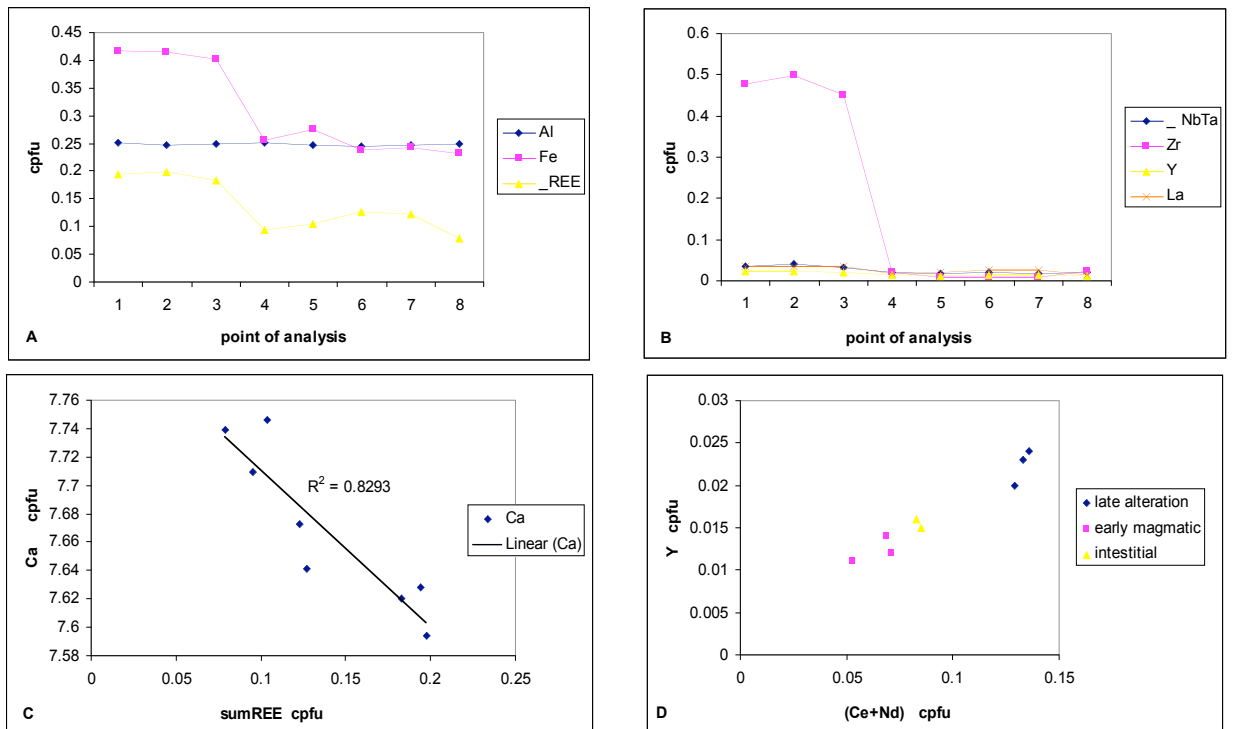
Figure 61: Geochemistry of ESd1-36.   A. Fe, Al and ΣREE variation. B. HFSE variation. C. Linear relationship between ΣREE and Ca. D. (Ce+Nd) vs. Y; represents the approximated slope of REE for sample ESd1.

(see Figure 61A-B**).** These points represent the largest difference between Zr and ΣREE concentration not including the late alteration zones.

There is reasonable correlation between the ΣREE and Ca, as can be seen by the graph in Figure 6C**,** where there is a good linear relationship, as expected from the known substitution mechanism: $Ca^{2+} + Ti^{4+} \leftrightarrow REE^{3+} + (Al, Fe)^{3}$ (Green and Pearson 1986).

When plotting (Ce+Nd) against Y, a reasonable linear relationship emerges (see Figure 61D). This plot represents the slope of the REE for titanite ESd1-36 and the three main textural groups of zoning (interstitial rim, magmatic and late alteration) form distinct groupings related to the magnitude of traces, although there is little change in the slope of itself. The (early) magmatic dark zoning has the lowest concentration of traces while the late alteration zoning displays the highest concentration of traces. The interstitial rim zone plots closer to the magmatic zone signature, suggesting an overall increase in the amount of traces available in the melt in the later stages of titanite crystallisation. This is likely to be related to slight contamination by fluids from the host granite that synplutonic dyke ESd1 intruded.

4.5.4 Summary of ESd1

Geochemically, there are two main groups that can be discerned from the analyses of the textural zones of the ESd1 titanites: a magmatic group and a late alteration group. Figure 62 below, is a plot of (Ce+Nd) against Y for all three titanites analysed, and it displays the approximate slope of REE for the dataset.
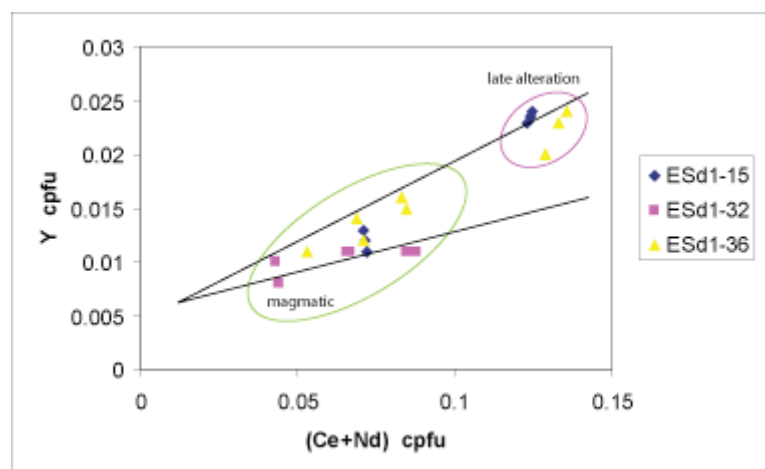
Figure 62: ESd1 total dataset; (Ce+Nd) vs Y (approximated slope of REE).

This plot clearly distinguishes the late alteration zoning from the magmatic zoning. There is also slight a change in slope associated with the late alteration. The most demonstrably magmatic of the crystals in ESd1-32, and bottom line is the REE slope of this crystal. The upper line is the REE slope of the textural zones relating to late alteration. The change in slope is most likely related to late alteration by fluids derived from the granite host which ESd1 intrudes. The late alteration is characterised by elevated Zr concentrations causing bright patchy zoning that is texturally related to cracks in the titanite, especially ESd-36.

4.6 RM1 (granite end-member)

RM1 is from the equigranular, quartz-rich, biotite monzogranite that forms the outer facies of the ROMG. It represents the most evolved rock of the whole complex and as such is the closest to a granitic "end-member". The titanites within this sample should give an indication of the type of geochemical signature expected to typify the more granitic rocks from the ROMG.

4.6.1 RM1-3

The overall shape of RM1-3 suggests that it is magmatic in origin; it has a good euhedral shape and the rim has margins that are straight and concordant with the internal zoning. Viewed in BSE, RM1-3 has simple zoning; a bright rim, less bright mantle and a darker outer rim. There is some sector zoning associated with the central long axis of the titanite. The inclusion of apatite would suggest that the crystal grew late. However, the overall euhedral shape and absence of interstitial rim features would also suggest that growth wasn't very late in the crystallisation process. The crystal displays some alteration to titanomagnetite along cracks proximal to where it abuts a magnetite crystal (see Figure 63).

The dark rim is characterised by low REE and Y concentration, this is a direct reflection of substitution (see Figure 64A-C). The rim has is slightly enriched in Zr and Nb compared to the mantle, this is to be expected based on the incompatibility of these two elements, however, the brighter central part of the crystal is characterised by higher concentrations of these two elements in addition to Ta. The brightest areas of the crystal in BSE imaging are linked to the highest concentrations of REE, and slightly lower concentrations of Al and Fe values show a similar pattern to each other as they both participate in the same coupled substitution mechanisms.
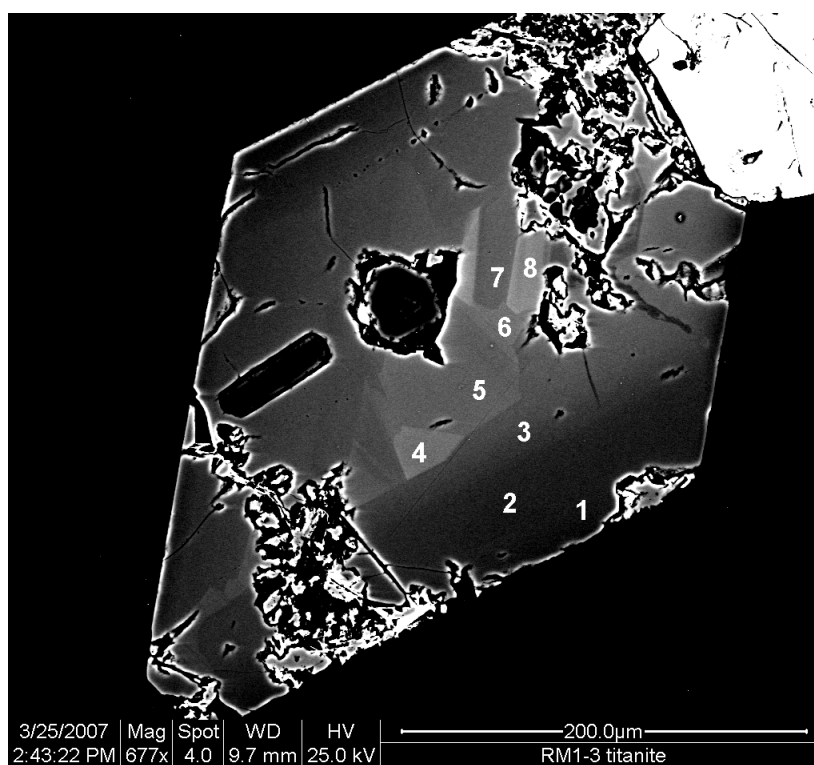
Figure 63: BSE image of RM1-3 and location of sample points.
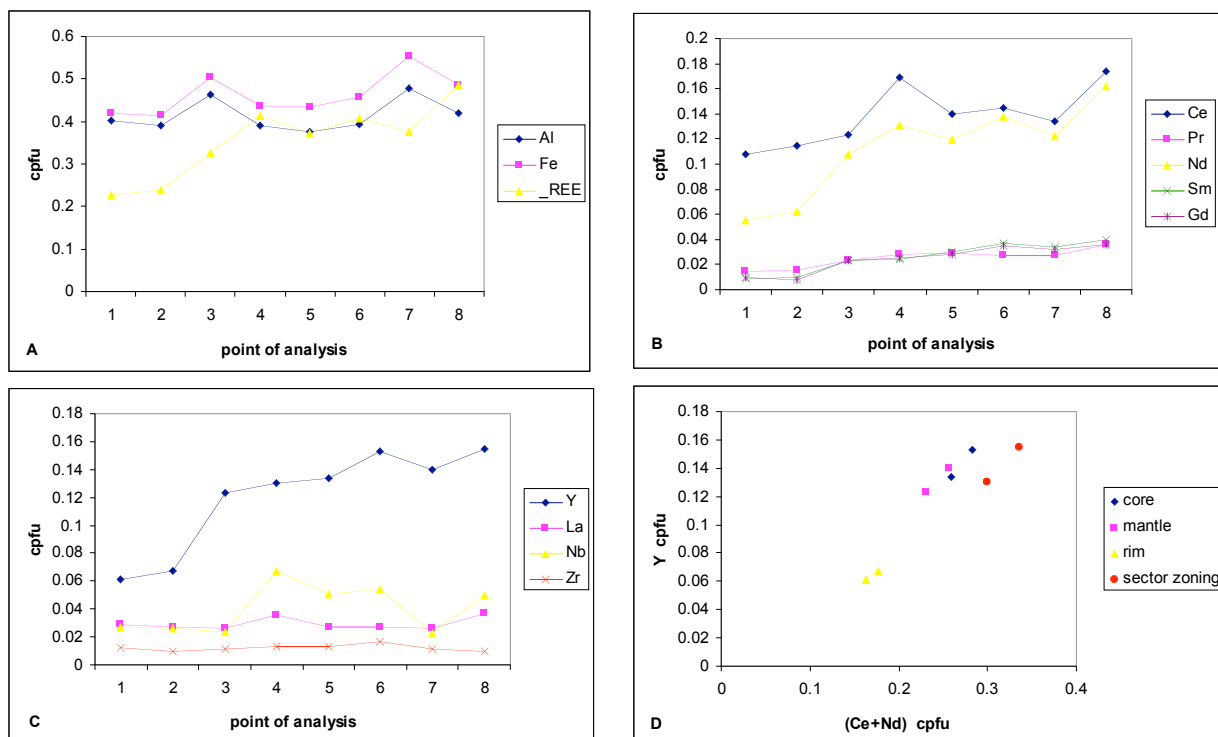
Figure 64: Geochemistry of RM1-3. A. Fe, Al and ΣREE variation across the crystal. B. REE variation. C. HFSE variation. D. REE slope approximation for textural groups of RM1-3, given by a plot of (Ce+Nd) against Y.

The pattern of variation displayed by the REE (see Figure 64B) is not uniform amongst the different REE, especially at analysis points 4 and 8. These analysis points are located on bright zones relating to sector zoning in the crystal. Certain crystal faces, namely the {111} face in titanite, preferentially incorporate trace elements that have equilibrium ratios greater than one; usually the REE, Y, and Nb (Paterson and Stephens 1992), and this is the likely cause for the elevated REE (especially Ce and Nd) and Nb values observed in the sector zones (analysis points 4 and 8).

(Ce+Nd) plotted against Y gives an approximation of the slope of REE for the crystal (see Figure 64D). The data set for RM1-3 creates a linear correlation that has very little spread in terms of REE slope. The main differences in REE slope are between the core and the sector zoning of the core area. The sector zoned portions of the crystal display a higher concentration of (Ce+Nd) compared to the rest of the core, which is to be expected since the sector zoning of the {111} crystal faces preferentially sequesters the REE.

This crystal can be summarised as follows:

- Core to rim REE pattern: high to low, suggests compatible behaviour.

- Core to rim HFSE pattern: high to low, suggests compatible behaviour

- Elevated trace element concentrations (especially Ce, Nd and Nb) of bright zones in the core are related to sector zoning.

4.6.2 RM1-7

The largest of all titanites from sample RM1, RM1-7 is over 1mm in length, euhedral in shape and displays excellent zoning in BSE. The centre of the crystal is characterised by bright zoning, including sector zoning along the long axis of the core. The bright core is mantled by a darker zone, which is uniform. This dark mantle is in turn succeeded by a thin, very bright inner rim that darkens towards the rim margin. The textural characteristics of RM1-7 are certainly magmatic (see Figure 65)

The REE are concentrated in the bright zones of the central part of the crystal (analysis points 6, 7, 8 and 9) while they are less concentrated in the dark mantle (analysis point 4), bright rim (analysis points 2, 5 and 10) and dark rim (points 1 and 3) (see Figure 66B-C).

Nb concentrations for the thin bright inner rim (analysis points 2, 5 and10) are extremely high, ranging from 0.245cpfu (analysis point 10) to 0.448cpfu (analysis point 5) (see Figure 66C). The average for the entire ROMG dataset is 0.038cpfu and there are only 8 out of a total of 234 data points that are over 0.100cpfu. For the same thin bright inner rim (analysis points 2, 5 and 10), Al and Fe both show a similar pattern of variation to Nb (see Figure 66A). These are matched by a corresponding drop in the values of Ti, whereas for the rest of the crystal, Ti otherwise follows the same trend in concentration as Ca (see Figure 66B). The substitution of pentavalent cations (like Nb and Ta) for Ti is charge balanced by additional replacement of Ti by Al and Fe, as show by the substitution mechanism: $2Ti^{4+} \leftrightarrow (Nb, Ta)^{5+} + (Al, Fe)^{3+}$ (Cerny, Novak et al. 1995). None of the other HFSE show such a pattern with respect to the thin bright inner rim, and in fact, the overall variation in Y and La for the whole crystal is more similar to that of the REE.

According to the titanite-melt partition coefficients derived by Prowatke and Klemme (2005) for intermediate to silicic melts, Nb should display compatible behaviour, albeit slightly less compatible than the REE. There is no evidence for a steady increase in Nb concentration from core to rim. Rather, there is a very large jump in concentration associated with the bright inner rim of the crystal, and the Nb concentration very rapidly decreases towards the outer margin of the rim. The subsequent rapid decrease would suggest that the Nb spike associated with the inner rim is not due to incompatible behaviour, if it was, then a steady increase in Nb towards the rim would be expected. The Nb spike associated with the bright inner rim is more likely due to a very late change in melt composition or the cessation of crystallisation of a phase that was previously sequestering the majority of the Nb in the melt. The likelihood is that the former situation is more plausible.

Plotting (Ce+Nd) against Y displays a reasonable linear trend that represents the slope of REE for the dataset (see Figure 66D). The dataset points are separated into textural groups which plot together. The outer core (analysis points 9 and 6) correspond to sector zoning and this explains the elevated (Ce+Nd), as sector zones tend to preferentially sequester the REE (Paterson and Stephens 1992). The bright rim (analysis points 5 and 10) plots off the trend line towards the Y axis. This is due to the relative depletion of REE compared to Y and the very elevated concentration of Nb. Such changes in the REE slope suggest that changes in the melt chemistry or key changes in the paragenesis have occurred. A single
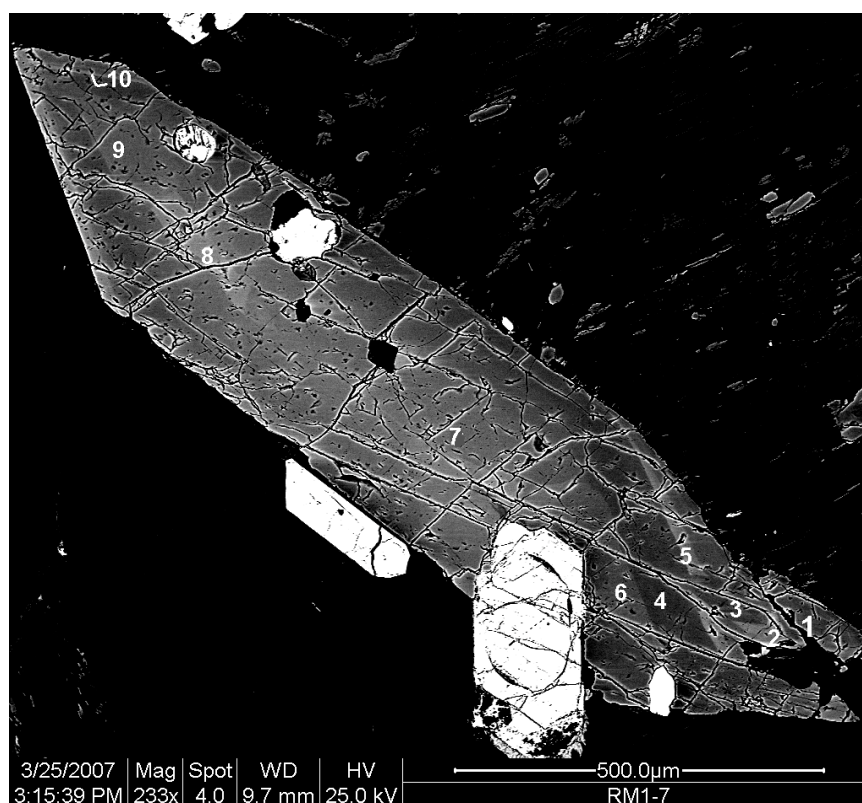
Figure 65: BSE image of RM1-7 and location of sample points.
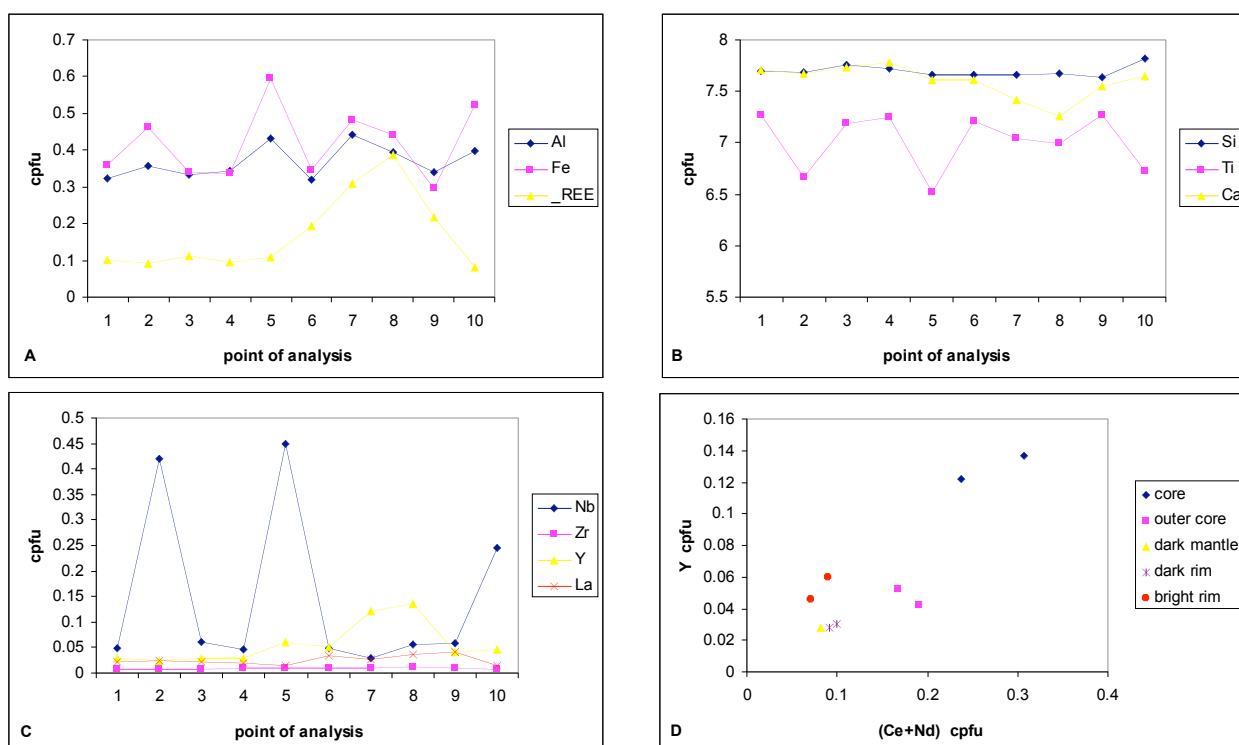
Figure 66: Geochemistry of RM1-7. A. Fe, Al and ΣREE variation across the crystal. B. REE variation. C. HFSE variation. D. REE slope for textural groups of RM1-7 given by a plot of (Ce+Nd) against Y.

linear trend with no off-lying points would suggest a more closed system or fractional crystallisation.

RM1-7 can be summarised as follows:

- REE rich core, REE poor mantle and rim, indicating compatible REE behaviour and magmatic crystallisation.

- REE enriched sector zoning characterising the outer core and central long axis of the crystal.

- Thin, bright inner rim characterised by extremely elevated Nb concentration, indicating a change of melt chemistry late on.

4.6.3 Summary of RM1

Compared to the entire ROMG dataset (234 analysis points), RM1 has some of the highest values for ΣREE, especially RM1-3, which occupies three of the top ten values for ΣREE. Analysis point RM1-3.8 (bright core) is the second highest recorded ΣREE of the whole ROMG dataset with 0.448cpfu. RM1-7 registers as the sixth highest value for the whole dataset with a value 0.389cpfu for analysis point 8 (bright core/sector zoning). The average ΣREE for the ROMG is 0.188cpfu compared to 0.267cpfu for RM1. Clearly, RM1 is distinguished by a higher than average REE content for the entire suite of ROMG rocks, which may be expected based on it being the granitic "end-member" in this study.

One unusual aspect of the geochemistry of RM1 is the extremely high concentration of Nb found in sample RM1-7. The average Nb concentration per spot analysed for the whole ROMG dataset is 0.038cpfu, while in RM1 the average is 0.099cpfu. RM1-3 has an average of 0.040cpfu, comparable with the ROMG average. However, RM1-7 has an average of 0.156cpfu, significantly higher than the ROMG average. The highest Nb concentrations were found in the bright inner rim of RM1-7, peaking at 0.448cpfu. Nb is the only trace element found in unusually high concentration in the bright inner rim of RM1-7, and a plot of Nb against ΣREE for the whole ROMG dataset (see Figure 67 below) shows these outlying points clearly.
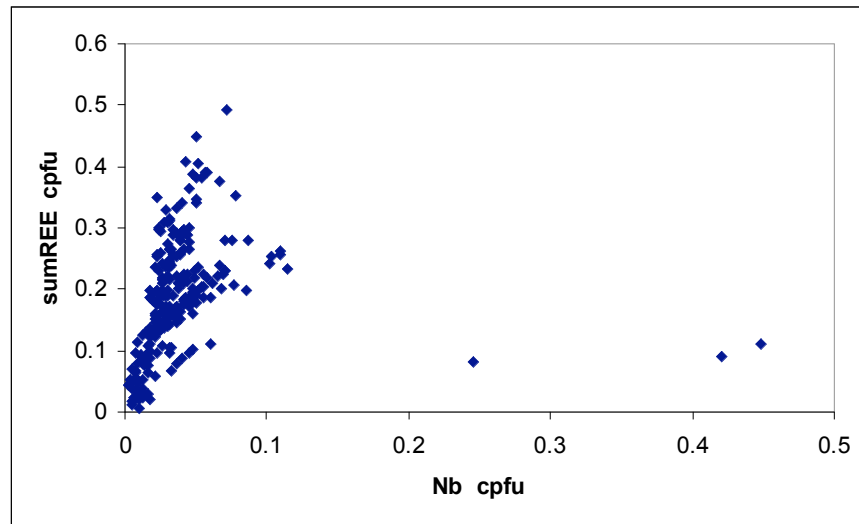
Figure 67: Nb vs ΣREE for entire ROMG data set. Outlying points with Nb values above 0.2 cpfu represent the most elevated Nb values of the dataset and belong to RM1-7.

A plot of (Ce+Nd) against Y for both RM1-3 and RM1-7 gives the approximate slope of REE for RM1 (see Figure 68below).
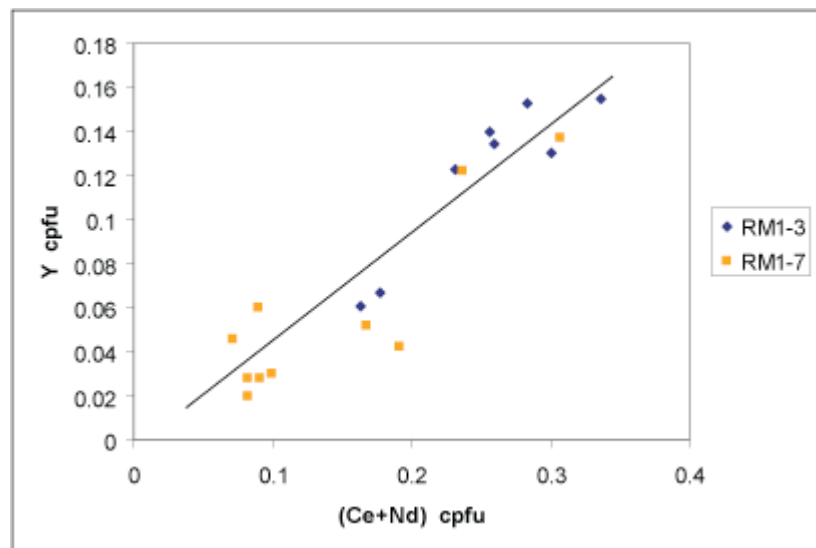
Figure 68: (Ce+Nd) vs Y for RM1 dataset, including RM1-3 and RM1-7Fig

The trend is fairly linear, with some outlying points being due to sector zoning and REE depletion relative to Y late in the crystallisation history. There is some overlap between RM1-3 and RM1-7, indicating a genetic relationship. The fairly linear trend indicates a closed system. The geochemistry and textural criteria both point towards a wholly magmatic origin for the titanites in RM1.

4.7 ES3A (advanced mechanical mixing)

This sample displays mingling and mixing on a fine scale, where granite is interspersed and streaked within a large body of diorite. The smallest streaks are less that 0.5cm wide and can be as long as 25cm. ES3A was analysed in order to assess the differences and similarities in texture and chemistry between the granitic and dioritic portions of the rock.

4.7.1 ES3A-27 (boundary zone)

This crystal formed close to the margin of the granite/diorite streak, and may be considered to have formed in the mixing zone between the two melts. It is one of the largest titanites in sample ES3A and is euhedral with a very thin rim perhaps shows interstitial features. The inference is that it records the early as well as the very latest stages of crystallisation. The overall texture is best described as patchy in the centre, with some sector zoning in the long axis of the mantle, plus a dark rim showing some faint oscillatory zoning. The central portion is mostly brightly zoned in BSE, apart from patchy areas, having no particular geometry, which vary in darker shades compared to the majority of the central portion of the crystal (see Figure 69).

The most interesting aspect of the geochemistry for the crystal relates to the differences in ΣREE between the bright and dark zones of the patchy zoning in the central area. Analysis points 5, 6, 9 and 10 correspond to dark patches in the central area of the crystal (see Figure 70A-B) and show a marked decrease compared with the brighter zones of the central area (analysis points 4, 7, 8 and 11). The analyses with the lowest concentration of REE are the dark margins/rims (analysis point 3) of the crystal, including the interstitial finger-like protrusion (analyses 1 and 2). This is not surprising, especially considering that the majority of REEs should exhibit compatible behaviour. These three analyses also have a low concentration of Zr, which usually behaves incompatibly (see Figure 70C). Analysis point 2 has the highest concentration of Al, possibly linked to the diminished activity of coupled substitutions linked to REE occurring at the late stages of crystallisation. Nb shows a trend similar to that of the REE, and according to Prowatke and Klemme's (2005) research, in dioritic melts, they are about as compatible as the REE. This study also shows that Zr has a partition coefficient similar to the REE for intermediate liquids, but for dacitic and rhoylitic liquids, Zr is less compatible than the REE. The study shows a variation in REE partition coefficients for titanite based on different melt compositions, whereas Zr
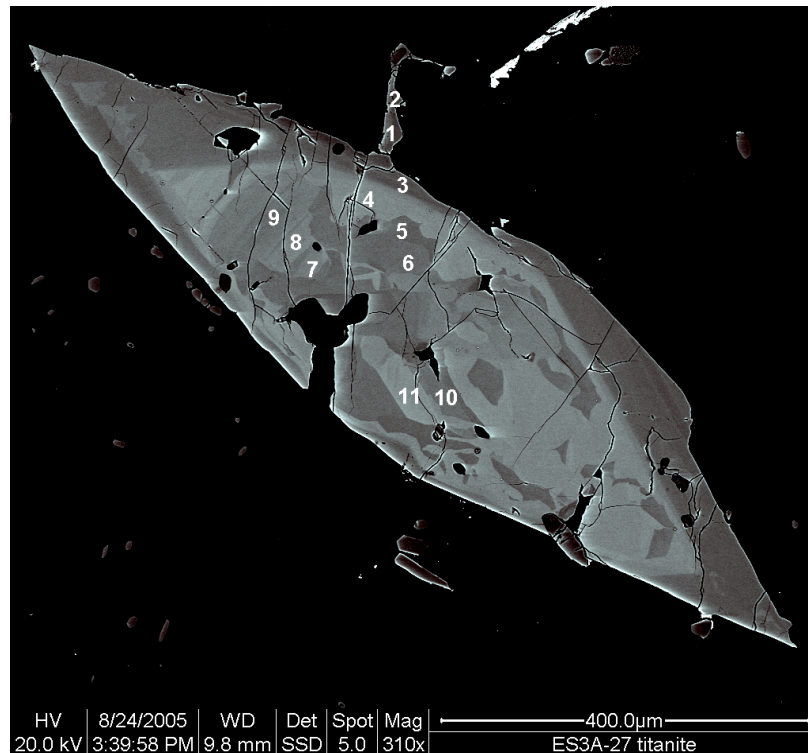
Figure 69: BSE image of ES3A-27 and location of sample points.
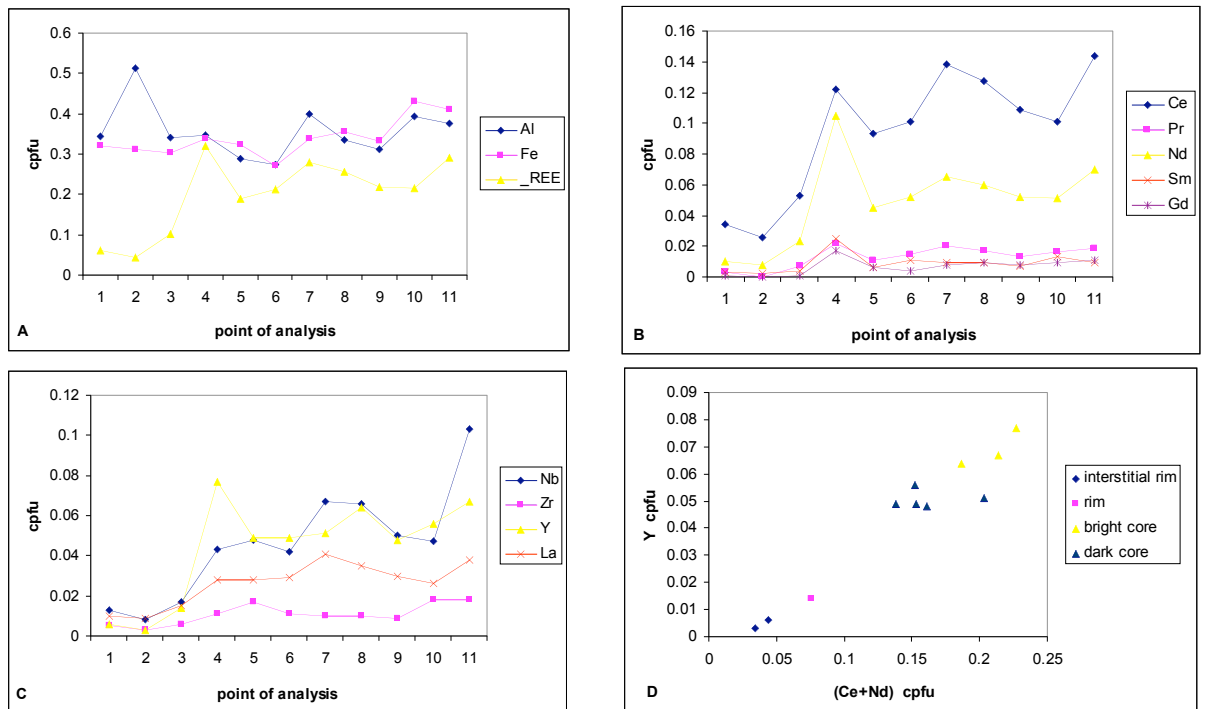
Figure 70: Geochemistry of ES3A-27. A. Fe, Al and ΣREE variation across the crystal. B. REE variation. C. HFSE variation. D. REE slope for textural groups of ES3A-27 given by a plot of (Ce+Nd) against Y.

compatibility is not affected by melt composition. In this instance, it is not surprising that Zr is behaving similarly to the REE.

The origin of the patchy texture of zoning in the crystal core is likely to be related to dissolution and re-growth of titanite. The texture alone suggest that there has been an initial period of titanite growth, producing the bright zoning (with faint sector zoning), a subsequent period of partial dissolution of titanite to produce a network of dissolution throughout the crystal, and a final period of re-growth of titanite filling in the patchy network and creating the mantle and rim. This scenario is backed up by the geochemistry of the textural zones. The REE content of the bright inner zones of the core are higher than those of the darker patchy areas. However, the REE content of the dark patches in the core is much higher than the REE content of the rim with interstitial protrusions (analysis points 1 2 and 3). The compatible behaviour of the REE would mean that the first stage of crystallisation would sequester the REE, and this is reflected in the high REE content of the bright core. This titanite is from the boundary between the diorite and granite and a possible explanation for the dissolution texture is that the crystal originated from the granite and crystallised fairly early on prior to the influx of hotter mafic melt and subsequent fine-scale mechanical mixing event. Heat transfer from the mafic melt could have caused the titanite to partially dissolve. Once the melt began to cool again, subsequent growth filled the dissolution network with a lower REE titanite, but since this occurred before the growth of the rim, the compatible behaviour of the REE would mean that the titanite growth in the network would sequester the REE, leaving the melt relatively depleted in REE by the time the rim crystallised. The REE content of the rim and interstitial rim is significantly lower than the dark patchy core areas.

An approximation of the REE slope is achieved by plotting (Ce+Nd) against Y (see Figure 70D). A linear trend with little scatter is displayed for this crystal. The data points on the graph are defined by textural group. The minimal scatter suggests a genetic relationship between the textural groups, and it can be seen that the bright and patchy areas of the core are more closely related in terms of REE content than they are to the rim/interstitial rim. The influence the diorite has had on the REE content of the melt is reflected in the very large difference between the core and rim.

ES3A-27 may be summarised as follows:

- Long record of magmatic growth reflected in both texture and geochemistry, especially by the differences in REE content of the textural groups.

- Compatible REE behaviour; elevated in the bright core and dark patchy core compared to the interstitial protrusions and rim.

- Early magmatic growth, dissolution then re-growth; dissolution likely brought about by heating from input and mixing of granite melt with diorite melt.

4.7.2 ES3A-49 (diorite)

Another fairly large titanite from the dioritic portion of sample ES3A, this crystal is not unlike ES3A-27 in that is euhedral and sports finger-like interstitial protrusions from the margins, but unlike ES3A-27, it has a simpler pattern of zoning. The zoning consists of a bright, small, semi-patchy core that shows some evidence of sector zoning. The mantle is darker and more uniform, with hints of sector zoning along the long axis of the crystal; the rim/protrusions are dark and uniform (see Figure 71).

Points analysed with the highest concentration of REE are 2 and 4, these correspond to the brightest zones of the crystal (see Figure 72A). The individual REE variation pattern across analyses is very coherent with no virtually no change in slope amongst the REE (see Figure 72B). Unsurprisingly, analysis points 2 and 4 also have the lowest Ca concentrations, again pointing to substitution of Ca at the 8-fold coordination site for REE. By looking at the variation in concentration of Al and Fe with respect to that variation on Ti (Figure 72D) , it is clear there is a direct antipathy, and this is good indication of the charge balancing expected to occur concomitantly with the substitution of Ca for REE, the overall equation being: $Ca^{2+} + Ti^{4+} \leftrightarrow REE^{3+} + (Al, Fe)^3$ (Green and Pearson 1986). Areas with the lowest concentration of REE are the darkest zones of the crystal analysed, these are points 5, 6 and 7, which correspond to patchy areas of the core mantle boundary. Analysis point 1 is from the central dark patchy portion of the crystal, which looks like it may be the same sort of patchy texture seen in the centre of ES3A-27. The early crystallisation history of this crystal may also have had a brief period of dissolution associated with it.

The trace elements which are generally thought of as being incompatible, Nb, Ta and Zr, are found at their highest concentration in the brightest zone at the centre of the crystal, point 2 (see Figure 72C), and looks to be related to preferential sequestering of these

elements due to sector zoning. This mirrors the findings for ES3A-27, where the partition coefficients for Zr, Ta and Nb, are similar to that of the REE, again relating to the findings of Prowatke and Klemme, (2005) where they show how melt composition affects the fractionation of Zr, Nb and Ta with respect to the REE.

Analysis point 2, the bright sector zoning of the core, has the highest overall concentration of REE for the whole ROMG dataset. This would seem to be unusual considering this titanite is from the diorite enclave portion of this sample. The preferential sequestering of REE by the {111} face of the long axis of the crystal may partly explain the REE enrichment. However, sector zoning alone would seem unlikely to produce such a high concentration, especially in a titanite from a diorite melt. Another possible explanation for such enrichment could be explained by the incorporation of REE from the granitic melt into the diorite prior to crystallisation. As mentioned in section 4.7.1, the patchy centre of crystal ES3A-27 may be due to heat assisted dissolution brought about by the mixing of cooler granitic magma with an influx of hotter dioritic melt. Sample ES3A displays a very advanced stage of mechanical mixing between diorite and granite, with cm-scale inter-fingering of the two melts. It is possible that the heat associated with the influx of the more mafic magma assisted in the mechanical mixing by thermally rejuvenating the granitic melt. The thermal rejuvenation of the granitic melt, combined with the small scale inter-fingering, may have made it possible for effective diffusion of REE from the granitic melt into the dioritic melt. The associated loss of heat from the diorite could bring on the crystallisation of titanite in diorite which would then be able to freely take up some of the REE diffusing out of the granitic melt as the two liquids were equilibrating.

ES3A-49 may be summarised as follows:

- Contains an extremely high REE rich core for a titanite in a dioritic enclave.

- High REE core represents the preservation of heat/diffusion driven trace element contamination from granitic melt; an artefact of small scale mechanical mixing of granitic and dioritic melts prior to titanite crystallisation.

- Very late crystallisation geochemistry characterised by interstitial rims with extremely low trace element concentration.
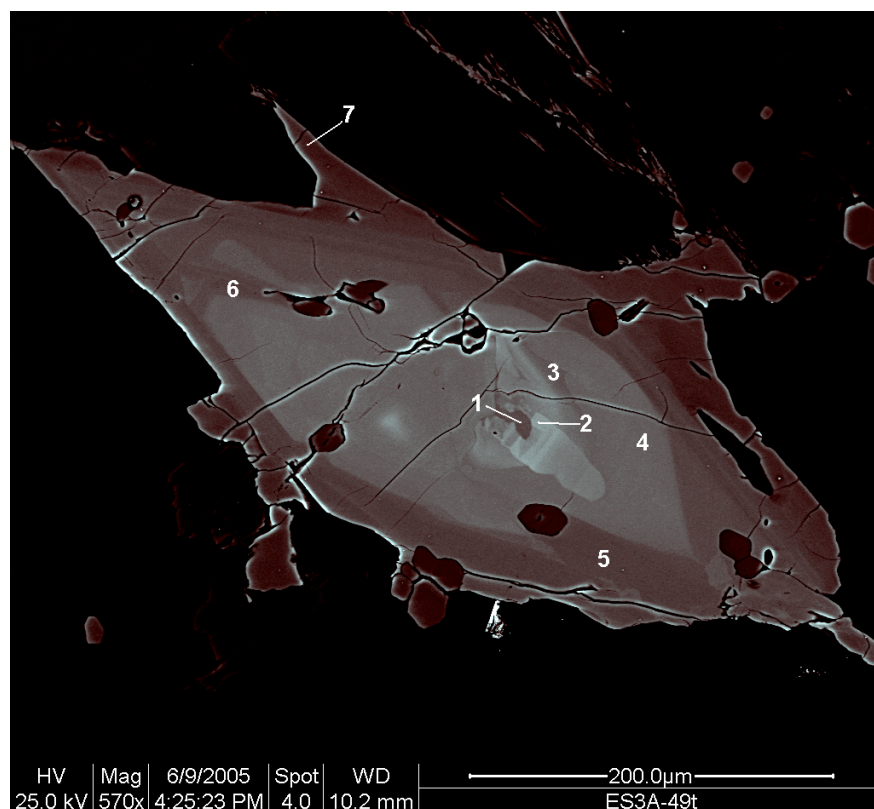
Figure 71: BSE image of ES3A-49 and sample point location.
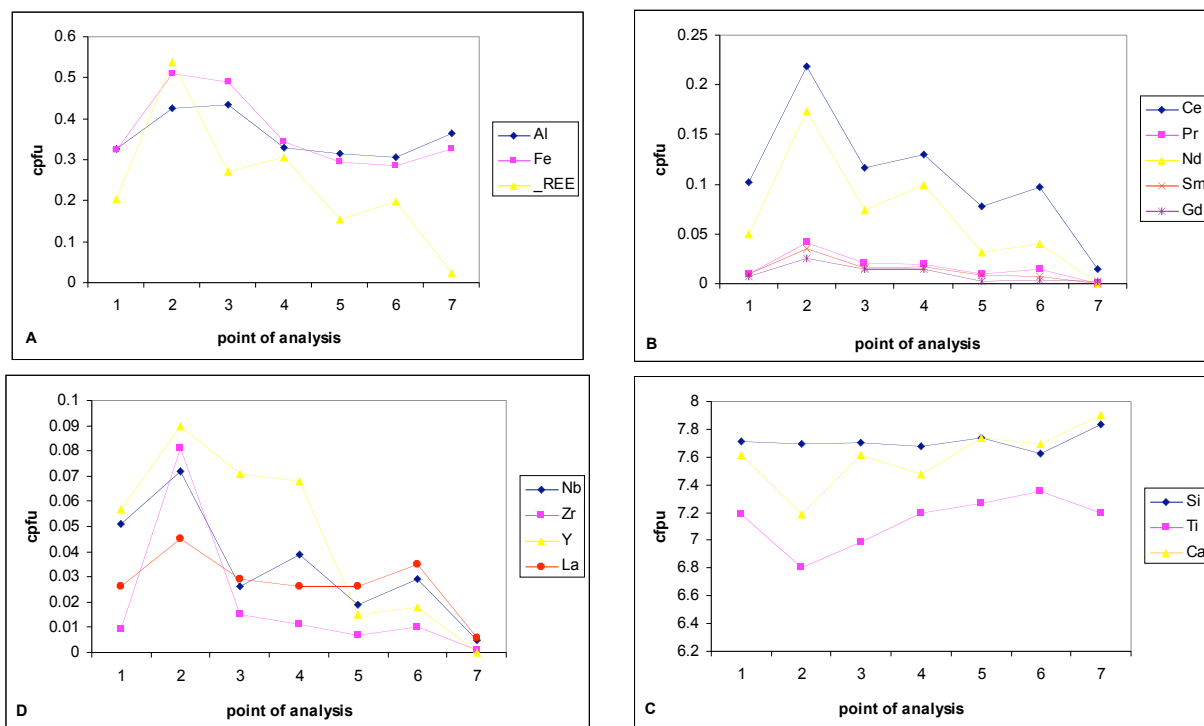
Figure 72: Geochemistry of ES3A-49. A. Fe, Al and ΣREE variation across the crystal. B. REE variation. C. HFSE variation. D. Ca, Ti, and Si variation.

4.7.3 ES3A-59

The only titanite analysed from the granitic portion of sample ES3A, ES3A-59 comprises two large (400µ long) euhedral titanites that have grown together. An irregular margin of growth impingement separates the two crystals (see Figure 73) Good magmatic zoning is clearly displayed, with fir-tree style sector zoning and well developed oscillatory zoning. The site where the crystals are twinned is the only area of the two crystals to exhibit peculiar patchy zoning. This zoning is darker than the zoning anywhere except perhaps the dark rim. There are large cracks associated with this area where the crystals impinge upon each other, and as such may have a part to play in the texture of the zoning observed. There are two possibilities of interpretation of this texture; it could be sub-solidus alteration facilitated by infiltration of fluids along the boundary between the crystals, or it could be linked to dissolution and re-growth brought about by magma mixing. The crystal on the left has a centre that looks like there may have been dissolution and re-growth due to the nature of the discontinuities in zoning, whereas the crystal on the right has a patchy pattern of zoning that is linked only to the border between the two, and looks more like later alteration.

Analysis points 1 and 2 correspond to the area of junction between the crystals, with point 1 analysing the darkest zone of the whole area and point analysing the slightly brighter zoning adjacent to point 1. The lowest concentration of total REE content of the whole crystal is found in point 1, comparable only with point 6, the dark outer rim of the crystal (see Figure 74A-B). Analysis point 2 also has a low concentration REE, possibly due to late stage sub-solidus alteration.

The REE are in their highest concentration at analysis point 3, which corresponds to the brightest zoning of the whole crystal, and looks to be related to fir-tree style sector zoning, described by Paterson and Stephens (1992), who relate the preferential uptake of REE, Y and Nb by the morphologically less important {111} crystal faces to a kinetically induced differential of growth between the {111} and the morphologically dominant {100} crystal face which tend to preferentially sequester Al and Fe. By inspection of Figure 74**A**, one can see that point three is the only point where the REE total concentration is greater than that of Fe or Al. Analysis point 3 also has the highest concentration of the HFSEs: Nb, Zr and Ta (see Figure 74**C**). For a titanite that has grown in the more granitic portion of the rock, one would assume that these elements to be slightly less compatible than the REE if the partition coefficients of Prowatke and Klemme (2005) are correct. However, by

inspection of the variation on REE and the HFSE for analysis points 4, 5, 6 and 7 (see Figure 74A-C) it is clear that Nb and Ta follow an overall similar variation to the ΣREE, while Zr is the only element to actually increase in concentration from the mantle (point 7) to the rim (point 6). This would seem to indicate that Zr behaved incompatibly compared to the REE only towards the end of crystallisation. Nb and Y show the largest shift in concentration from mantle (point 7) to rim (point 6), compared the other trace elements, indeed these two elements are at their highest concentration at point 7, the mantle area, if we exclude the bright central point 3. Analysis points 4 and 5 which immediately are adjacent to point 3 have lower concentrations of these two elements, perhaps suggesting some change in melt chemistry, or availability of these elements between the core/inner mantle growth and the outer mantle growth. Zr and La are the only elements to be in higher concentration at the rim than in the mantle, suggesting incompatible behaviour overall, if the sector zoning (analysis point 3) is disregarded. Sector zoning occurs due to preferential sequestering of trace HFSE and REE by certain crystal faces, and therefore should not be relied on to ascertain mineral-melt partitioning behaviour.

Oscillatory zoning is well developed in the crystal and this may be recording fluctuations in the melt associated with the fine-scale mingling between the diorite enclaves and host granitoid. As speculated in sections 1.4.1 and 1.4.2, it is possible that the input of heat from the diorite may have caused increased diffusion of trace elements from a thermally rejuvenated granitic melt into the dioritic melt. Since the inter-fingering of the two magmas is on the centimetre scale, it may be postulated that during mechanical mingling there wasn't a steady transfer of heat, but the process may have been step-wise, resulting in the coarse oscillatory zoning that characterises this crystal. The presence of very few inclusions and the good euhedral shape of the crystal would indicate growth that wasn't very late, otherwise more inclusions and interstitial rim characteristics would be expected. It is unclear whether the patchy zoning is due to later sub-solidus alteration or is a very early dissolution/re-growth texture, but because it is centred on the join between the two crystals, and is also linked to cracks in the crystal, it seems more likely that it is related to late fluid alteration.

The REE slope plot, (Ce+Nd) against Y, (see Figure 74D) clearly displays two groups spread out along a roughly linear trend (with some spread). One group is represented by the magmatic earlier magmatic oscillatory and sector zoning, richer in REE, while the very late magmatic rim and post magmatic alteration form another group which is poor in REE.
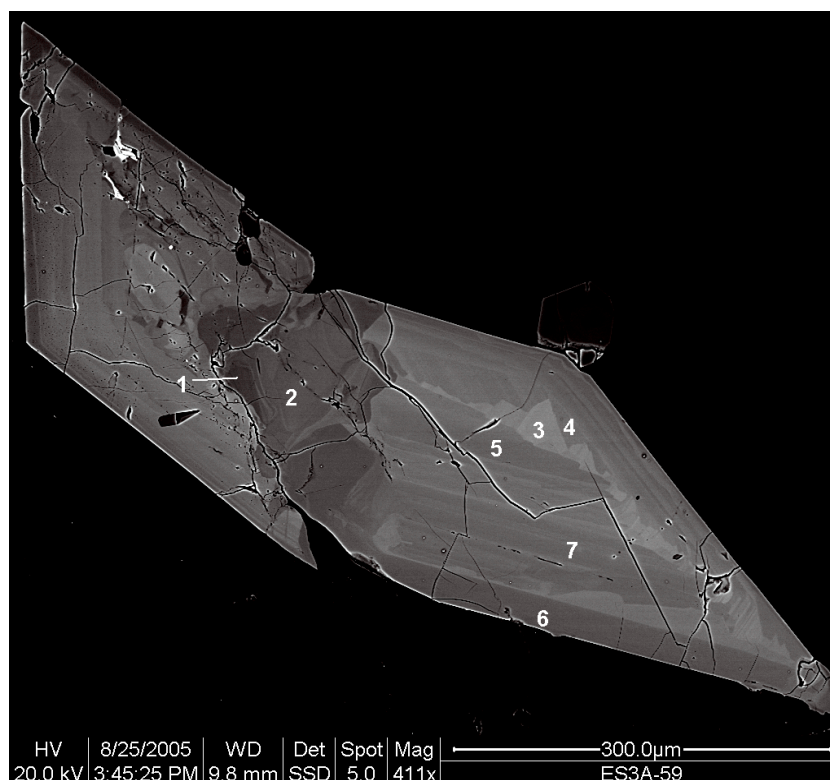
Figure 73: BSE image of ES3A-59 and location of sample points.
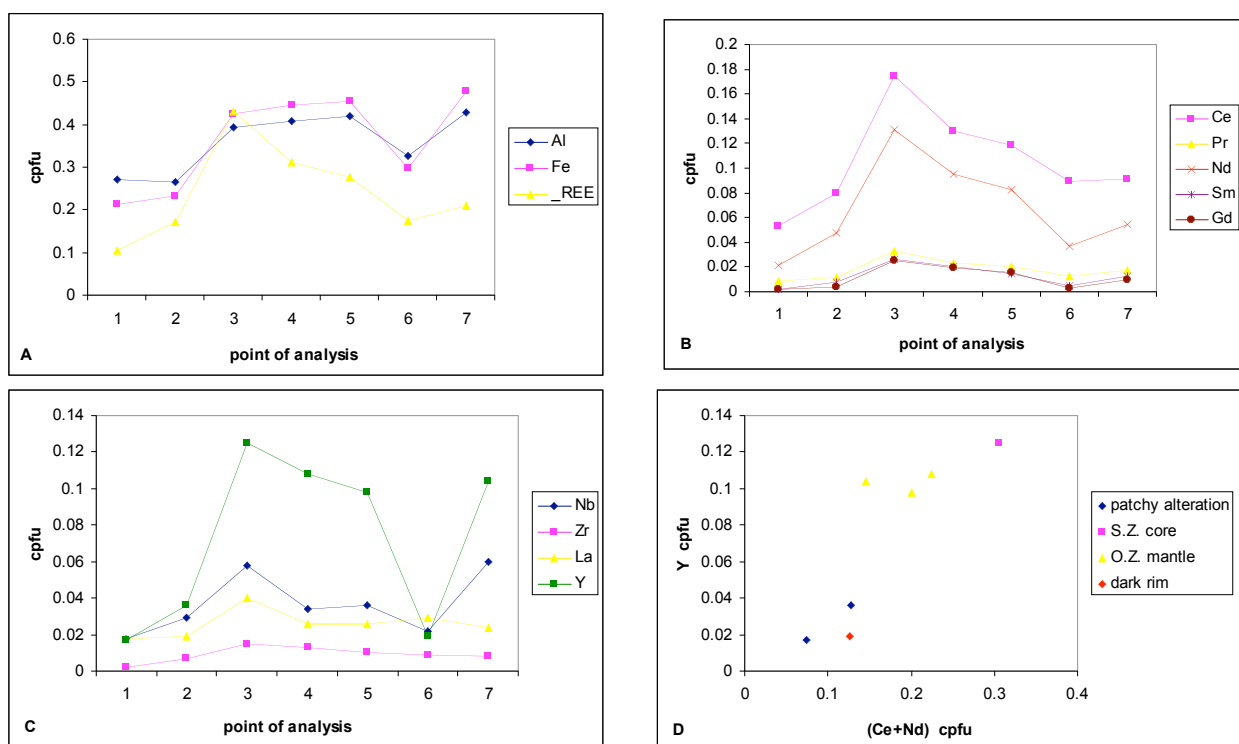
**Figure 74: Geochemistry of ES3A-59. A. Fe, Al and ΣREE variation across the crystal.
B. REE variation. C. HFSE variation. D. REE slope for textural groups of ES3A-49
given by a plot of (Ce+Nd) against Y.**

ES3A-59 may be summarised as follows:

- Textural features are strongly magmatic with well developed sector zoning, oscillatory zoning and good euhedral shape.

- Coarse oscillatory zoning likely to be a product of variable heat transfer from the mafic melt during small scale-mixing with the host granitoid, causing punctuated diffusion of trace elements out of the granitic melt and into the mafic melt.

- REE, Y and Nb display compatible behaviour; La and Zr display incompatible behaviour.

- Plotting (Ce+Nd) against Y displays a linear trend with two main groups related to textural features; one early magmatic and one late magmatic/post magmatic.

4.7.4 Summary of ES3A

The suite of three titanites from this sample display textural features that relate to the fine-scale mechanical mingling and mixing between the host granitoid and mafic enclaves that defines ES3A. The overall geochemical similarity of all three titanites, despite each of them being from a different location (mixing boundary, diorite enclave and host granite) reflects an attempt at equilibration between the liquids facilitated by the fine scale mingling between the liquids.

Dissolution and re-growth textures observed in ES3A-27 (mixing boundary) would suggest that the there was sufficient heat transfer between the two melts to alter the stability of titanites already growing. Heat transfer between the mingling liquids, and the fine-scale of the mixing, facilitated diffusion of REE and HFSE, such that the spread in geochemical signature between the diorite and granite titanites is very little.

A combined plot of (Ce+ Nd) against Y (see Figure 75) for each of the three titanites in the dataset shows considerable overlap between all three, with ES3A-27 (from the boundary of the host and enclave) spanning the middle of the roughly linear spread. The slope of each of the three titanites is slightly different, indicating an open system/magma-mixing. Outlying points and scatter are mainly due to sector zoning and post magmatic alteration.
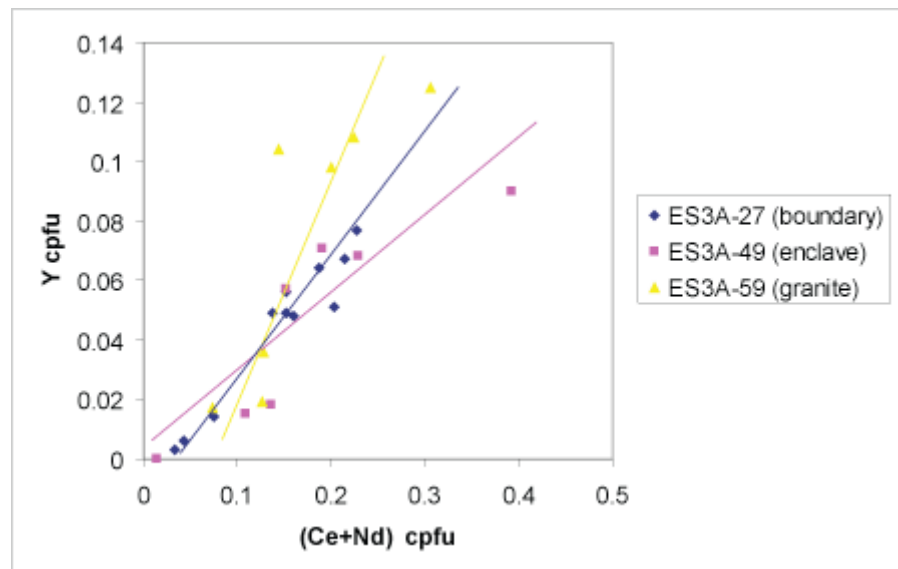
Figure 75: (Ce+Nd) vs Y, an approximation of the REE slope for the complete ES3A data set.

4.8 ROM1 (vesicular mafic enclave)

This sample represents a particular group of dioritic enclaves from the ROMG that is characterised by the presence of micropegmatitic clots of amphibole 3 to 10mm in length. These clots are best described as glomerocrysts, primarily composed of amphibole crystals, which are surrounded by altered feldspar crystals. There are often voids found in the centre of these clots, and it is postulated that they may represent late stage filling of vesicles. Titanite also occurs within these clots. The groundmass of ROM1 also contains very texturally interesting titanites. These fairly large titanites (up to 1.5mm in length) have evidence of periods of dissolution and re-growth. The solution horizons are often accompanied by inclusions of Fe-Ti oxides, indicating a change of oxygen fugacity and associated change in stability of titanite and ilmenite. Geochemical investigation of these titanites is crucial in understanding the possible role magma-mixing in bringing about such oxygen fugacity changes.

4.8.1 ROM1-40

This titanite is the largest and most texturally varied titanite to have been geochemically analysed. It is 1.5mm in length and is characterised by at least three distinct episodes of growth, punctuated by at least two periods of transient instability with respect to titanite crystallisation (see Figure 76). The first period of growth represents the inner core of the crystal which has a patchy pattern of zoning and includes many randomly orientated and shaped inclusions of Fe-Ti oxides (see Figure 77A). Some vestiges of oscillatory and

sector zoning are present, but are poorly defined. This zone is bordered by a solution horizon, most likely representing a brief departure from titanite stability, where titanite may have been subject to dissolution before re-growth. The period of re-growth, a return to conditions stabilising titanite, is represented by the oscillatory zoned mantle (see Figure 77B). This is separated from the rim by another solution horizon with Fe-Ti oxide inclusions. The rim itself is interstitial in texture and most likely represents the final period of growth at a late stage in the magmatic history (see Figure 78).
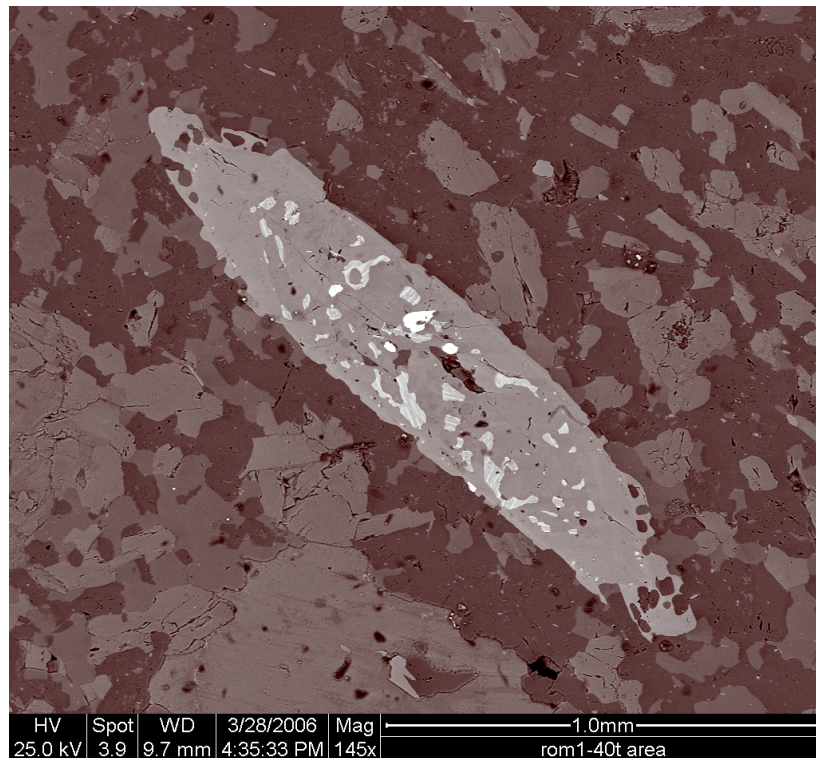
Figure 76: BSE image of whole of titanite ROM1-40. The crystal is characterised by 3 periods of growth: a central ilmenite inclusion rich zone, an oscillatory zoned mantle, and an interstitial rim separated form the mantle by a thin dissolution horizon with small ilmenite inclusions.

Since there are so many data points analysed from the three main different sections of the crystal, the data will be presented for each section in order of the growth history of the crystal, which would follow as such: central/core area, oscillatory zoned mantle, and finally the rim/interstitial protrusions.

4.8.1.1 ROM1-40 central area/core

Many inclusions of Fe-Ti oxides are within the core of ROM1-40. They are of different sizes and different shapes. Some look to be genetically related to the dark areas that characterise the patchy zoning of the core of this titanite; the exsolution textures of the Fe-Ti oxides form linear patterns which correspond with sector zoning in the adjacent titanite.

This section of the crystal should contain the earliest growth history and hence represent the geochemistry of the early melt environment. Analysis points 9 and 10 (see Figure 77A) are from the very centre of the crystal and sample bright zoning that looks to be original and not affected by the first event which caused the destabilisation of titanite and growth of Fe-Ti oxides. Analysis points 11 and 12 represent two irregularly shaped patches of dark zoning, which are thought to represent areas of dissolution during the event causing titanite instability, which subsequently re-grew after melt conditions regained stability with respect to titanite. Whether or not these dark patches once contained ilmenite inclusions is not known. Analysis points 13 and 14 are from the brighter area just adjacent to the dark patches of points 11 and 12.

Points 9 and 10 show the highest concentration of REE out of the analyses in the central area (see Figure 79A-B)**,** whereas, analysis points 11 and 12 have very little total REE. Points 13 and 14 have slightly less concentrations of total REE than points 9 and 10. The Fe and Al values for points 11 and 12, the dark patchy zones, are very different from the other analyses in that they are the only two where the Fe concentration is less than the Al concentration, and they are considerably less, almost half as much. Similarly, the Ca and Ti concentrations for these dark patches is elevated (see Figure 79D**)** In analyses 9, 10, 13 and 14, Fe is greater than Al by about 25% at most, or equal to the Al concentration.

If these areas once had ilmenite inclusions which were subject to dissolution due to a change in oxygen fugacity (a reduction event favours ilmenite stability over titanite), or if they represent areas of titanite dissolution due to a reduction event, followed by re-growth once conditions stared to favour titanite nucleation again, then the Fe available in the melt would be reduced to ferrous iron. This would lower the activity of the coupled substitutions involving the uptake of REE ($Ca^{2+} + Ti^{4+} \leftrightarrow REE^{3+} + Fe^3$)**.** Any new growth of titanite at this lowered oxygen fugacity would have very low Fe and REE content but also have higher Ca and Ti content; the same has been reported by other workers, and this is perhaps this same process is recorded in the geochemistry and texture of the central portion of this titanite (Nakada 1991; Xirouchakis and Lindsley 1998; Della Ventura, Bellatreccia et al. 1999; Piccoli, Candela et al. 2000; Tiepolo, Oberti et al. 2002; Harlov, Tropper et al. 2006).

The behaviour of the HFSE follows the same pattern as the REE for analyses 9-13. The highest values are recorded in analyses 9 and 10 and lowest values in 11 and 12, with analyses 13 and 14 just below the concentration of 9 and 10 (see Figure 79**C**).
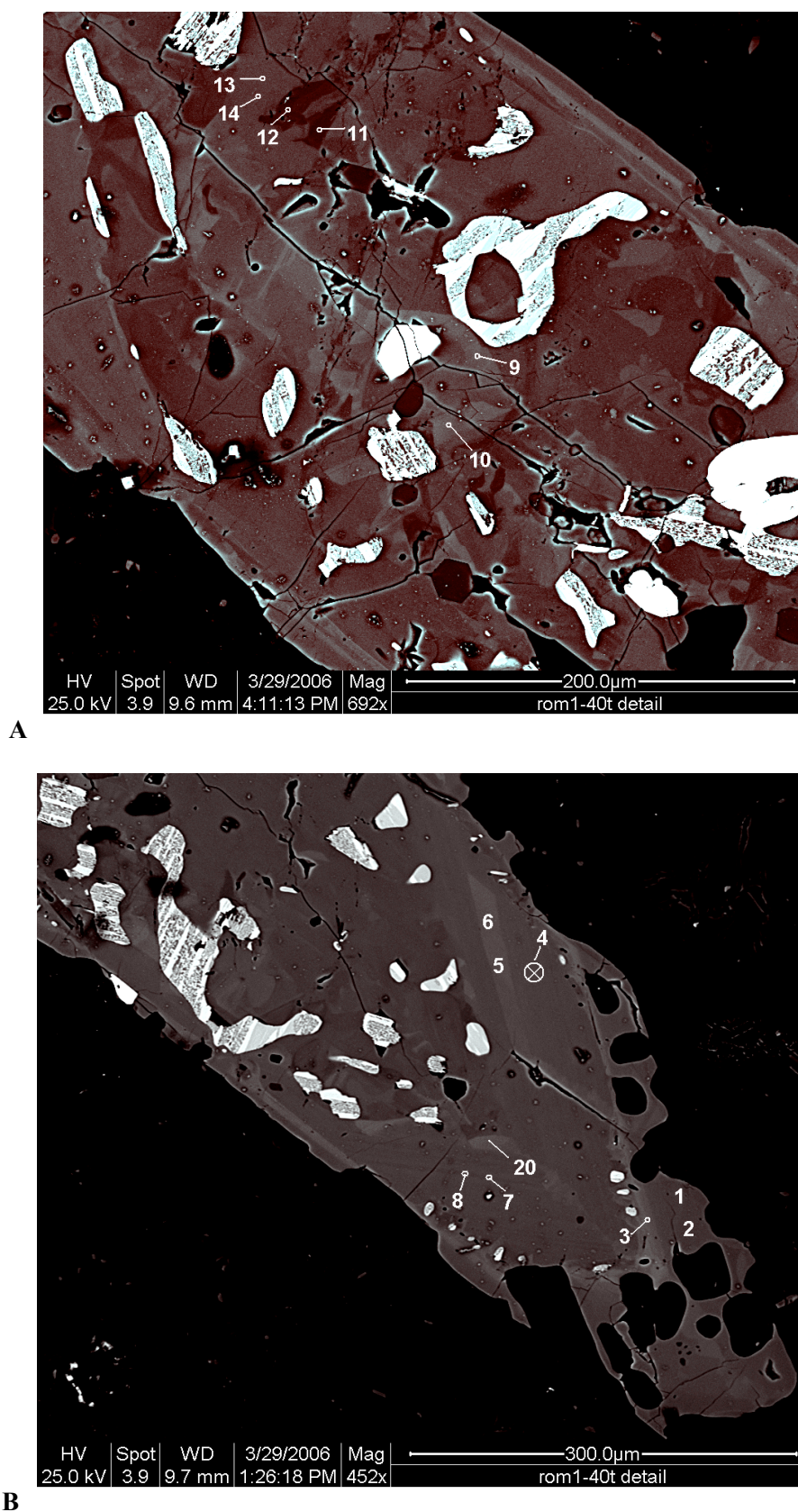
Figure 77: BSE images of ROM1-40 showing detail of zoning and location of sample points. A. Central area/core with patchy zoning and ilmenite inclusions. B. Oscillatory zoned mantle and interstitial rim. Note the ilmenite inclusions and solution surface separating the mantle from the core.
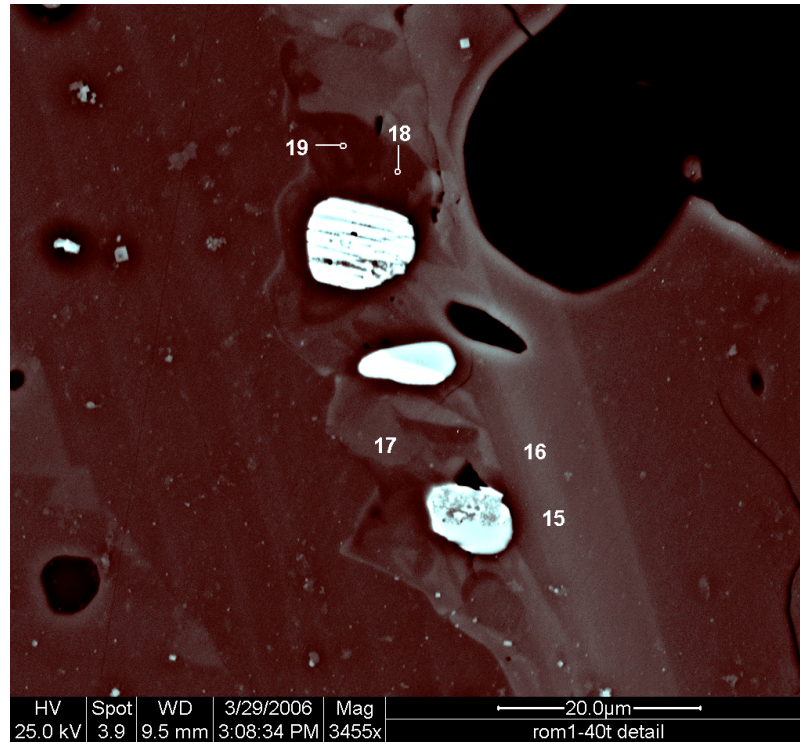
Figure 78: BSE image of ROM1-40 showing detail of mantle-rim boundary and sample location points. Note the discontinuous zoning which forms the boundary between the mantle and rim and the associated ilmenite inclusions and patchy titanite zoning.
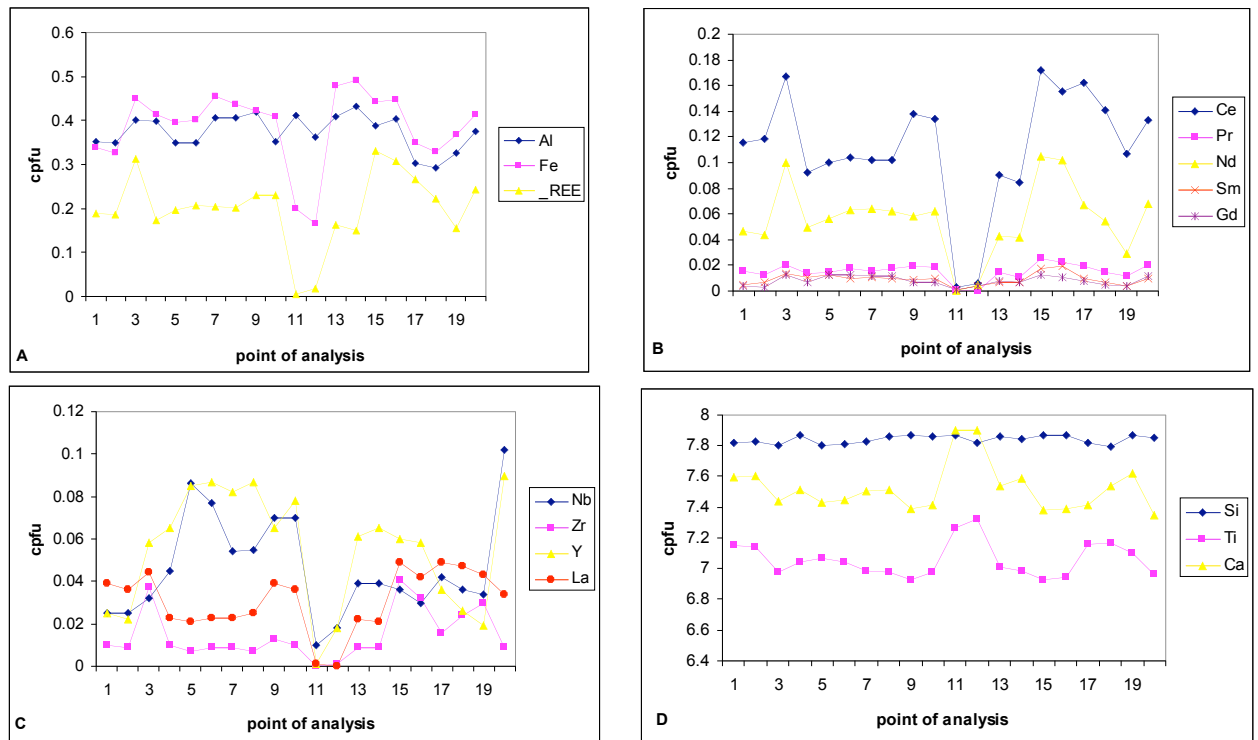
Figure 79: Geochemistry of ROM1-40. A. Fe, Al and ΣREE variation across the crystal. B. REE variation. C. HFSE variation. D. Ca, Ti, and Si variation

4.8.1.2 ROM1-40 oscillatory zoned mantle

The oscillatory zoned mantle of ROM1-40 is separated from the core by an irregular solution surface that cross-cuts zoning. The mantle is fairly uniform in character and is characterised by oscillatory zoning on a fine scale and by its lack of Fe-Ti oxide inclusions. There is fir-tree style sector zoning along the long axis of the titanite. Sample points 5 and 6 were chosen in order to characterise the chemistry of the brightest and widest of the oscillatory zoning visible which is adjacent to the core-mantle boundary; analysis point 4 was analysed as a 10µm spot defocused beam in order to characterise the finer scale zoning of the mantle; analysis points 7 and 8 are from a thin dark zone of the mantle; and point 20 analyses the brightest part of sector zoning in the mantle, directly adjacent to the core-mantle boundary (see Figure 77B for sample point location).

There isn't much variation in the REE totals or the REE patterns from points 4 to 8, and 20, although there is nearly four times as much Y compared to La for the data points 4 to 8. Points 5 and 6, closest to the core of the crystal, record the highest concentrations of Nb and Y, with points 7 and 8 next highest (see Figure 79A-C). The variation alone within the mantle of the crystal is not very significant in itself, but the Y/La, and the general REE, Nb, and Zr trend seen here is more interesting when compared with trends observed in the core and rim of the crystal; the HFSE element behaviour is not consistent with the REE pattern, they seem to be decoupled. Of note, analysis point 20 is significantly different from the others in the mantle, especially with respect to Nb and REE, where the concentrations are higher. This may be explained it terms of enrichment related to preferential uptake by the {111} crystal face, which is related to sector zoning (Paterson and Stephens 1992).

4.8.1.3 ROM1-40 rim/interstitial area

The analyses in the mantle area which are of most interest are 15, 16 and 3 -which all sample the area of the rim immediately adjacent to the solution surface separating the mantle from the rim (see Figure 78). These analyses show a similar chemistry in terms of overall concentration and they also contain the highest concentrations of total REE, Zr and La, found anywhere in the crystal. The main points of interest come from inspection of Figure 79A-C, where it can be seen there is less fractionation occurring between Zr and Nb, as well as less fractionation occurring between Y and La when compared to values for the mantle and analyses 9, 10, 13 and 14 of the core area. The largest fractionation of these pairs (Zr and Nb; Y and La), occurs in the mantle area, and the least amount of

fractionation occurs in the bright first part of the rim. Concentrations of La and Zr increase relative to Nb and Y for the inner rim of the crystal. If these trends are compared to the chemistry of analyses 1 and 2, which are from the outermost parts of the rim area, we can see that for Y and La, the trend actually changes completely, with La becoming more concentrated than Y. Whereas with Nb and Zr, the degree of fractionation increases again slightly, although it's still less than in the mantle of the titanite. Analyses 17 and 18 show the same trend. The dark zoning of the immediate rim area adjacent to an inclusion of ilmenite (analysis point 19), is again similar although it has a higher concentration of Zr and a lower concentration of REEs.

The fractionation trends of Y - La, and Nb - Zr, so far, are the main geochemical trends (in addition to the changes in REE concentration) sufficiently different between the core, mantle and rim that point to the major changes in melt chemistry that brought about the periods of titanite stability and instability (which are plainly marked by the textural evidence of the core's patchy zoning and partially digested ilmenite inclusions, as well as by the solution surfaces and their associated ilmenite inclusions). Nb and La seem to be relatively more concentrated than the REE or Zr and Y in the dark zones of the crystal and the patchy zones that look to be areas of titanite/ilmenite dissolution and re-growth; the converse is true for the brighter zones.

It is clear that this crystal has a significant amount of history preserved within its compositional zoning. Plotting (Ce+Nd) against Y (approximation of the REE slope) reveals a significant amount of spread in the slope that relates to the different textural groups of the crystal (see Figure 80, below).

Figure 80: (Ce+Nd) vs Y (REE slope) plot for textural groups from entire ROM1-40 dataset.
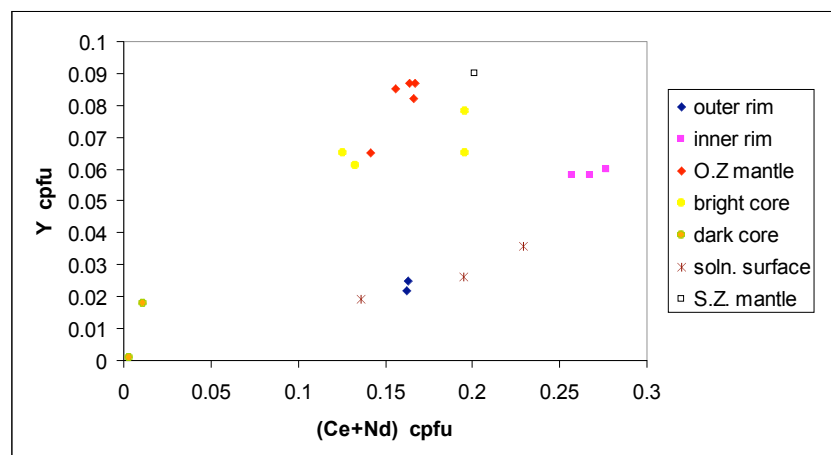
These shifts in the REE slope indicate a clearly open system at work, whereby changes in the melt are reflected in the chemistry of titanite. The textural and geochemical evidence for magma-mixing and associated processes (oxidation/reduction of melt, changes in temperature) having played a role in the history of formation of sample ROM1 is very compelling.

Titanite ROM1-40 may be summarised as follow:

- Textural evidence of at least two periods of titanite instability and subsequent re-growth is reflected in the geochemical differences between the textural zoning groups.

- Dark patchy zoning associated with re-growth of titanite (following transient instability and dissolution) is characterised by lower concentrations of trace elements (especially REE) as well as lower Fe. This is due to reduced activity of the coupled substitution $Ca^{2+} + Ti^{4+} \leftrightarrow REE^{3+} + Fe^{3}$, brought about by the reduction event causing transient titanite instability since a lowering of oxygen fugacity in the melt would reduce ferric iron to ferrous iron. The lag in oxygen fugacity increase after a return to titanite stability would explain the reduced REE uptake and concomitant reduced Fe.

- La behaviour is incompatible, with higher concentration in the rim compared to the mantle. La behaviour is also decoupled with respect to the REE. Nb and Y show more compatible behaviour.

- The inner rim (analyses points 3, 15 and 16) has the highest concentrations of REE and also observes a significant increase in Zr and Y. This may reflect a change in melt chemistry after the transient lowering of oxygen fugacity. If input of mafic magma to the system lowered the overall oxygen fugacity of the existing different melt component (both dioritic and granitic), then there may also be an associated transfer of heat to the existing melt components (of which ROM1 belongs to). This may increase the trace element content of the ROM1 enclave by increasing the temperature of the host granite and facilitating diffusion.

- It's not impossible that ROM1-40 may be a crystal that has been scavenged from the granite host by the ROM1 enclave during mechanical mixing. This scavenging process could also explain the alternating periods of dissolution and re-growth.

4.8.2 ROM1-21

The glomerocrystic clots of amphibole and feldspar that characterise sample ROM1 also contain numerous titanite crystals, usually within the amphibole but also sometimes within the feldspar of the clot's outer margin. ROM1-21 is an example of such a titanite. It is an elongate (50μm wide, 400μm long) twinned titanite with a bright but irregularly zoned core, a patchy zoned mantle with inclusions of Fe-Ti oxides, and a euhedral zoned bright rim. The mantle has evidence of dissolution/re-growth at its junction with both the core and rim. It is likely that this titanite has been subject to one of the transient changes in melt chemistry that generated similar solution surfaces in ROM1-40. Analysis points were chosen in order to characterise the chemistry of all three zones (see Figure 81).

The behaviour and trends of the HFSE, (Zr, La, Y and Nb) in this sample are similar to that of ROM1-40, which also displays discontinuous zoning and evidence of dissolution/re-growth. The overall pattern of behaviour for Zr and La shows them both behaving incompatibly -they are more concentrated in the dark zoning of the mantle and rim than they are in the brighter zoning of the core (see Figure 82C). Zr and La are concentrated most in analysis points 3 and 4 of the mantle and 1 and 2 of the rim. This is in contrast with their lower concentrations in points 5 and 6 from the bright zone at centre of the crystal's core. Analyses 7 and 8 are not as low in Zr and La as 5 and 6. However, they still are lower than the concentration found in the mantle and rim. If the darker zone of the core, which points 7 and 8 sample, is the latest part of the core to crystallise, then the trend for incompatibility holds true.

Y and Nb show the opposite trends to La and Zr; they are more concentrated in the bright portions of the core area (points 5 and 6) and less concentrated in the patchy mantle zones (points 3 and 4) -behaviour that can be considered to be compatible, or at least that they were more prevalent in the early melt history. If the core area is considered to represent the earliest history, with a bright zone (sampled by points 5 and 6) which gives way to a darker rim (sampled by points 7 and 8), before being subject to dissolution and re-growth (represented by the patchy mantle with ilmenite inclusions and the rim), then the pattern of compatibility shown by Y and Nb for points 7 and 8 also makes sense. If the dark zoning is not later than the bright zoning of the core in terms of crystallisation, then the inference would not hold. Another consideration is that the darker zone sampled by points 7 and 8 represents a sub-solidus alteration associated with the large crack that running along the area where the two joined crystals meet.

The ratios between the LREE and HREE is least in the core area of the crystal, at analysis points 5 and 6 (see Figure 82A-B). When comparing the concentrations of Ce and Nd to Gd and Sm at the rim (point 2) and in the core (points 5 and 6), it is also apparent that the behaviour of the former pair is more incompatible than the latter pair. The melt composition being dealt with here is dioritic, and according to the partition coefficients given by Prowatke and Klemme (2005), in general for intermediate melts, titanite accommodates the middle REE more readily than it does the LREE and HREE. In this case, the data matches the predictions of their findings, with Gd and Sm displaying more compatible behaviour than Ce. There is a similarity of behaviour between the middle REE (Sm and Gd) and Y.

It is most likely that the trends in partitioning are not solely related to the compatibility/incompatibility of the respective elements, but that there may be an element of influence from the observed changes in melt conditions evidenced by the solution surface textural features and associated ilmenite inclusions. Due to the presence ilmenite inclusions and patchy zoning, it is most likely that the major change in magmatic conditions is indeed due to a reduction event (such as an input of mafic magma) which transiently destabilised titanite formation (perhaps also dissolving some of the titanite) and promoted ilmenite nucleation. If reducing conditions lingered after titanite stabilised again, then the amount of and hence activity of ferric iron would be diminished, and this would in turn cause a limiting of the incorporation of REE into the titanite structure due to the coupled nature of the substitution of REE and Fe for Ca and Ti. These textures and geochemical signatures are represented well in ROM1-40 and ROM1-21.

A plot of (Ce+Nd)/Y against ΣREE represents the variation of the approximated REE slope with respect to the total REE (see Figure 82D). The change in value for the slope of REE for each of the textural groups indicates that the system in an open one, which is compatible with the idea of mixing magmas and the resultant changes in oxygen fugacity. Within the textural groups, the change in REE slope is less pronounced, but there is more change in the total REE concentration; this pattern indicates that there is less control on the trace element fractionation by open system processes (magma mixing) and more influence by closed system processes (fractional crystallisation).

Figure 81: BSE image of ROM1-21 and location of sample points
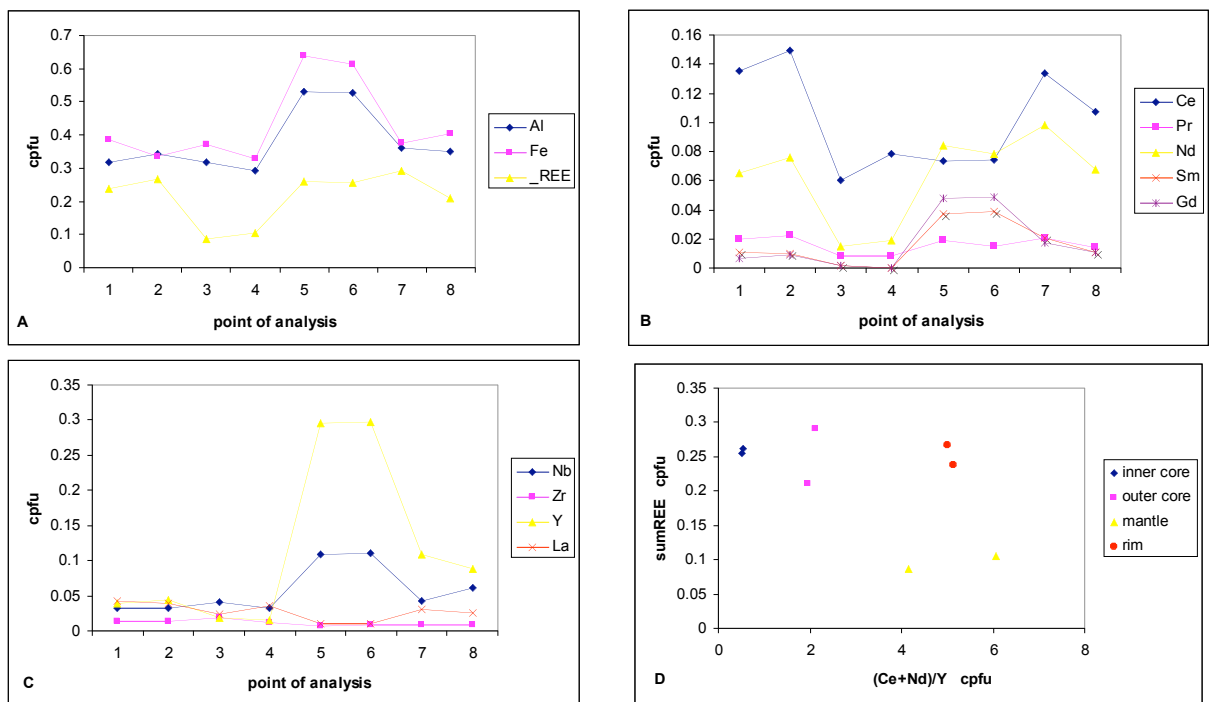
Figure 82: Geochemistry of ROM1-21. A. Fe, Al and ΣREE variation across the crystal. B. REE variation. C. HFSE variation. D. A plot of (Ce+Nd)/Y (value of REE slope) against sumREE; this plots helps to differentiate textural groups within ROM1-21 that have different REE slopes while also giving a comparison of REE enrichment.

ROM1-21 may be summarised as follows:

- Zr and La display incompatible behaviour; Nb and Y display compatible behaviour.

- REE depleted in the dark-zoned mantle, relative to the core and rim.

- Textural evidence of transient titanite instability (causing dissolution and re-growth creating the mantle area) is reflected in differences in the geochemical signature between the core, mantle and rim.

- Variation of the REE slope between textural zones in the crystal indicates an open system (magma mixing). Similar REE slopes, but different values for ΣREE for analysis points within the same textural zone, indicates fractional crystallisation as the dominant control over trace element partitioning.

4.8.3 ROM1-31

Another titanite from one of the amphibole-rich clots that characterise sample ROM1, ROM1-31 is different from ROM1-21 in that it has no textural evidence of dissolution and re-growth. It is composed of three titanites that have inter-grown at the margin of the clot and it is primarily surrounded by amphibole. The zoning pattern is similar for the three crystals: medium bright small inner cores; brighter outer cores; thin dark inner mantle, and a final slightly brighter outer mantle and rim (see Figure 83). All of the crystals contain thin, crack related areas with dark zoning in BSE, which looks like late, sub-solidus alteration.

Analyses 11, 12, 13 and 14 are taken from the area of re-crystallised titanite, perhaps sub-solidus alteration associated with the cracks visible in the immediate area. The dark zoning pattern can be seen proximal to cracks and cross-cutting the oscillatory zoning and sector zoning of all three crystals. These analysis points also have the lowest concentration of trace elements in conjunction with the dark rim zones sampled by analyses 1, 2, 3 and 4. (see Figure 84A-C)

Analyses 15 and 16 correlate to a moderately bright zone in the central portion of one of the crystal and these points show unusually high concentrations of Zr however, there is nothing unusual about the geochemistry of the other trace elements for these two points, although they record the second highest concentrations for REE, they do not show any

unusual fractionation trends at all. The variation seen in the other elements is all very similar, except for Fe, where again for points 15 and 16, the Fe concentration is higher than seen anywhere else in the three crystals.

The REE concentration is at its highest at analysis points 17 and 18, which represent the brightest zoning sampled and also corresponds to the core of one of the crystals (see Figure 84A-C). Analyses 5, 6, 7, 8 sample the next brightest central area, and also display the next highest concentrations of REE, followed by points 9 and 10. The lowest concentration of HFSE and REE is from points 1, 2, 3 and 4. The absolute lowest concentrations are from points 3 and 4, which correspond to the darkest zoning observed in that is definitely magmatic in origin. In the largest of the crystal, this dark inner mantle, along with the analyses 1 and 2 from the rim, possibly represents the last period of crystallisation of these three crystals. The dark zoning in the three bands of the rim and mantle here do not seem to be represented in the other two crystals. Points 1 and 2 are from a decidedly wider band of zoning which is closer to the rim edge than points 3 and 4, and the fact that they also show slightly higher concentrations of REE and traces elements, indicates a possible rejuvenation in magma associated with the very final stages of crystallisation or an influx if very late fluid/volatile phase rich in trace elements. These crystals are part of the glomerocrystic clot, which is thought to represent a late stage vesicle fill, and hence possibly also show the characteristics of the late stage chemistry of the melt. The variation in trace element concentration shows broadly compatible behaviour with the exception of the differences between analysis points 19, 20 and 15, 16 -both of which represent the very cores of two of the crystals. These points have lower REE values than the bright zoning sampled by 17 and 18. However, these last two points may have a chemical signature that is related to sector zoning. Analyses 17 and 18 have the highest total REE concentration of any of the zones analysed in the whole of sample ROM1. Analyses 1, 2, 3 and 4 are also amongst the lowest concentrations for total REE analysed for ROM1, and as such, the degree of variation in REE is the largest in sample ROM1-31.

An approximation of the REE slope is given by a plot of (Ce+Nd) against Y (see Figure 84D) and although there is a roughly linear trend for the ROM1-31 dataset, there is also some spread within certain textural groups. The textural groups relating to the core of the crystal show the most spread, a possible indication of an open system whereby the melt chemistry is changing due to outside influences, and seeing as these crystals are associated with the filling of a vesicle, perhaps volatiles rich in trace elements already present in the vesicle prior to crystallisation of the titanites have played a role.
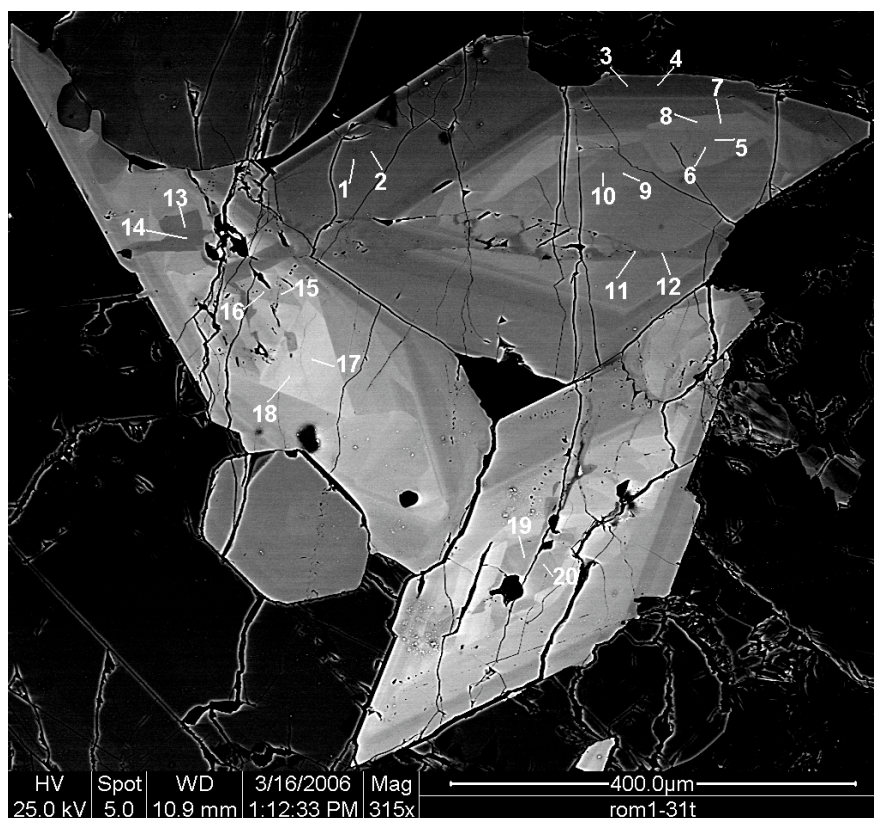
Figure 83: BSE image of ROM1-31 and location of sample points.
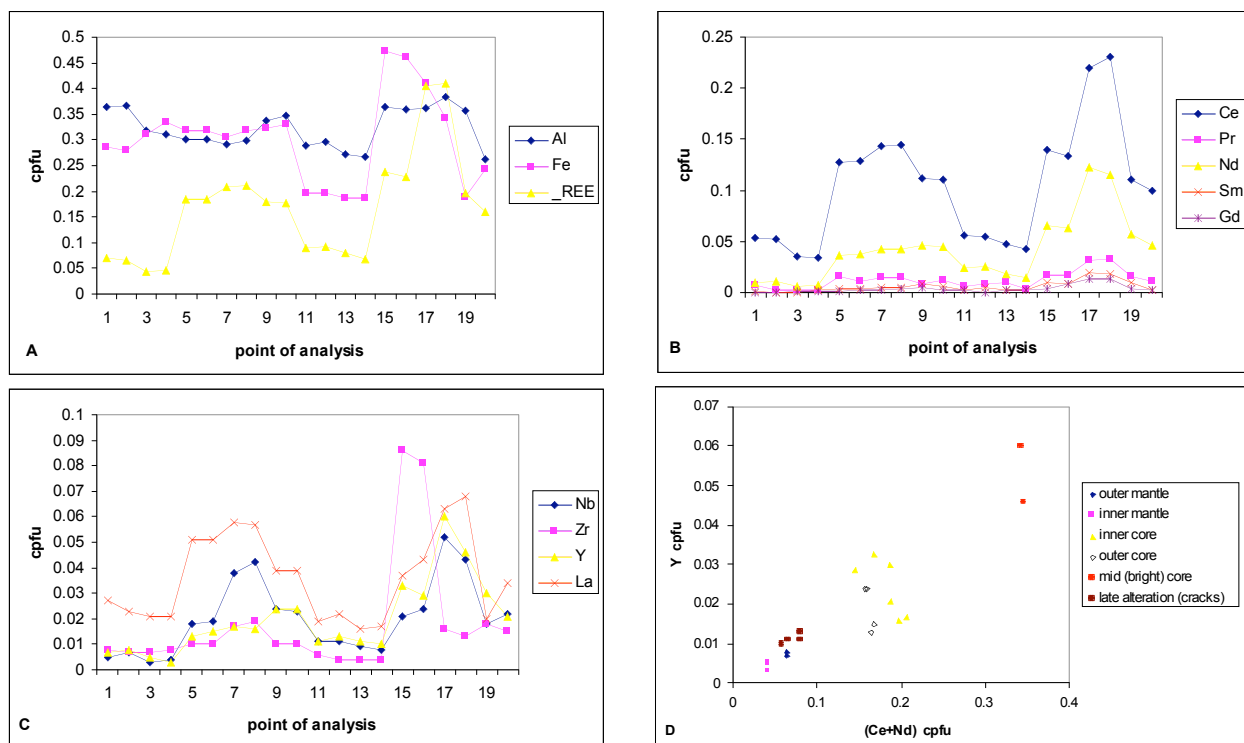
**Figure 84: Geochemistry of ROM1-31. A. Fe, Al and ΣREE variation across the crystal.
B. REE variation. C. HFSE variation. D. REE slope for textural groups of ROM1-31
given by a plot of (Ce+Nd) against Y.**

ROM1-31 may be summarised as follows:

- REE behaviour is broadly compatible.

- Complex changes in zoning of the cores of the crystals indicate changes in melt conditions during the waning stages of ROM1 crystallisation.

- Late stage volatile rich fluids present in the vesicle (prior to crystallisation of the minerals filling the vesicle) may have played a role in the variation observed in the zoning of the crystal cores.

- Late, subsolidus alteration of the titanites is displays trace element concentrations that are slightly elevated compared to the rim of the crystal.

4.8.4 ROM1 summary

Sample ROM1 boasts a large variety of textural and geochemical information with respect to the nature of its titanites. The most striking textural aspect of titanite is that of the dissolution and re-growth preserved within samples ROM1-40 and ROM1-21. The textural discontinuities and associated ilmenite inclusions indicate episodes of transient instability of titanite with concomitant transient stabilisation of ilmenite. Growth of titanite is promoted by oxidizing conditions, and the associated Fe rich phase tends to be magnetite. A reduction of oxygen fugacity change brought about by an influx of mafic melt altering the conditions in the magma chamber, could destabilise titanite and favour nucleation of ilmenite. A return to oxidizing conditions would cause partial or complete dissolution of ilmenite and promote re-growth of titanite. A lag in return to fully oxidising conditions could cause a period of reduced uptake in REE by titanite due to a reduction in the coupled substitutions involving REE and ferric iron (Nakada 1991; Xirouchakis and Lindsley 1998; Della Ventura, Bellatreccia et al. 1999; Piccoli, Candela et al. 2000; Tiepolo, Oberti et al. 2002; Harlov, Tropper et al. 2006). These processes are recorded both texturally and geochemically by titanites ROM1-21 and ROM-40, with ROM1-40 recording at least two transient titanite destabilisation events. Titanite is clearly capable of recording large scale, chamber-wide, processes from the magmatic environment.

Geochemical variation is significant with respect to the REE and HFSE signature of titanites within ROM1. Overall, the REE behave compatibly, being concentrated in the cores and relatively depleted at the margins A departure from this pattern could indicate a

change in melt chemistry, although could equally represent key crystallisation changes in the paragenesis of the rock. In order to rule this out, it would be necessary to undertake a study of the geochemical history of the other minerals in the paragenesis that would be likely to have a fractionating affect on the trace elements within the melt. The HFSE show variability in partitioning behaviour, with Zr and La displaying less compatible behaviour than Nb or Y. La can be strongly fractionated from the REE (except for Ce) which is curious as it usually mirrors the REE (especially the LREE).
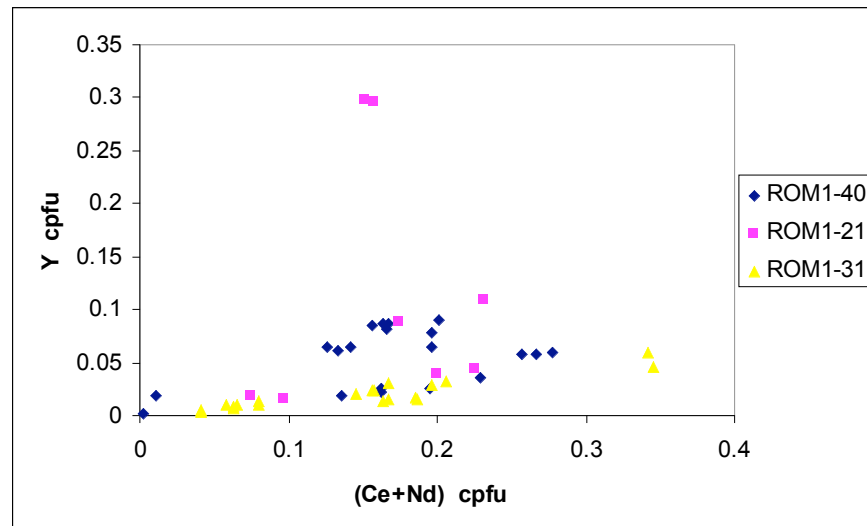
Figure 85: REE slope plot given by (Ce+Nd) vs Y for entire ROM1 dataset; values in cations per formula unit.

The variation in REE slope for the entire ROM1 dataset (given by plotting (Ce+Nd) against Y; see Figure 85 above) is a strong indication of crystallisation in an open system. The slope of REE would be more constrained and constant if the system was closed; in this case, fractional crystallisation processes would account for variations in the total REE. The variation in REE slope, outlying points and scatter may be explained due to:

- Changes in melt chemistry related to magma mixing processes (and changes in melt temperature and oxygen fugacity).

- Later, sub-solidus alteration of titanite.

- Crystal chemical controls on partitioning behaviour, especially preferential uptake of REE, Y, Nb and La due to kinetically-induced sector zoning.

4.9 ES16 (hybrid)

This sample represents the most hybridised of all rocks collected from the ROMG. It is has a texture which shows evidence of mechanical mixing of an advanced stage, with localised flow and swirl textures in addition to large partially resorbed megacrystic feldspars. The mineralogy is intermediate between the monzogranite of RM2 and the diorite of the synplutonic dykes (ESd1) and mafic microgranular enclaves (MMEs), such as ROM1. As such, it represents the most advanced stage of hybridisation sampled from the facies seen at the current level if un-roofing of the pluton. The majority of titanites from sample ES16 are subhedral to anhedral, with interstitial protrusions characterising the texture of the outer margins. Prince (1943) reported that the crystal morphology of titanites from mafic rocks tends to be more interstitial than compared to silicic rocks, where the titanites tend to be euhedral.

4.9.1 ES16-7

ES16-7 is a subhebdral titanite over 1mm in length with interstitial margins. There is very little zoning visible in BSE except for some sector zoning along the long axis of the crystal, one dark patch at the centre -points 3 and 4 analyse this, and some dark patches at one margin -points 1 and 2 have been placed here (see Figure 86). The lack of zoning in BSE imaging is a distinctly common feature among the titanites of ES16. If zoning is present it tends to be very simple, broad zoning or sector zoning.

The most striking feature of the variation in trace elements is apparent from inspection of the sum of REE -overall there is very little variation, and even among the individual REE, there is not much variation at all (refer to Figure 87A-B). The REE are most concentrated at analysis points 5 and 6, which correspond to the mantle. The mantle area is uniform in character with respect to zoning; there is no oscillatory zoning at all.

The Zr and La are slightly less concentrated in the "core" area (analysis points 3 and 4) than they are in the mantle or dark portions of the rims (points 5, 6 and 1, 2 respectively). The opposite in true for Y and Nb, which are more concentrated in points 3 and 4 than the rest (see Figure 87C). The behaviour of Y and Nb may thus be considered to be more compatible and that of Zr and La incompatible.

Overall, the paucity of real variation of REE in this sample suggests that it is quite chemically homogenous. It ranks just about in the middle when compared to most samples in the study when it comes to total mean REE concentration, perhaps unsurprisingly so.
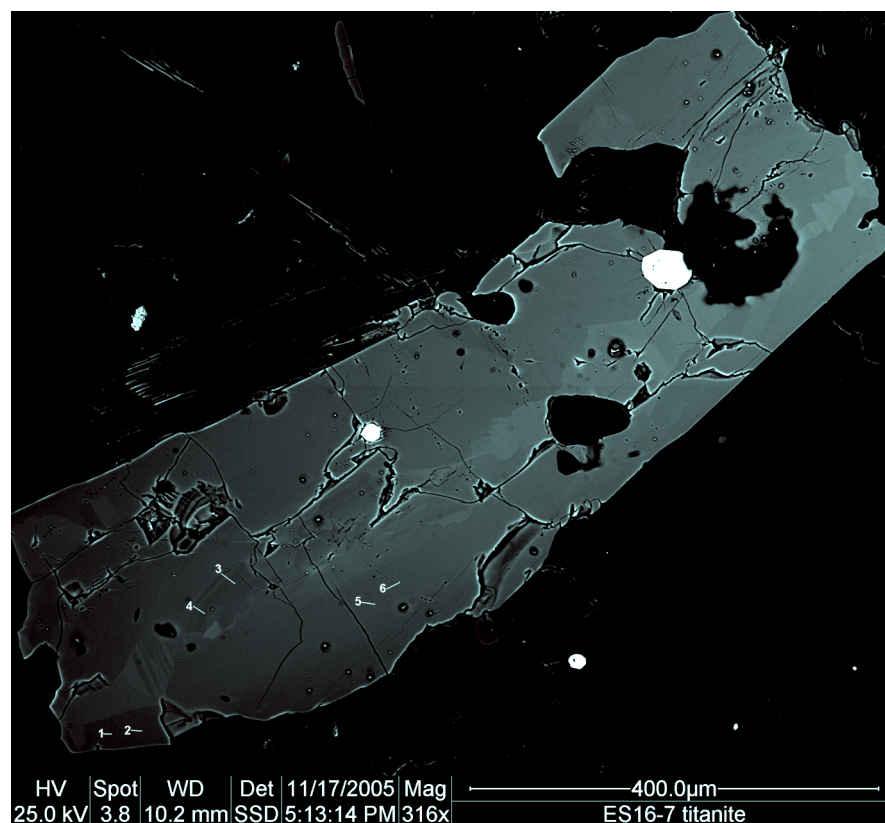
**Figure 86: BSE image of ES16-7 (hybrid) titanite with sample point location.**
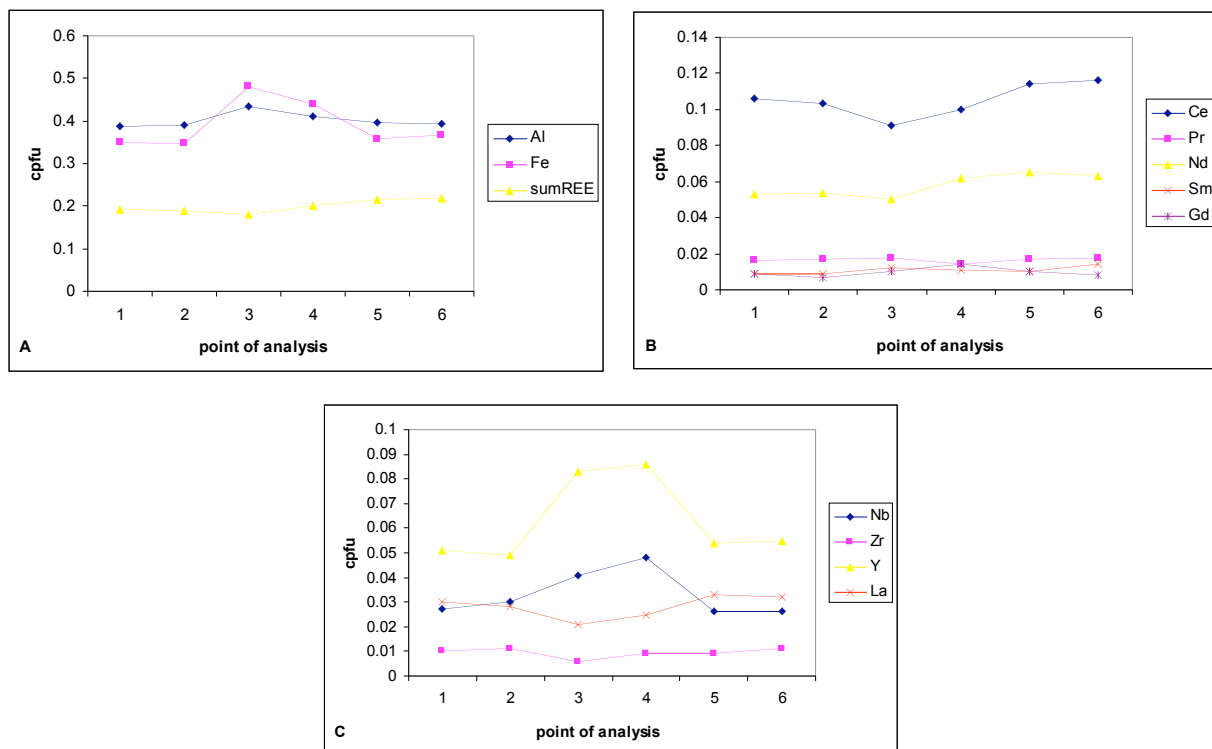
Figure 87: Geochemistry of ES16-7. A. Fe, Al and ΣREE variation across the crystal. B. REE variation. C. HFSE variation.

The mean total REE for ES16 is about 0.200cpfu, compared to a max of 0.493cpfu and minimum 0.013cpfu for ES3A, which displays the maximum spread observed in all of the ROMG. ES16 is the most hybridised of all the ROMG samples, and as such represents the most advanced example of chemical and mechanical mixing between the granitic and dioritic end-members of the entire co-genetic suite. Mixing and mingling is facilitated by a low temperature and viscosity contrast between the magmas, and it is very likely that the melts which have mixed in order to create ES16 where of sufficiently similar viscosity to allow for mechanical hybridisation to occur. Fine-scale mechanical mixing of two magmas with sufficient heat would also have a significant effect on the chemical characteristics of the melt since thorough mechanical mixing will facilitate chemical mixing. Diffusion of trace elements would be enhanced if the melts were mechanically mixed to a fine degree, and as such, the likelihood of attaining chemical homogeneity would be great. Since this sample shows very little variation in trace element composition with respect to the REE, despite showing some HFSE variation, it is reasonable to assume that a certain degree of chemical homogeneity was achieved in ES16 prior to titanite formation. Since titanite is considered to be refractory in nature, it would be expected that any titanites forming early in the component may retain their early chemical signature. However, there are no examples of titanite in ES16 that show a significantly different pattern of compositional zoning to suggest there were titanites crystallising in precursor melts. It is possible that the melts which have mixed to form ES16 were both still very hot and had an extremely low crystal content (probably no titanite at all) just prior to mixing. If this were the case, then thorough mechanical and chemical mixing would achieve a degree of chemical homogeneity in the hybrid melt and the geochemistry of ES16-7 reflects a very low degree of REE variation. The fact that sector zoning exists is not dependant on wholesale chemical homogeneity or heterogeneity of the melt; rather, it is a crystal chemical factor whereby certain crystal faces preferentially take up certain trace elements. Hence, it is not a factor that can dispute relative homogeneity being achieved in the melt prior to titanite formation.

ES16-7 may be summarised as follows:

- Interstitial shape of titanite suggests a late crystallisation.

- REE profile across the crystal is very flat, such an absence of variation is indicative of a chemically homogenised melt.

- Some fractionation between the HFSE exists; Y and Nb behave compatibly and La and Zr behave incompatibly. ES5

- Distinct absence of zoning other than sector zoning suggests a degree of chemical homogeneity in the melt was achieved prior to titanite formation.

- ES16 is a hybridised rock, and as the most mixed rock of the ROMG co-genetic suite, it represents a very advanced stage of mechanical and chemical mixing. This thorough mixing and homogenisation of the component melts is reflected in the simple compositional zoning of titanite ES16-7.

4.10 ES5 (early mingling)

Mingling of granite and diorite is common in the ROMG. ES5 samples an early stage of mechanical mingling between the two magmas, where the boundary between the diorite enclave and host granitoid is considered as un-reactive. There is some small-scale inter-fingering of the two at the boundary, but this is very limited and there is little to no evidence of significant mechanical mixing. The sample enables characterisation of the chemistry of titanites from host-enclave samples where mingling is evident but mixing is very limited.

4.10.1 ES5-30 (host granite titanite)

Titanite ES5-30 is from the granite (host) portion of the sample. It is a 100μm long titanite that is juxtaposed with a zircon of similar size, with evidence of the titanite growth being limited and impinged upon by the zircon, which has looks like it has formed first. The zoning of the titanite is simple, with a bright zoned core area generally becoming successively darker towards the rim. There is evidence of some sector zoning and a curious dark zoning that lies adjacent to where the zircon impinges on the titanite. This dark zoning next to the zircon may be due to some type of sub-solidus alteration linked to the grain boundary, however, the margins of this dark zone meet the sector zoning of the middle at normal looking geometrical angles, typical of almost all fir-tree sector zoning. This dark zoning may be an artefact of the sector zoning and the angle at which the titanite is sectioned. If this is not the case, and alteration is the reason for this dark zoning, then it may be argued that for alteration of titanite to succeed it needs irregular surfaces for effective progression. In this case the well-developed surfaces of the internal sector zoning may be halting the progression of alteration (see Figure 88).
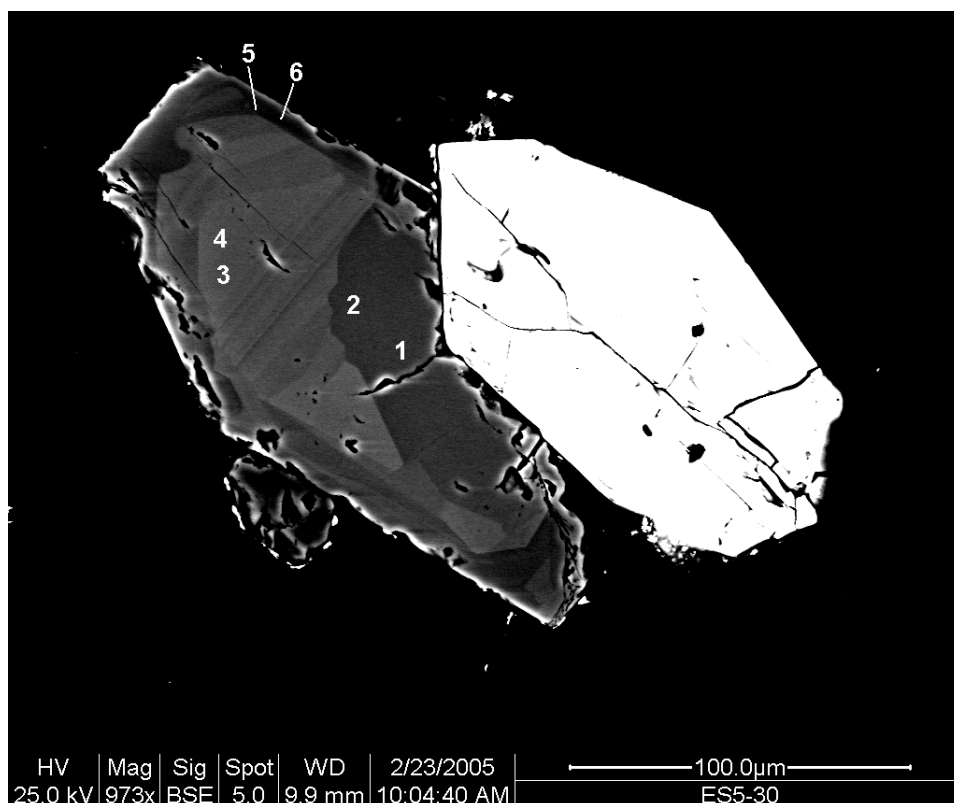
Figure 88: BSE image of ES5-30 (granite) and location of sample points.
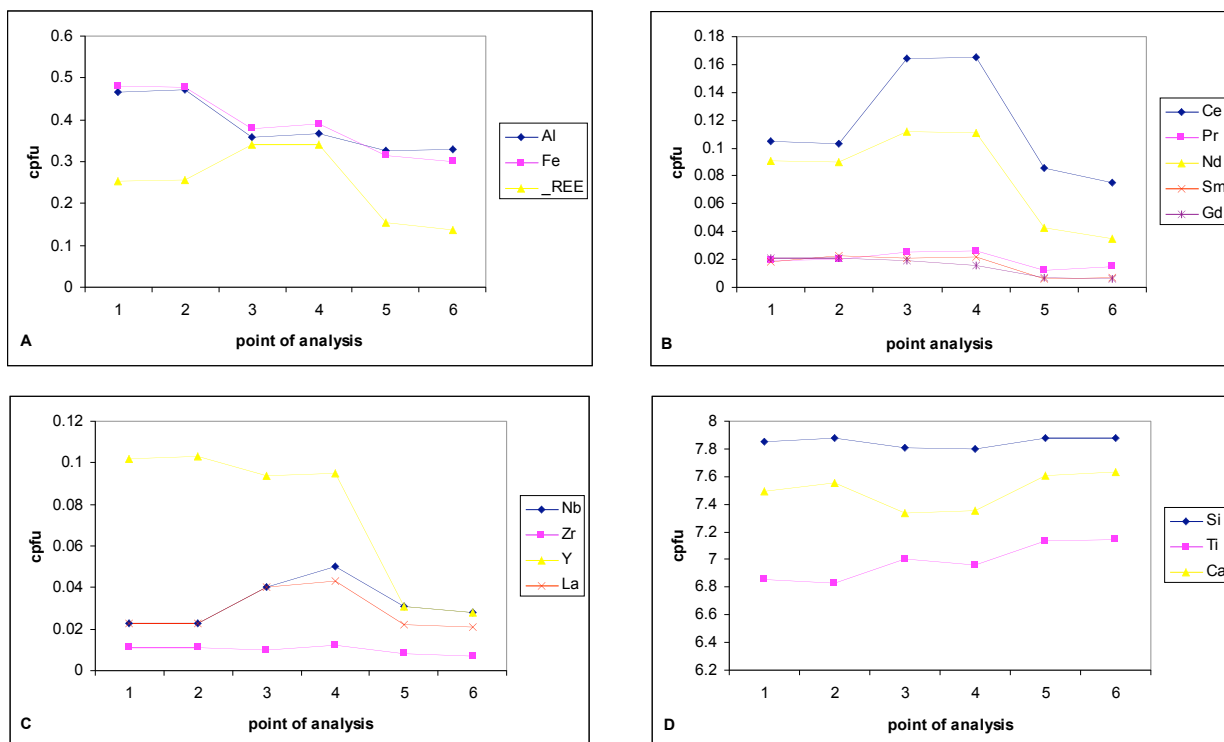
Figure 89: Major and trace element geochemistry of ES5-30. A. Fe, Al and ΣREE variation across the crystal. B. REE variation. C. HFSE variation. D. Ca, Ti, and Si variation

From inspection of the variation in REE and ΣREE (see Figure 89A-B) it is clear that the bright zones sampled by points 3 and 4 have the highest concentration followed by points 1 and 2, with the dark rim (points 5 and 6) being lowest in concentration. Ce and Nd have the highest values of all REE and show the most variation in concentration. The bright zones sampled by points 3 and 4 appear to be related to sector zoning and not necessarily oscillatory zoning, since the dark zones sampled by points 1 and 2 have correspondingly lower REE totals but also have higher Fe and Al than points 3 and 4. This is the same type of pattern that Patterson and Stephens (1992) report from sector zoned titanites, stating that kinetically-induced sector zoning results preferential uptake of REE on certain morphologically key faces (the {111} and {110) faces), while the corresponding morphologically dominant (and faster growing) {100} crystal face preferentially sequesters elements such as Al and Fe. The trace element patterns observed in this crystal, at least with respect to points 1 to 4, are most likely related to sector zoning processes. Further indication of this possibility comes when the variation in Ca and Ti concentration is taken into account (see Figure 89D). The REE substitute for Ca and Fe and Al substitute for Ti, so where there is little REE but lots of Fe and Al in points 1and 2, we can see a corresponding dip in the Ti values and rise in Ca values compared to points 3 and 4, where we see the opposite. There is a high concentration of Nb detected in analyses 1 and 2 (see Figure 89C), and seeing as Nb also substitutes for Ti, the low values for Ti for these points is further explained. Perhaps the reason for high uptake of Nb here is due to forced uptake relating to the sector zoning preferential sequestering mechanism.

The rim of this crystal is dark and subsequently it is unsurprising that there is a lack of REE detected in analyses 5 and 6 when compared to analyses 1 to 4 (see Figure 89A-B). It is also clear that the general trend of behaviour for the HFSE is generally compatible (see Figure 89C), however, there is a noticeable lack of Zr altogether in the crystal, and perhaps this is best explained due to the proximal growth of a zircon crystal causing a local reduction in the available Zr in the melt.

ES5-30 may be summarised as follows:

- The REE and HFSE behave compatibly.

- Lack of Zr due to proximity to Zircon.

- Textural character dominated by sector zoning.

4.10.2 ES5-66 (host granite titanite)

This is a large (300µm) titanite from the granite host portion of the sample, characterised by subhedral morphology with an interstitial rim, and thus it should contain a signature of the late crystallisation history of the melt. It has a bright interior, most likely due to sector zoning, and has some weak oscillatory zoning in the mantle, with one prominent bright zone, before terminating in a dark rim/interstitial area (see Figure 90).

The overall patterns of trace element variation are as expected in terms of concentration when dark zones are compared to light zones. There is, however, a fairly large range of REE values, from less than 0.05cpfu to over 0.375cpfu. The brightest zones sampled (points 5 and 7) have the highest concentration of REE as well as the highest concentration of total HFSE (Y, Zr, La and Nb). The pattern of variation across all points is broadly the same for the REE as it is for the HFSE (see Figure 91A to C). The analyses with the lowest concentration of trace elements are the rim/interstitial areas sampled by points 3, 4, 9 and 10; with points 11 and 12 sampling the outer mantle having slightly higher trace element values. The behaviour of all the trace elements is fairly compatible, as there are no elements which increase in concentration towards the rim. The bright zone denoted by point 7 is the only zone that marks an increase in trace element concentration; otherwise, there is a steady decrease from core to rim.

The REE slope (given by a plot of (Ce+Nd) against Y) shows a roughly linear trend with some outlying points (see Figure 91D). The textural groups form groups that are spread out along the linear trend, indicating a genetic coherence. The fact there is little spread in the slope of REE indicates a fairly closed system, which is coherent with the sample displaying limited physical interaction between the host granite and microdiorite enclave.

ES5-66 may be summarised as follows:

- Compatible trace element behaviour.

- HFSE and REE show very similar variation patterns across the crystal.

- Rim/interstitial areas characterised by very low trace element concentration.

- Linear trend of REE slope is indicative of a fairly closed system, expected of a sample displaying limited mechanical mixing between enclaves and host.
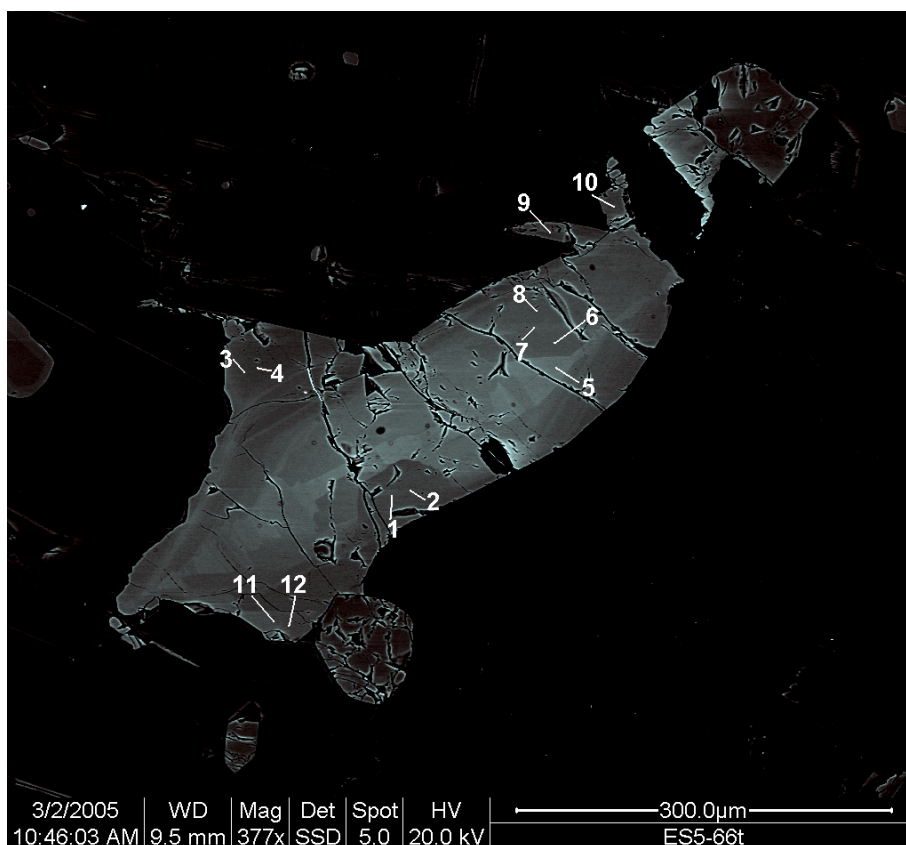
Figure 90: BSE image of ES5-66 (granite) and location of sample points

**Figure 91: Geochemistry of ES5-66. A. Fe, Al and ΣREE variation across the crystal. B. REE variation. C. HFSE variation. D. REE slope for textural groups of ES5-66, given by a plot of (Ce+Nd) against Y (cpfu).**

4.10.3 ES5-8 (diorite enclave titanite)

The enclave portion of sample ES5 is a microdiorite with no extra discerning features that are visible in some of the diorite enclaves, such as amphibole clots, megacrysts of alkali feldspar, or networked veins of granitic material. It is apparently homogeneous. Titanite ES5-8 is the only titanite to be chemically assessed from the enclave portion of sample ES5. The titanite has an anhedral/interstitial texture, which is typical of titanite crystallised from mafic to intermediate melts (Prince 1943; Piccoli, Candela et al. 2000). There is no clear or distinctive pattern of zoning apart from some changes in BSE intensity from core to rim, and indeed it is difficult to discern what may be true core and what may be true rim due to the very anhedral/interstitial nature of the titanite itself. One of the interstitial finger-like protrusions of the crystal has a very bright zoning, which is unusual for titanite in general, where the rims are normally the darker zoned areas when viewed in BSE. (See Figure 92).

Overall, the main thing to note is that fact that there is a lower concentration of trace elements and a smaller spread in values for both the REE and HFSE, when compared to the titanites from the granite portion of sample ES5 (see Figure 93A-C). The ΣREE varies between 0.126 and 0.210cpfu for ES5-8, compared to a range of 0.138 to 0.341cpfu for ES5-30, and a range of 0.020 to 0.382cpfu for ES5-66. The peak values for Y (the most concentrated HFSE in all three titanites), in ES5-8 is less than half of those in both titanites from the granitic part of ES5.

The fact that the highest values for REE and HFSE concentration are from point 9, which samples the very rim of one of the interstitial margins of the rim, is either an indication that there is some late stage change to the melt chemistry or that the trace elements are showing behaviour that is incompatible. Considering sample point 3 is also from a bright zone near the margin of the crystal (and that it is the point with the second highest concentration of trace elements) but points 7 and 8 are also sampling the rim but do not show similar REE values, it is more likely there may have been some late stage change in melt chemistry that was diffusion controlled. The very last parts of the titanite to crystallise may have been affected by some limited diffusion of trace elements from the granite host; this is possible seeing as ES5-8 lies very close to the margin of the enclave and host granite. Titanites from the granite host (ES5-30 and ES5-66) do not show evidence of being geochemically influenced by the diorite enclave, but this may be due to the small size of the enclave
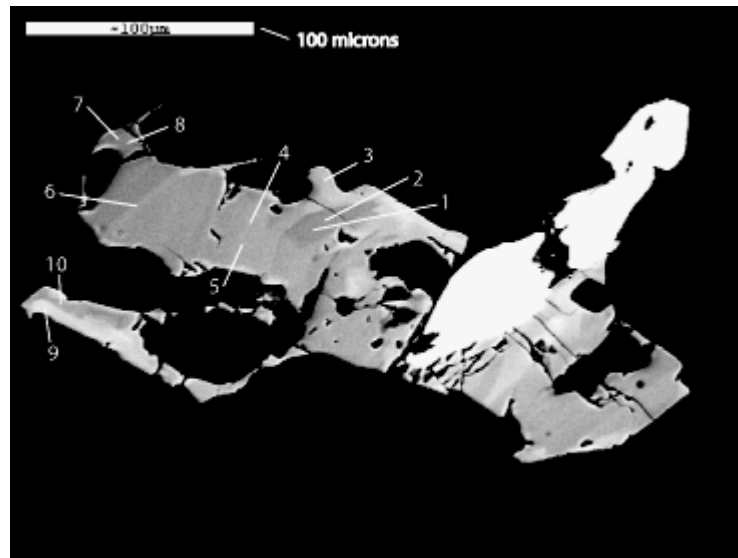
Figure 92: BSE image of ES5-8 (enclave) and location of sample points.
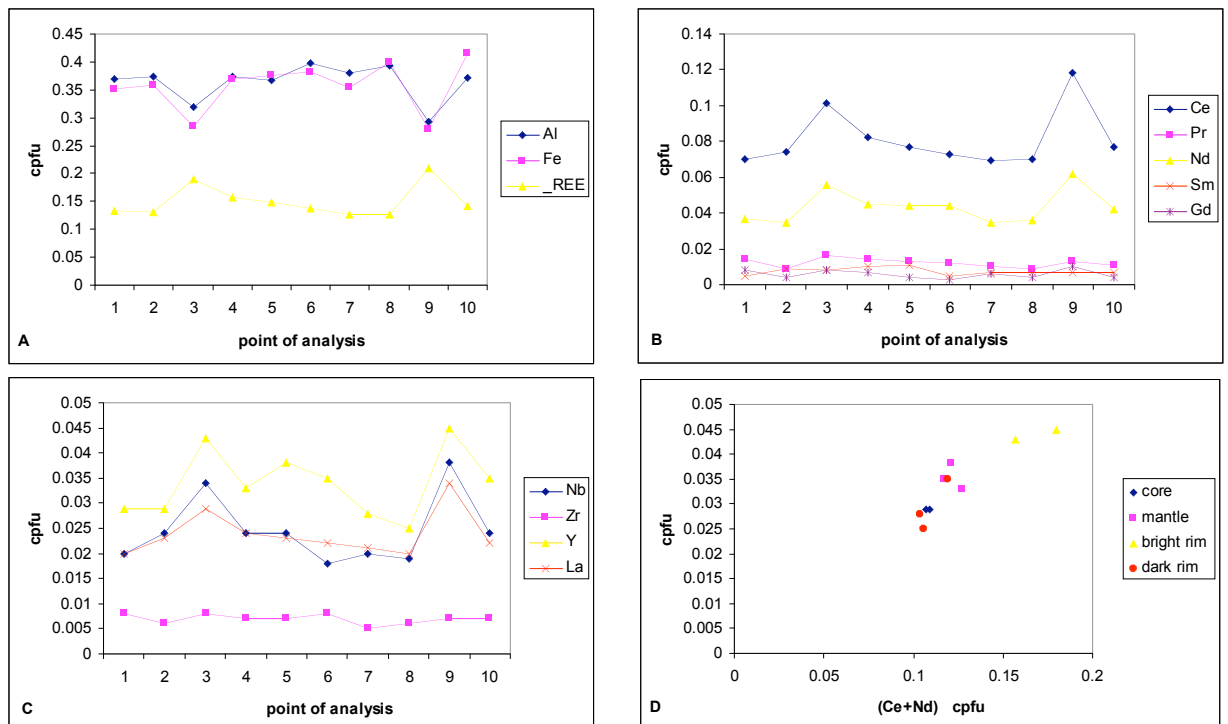
**Figure 93: Geochemistry of ES5-8 (enclave). A. Fe, Al and ΣREE variation across
the crystal. B. REE variation. C. HFSE variation. D. REE slope for textural groups
of ES5-8 given by a plot of (Ce+Nd) against Y (cpfu).**

compared to the host granite. The geochemical gradient between the host and enclave would be such that diffusion would be directed from the granite to the enclave.

ES5-8 may be summarised as follows:

- Interstitial shape, characteristic of titanites form a mafic source.

- Lower concentration and less variation of REE and HFSE than observed in the titanites from the host granite in ES5.

- REE and HFSE enriched in the rim compared to core; possible indication of some limited diffusion of trace elements from the host granite into the diorite enclave.

4.10.4 Summary of ES5

ES5 is a sample displaying a host-enclave relationship that is from an early stage of mingling where there has been limited physical or chemical interaction between the diorite and granite. The geochemistry also reflects this. The titanites from the host granite (ES5-30 and ES5-66) have higher concentrations of REE and HFSE than titanite from the diorite enclave (ES5-8). There is also a significant difference in the textural character of the granite versus enclave titanites in this sample; ES5-8 is extremely anhedral and interstitial in shape compared to ES5-66 and ES5-30, which are euhedral with only the rim ES5-66 displaying a late interstitial component of crystallisation.

 Finally, the reverse zoning (enrichment of REE and HFSE in the rim compared to core) of sample ES5-8 must indicate contamination of trace elements from the host granite. Neither the REE nor HFSE are actually incompatible with respect to titanite in intermediate nor granodioritic melts (Prowatke and Klemme 2005), and therefore normal zoning would be expected unless there has been contamination from an outside source. Although there is limited physical interaction between the enclave and granite, the volumetrically superior granite host has had some influence on the geochemical signature of the diorite enclave; this is likely to be a direct result of diffusion driven by chemical gradients of REE and HFSE between the large host and small enclave.

4.11 A (mixing margin)

Sample A displays a mixing boundary between host granite and diorite enclave that has had sufficient time to interact and produce a reaction zone between the two melts. The fact that the two melts were of sufficient temperature and rheology to mechanically and chemically mix since the titanites within the mixing zone (as well as within the granite and enclave) of the sample may hold a record of the mixing.

4.11.1 A-13 (granite)

The only titanite to be analysed that is from the granitic portion of sample A, A-13 is a euhedral titanite about 300μm long. It displays a central core that appears to have been subject to dissolution, as it forms a non-linear, non-crystal margin parallel boundary with the bright zoned mantle. The core shows evidence of oscillatory zoning that is truncated by the zoning of the mantle. The crystal's growth history is terminated with a dark rim (see Figure 94).

As would be expected, the zoning with the highest concentration of REE is the brightest, which is sampled by point 1 and is in the core of the crystal. The variation in values for ΣREE is from 0.173 (for point 5) to 0.352cpfu (for point 1) which is moderately high considering there are no extremely low values (see Figure 95A-B). The pattern of ΣREE is broadly mirrored by the individual rare earths, with Ce and Nd having the highest values. Analyses 3 and 4 are from the bright mantle and have the next highest values for REE concentration. Analyses 5 and 6 have the lowest values for ΣREE, and as they represent the dark rim of the crystal, this is not surprising. Point 7 is a 10μm spot that samples the fine scale oscillatory zoning of the core, and it records REE values that are less than that of the bright zoning of the rim (points 3 and 4) but greater than the values recorded at the rim (points 5 and 6). This would seem to indicate that there has been a major change to the melt chemistry between the mantle/rim and the core. This is ratified by the solution surface that defines the boundary between the core and the mantle. The cause of such a change may be related to a reduction event brought about by the input of diorite magma into the melt. Sample A is from an area of very high density mingling between granite and diorite enclaves.

Of the HFSE, Y is the only one to mirror the variation of the REE (see Figure 95 C). Nb seems to be significant in that it shows compatible behaviour in both the core and mantle/rim areas, but it is in higher concentration overall in the core area (both the bright
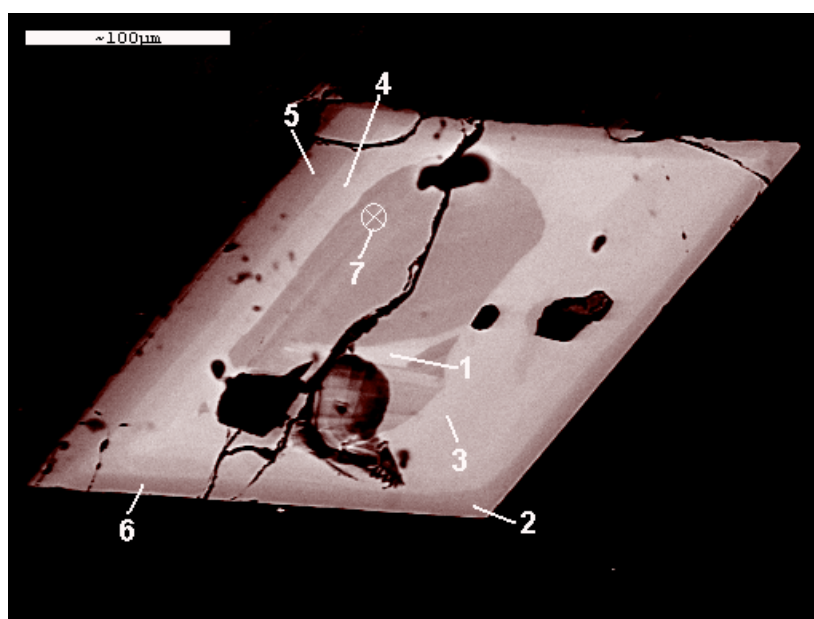
Figure 94: BSE image of A-13 (granite) and location of sample points. Scale bar is 100 microns in length.
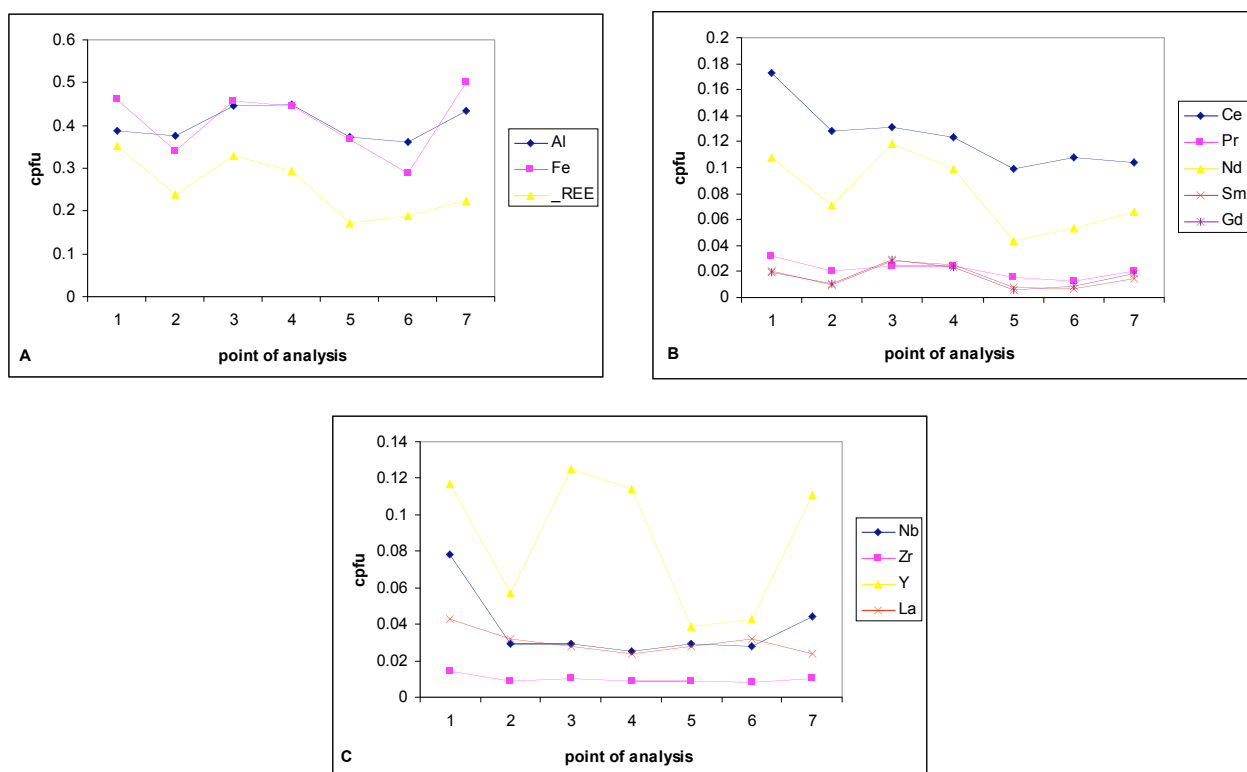
Figure 95: Geochemistry of A-13 (granite) A. Fe, Al and ΣREE variation across the crystal. B. REE variation. C. HFSE variation.

portion of the core -point 1, and the oscillatory zoned outer core -point 7) than it is in the mantle and rim (points 3, 4, and points 5, 6 respectively). The inference made from this information is that the overall change in melt chemistry between the core and mantle/rim is characterised by a diminished concentration or activity of Nb. Zr and La show little variation and are of very low values.

Plotting (Ce+Nd) against Y provides an approximation of the REE slope for A-13. (see Figure 96 below). The textural groups may be divided by the dissolution horizon into two categories: the core area (comprising the bright inner core and oscillatory zoned (O.Z) outer core) and the mantle/rim area.
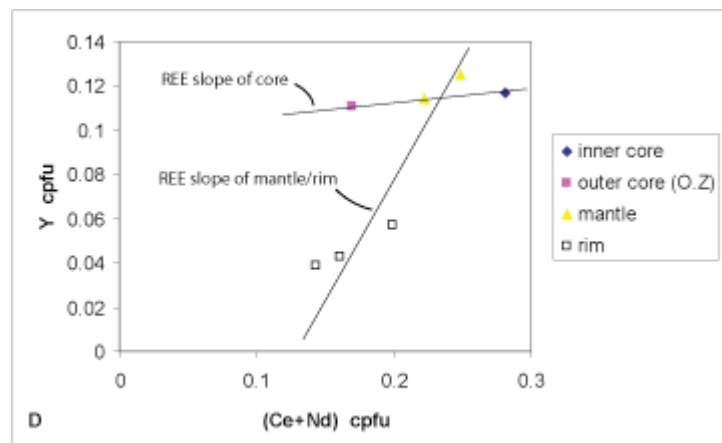
Figure 96: REE slopes of textural groups from A-13 (granite) given by a plot of (Ce+Nd) against Y. Note the significant change in slope between the core and mantle/rim textural areas of the titanite.

The mantle and rim form zoning that is continuous and as such a slope may be drawn through these groups. The inner and outer core also form part zoning that is continuous, and as such, it is reasonable to assume a slope may be drawn through these values. The REE slope for the core area is extremely different from that of the rim and mantle area. Such a change in slope for the REE would indicate that the melt chemistry has been altered due to an open system process, such as magma-mixing. The textural evidence also suggests that there has been a period of dissolution and re-growth of titanite between the formation of the core and the mantle/rim. Sample A displays an advanced stage of chemical interaction between the host granite and its enclaves, whereby the boundary between the two displays evidence of reaction. It is reasonable to assume that the input of mafic magma could have initiated transient dissolution of titanite due to thermal rejuvenation of the granite. Once titanite became stable again, the melt chemistry had been altered to become less fractionated between the LREE and HREE than it was before.

A-13 may be summarised as follows:

- REE and HFSE display compatible behaviour.

- Textural evidence of a transient period of titanite instability is reflected in the compositional zoning, namely, an attenuation of the LREE signature in the mantle/rim compared to the core.

4.11.2 A-57 (enclave)

The enclave portion of sample A is a microdiorite with glomerocrystic clots of amphibole. Titanite A-57 is an elongate subhedral crystal that measures greater than 300μm along the long axis. It is distinguished by the presence of a solution surface separating an inner core with zoning, from a bright outer mantle and darker rim (see Figure 97).

Zoning showing the highest values for REE are the bright parts of the mantle (points 4 and 5), closely followed by the bright portion of the core (point 6). The lowest concentration of REE is from point 7, which analyses the fine scale oscillatory zoning of the core area (see Figure 98A-B). The values for REE for the oscillatory zoned portion of the core (analyses 7 and 3) are lower than those for the rim (points 1 and 2), which would suggest that the overall change in melt chemistry, which has caused the dissolution and re-growth of the crystal, has been one of an overall increase in REE when the core is compared to the mantle and rim. However, the opposite is true for Y and Nb, (see Figure 98C) which register highest in points 3 and 6.

It is clear from the differences in REE and HFSE between the mantle/rim area and the core, that there has been some significant change in melt chemistry. This is most likely to have been a direct influence of mingling and mixing of granitic and dioritic melts. Compared to A-13, this sample has slightly lower max values for REE and for HFSE, this is likely a direct result of the fact that A-57 is from the diorite and A-13 is from the granite. This inference is backed up by the significant difference in the positioning of the core and rim/mantle textural groups when (Ce+Nd) is plotted against Y (see Figure 98D).

A-57 may be summarised as follows:

- Textural evidence of titanite dissolution and re-growth indicates changes in melt chemistry have taken place.
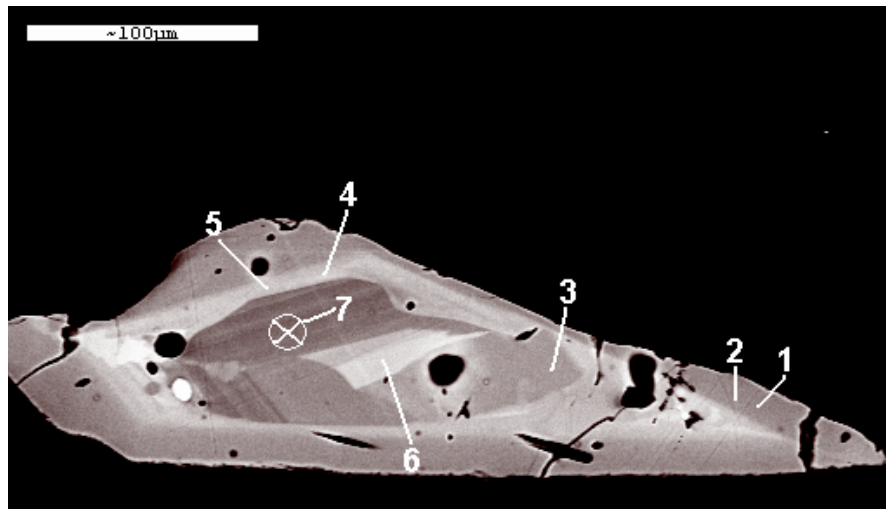
Figure 97: BSE image of A-57 (enclave) and location of sample points. Note the discontinuous zoning marked by the solution surface which separates an oscillatory zoned core from a simply zoned mantle/rim.
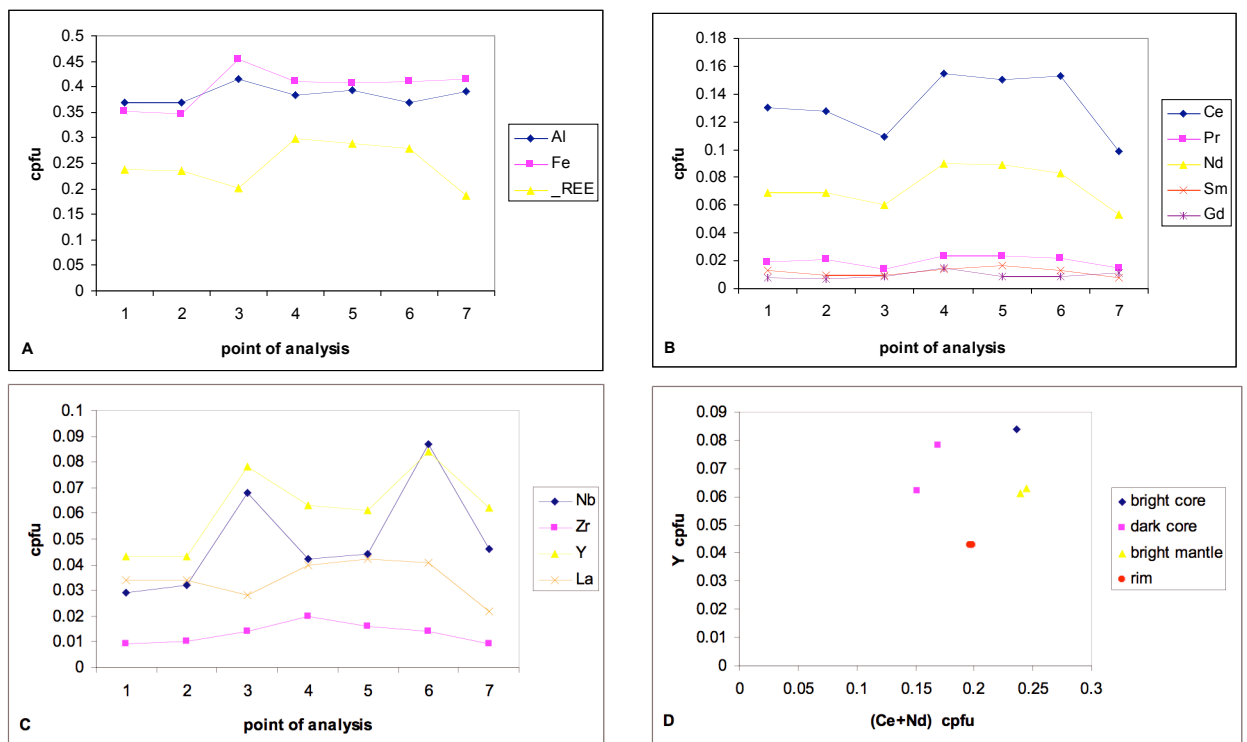
Figure 98: Geochemistry of A-57 (enclave). A. Fe, Al and ΣREE variation across the crystal. B. REE variation. C. HFSE variation. D. REE slope for textural groups of A-57 (enclave) given by a plot of (Ce+Nd) against Y (cpfu).

- The core is less enriched in REE compared to mantle and rim, which indicates a change in melt chemistry involving REE enrichment. Mingling and chemical mixing with the host granite would cause such an increase in REE content.

4.11.3 Summary of A (mixing margin)

Both titanites form this sample show evidence of significant changes in the melt during the crystallisation history. The textural evidence is the same for both crystals: discontinuous zoning. In each case, there is a core area separated from a mantle/rim area by a solution surface. The geochemical signature of the central and outer zones indicates a change in chemistry. For A-13, from the granite portion of the sample, the change in geochemical signature indicates a lowering of REE concentration and especially a relative depletion of LREE, which would be indicative of mixing with a mafic magma. For A-57, the opposite is true, and the mantle/rim area shows relative enrichment in the REE compared to the core, an observation concordant with an influence from a more REE rich granitic melt.

4.12 Discussion and conclusions

The great variety of textures displayed by titanite from the ROMG, with respect to both crystal shape and compositional zoning, is by and large corroborated by the geochemical signatures that are a reflection of the processes which have led to the formation of the rocks they come from.

The variation of the trace elements observed in titanite is a direct reflection of the compositional zoning pattern. Melts that are enriched in particular trace elements will pass on that signature to the titanites. If melts of significant contrasting chemistries mix or mingle, then titanite may record any significant instance of trace element diffusion between the melts. More importantly, there doesn't need to be a transfer of trace elements between mingling/mixing melts for titanite to record evidence of the interaction. If the melts are of significantly different oxygen fugacities, then titanite may become destabilised and partially dissolve. This dissolution may only be temporary, but it may be difficult to tell if it was a product of increasing heat of the melt of if it was due to a change in oxygen fugacity. Titanite however, may record evidence of the cause of dissolution based on the nature of re-growth. As shown by some of the titanites within the ROMG (ROM1-40, ROM-21, ES3A-27), re-growth following a period of dissolution may be attributed to a change in oxygen fugacity if the new titanite growth is characterised by unusually low REE content. This is related to the nature of trace element incorporation in the titanite

structure; REE are taken up due to coupled substitution mechanisms involving tetravalant Al and Fe. If a melt becomes reduced then the activity of ferric Fe will also be reduced, thus inhibiting the ability of titanite to take up REE by affecting the activity of the coupled substitution (Wones 1989; Piccoli, Candela et al. 2000).

The trace element content of titanite will reflect the trace element content of the rocks that it formed in, especially with respect to the REE and HFSE signature. In the ROMG sample set there are two main lithological end-members: the RM1 granodiorite (silicic end-member) and the ESd1 synplutonic diorite dyke (mafic end-member). The other samples analysed represent mingled and mixed occurrences of these two lithologies. Arguably, ES16 represents a fully hybridised variant of RM1 and ESd1. In essence, if titanite is able to retain a signature of the trace-element content of the melt it formed in, then titanite analysed from each of these rocks should display a different geochemical fingerprint. Since the rocks are part of a co-genetic suite formed in part by magma-mixing processes, then it stands to reason that titanite may also record evidence of this magma mixing in the trace element signature. A plot of (Ce+Nd) against Y gives an approximation of the REE slope of titanite, and if RM1, ESd1 and ES16 are plotted together the results show an interesting relationship between the three.
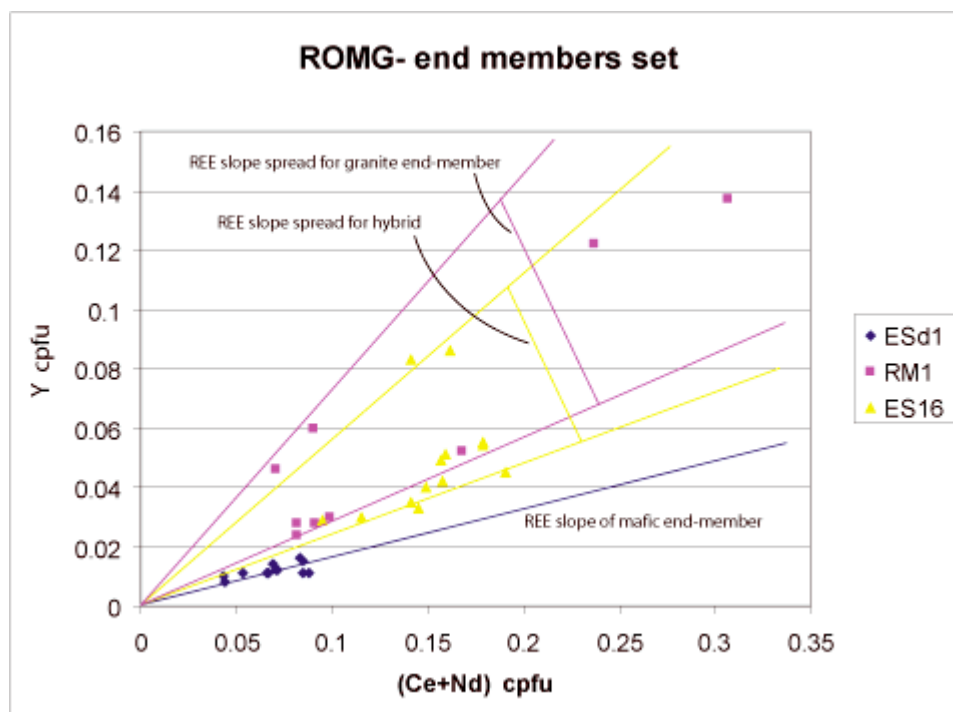
Figure 99: REE slope of ROMG end-members (RM1, ESd1) and hybrid variant (ES16).

The first thing to note is that this plot is very effective at graphically separating different lithologies based on the REE slope of titanite. The slope of the ESd1 is relatively LREE enriched compared to the slope of RM1 and the slope of ES16 lies (variably) between the two. The spread on the REE slope for both RM1 and ES16 is significant, whereas the spread of slope for ESd1 is almost non existent by comparison (at least on the scale of this graph).

The ROMG is a very complex suite of rocks, and it's difficult to be certain of the true nature of any of its facies in terms of being an end-member lithology. RM1 is almost certainly not an end-member in the truest sense, although it is the most evolved rock to be sampled form the ROMG. It is likely that fractional crystallisation and partial melting processes at depth have both played a part in the formation of RM1 prior to emplacement, and hence it is unlikely to be a true end-member. RM1 is likely to be a product of open system processes. On the other hand, ESd1, as a synplutonic dyke, is more likely to be representative of a melt source which has seen less mixing or contamination prior to emplacement in the ROMG. If this is the case, then is makes sense that there is less spread on the REE slope for ESd1, as fractional crystallisation is more likely to be the main petrogenetic process involved in its formation.

When considering the overlap of the REE slope spread of RM1 and ES16 and their relation to the REE slope of ESd1, it is reasonable to assume that the pattern is a reflection of the magma-mixing processes that have operated in their formation. ES16 is a lithology that represents a hybridised mixture of RM1 and ESd1, and this mixing process is reflected in the REE slope of titanite.

Titanite from the ROMG displays trace element partitioning behaviour that, for the most part, reflects the published work of Prowatke and Klemme (2005). However, there are instances where the behaviour of certain trace elements, especially the REE, does not reflect normal partitioning behaviour at all. This is almost exclusively related to petrogenetic processes that have led to significant changes in melt chemistry. Prowatke and Klemme (2005) show that melt composition is a very important factor in the partitioning behaviour of trace elements with respect to titanite, and this is confirmed by the record of compositional zoning in titanite from mixed-magma rocks form the ROMG. Titanite ES5-8 is from the diorite enclave of a sample and it displays reverse zoning; it is enriched in REE in the rim and not the core. This is certainly due to contamination from the host granite, otherwise normal REE partitioning behaviour would be observed.

Another way in which titanite reflects the petrogenetic processes operating to form the rocks in which it is found, is that it has been found to reflect the degree of homogenisation of the melt. ES16 is a hybridised rock, and as the most mixed rock of the ROMG co-genetic suite which represents a very advanced stage of mechanical and chemical mixing. This thorough mixing and homogenisation of the component melts is reflected in the simple compositional zoning of titanite ES16-7. It has very little REE variation and the only zoning visible is sector zoning, which is driven by crystal chemical controls and not melt.

A plot of the titanite REE slope for the whole ROMG data set clearly shows that there have been significant changes in slope, indicating an open system. Each sample reflects a different stage of the mixing/mingling process and also has its own unique spread in REE slope. It is possible to differentiate between these lithological groups and also to asses their degree of relatedness by using information stored in the compositional zoning of titanite.
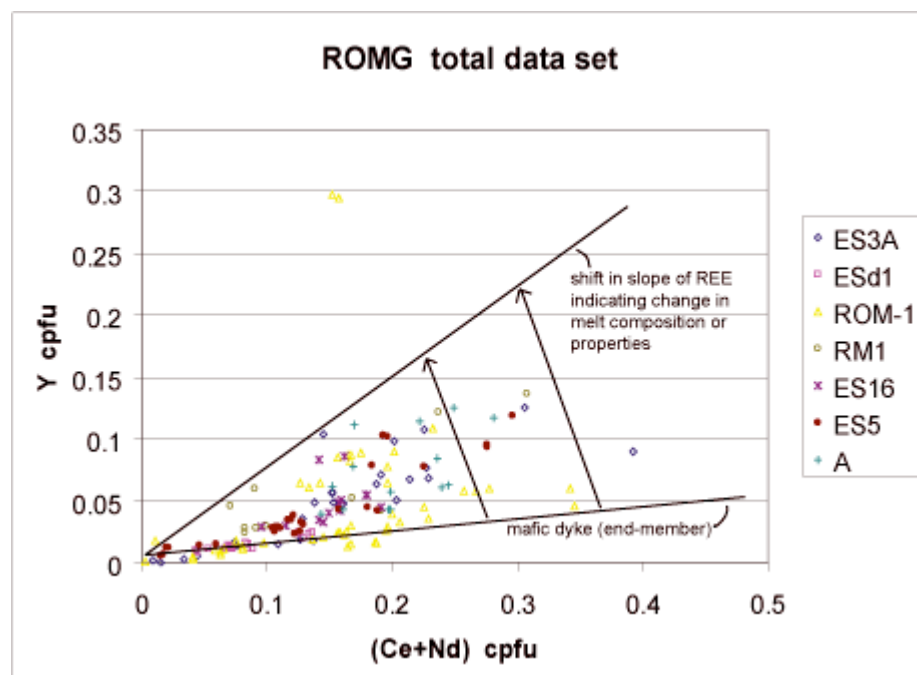
Figure 100: REE slope plot for the entire ROMG dataset.

In conclusion, titanite from the ROMG displays a variety of complex textures, both with respect to crystal shape and compositional zoning that are the result of the petrogenetic processes which have operated to form the rocks they are found in. In the case of the ROMG, magma-mingling and mixing are the dominant petrogenetic processes, and titanite can record evidence of both simple mingling and thorough mixing in its textural history.

5

Fish Canyon Tuff

5.1 Introduction

The aim of the project is to ascertain whether of not titanite is able to preserve evidence of magma-mixing processes in the chemical zoning of the crystal. The ROMG has served as a plutonic end-member for the study as it has clear evidence for magma-mixing at depth, and on a variety of scales. Magma-mixing is thought to be an important mechanism for initiating large-scale pyroclastic eruptions (Lipman, Doe et al. 1978; Didier and Barbarin 1991; Clarke 1992; Lipman, Dungan et al. 1996; Lipman, Dungan et al. 1997; Bachmann, Dungan et al. 2000; Bachmann, Dungan et al. 2005)and as such may play an important role in the petrogenetic history of such eruptions which may be easily hidden due to the fact that pyroclastic deposits are prone to alteration. In addition to this, the quenched and glassy nature of pyroclastic deposits and to some extent the homogenisation associated with emplacement at the surface, may act to mask the details of petrogenesis. Cognate magmatic material may not contain evidence of mixing at depth and unless there is textural or geochemical alteration of phenocrysts prior to eruption, then evidence may be very sparse. Titanite is a very geochemically robust accessory mineral that has the ability to serve as a sink for trace elements, the REE and HFSE in particular, and hence it may possible preserve a record of the changing conditions within a magma chamber during petrogenesis, including evidence of magma-mixing processes. The Fish Canyon Tuff is the largest documented pyroclastic eruption and serves as the volcanic end-member in this study to asses the ability of titanite to record evidence of magma mixing processes. (Lipman, Doe et al. 1978; Whitney and Stormer 1985; Ellwood, Stormer et al. 1989; Lipman, Dungan et al. 1996; Lipman, Dungan et al. 1997)

5.2 Literature Review

Study of the Fish Canyon Tuff has been ongoing for more than 35 years (Lipman, Doe et al. 1978; Hildreth 1981; Whitney and Stormer 1985). It is the largest ever documented

pyroclastic eruption with a total estimated erupted output in excess of 5000 km^3 occurring in less than 2.5 Ma years (Lipman, Dungan et al. 1996). The tuff has also received much attention due to the peculiar nature of the rock itself; it is an extremely voluminous crystal rich dacite that is compositionally homogenous. Hildreth (1981) referred to the Fish Canyon Tuff as his archetypal voluminous silicic ignimbrite, a type of deposit he referred to as "Monotonous Intermediates". The study of such batholith size pyroclastic deposits, erupted from relatively shallow but large magma chambers, is very important in gaining an understanding of magmatic processes occurring in crustal settings; not simply because of their size, but also because they represent the largest known explosive volcanic phenomena and ignimbrites like these represent rapidly erupted and quenched magmas, allowing glimpses into the nature of the plutonic environment from which they came (Bachmann, Dungan et al. 2000; Bachmann, Dungan et al. 2002; Bachmann and Bergantz 2003; Bachmann, Dungan et al. 2005)

The Fish Canyon Tuff is the largest of the 17 pyroclastic ash-flow deposits that comprise the Tertiary San Juan volcanic field, which is located on the eastern edge of the Colorado Plateau, southwest Colorado, USA (see Figure 101 below). The entire San Juan field covers an area of over 25 000 km^2 and comprises a volume of rock in excess of 40 000 km^3 (Bachmann et al 2002).
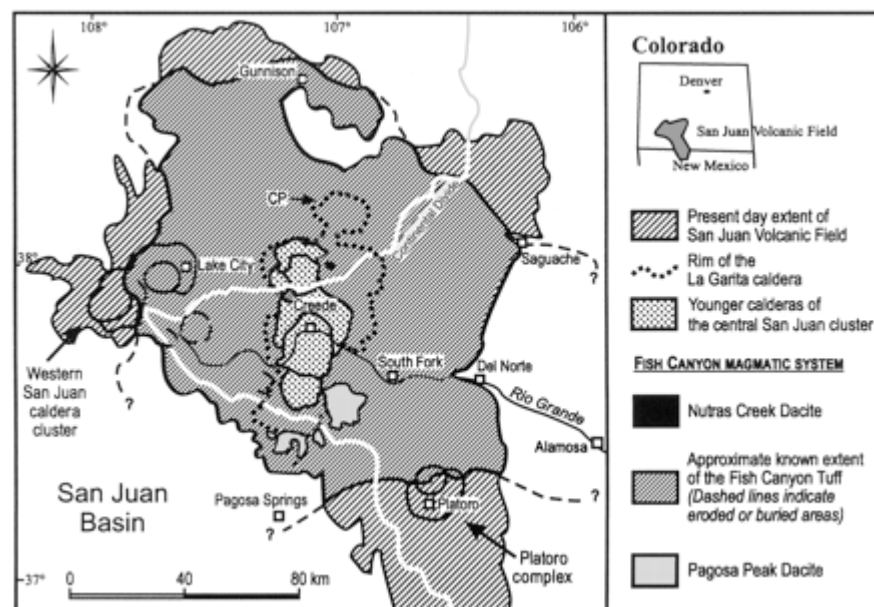
Figure 101: San Juan Volcanic Field and Fish Canyon Tuff location map. From Bachmann et al (2002).

Magmatic activity in the San Juan volcanic field commenced roughly 33.5 Ma years ago, with Fish Canyon erupting in the period 28.5-26 Ma years ago (Lipman, Dungan et al.

1996; Oberli, Bachmann et al. 2002; Bachmann, Oberli et al. 2007; Charlier, Bachmann et al. 2007). The magma body involved in the Fish Canyon Tuff eruption is thought to have been involved in three major eruptions. The first produced the Pagosa Peak Dacite; a small (200km^3) poorly vesiculated and poorly fragmented rheomorphic ignimbrite. This eruption was the pre-caldera phase with respect to the creation of La Garita caldera, the caldera created by the Fish Canyon eruption. The second eruptive phase was that of the Fish Canyon Tuff itself, and is considered to have occurred concomitantly with caldera collapse. The final stage of eruption produced a volumetrically minor dacitic lava, the Nutras Creek Dacite (Bachmann 2002).

The Fish Canyon Tuff is thought to have erupted from a compositionally monotonous and un-zoned magma chamber, and is characterised by its bulk chemical homogeneity (67.5-68.5 % SiO_2), the high crystal content (35-50% of the rock) and the near-solidus phenocryst assemblage (quartz, sanidine, biotite, plagioclase, hornblende, titanite, apatite, zircon, magnetite and ilmenite) (Lipman, Doe et al. 1978; Lipman, Dungan et al. 1997; Bachmann, Dungan et al. 2002). The Pagosa Peak dacite is identical to the Fish Canyon Tuff in bulk chemistry and phenocryst assemblage but differs in degree of vesiculation; it is a poorly fragmented dacite with rheomorphic features as opposed to a highly vesiculated, pumice-rich tuff like the Fish Canyon deposit. Essentially, although they are identical in bulk chemistry and phenocrysts assemblage, they are different in terms of eruption style and degree of inclusion of juvenile/co-magmatic clasts of dacite. The Pagoska Peak dacite is more representative of the Fish Canyon magma body since it was produced by effusive fire-fountaining phenomena as opposed to violent pyroclastic eruptions producing the highly fragmental and glassy Fish Canyon Tuff. The magma chamber is considered to have cooled to a near solidus temperature, rigid crystal mush prior to eruption (Grunder and Boden 1987; Johnson and Rutherford 1989; Bachmann, Dungan et al. 2002; Bachmann, Dungan et al. 2005; Charlier, Bachmann et al. 2007). The eruption mechanism has been proposed as thermal rejuvenation of the magma body brought about by the upward percolation of a hot, low density water, carbon dioxide and fluorine rich fluid derived from a mafic magma which underplated the magma body (Bachmann et al, 2003).

5.3 Sample description

Samples for study were provided by Olivier Bachmann, who has written and co-authored many papers on the Fish Canyon Tuff and the Pagosa Peak Dacite. (Bachmann and Dungan 2002; Bachmann, Dungan et al. 2002; Bachmann and Bergantz 2003; Bachmann,

Dungan et al. 2005; Bachmann, Oberli et al. 2007). The samples provided came from the intracaldera facies of Fish Canyon tuff (BFC-104b and BFC-129), and the outflow (extra-caldera) facies of the Fish Canyon Tuff (BFC-124). Also included was a sample of the Pagosa Peak Dacite (BFC-55). All of these samples are referred to in Bachmann et al's 2002 paper "The Fish Canyon Magma Body, San Juan Volcanic Field Colorado: Rejuvenation and Eruption of an Upper-Crustal Batholith.

Since the bulk chemistry and phenocrysts assemblage of the Fish Canyon Tuff and Pagosa Peak Dacite is identical, and a general description of the chemistry and phenocryst assemblage has already been given in section 6.2 above, it isn't necessary to describe each sample in turn again. However, there are key differences between the samples in terms of eruptive history that may have significance to this study, and these are outlined below.

BFC-129 and BFC-104b are from the intracaldera facies of the Fish Canyon Tuff, and as such, they are products of the waning stages of eruption. Collapse of La Garita caldera during the end stages of chamber evacuation allowed the final erupted pyroclastic material to accumulate within the caldera. This may be significant in terms of the textural and geochemical attributes of the titanites. The final stages of eruption are likely to be sampling magma from the deeper reaches of the magma chamber, and if melt conditions were not homogenous within the chamber or if petrogenetic processes in operation prior to eruption were different in different parts of the chamber, then titanite may record these incongruities in its texture and compositional zoning.

Bachmann et al. (2002) report previously unrecognised quenched andesite inclusions from the Fish Canyon Tuff. While they acknowledge that volumetrically significant mingling or mixing with a more mafic component is unlikely to produce such a small amount of andesite inclusions found in main the Fish Canyon Tuff (outflow), they do confirm the possibility that the magma chamber was weakly heterogeneous and such heterogeneity may be indicated by the preferential occurrence of andesitic inclusions in the late-erupted intracaldera facies. BFC-124 is from the outflow (extra-caldera) facies of the Fish Canyon Tuff. The only consideration here is that it represents the main phase of eruption and should therefore reflect the majority of the magma from the main body of the magma chamber. The main petrological difference between the outflow and the later intracaldera deposits is the preferential presence of andesitic inclusions in the latter.

BFC-55 is from the Pagosa Peak Dacite. It represents a precursor eruption to the Fish Canyon Tuff, with a comparatively low-energy eruption with respect to the main Fish

Canyon Tuff. It is a poorly vesiculated and poorly fragmented pyroclastic deposit containing a high proportion of juvenile clasts (40-60%) up to 4m in length, that were emplaced as viscous magma with finer fractions of pumice, ash and phenocrysts (Lipman, Dungan et al. 1997; Bachmann, Dungan et al. 2000; Bachmann, Dungan et al. 2002; Bachmann and Bergantz 2003; Bachmann, Dungan et al. 2005). These juvenile magma "blobs" represent unmodified samples of the Fish Canyon magma body, and they preserve textural criteria hitherto unrecognised from the main Fish Canyon Tuff; in particular, resorption textures are not seen only in quartz, but are also found in feldspar, and amphibole. Furthermore, evidence of grain-boundary melting is also preserved where to feldspar phases, or feldspar and quartz, are in contact(Bachmann, Dungan et al. 2002). As the precursor eruption to the Fish Canyon Tuff, the Pagosa Peak dacite may have been tapped from the upper reaches of the magma chamber, and is likely to preserve characteristics of that portion of the melt. If it preserves resorption textures in feldspar and amphibole that were hitherto unrecognised from the Fish Canyon Tuff, it may also preserve such textures in titanite. Below are typical examples of the texture of the Fish Canyon Tuff (Figure 102) and Pagosa Peak Dacite (Figure 103).
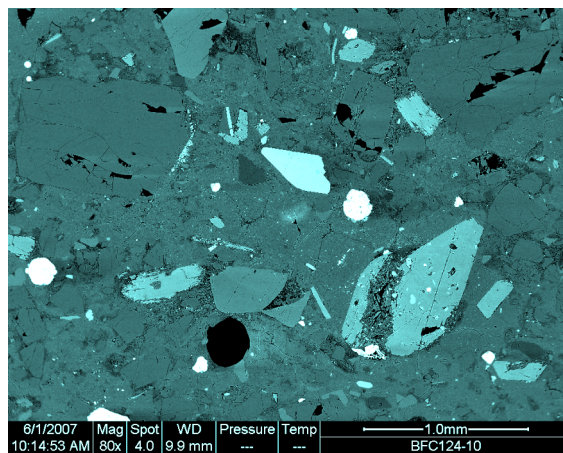
Figure 102: BSE image of Fish Canyon Tuff outflow, sample BFC-124. The bright euhedral crystal near the middle of the image is a titanite (BFC-124-10). Note the glassy, pyroclastic matrix in which the phenocrysts are set. Phenocrysts include: amphibole (large, bottom right); small, bright, rounded Fe-oxides (next to titanite and also at the left edge); large feldspar (upper left corner).
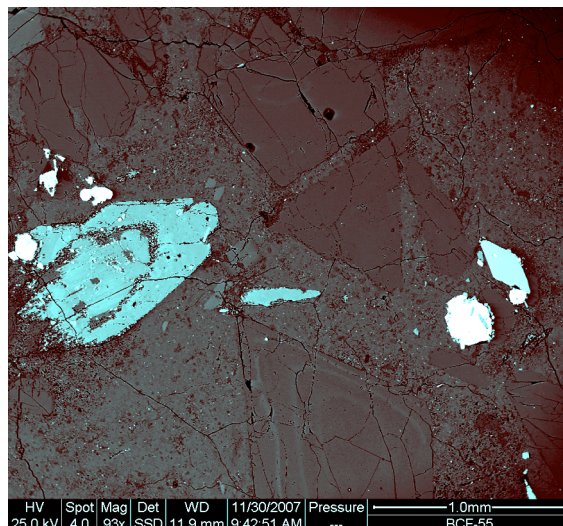
Figure 103: BSE image of the Pagosa Peak Dacite. Note the bright euhedral titanite at the right, sitting next to a round bright Fe-oxide. On the left there is a large, partially altered hornblende.

5.4 Geochemistry

Geochemical analysis was done by electron microprobe analysis (EMPA) at the Grant Institute for Earth Sciences at the University of Edinburgh and was achieved with technical support from Dr David Steele. The EMPA unit employs a Cameca SX100 equipped with 5 vertical crystal spectrometers and a PGT Spirit energy dispersive analyser. The instrument operates under Windows 2000 and uses Cameca's PeakSight software.

For details of analytical methods and sampling rationale refer to the analytical methods section in Chapter 5, ROMG titanite geochemistry.

5.4.1 BFC-124 (outflow sample)

Sample BFC-124 is from the outflow of the Fish Canyon Tuff, and most represents the early stages of magma chamber evacuation and hence the phenocrysts within it most likely sample the shallower parts of the magma chamber. Two main textural types of titanite are found in this sample, titanites with no visible zoning in BSE imaging and those with visible zoning. Two of the samples showing good zoning features also show evidence of dissolution/re-growth and inclusion of ilmenite along the solution horizons. Similar solution features where seen in titanite from the ROMG and are thought to be related to the changes in oxygen fugacity or melt temperature brought about by the input of a reducing mafic magma component. Three titanites where chosen to geochemically characterise; two that show dissolution/re-growth with ilmenite inclusions, and one subhedral un-zoned titanite. The following is an account of the textures and geochemistry of the analysed titanites from BFC-124.

5.4.1.1 BFC-124-5

Points of analysis were chosen in order to characterise the three main textural zones of titanite BFC-124-5: the bright core, the darker ilmenite inclusion rich mantle, and the oscillatory zoned rim. The boundary between the core and the mantle represents a solution surface, and zoning from the mantle can be seen to cross-cut the core zoning (see Figure 104 for BSE image and sample point location)**.**

BFC-124-5 contains the second highest concentration of REE in all of sample BFC-124 (analysis point 3), yet also contains the second lowest REE concentration (analysis point 1) and as such it contains the widest range of REE. The REE concentration is highest in the core (see Figure 105A-B), which is represented by sample points 3 and 4. Analysis point 3 corresponds to the brightest portion, however, it looks to be sector zoning. Point 4 samples

Figure 104: BSE image BFC-124-5 and location of sample points. Points 1 and 4 are 10μm defocused spots, the others are 1 μm spots.
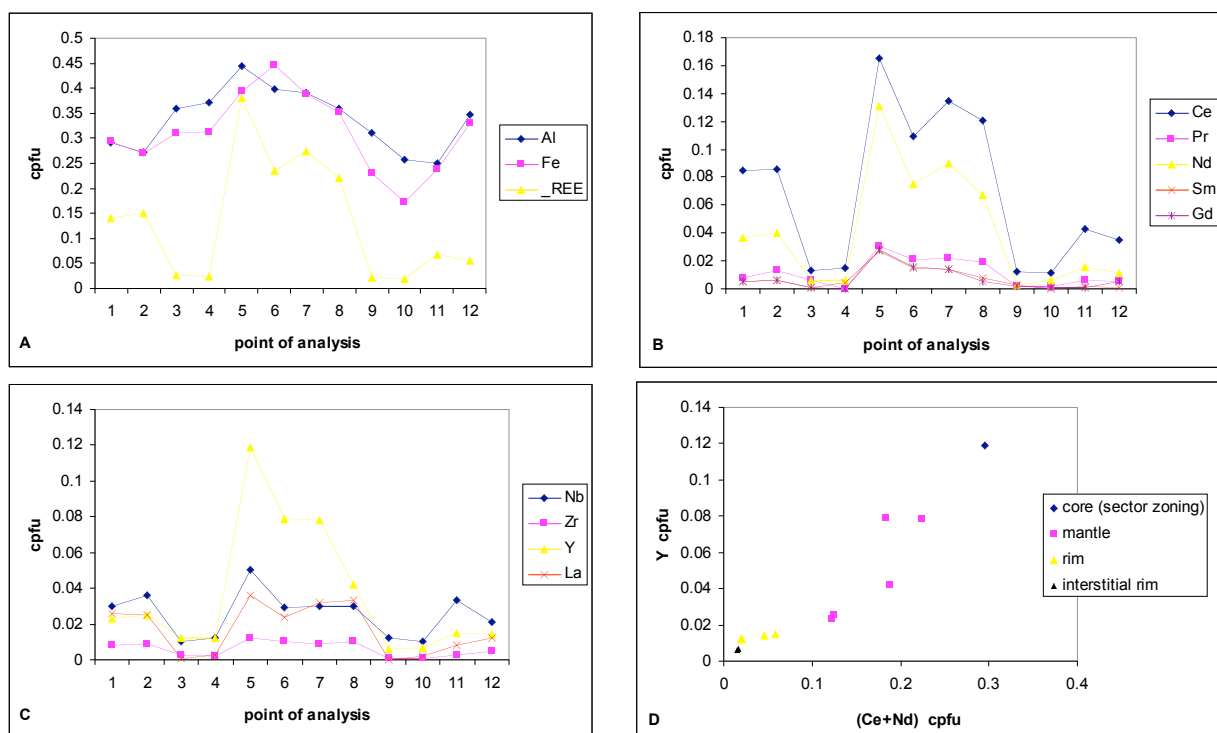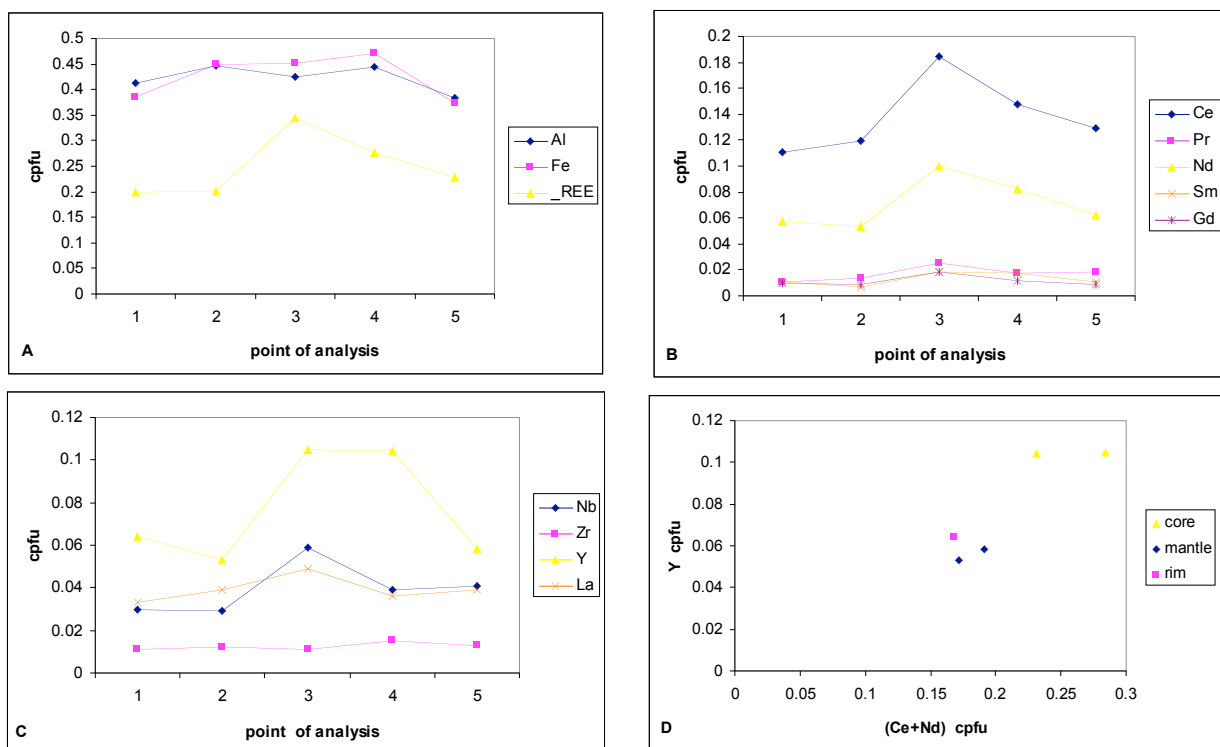

Figure 105: Geochemistry of BFC-125-5. A. Fe, Al and ΣREE variation across the crystal. B. REE variation. C. HFSE and La variation. D. REE slope for textural groups of BFC-124-5, given by a plot of (Ce+Nd) against Y.

a different sector face than point 3, and is hence slightly poorer in total REE content, however, it does show similar concentrations of Zr and Y (see Figure 105B-C). When sector zoning develops, less compatible elements (as well as Al and Fe) tend to be taken up by the morphologically dominant and faster growing {100} crystal face, compared to the {111} face, which is less dominant yet tends to take up the REE and more compatible elements (Paterson and Stephens 1992). Analysis 4 records the highest values for Fe and Al as well having substantial Zr and Y which are less compatible than the REE; hence, the chemical differences between point 4 and point 3 are most likely due to sector zoning. One unusual aspect of the REE totals is revealed by a comparison of analyses 5 and 2, which both sample the mantle. Analysis point 5 samples a darker zone but it has a higher total REE value (0.229cpfu) compared to point 2 (0.202 cpfu). There isn't much difference and there is nothing in the other graphs to indicate why there would be such a difference, however, point 5 is very close to a bright portion of the rim, and there may be an influence from this.

Analyses 1 and 2 sample the rim and mantle respectively. The ΣREE for both of these points is nearly identical; although a quick look at the individual REE variation (see Figure 105B) shows that there are slight differences between the rim and mantle. The rim (point 1) is slightly richer in Nd, whereas the mantle (point 2) is slightly richer in Ce and Pr. There are also differences between the rim and mantle when it comes to the HFSE, with Y increasing from mantle to rim, and Zr and La decreasing from mantle to rim (see Figure 105C).

A plot of (Ce+Nd)/Y shows definite groupings where the mantle and rim sample points plot together and the core sample points plots together (see Figure 105D). This plot, in conjunction with the overall pattern of REE variation, and when combined with the textural zoning of the crystal (solution surface with ilmenite inclusions, re-growth), seems to suggest a clear evidence for a magmatic event that significantly changed the melt chemistry between growth of the core and growth of the mantle/rim. The main points of interest in geochemical terms may be summarised as follows:

- Melt chemistry change between the core and mantle/rim. Possible link to reduction event, such as the introduction of a mafic magma.

- Overall the core to rim pattern is one of compatibility for most elements, especially the REE.

- Sector zoning is the most likely reason for differences between sample points in the core (compare analyses 3 and 4).

- The rim is richer in Nd and Y compared to the mantle, but it is also poorer in La and Zr, Ce and Pr.

5.4.1.2 BFC-124-7

Titanite BFC-125-7 is similar to BFC-124-5 in textural characteristics, especially the presence of a solution horizon with ilmenite inclusions and subsequent re-growth. The overall pattern of zoning is also very similar: a bright core with some evidence of sector zoning, separated from a dark mantle (with ilmenite inclusions) by an irregular solution surface, and a dark uniform rim. The main difference between the two titanites lies in the fact the BFC-124-7 is a fragmented phenocryst, probably just less than half its original size. A large number of phenocrysts from the Canyon Tuff are fragmented due to the violent pyroclastic nature of the eruption. Points of analysis were chosen to characterise the geochemistry of each of these zones (see Figure 106 BSE image of BFC-124-7 and points of analysis). One interesting aspect of the crystal is the presence of some small Fe-Ti oxides on the very outside of the rim.

The first thing to note is that the results for analysis points 2 and 6 are almost identical (see Figure 108A-C). They both sample the bright outer core which has relatively uniform zoning; there is some very fine scale oscillatory zoning visible, but it is quite faint. Sample point 6 is an analysis which has employed a 10 micron de-focused beam and it was situated to sample the brightest patch of zoning of the outer core. The REE content of point 6 (0.331cpfu) is just slightly higher than point 2 (0.319cpfu). The Y and Nb values show a similar pattern, where titanite-6 is ever so slightly higher in concentration. The overall pattern of all trace elements between the two points is similar, and this is most likely due to the overall uniformity of the zoning found in the outer core. This may be evidence of the melt being fairly stable at the time, with temperatures stable but high enough for diffusion to occur, and little in the way of input of new material to effectively alter the melt chemistry or conditions.

The highest values for REE concentration are from analysis point 1, the brightest part of the whole crystal and essentially the only remnant of the central portion of the core (see Figure 108A-B). The highest value of ΣREE is also from point 1 and is 0.396cpfu.
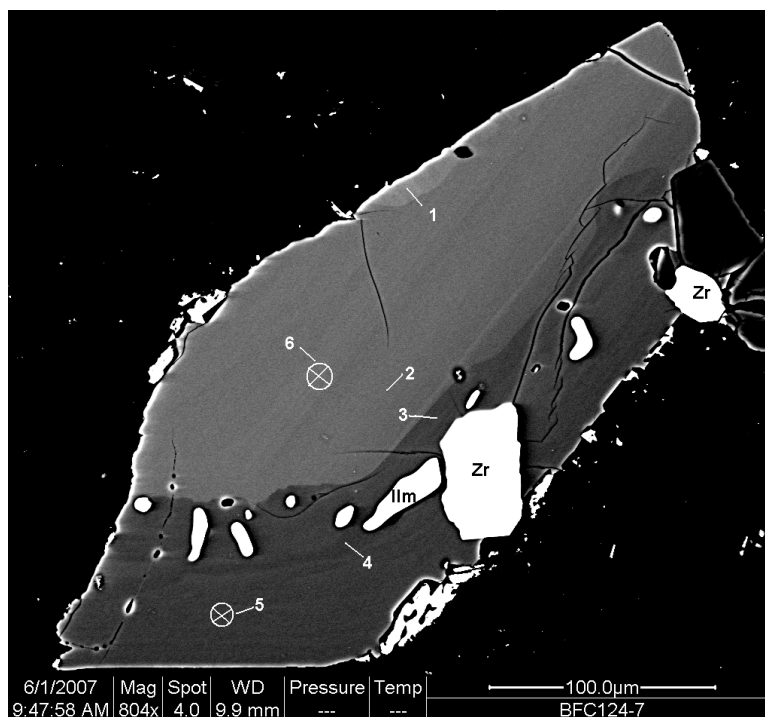
Figure 106: BSE image of BFC-124-7 and location of sample points. Points 5 and 6 are Figure 107, the rest are 1 μm spots. Note the inclusions of zircon and ilmenite along the core-rim boundary.
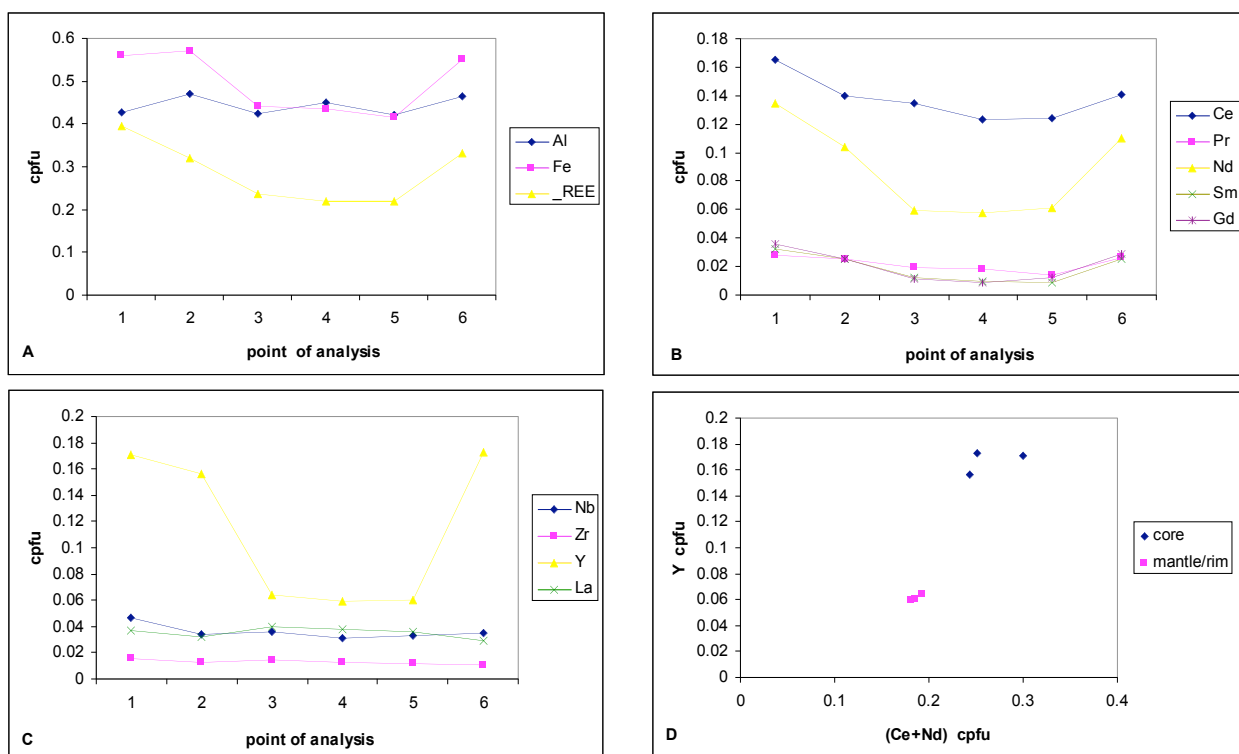
Figure 108: Geochemistry of BFC-125-7. A. Fe, Al and ΣREE variation across the crystal. B. REE variation. C. HFSE and La variation. D. REE slope for textural groups of BFC-124-7, given by a plot of (Ce+Nd) against Y.

The lowest value recorded (0.218cpfu) is from point 4, which samples the darkest portion of the mantle. The boundary between the mantle and rim portions of the crystal is poorly defined in terms of zoning, but the mantle is defined from the rim more readily by the presence of ilmenite inclusions in the former. Analysis point 4 seems to sample the very last part of the mantle, a dark zone that precedes the oscillatory zoning of the rim. Point 3 samples the initial chemistry of the mantle where it borders the core. A solution surface separates the two zones. The total REE concentration in the mantle/rim is at its highest at point 3. Analysis 5 is a 10 micron spot that measures the oscillatory zoning of the rim and shows REE values very close to those of analysis point 4. The behaviour of Ce and Nd is different in the mantle/rim when compared to the core, with Nd values dropping significantly more in the mantle/rim than Ce does, and a plot of (Ce+Nd) against Y distinguishes the rim/mantle chemistry from that of the core (see Figure 108D). Of all the HFSE, Y by far shows the largest variation between core and mantle/rim, which also helps to distinguish the two areas in the plot mentioned above.

La is behaving curiously, as it does not mirror the LREE, as would be expected. It seems to behave in an opposite manner from the REE, overall it is more enriched in the mantle/rim than it is in the core. The highest concentration of La is found in the first portion of the mantle (point 3), and there is a uniform drop in concentration from analyses 3 through 5. The pattern for La in the core area is highest at the brightest spot (point 1). Analysis point 6 is less concentrated in La than point 2, so there is not a progressive decrease along the core profile. The behaviour of La can be described as compatible; however, the instance of increased values in mantle/rim versus core would suggest that whatever event caused the change in melt conditions between core and mantle also possibly served to increase the La content of the melt. A summary of the main points of interest are as follows:

- All of the trace element trends define two main groups: a core area defined by high REE content and a mantle/rim area defined by lower REE content.

- The mantle-core contact is characterised by dissolution and re-growth of titanite, accompanied by ilmenite inclusions; an indication of transient instability of titanite, possibly brought about by input of a mafic magma and ensuing reduction of the melt.

- La behaviour is very different from the remainder of the REE, showing higher values in the mantle/rim than in the core, however, the overall behaviour of La in each zone is compatible.

5.4.1.3 BFC-124-1

BFC-124-1 is a fairly small (less than 150 microns wide) un-zoned titanite. Like most titanites from Fish Canyon it is fragmented and is most likely a small part of a larger phenocryst. There are 2 fairly straight edges to the crystal and since there is no visible zoning it is possible that this fragment represents an un-zoned rim. It is also possible that the whole original crystal itself was un-zoned and we are just seeing a fragment of it. Two points of analysis were chosen, one using a 1 micron focused beam and the other using a defocused 10µm beam. The reason for this was to make sure that there weren't any fine scale changes in chemistry that the 1 micron beam might miss (see Figure 109 for BSE image and sample point location).

Both analyses (point 1 and point 2) show nearly identical geochemistry, so it is fair to assume that the crystal is homogeneous chemically. In comparison with the other two titanites examined from BFC-124, this titanite displays a similar chemistry to the mantle and rim of BFC-124-5 and BFC-124-7. A plot of (Ce+Nd) against Y for all data points from BFC-124 (see Figure 110) demonstrates how geochemically similar BFC-124-1 is to the mantle/rim of both BFC-124-5 and BFC-124-7. It is entirely possible that this titanite represents a late crystallisation, and hence why it is similar chemically and texturally to the fairly uniform rims of BFC-124-7 and BFC-124-5. It is also possible that BFC-124-1 is a broken portion of a much larger crystal and is from the rim of that crystal; however, the overall shape would seem to suggest this is not the case as it looks subhedral and would perhaps be longer and thinner if it was a rim fragment.

5.4.1.4 BFC-124 summary

It is interesting to compare the data from all three titanites from the outflow sample and see clear groups of data points which correspond to specific textural features; the mantle/rim signature is similar between BFC-124-7 and BFC-124-5, and BFC-124-1 has a similar chemistry. The (Ce+Nd)/Y plots illustrate this very well (compare Figure 105D, Figure 108D and Figure 110). The plots show that BFC-124-7 has a core that is more enriched in Y compared to BFC-124-5. According to Prowatke and Klemme (2005) Y is moderately compatible with respect to titanite from intermediate melts, so perhaps BFC-124-7 started to crystallise slightly earlier than BFC-124-5.
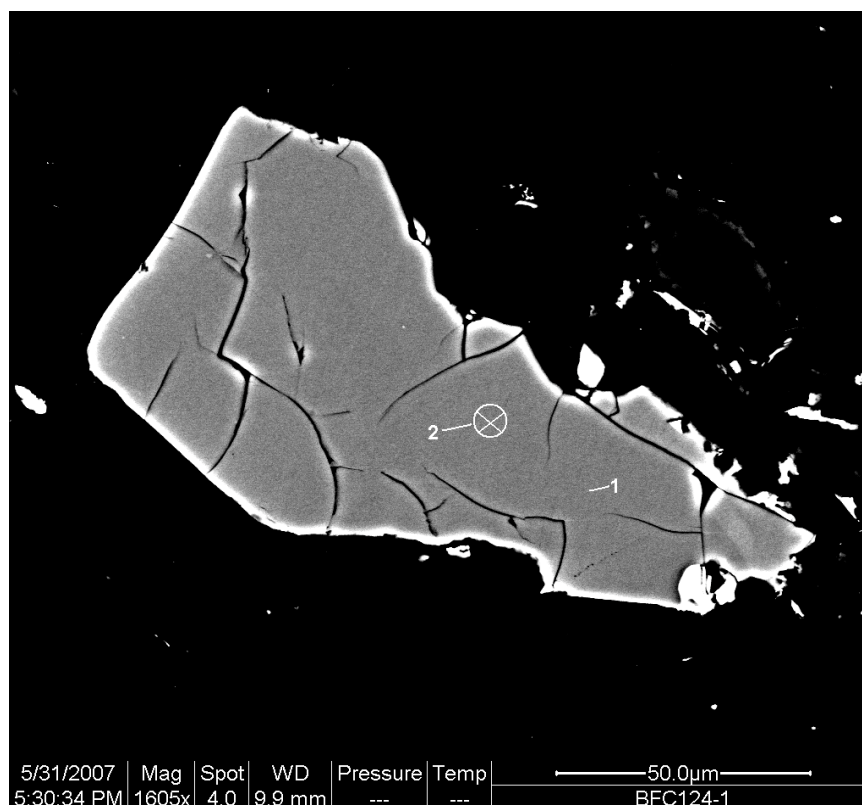
Figure 109: BSE image of BFC-124-1 and location of sample points. Note that point 2 is a 10μm defocused spot and point 1 is a normal 1 μm spot.
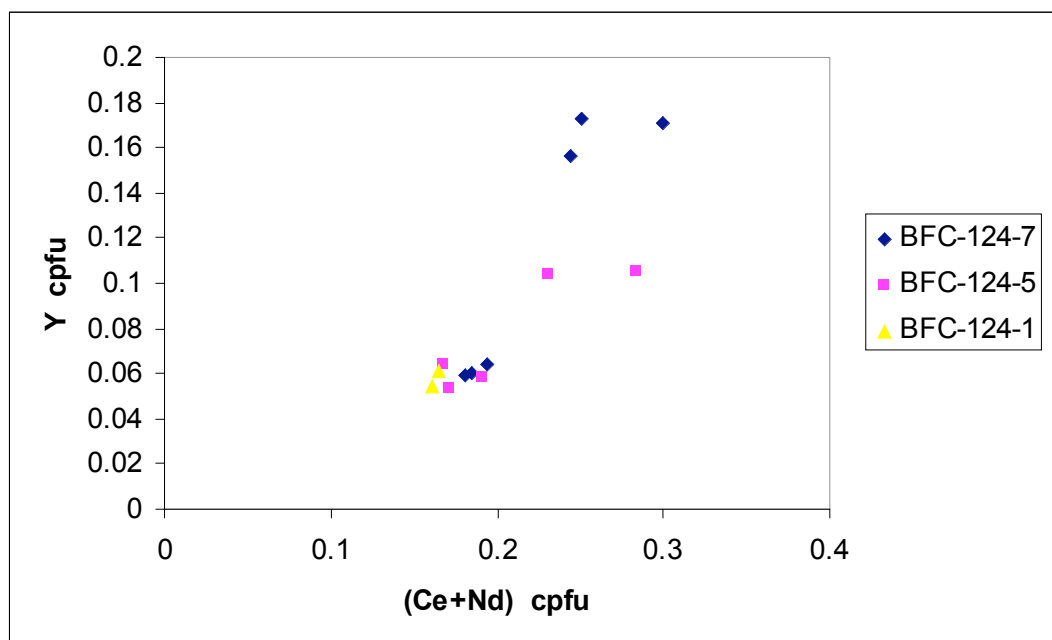
Figure 110: REE slope plot for entire BFC-124 (outflow) dataset, given by plotting (Ce+Nd) against Y.

The clear geochemical differences between core and mantle/rim for BFC-124-5 and BFC-124-7, in conjunction with their textural features, would seem to suggest that an event occurred that significantly altered the melt chemistry. This signature has been preserved by the titanites. The solution surfaces and ilmenite inclusions indicate a transient destabilising of titanite and concomitant nucleation of ilmenite, most likely brought about by a reducing event, such as the input of mafic magma into the magma chamber (Nakada 1991; Piccoli, Candela et al. 2000; Tiepolo, Oberti et al. 2002). Sample BFC-124 is from the outflow of Fish Canyon, and as such most likely represents the later stages of eruption and possibly is from the deeper portions of the magma chamber where there was interaction between a silicic crystal mush and an underlying hotter mafic melt prior to eruption (Bachmann, Dungan et al. 2002; Bachmann and Bergantz 2003; Bachmann, Dungan et al. 2005).

5.4.2 BFC-104b-5 (intracaldera)

The intracaldera rocks from Fish Canyon represent the final stages of the voluminous eruption and as such is likely to represent magma from the deeper reaches of the chamber (Bachmann, Dungan et al. 2002). BFC-104b-5 is the only titanite to be analysed from sample BFC-104b. It is a large euhedral titanite, over 600 microns long, with very well developed oscillatory zoning and fir-tree style sector zoning along its centre (see Figure 111). The overall pattern of zoning is simple: a bright central area which becomes progressively darker towards the rim. However, the rim itself is more complex. It contains numerous ilmenite inclusions and is has a darker and sometimes patchy pattern of zoning. The textural evidence would indicate that melt conditions changed enough to destabilise titanite and allow the nucleation of ilmenite. Titanite must have become stable again as the margins of the rim are straight. Points of analysis were chosen in order to sample the different zones (see Figure 112).

The geochemistry of this titanite reflects the same patterns seen in those of sample BFC-124; the elevated values of REE correspond to the bright core and the lower values correspond to the dark rim. The highest values for REE are from the sector zoned parts of the core (analysis point 5) which has a ΣREE content of 0.325cpfu. The lowest ΣREE is 0.202cpfu and is from analysis point 4, which samples the dark rim (see Figure 113A). The REE all show a similar variation, however, Sm, Gd, and Pr are very low in concentration. The main REE signature is from Ce and Nd (see Figure 113B).

6/1/2007 | Mag | Spot | WD | Pressure | Temp | 300.0µm
1:00:39 PM | 329x | 4.0 | 10.0 mm | --- | --- | BFC104-5
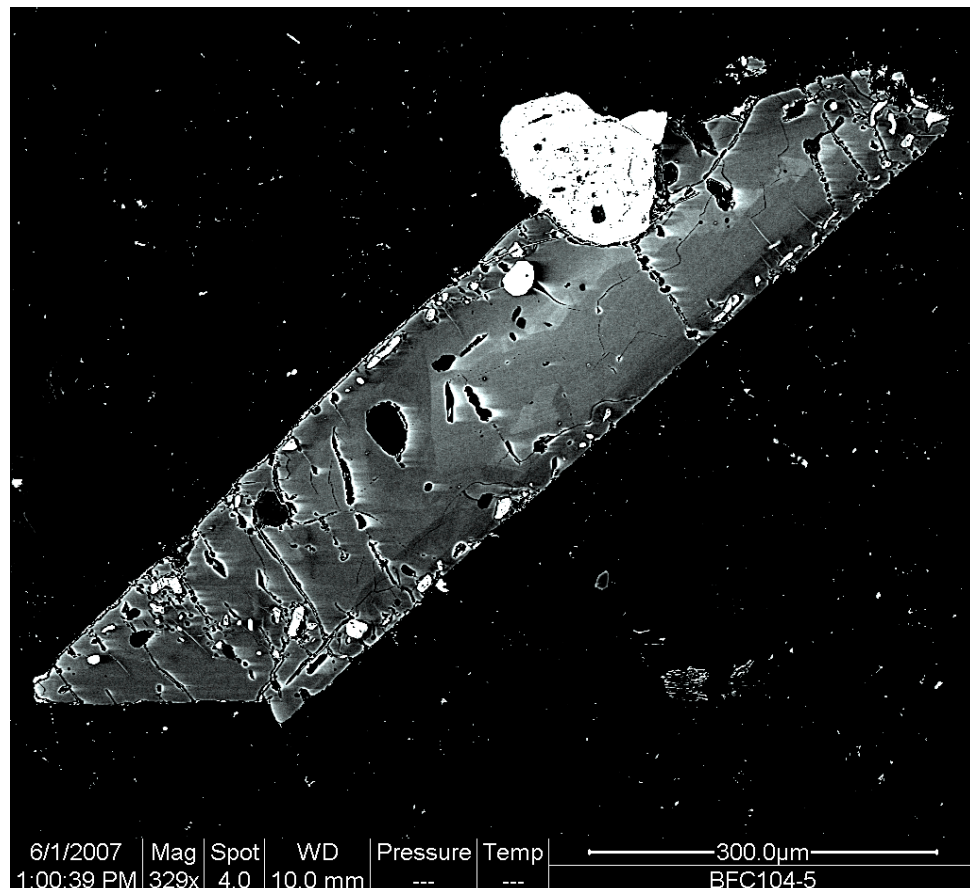
**Figure 111: BSE image of whole crystal of titanite BFC-104b-5 (intracaldera).
Note the bright zoning of the interior compared to the dark rim. The dark rim
has many small bright inclusions of ilmenite.**

Upon inspection of the HFSE, the patterns of variation seem to mimic that of the REE (see Figure 113, compare B and C) with one exception, Zr, which seems to show the opposite pattern: it is more enriched in the rim than it is in the core. Zr may be considered incompatible in this case, or another explanation would be that the melt later became enriched in Zr. La follows a pattern very similar to the REE, which is more like the behaviour expected for La. In samples from the Ross of Mull Granite (ES3A-59, ROM1-40, ROM1-21, A-13) La behaviour has diverted significantly from that of the of other REE, and from Y and Nb; however, in this titanite they all show a very similar pattern, especially La and Nb.

As shown for other samples, plotting (Ce+Nd) against Y for all data points displays geochemical groups that correspond to zoning and how it is linked to the slope of the REE for the sample. In such a plot for BFC-104b-5 (see Figure 113D), it is clear that the rim and core have different geochemical characteristics. Furthermore, it can be seen that the sector zoning of the core (point 5) is slightly more enriched in trace elements compared to
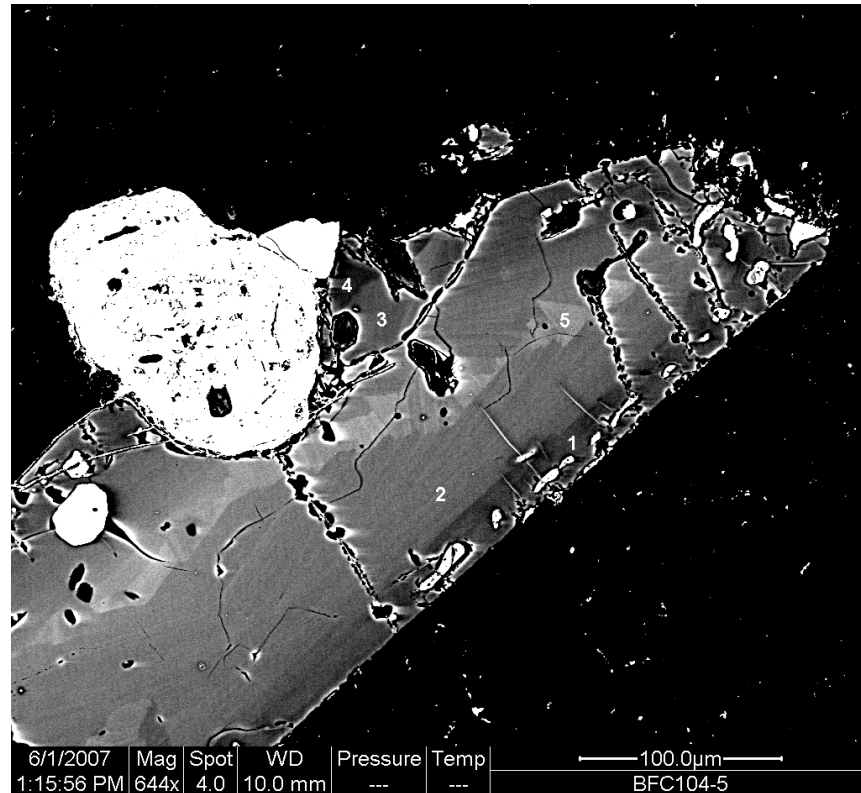
Figure 112: BSE image of zoning detail from titanite BFC-104b-5 (intracaldera) and location of sample points.
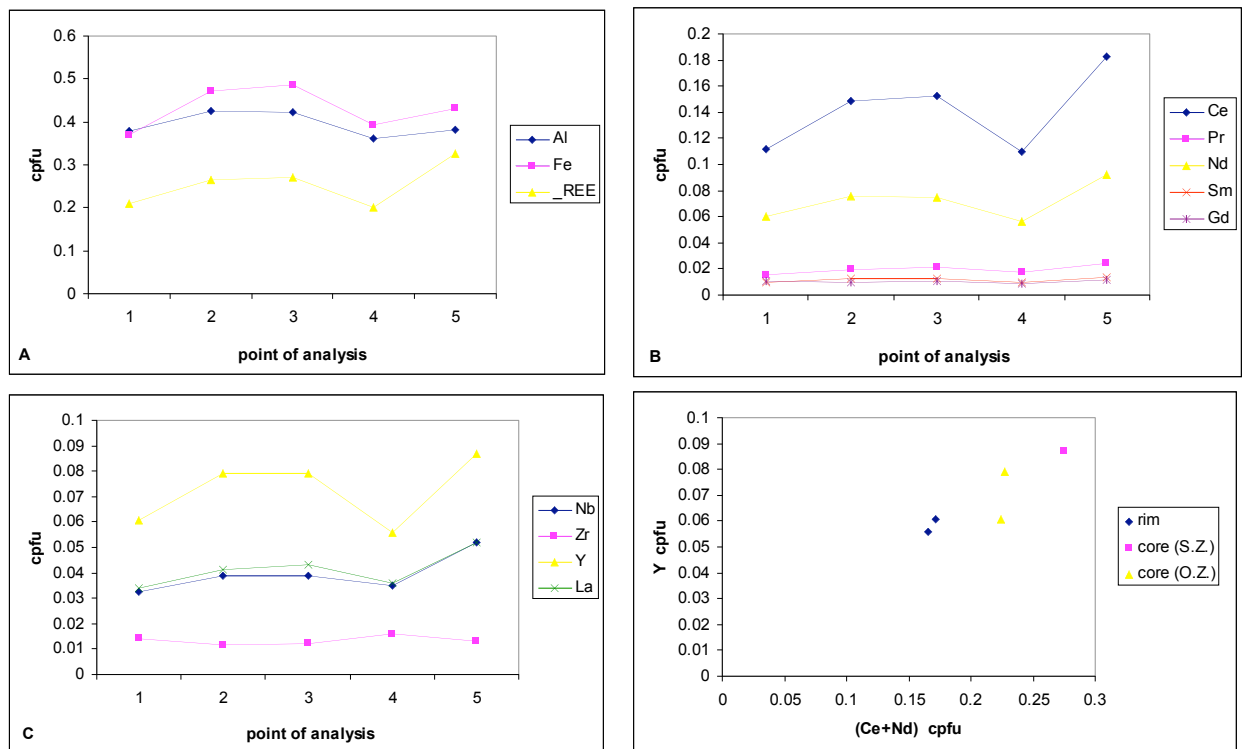
Figure 113: Geochemistry of BFC-104b-5 (intracaldera). A. Fe, Al and ΣREE variation across the crystal. B. REE variation. C. HFSE and La variation. D. REE slope for textural groups of BFC-104b-5, given by a plot of (Ce+Nd) against Y.

the oscillatory zoned core (points 2 and 3). The main geochemical points for BFC-104b-5 may be summarised as follows:

- Plotting (Ce+Nd) against Y clearly defines the rim from the core, where the latter is more enriched in trace elements.

- La variation is similar to the total REE, which is unusual compared to other samples (especially those from the Ross of Mull Granite).

- Zr displays a variation that is the opposite of the REE pattern as it is enriched in the rim relative to the core; interpreted as either incompatible behaviour or the melt subsequently becoming enriched in Zr.

- The textural evidence for titanite becoming unstable prior to rim formation, with concomitant ilmenite nucleation, is reflected by the changes in geochemistry between the rim and core.

5.4.3 BFC-129 (intracaldera)

BFC-129 is a sample of the intracaldera part of Fish Canyon, just like BFC-104b. As such, it possibly samples the deeper reaches of the chamber, as it formed from the final stages of eruption, during caldera collapse. Most titanites from this sample show evidence of 3 main episodes of growth and one episode of dissolution. Numerous ilmenite inclusions are associated with the dissolution horizons. Titanite BFC-129-10 typifies the geochemical patterns observed from BFC-129.

5.4.3.1 BFC-129-10

The textural characteristics of this crystal hint at a period of instability of titanite early on in the crystallisation history. The core has a uniform zoning, which is moderately bright in BSE; this core, however has been subject to dissolution, creating an undulose solution surface. The solution surface is also associated with the growth of ilmenite inclusions. When titanite growth resumed the resulting pattern of zoning produced was very patchy, and this forms the inner mantle of the crystal. This patchy zoning is succeeded by a more uniform outer mantle. The rim is also relatively uniform and thick while also being slightly brighter than the inner and outer mantle; fine-scale oscillatory zoning is well developed. Points for analysis were chosen to sample each of the textural features described (see **Figure 114** for BSE image and analysis points).
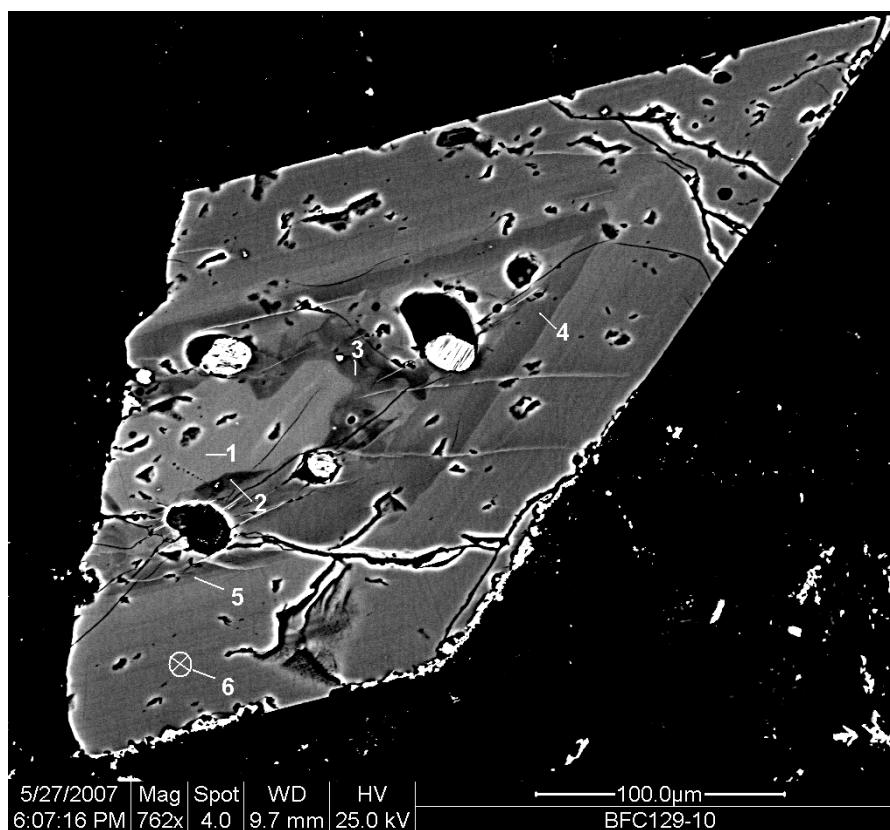
Figure 114: BSE image of titanite BFC-129-10 (intracaldera) and location of sample points. Note that point 6 in a 10 spot, the rest are 1µm.
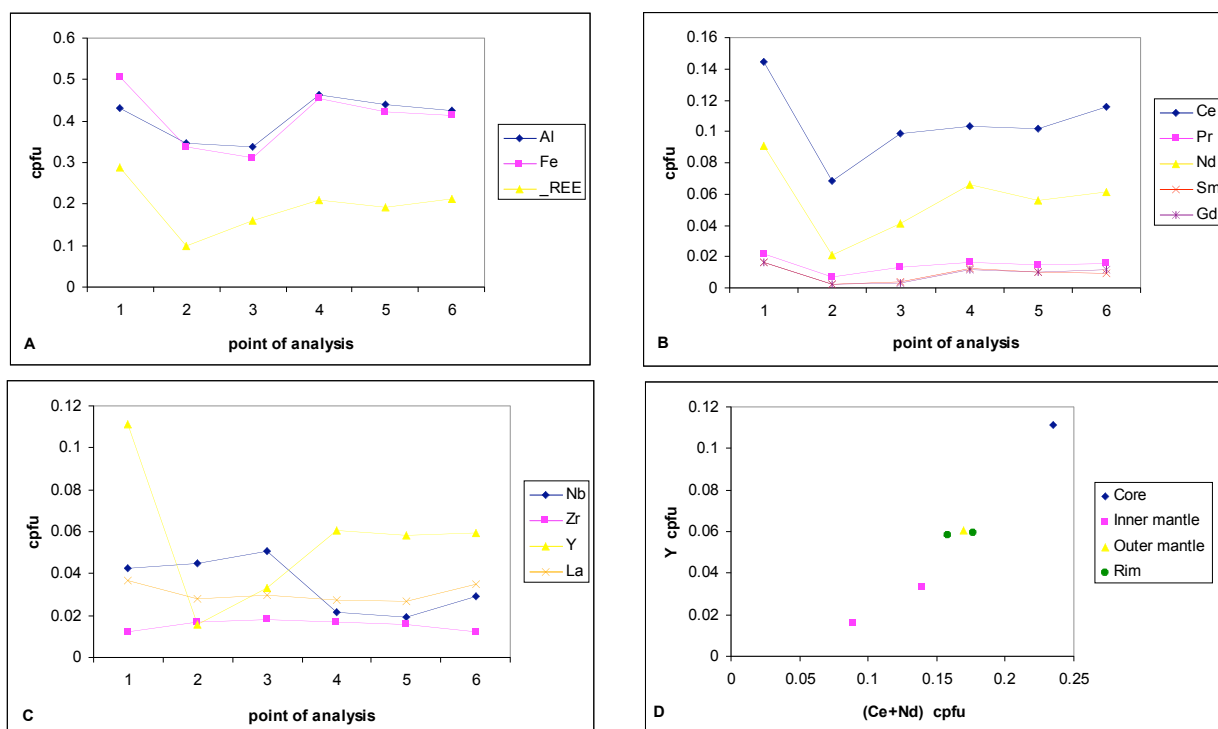
Figure 115: Geochemistry of BFC-129-10 (intracaldera). A. Fe, Al and ΣREE variation across the crystal. B. REE variation. C. HFSE and La variation. D. REE slope for textural groups of BFC-129-10 given by a plot of (Ce+Nd) against Y.

The total REE content varies between 0.289cpfu for the bright centre (analysis point 1), and 0.100pcfu for dark zoning of the inner mantle (point 2) (see Figure 115A-B). Analysis point 3, another data point form the inner mantle, is slightly richer in total REE compared to point 2, but not as rich as the outer mantle (point 4). The rim seems to be about as rich in total REE as the inner mantle; a comparison of analyses 5 and 6 with 4 shows that the values are very similar, with point 4 being ever so slightly more REE rich. This is surprising given that analysis point 4 is from the inner mantle which is darker than the rim. The overall variation in the REE is similar to the variation in ΣREE for all the data points, and all of the REE show a similar pattern. Only La and Ce shows some deviation. Ce is slightly more concentrated in analysis point 6 which would seem to indicate that for the rim, Ce content is increasing toward the outer margin of the crystal indicating either slight incompatibility or enrichment in Ce in the melt.

La does not mimic the REE at all, while Y does (compare Figure 115B and Figure 115C). It would be expected that Y should mimic the HREE, yet it seems to follow the general variation shown by the LREE, especially Ce. La is most enriched in the bright core (point 1) and in the outer rim (point 6), and does not vary much in the mantle of the titanite at all. It appears to behave compatibly from the core to mantle, with progressive decrease in concentration from point 1 to point 4. However, when looking at the values for La in the rim, it is clear that it is more concentrated in the outer part of the rim (point 6) compared to the inner part of the rim (point 5), which would seem to indicate incompatible behaviour. According to Prowatke and Klemme (2005) La should behave compatibly for titanite in intermediate to silicic liquids. Thus, the increase in concentration of La in the outer rim may be linked to changes in the melt composition rather than due to strictly incompatible behaviour.

Nb behaviour is moderately incompatible, and it can be seen to increase from core through mantle, and it increases from inner rim to outer rim (see Figure 115C). This behaviour is expected according to the partition coefficients reported for titanite in silicic rocks by Prowatke and Klemme (2005). The highest values for Nb are from the very dark part of the patchy zoned inner mantle (see analyses 2 and 3). This inner mantle area of the crystal looks to have been subjected to a period of titanite dissolution, concomitant ilmenite nucleation and growth, before a return to titanite stability. A change in oxygen fugacity could have brought about such changes in mineral stability and also could have reduced the REE uptake in titanite by affecting the coupled substitutions involving ferric iron (Ca^{2+} + $Ti^{4+} \leftrightarrow REE^{3+} + Fe^{3+}$) as there would be less Fe^{3+} to participate in such substitutions in a

reducing melt (Wones 1989; Nakada 1991; Xirouchakis and Lindsley 1998; Piccoli, Candela et al. 2000). On the other hand, Nb would be free to participate in more reactions as it does not depend on Fe^{3+} for charge balancing. Zr is enriched in the inner core, and this may also be due to the reduced activity of the REE and Fe exchange vector, which would free up the octahedral Ti site for exchange directly with Zr.

A plot of (Ce+Nd) against Y shows a geochemical link between the three main textural features of this titanite (see Figure 115D). The textural features (discontinuous zoning and a solution surface) are most likely due to a change in melt conditions brought about by an influx of reducing mafic magma. The plot shows how the core (point1) and inner mantle (analyses 2 and 3) are sufficiently different chemically that it may be inferred that some event has taken place between the two which has altered the melt composition. The outer mantle (point 4) and rim (points 5 and 6) plot near each other midway between the core and inner rim values, indicating that the change in melt chemistry was a short lived event that eventually reached equilibrium. BFC-129-10 contains the lowest set of plotting values for (Ce+Nd)/Y in all of the analyses for Fish Canyon Tuff, and this is from the inner core (point 2).

Summary of the main geochemical features of BFC-129-10:

- Textural evidence for a transient change of melt chemistry is reflected by the distinct chemical signatures of the relevant growth zones (core, mantle and rim).

- La behaviour doe not reflect the behaviour of the REE, although Y does.

- Zr and Nb are enriched in the dark patchy zoning associated with the dissolution and re-growth of the inner mantle. This is likely due to the reduced activity of ferric iron and subsequent reduction of REE uptake allowing Zr and Nb more opportunity to participate in substitution reactions involving Ti.

5.4.4 BFC-55 Pagosa Peak Dacite

This sample is from a voluminous lava-like eruption that predates the main Fish Canyon Tuff eruption. The bulk rock chemistry and phenocryst compositions and assemblage of this rock are indistinguishable from the overlying Fish Canyon Tuff. The only main differences are that the Pagosa Peak Dacite is less vesiculated than the Fish Canyon Tuff and it also contains a high proportion (40-60%) of juvenile clasts of dacite and occasional pumice that were emplaced as viscous magma. The explosive potential of the magma is

thought to have been reduced by degassing during gradual ascent through fissure conduits, resulting in a fracture dominated fragmentation with low vesicularity (Lipman, Dungan et al. 1997; Bachmann, Dungan et al. 2000; Bachmann, Dungan et al. 2002). Since the chemistry is similar to the Fish Canyon Tuff, it is worth while seeing if there are similarities in the overall geochemical signature of titanites from the two units.

The titanites from BFC-55 are all very similar in overall texture and zoning. They all contain evidence of magmatic zoning in the form of oscillatory zoning and sector zoning. The zoning is quite uniform for all titanites with an overall faint darkening from core to rim when observed in BSE. Nearly all the large unfractured titanites contain evidence of a period of dissolution, where oscillatory zoning can be seen to be truncated by a solution surface and re-growth mantling it. There are few or no ilmenite inclusions associated with these solutions horizons.

5.4.4.1 BFC-55-18

Titanite BFC-55-18 is a typical example of titanite from BFC-55. It is euhedral, roughly 350 microns in length and has the general textural features described above: a core with well developed zoning, truncated by a solution surface which is mantled by further growth becoming progressively darker towards the rim. Each of these textural features were analysed geochemically (see Figure 116 for BSE image and data points).

The overall variation in total REE is very small, with the largest value (0.342cpfu) coming from the initial bright part of the mantle (analysis point 3) that represents the first period of growth after the partial solution of the core (see Figure 117A). The smallest recorded value for total REE comes from the rim of the crystal (point 7) which also happens to be the darkest portion. In the core, the bright central zoning (point 2) records a higher ΣREE than the outer darker part of the core (analysis point 1). The mantle records a progressive decrease in REE content from the initial bright rim (point 3) to the dark edge (point 7). The pattern of individual REE (see Figure 117B) variation broadly mirrors the ΣREE pattern, there are no individual rare-earth elements that are behaving differently, with Ce and Nd the most concentrated overall, a pattern observed in all samples from the Fish Canyon rocks.

The HFSE broadly mirror the patterns seen in the REE variation (compare Figure 117B and Figure 117C). La is behaving as would be expected in this sample, and shows a
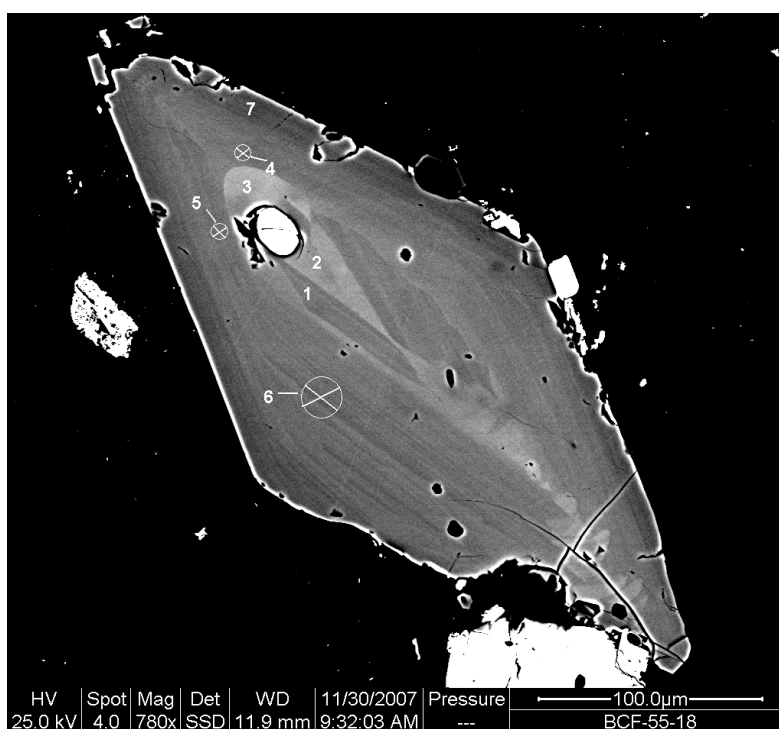
Figure 116: BSE image of BFC-55- 18 (Pagosa Peak Dacite) and location of sample points. Points 4 and 5 and 10micron spots, point 6 is a 20 micron spot. The bright, round inclusion within the core of the titanite is zircon.
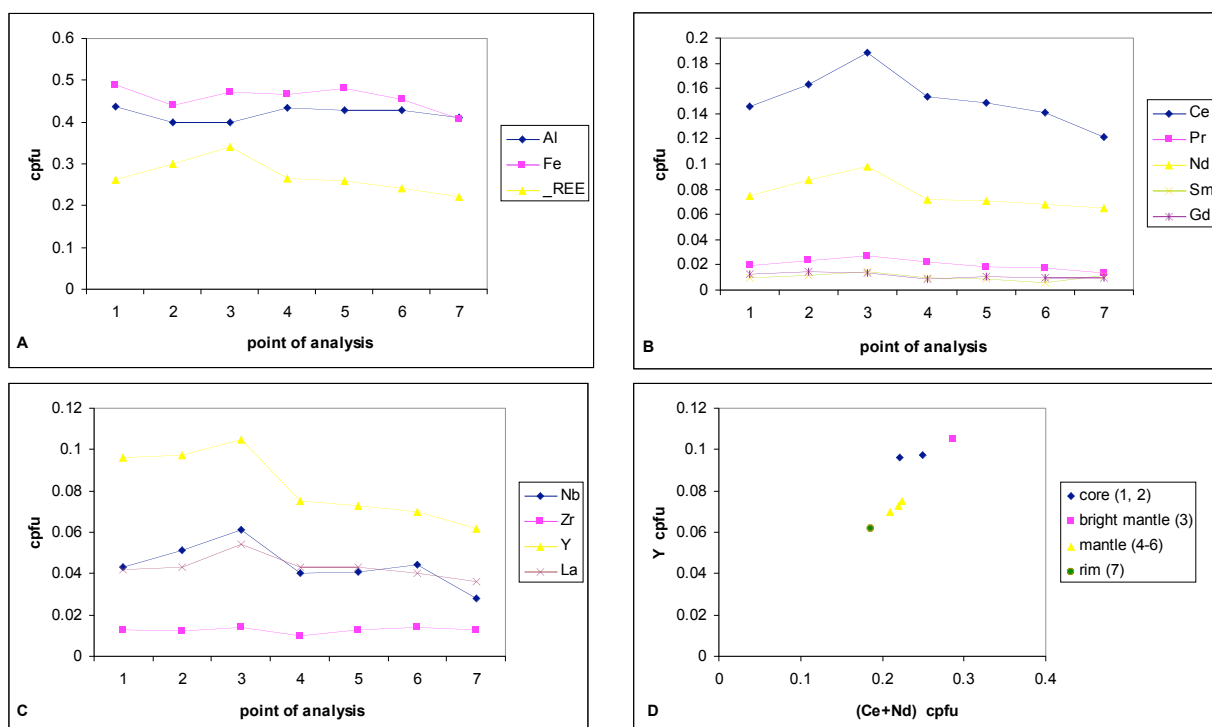
Figure 117: Geochemistry of BFC-55-18 (Pagosa Peak Dacite). A. Fe, Al and ΣREE variation across the crystal. B. REE variation. C. HFSE and La variation. D. REE slope for textural groups of BFC-55-18 given by a plot of (Ce+Nd) against Y

similar pattern of behaviour as the LREE. All of the trace elements seem to be adopting compatible behaviour with respect to titanite, except for Zr which increases slightly in concentration towards the rim. However, according to Prowatke and Klemme (2005) for a rock of dacitic composition, such behaviour is normal for Zr.

A plot of (Ce+Nd) against Y differentiates between the main textural zones of BFC-55-18 (see Figure 117D). The evolution of the trace element concentration in the crystal is centred around changes in the melt that relate to the solution horizon that separates the zoned core from the zoned mantle/rim area. The initial geochemistry of the core shows a lower concentration of REE compared to the very bright initial rim of the mantle (sampled by point 3). The solution surface indicates a change in melt conditions that transiently destabilised titanite, allowing it to become partly resorbed. In some of the titanites from the Fish Canyon Tuff (BFC-129-10, BFC-104b-5, BFC-124-5 and BFC145-7), dissolution/re-growth textures are almost always associated with ilmenite inclusions, but this is not the case seen here. Also, the immediate area of re-growth is usually characterised by dark patchy zoning, but in this case, the renewed growth is very brightly zoned and represents the highest concentrations of REE in the entire crystal.

The possible interpretation is that instead of a reduction event causing the titanite instability (where we would expect associated ilmenite nucleation), a heating event could destabilise titanite transiently (Wones 1989; Piccoli, Candela et al. 2000). Perhaps input of a new melt material could cause such a heating without affecting the oxygen fugacity of the melt. If the new magma was richer in trace elements, then the renewed growth would reflect that increase in trace element availability, and this is a possible explanation for the bright initial rim of the mantle (sample point 7). Nevertheless, the geochemistry of the titanite reflects the textural evidence of an event that altered the melt characteristics enough to dissolve titanite and re-grow titanite with higher concentrations of trace elements.

5.4.5 Comparison of (Ce+Nd)/Y plots and summary

For each of the samples from both the Fish Canyon Tuff and the Pagosa Peak Dacite, the plot of (Ce+Nd) against Y has consistently proved useful in geochemically differentiating between the main textural zones of the titanites, especially when the features relate to major changes in melt characteristics. A composite graph showing each titanite sample as a group may give indications about how the samples may be related to one another.
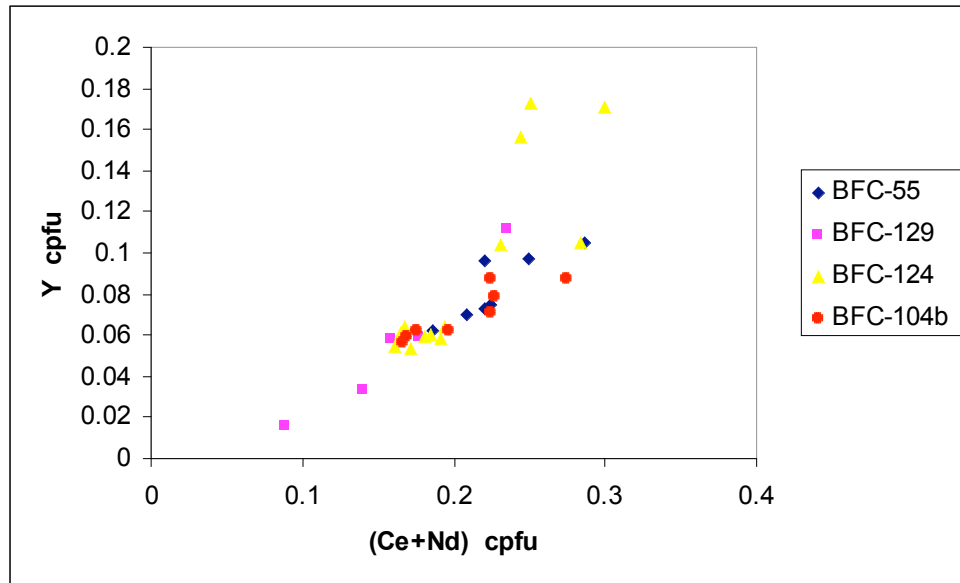
Figure 118: REE slope plot for Fish Canyon/Pagosa Peak dataset plotted by sample.

The first thing to note about the plot (above) is that all of the data sets overlap in the middle, a sure indication that the titanites are genetically related. There is evidence for a change in slope, especially for sample BFC-124, where there is a fair amount of spread on the data in the upper part of the plot. The data points that represent the core of BFC-124-7 are the ones that plot highest on the graph and are more enriched in Y relative to Ce and Nd compared to the rest of the dataset. The core of BFC-124 represents an early crystallisation form a melt that was richer in Y.
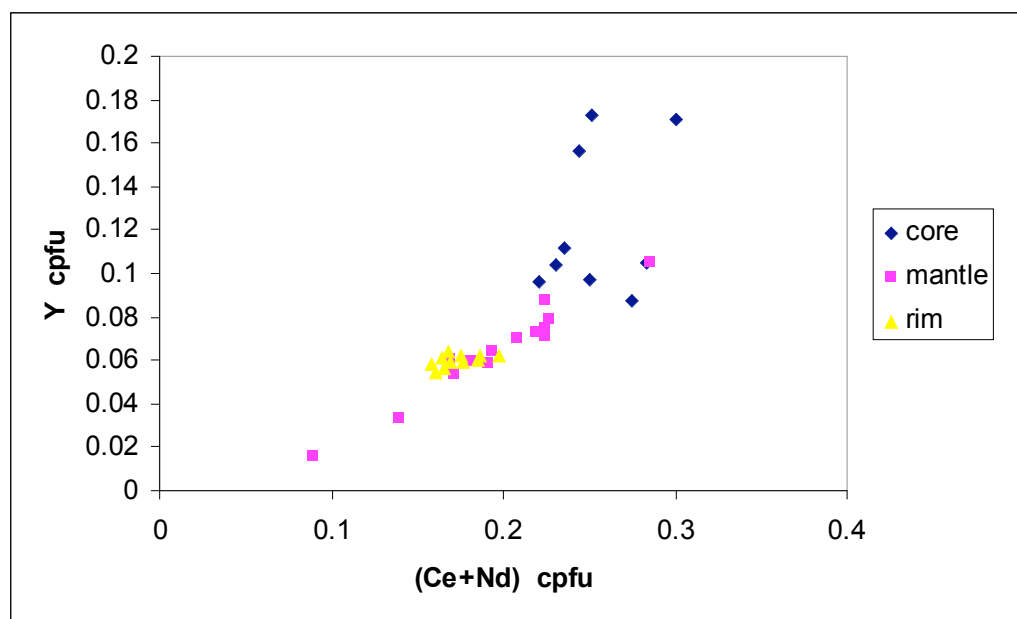
Figure 119: REE slope plot for Fish Canyon/Pagosa Peak dataset plotted as textural groups.

It's interesting to note that the same dataset plotted as textural groups (see Figure 119) provides a more consistent grouping than when plotted as sample groups. This indicates that there is some similarity between the crystals with respect to the melt chemistry they are recording within their compositional zoning. The general trend would indicate a core chemistry with a fair amount of spread but an overall enrichment in medium and heavy REE compared to light REE. There is less spread on the REE slope for the mantle group and the trend is far more linear and consistent, however, the range in values is greater than for the core group. The slope represents a chemistry that is more LREE enriched than the core group slope. The rim group has an even more LREE enriched slope; however, it also has a smaller range in absolute values than the mantle and core groups.

The overall trend for the REE slope for the Fish Canyon/Pagosa Peak textural group dataset may be summarised as follows:

- HREE and MREE enriched cores, with significant spread.

- Change of slope towards LREE enrichment, with less spread, for the mantle textural group.

- Rim textural groups shows the least overall spread in values and has a REE slope that indicates an overall enrichment in LREE vs MREE and HREE.

The titanite-melt partition coefficients given by Prowatke and Klemme (2005) indicate that the MREE are more compatible than the LREE, especially for dacitic and rhyolitic melt compositions. They also report that Y is more compatible than Ce for melts of dacitic composition. This is the trend observed for the Fish Canyon/Pagosa Peak dataset.

The entire dataset has a roughly linear trend, albeit with some spread; however, it is unsurprising if one considers that most of the titanites displayed textural evidence of dissolution and re-growth (also reflected in the geochemistry), and therefore may all be related to the same type of event that altered the melt characteristics. The inference from the textural features is that some sort of reduction event has taken place, perhaps due to input of a mafic melt into the system, which has caused the dissolution and re-growth, with a renewed chemistry.

If this is the case, then why doesn't every titanite have the same chemical signature at the rim? The answer could be simply because the titanites come from different parts of the

melt reservoir and may have been influenced to different extents by the event that changed the melt. Bachmann et al (2000, 2002, 2005) and Bachmann and Bergantz, (2003) argue that thermal rejuvenation of the Fish Canyon Tuff just prior to eruption was caused by intrusion of water rich mafic magmas at the base of the magma chamber. The crystal rich homogenous melt is thought to have cooled to a rigid crystal mush just prior to eruption, and the additional heat transferred throughout the magma chamber by gas "sparging" processes will have certainly affected the titanites at the bottom of the magma chamber first. Gas sparging is a term proposed by Bachmann and Bergantz (2003) to describe the upward percolation of a hot gas phase that acts as a "defrosting" agent for rigid crystal mushes that are near their solidus and therefore have reached their rheological locking point.

Titanites from the intracaldera portion of the Fish Canyon Tuff are likely to have come from deepest parts of the magma chamber and these possibly should show significant textural and geochemical evidence for such thermal rejuvenation. The titanite which shows the most textural evidence for dissolution and re-growth (features which could be brought about by heating and oxygen fugacity reduction of the melt by the mafic magma) is sample BFC129-10, which is from the intracaldera facies of Fish Canyon. The titanites which show the least evidence of being affected by thermal rejuvenation caused by a mafic melt at the base of the magma chamber would be those that were near the top of the chamber. The Pagosa Peak Dacite was sourced from the same magma chamber as the Fish Canyon Tuff itself, and is thought of as a less vesiculated precursor eruption. It may well be no coincidence that the titanites from the Pagosa Peak Dacite (BFC-55) are more uniform (with respect to zoning) than those from Fish canyon, and where they do show textural evidence of dissolution and re-growth, it is limited compared to the titanites from the Fish Canyon intracaldera facies, and lacks the ilmenite inclusions which tend to nucleate on titanite when it becomes unstable in a reducing melt.

A comparison of the textural features of BFC-129-10 (intracaldera; see Figure 114) with BFC-104b-5 (outflow, see Figure 111) reveals differences in the position and extent of the dissolution surface. BFC-104b-5 is only affected near the rim and the extent of dissolution and amount of re-growth is minimal compared to BFC-129-10. BFC-129-10 has had the majority of the crystal's centre dissolved, leaving only a small core, before re-growth occurred. The re-growth is also fairly substantial, creating a significant mantle and rim compared to BFC-104b-10. The explanation for this difference is perhaps related to the provenance of the titanites with respect to depth of the magma chamber. BFC-129-10 is

from the intracaldera facies, and as such is from the waning stages of eruption. Hence, it is likely to be sourced from the deeper reaches of the magma chamber, where the underplating of hot, water-rich mafic magma is likely to have had a prolonged effect compared to the upper reaches of the chamber. The gas "sparging" process involves the upward percolation of hot fluids, and this means that the lower reaches of the magma chamber will be subjected to continuous heating while the "defrosting" of the whole chamber takes place. This continuous movement of hot fluids through the bottom part of the chamber will certainly have a profound effect on the minerals near the bottom, which is where titanite BFC-129-10 is likely to have originated from, considering its provenance is from the intracaldera facies. The initial phase of hot fluid percolation will have caused the dissolution of titanite and possibly also allowed the stabilisation and growth of ilmenite due to changing oxygen fugacity (Wones 1989; Nakada 1991; Piccoli, Candela et al. 2000). Once the defrosting of the chamber was underway, the gas from the underplating mafic magma would begin to become exhausted and the base of the chamber would eventually start to cool slightly as the remainder of the gases percolated upwards. Once this occurred, the titanite would then start to crystallise again, hence why the titanites from the deeper reaches of the magma chamber would have had more time to re-grow.

The main conclusion from this study of titanites from the Fish Canyon Tuff and Pagosa Peak dacite, is that evidence for the thermal rejuvenation of the magma chamber by a mafic melt prior to eruption may very well be preserved in the textural and chemical signature preserved in the compositional zoning of the titanites. Solution and re-growth features of the titanites correlate very well with trace element patterns, especially the core/mantle/rim textural groups highlighted by the (Ce+Nd)/Y plots.

One note of caution would be to point out that it is impossible, without detailed whole rock chemistry and mineral melt partition coefficients for each phenocryst phase, to rule out the possibility that the geochemical variation of the titanites is more likely due to partitioning of elements driven in part by the timing and extent crystallisation of other phases present. However, the textural and geochemical evidence provided here seems to point towards a link with the thermal rejuvenation of the magma, an event brought about by a mafic magma interacting with the magma body.

6

Conclusions

Titanite is a mineral that has the ability to record a large variety of petrogenetic information within its textural features, both in terms of crystal shape and compositional zoning. This is mainly due to the fact that titanite serves as a sink for many trace elements of petrogenetic significance, namely, the rare-earth elements and the high-field-strength elements. Not only does titanite serve as one of the primary sinks for these elements in relatively oxidised intermediate to acidic melts, it also is very refractory in nature and resists diffusion of these trace elements out of its crystal structure. Thus, it is able to resist most alteration processes and has the potential to permanently record aspects of its crystallisation history and potentially reveal the nature of the petrogenetic processes that operated in its formation.

This study has shown that evidence of magma-mingling and mixing at depth (Ross of Mull Granite) can be recorded in the textural features of titanite compositional zoning. The most convincing evidence comes from the preservation of dissolution and re-growth textures in titanite, brought about by the mixing of magmas. This is significant since it shows that titanite is able to resist chemical homogenisation despite the very slow cooling it endures in the plutonic environments. It has also been shown that titanite is able to not only preserve evidence of magma mixing processes occurring at depth, but it is also able to preserve evidence of similar processes all the way through to the volcanic environment (Fish Canyon Tuff).

The study would have benefited greatly from having whole rock geochemical data as well as geochemical data for each of the main minerals within the paragenetic suite shared by titanite. This would have enabled trace element mineral-melt partition coefficients to be worked out all of the minerals involved, and thus, it would allow a better assessment of titanites ability to faithfully mirror the changing conditions of the melt in which it is crystallising, since it could be ascertained whether the trace element variations recorded in the compositional zoning of titanite is truly governed by melt processes or is also

significantly controlled by the partitioning of elements by other minerals in the paragenesis.

Suggestion for further research would include

- A thorough investigation into the nature of sector zoning in titanite and how it relates to other types of magmatic zoning; this would allow for a better understanding of how to avoid misinterpretation of partitioning behaviour of the trace elements with respect to titanite.

- A study into the manner in which La behaves in titanite. La behaviour seems to deviate significantly from the behaviour of the other REE in titanite, and this may mean that titanite has the ability to fractionate La with respect to the LREE in a way that other minerals do not.

- The most curious textural feature of titanite to emerge from this study is the patchy zoning that characterises those titanites which have experienced periods of dissolution and re-growth. The exact nature of the role of ilmenite in these reactions needs to be better understood with respect to the formation of the intricate patterns observed in BSE. These features are often associated with growth of very small REE-rich minerals, such as allanite, and there may be a link to their nucleation and the reduced uptake of REE by titanite which follows these transient periods of titanite instability.

A

A.1 Ross of Mull Granite titanite EMPA data (cpfu)

The data is presented as atoms per formula unit (most as cations, plus anions per formula unit for OH and F). The unit cell for titanite in this case is based on having 24 cations, 38 oxygen anions, plus an additional 2 anions of water/volatiles (OH, F).

A-13

Sample	Si	Ti	Ca	Al	Fe	La	Ce	Pr	Nd	Sm	Gd	ΣREE	Y
A13.1	7.704	6.93	7.312	0.388	0.459	0.043	0.173	0.032	0.11	0.02	0.019	0.352	0.117
A13.2	7.762	7.13	7.495	0.375	0.341	0.032	0.128	0.02	0.07	0.01	0.011	0.24	0.057
A13.3	7.757	6.965	7.372	0.446	0.457	0.028	0.131	0.024	0.12	0.03	0.029	0.33	0.125
A13.4	7.745	7.024	7.407	0.448	0.445	0.024	0.123	0.024	0.1	0.03	0.023	0.294	0.114
A13.5	7.83	7.105	7.559	0.373	0.366	0.028	0.099	0.016	0.04	0.01	0.006	0.173	0.039
A13.6	7.702	7.277	7.566	0.362	0.289	0.032	0.108	0.013	0.05	0.01	0.009	0.19	0.043
A13.7	7.769	6.938	7.497	0.435	0.5	0.024	0.104	0.02	0.07	0.02	0.018	0.223	0.111

Sample	Zr	Nb	Ta	Mg	P	Mn	OH	Na	K	F	Total
A13.1	0.014	0.078	0.009	0.005	0.026	0.054	1.985	0.027	0.001	0.015	25.524
A13.2	0.009	0.029	0.003	0.007	0.017	0.031	1.936	0.006	0	0.064	25.537
A13.3	0.01	0.029	0.004	0.005	0.016	0.034	1.839	0.008	0	0.161	25.587
A13.4	0.009	0.025	0.003	0.001	0.013	0.037	1.817	0.008	0	0.183	25.596
A13.5	0.009	0.029	0.003	0.005	0.014	0.029	1.863	0.003	0.003	0.137	25.57
A13.6	0.008	0.028	0.004	0.006	0.014	0.027	1.857	0.012	0	0.143	25.563
A13.7	0.01	0.044	0.004	0.004	0.007	0.064	1.829	0.016	0	0.171	25.649

A-57

Sample	Si	Ti	Ca	Al	Fe	La	Ce	Pr	Nd	Sm	Gd	ΣREE	Y
A57.1	7.693	7.215	7.555	0.369	0.351	0.034	0.13	0.019	0.07	0.01	0.008	0.239	0.043
A57.2	7.747	7.178	7.509	0.37	0.347	0.034	0.128	0.021	0.07	0.01	0.007	0.235	0.043
A57.3	7.741	6.996	7.541	0.416	0.455	0.028	0.109	0.014	0.06	0.01	0.009	0.202	0.078
A57.4	7.705	7.1	7.459	0.384	0.409	0.04	0.155	0.024	0.09	0.01	0.015	0.298	0.063
A57.5	7.714	7.118	7.412	0.394	0.408	0.042	0.15	0.024	0.09	0.02	0.009	0.289	0.061
A57.6	7.74	7.019	7.403	0.368	0.409	0.041	0.153	0.022	0.08	0.01	0.009	0.28	0.084
A57.7	7.772	7.082	7.591	0.391	0.415	0.022	0.099	0.015	0.05	0.01	0.011	0.186	0.062

Sample	Zr	Nb	Ta	Mg	P	Mn	OH	Na	K	F	Total
A57.1	0.009	0.029	0.001	0.004	0.017	0.028	1.788	0.004	0.021	0.212	25.613
A57.2	0.01	0.032	0.002	0.005	0.015	0.029	1.819	0.006	0.022	0.181	25.583
A57.3	0.014	0.068	0.005	0.009	0.014	0.074	1.75	0.02	0.002	0.25	25.666
A57.4	0.02	0.042	0.001	0.01	0.016	0.038	1.794	0.006	0.001	0.206	25.596
A57.5	0.016	0.044	0.002	0.006	0.015	0.034	1.799	0.011	0.002	0.201	25.57

Sample											
A57.6	0.014	0.087	0.005	0.005	0.023	0.057	1.835	0.017	0	0.165	25.554
A57.7	0.009	0.046	0.003	0.008	0.011	0.054	1.695	0.012	0.001	0.305	25.669

ES16-7

Sample	Si	Ti	Ca	Al	Fe	La	Ce	Pr	Nd	Sm	Gd	ΣREE	Y
ES16_7.1	7.86	7.067	7.589	0.386	0.35	0.03	0.106	0.016	0.05	0.01	0.009	0.193	0.051
ES16_7.2	7.797	7.138	7.586	0.389	0.347	0.028	0.103	0.017	0.05	0.01	0.007	0.19	0.049
ES16_7.3	7.83	6.994	7.507	0.434	0.481	0.021	0.091	0.018	0.05	0.01	0.01	0.181	0.083
ES16_7.4	7.818	6.969	7.567	0.412	0.44	0.025	0.1	0.014	0.06	0.01	0.014	0.201	0.086
ES16_7.5	7.843	7.078	7.518	0.395	0.359	0.033	0.114	0.017	0.07	0.01	0.01	0.216	0.054

Sample	Zr	Nb	Ta	Mg	P	Mn	OH	Na	K	F	Total
ES16_7.1	0.01	0.027	0	0.004	0.016	0.031	1.743	0.009	0.004	0.257	25.628
ES16_7.2	0.011	0.03	0.001	0.005	0.015	0.029	1.722	0.005	0.004	0.278	25.627
ES16_7.3	0.006	0.041	0.003	0.007	0.008	0.059	1.644	0.023	0.001	0.356	25.682
ES16_7.4	0.009	0.048	0.001	0.003	0.012	0.062	1.72	0.029	0.002	0.28	25.686
ES16_7.5	0.009	0.026	0.002	0.006	0.013	0.031	1.785	0.01	0	0.215	25.593

ES3A-27

Sample	Si	Ti	Ca	Al	Fe	La	Ce	Pr	Nd	Sm	Gd	ΣREE	Y
ES3A_27.1	7.817	7.198	7.851	0.345	0.32	0.01	0.034	0.003	0.01	0	0.001	0.051	0.006
ES3A_27.2	7.732	7.176	7.809	0.513	0.313	0.009	0.026	0	0.01	0	0	0.036	0.003
ES3A_27.3	7.74	7.299	7.77	0.344	0.304	0.015	0.053	0.007	0.02	0	0.001	0.088	0.014
ES3A_27.4	7.671	7.186	7.462	0.346	0.339	0.028	0.122	0.022	0.11	0.03	0.017	0.291	0.077
ES3A_27.5	7.692	7.258	7.658	0.287	0.322	0.028	0.093	0.011	0.05	0.01	0.006	0.161	0.049
ES3A_27.6	7.643	7.366	7.591	0.273	0.272	0.029	0.101	0.015	0.05	0.01	0.004	0.183	0.049
ES3A_27.7	7.687	7.145	7.463	0.399	0.338	0.041	0.138	0.02	0.07	0.01	0.008	0.24	0.051
ES3A_27.8	7.65	7.184	7.536	0.335	0.355	0.035	0.127	0.017	0.06	0.01	0.009	0.222	0.044
ES3A_27.9	7.753	7.18	7.576	0.312	0.332	0.03	0.109	0.013	0.05	0.01	0.008	0.189	0.048
ES3A_27.10	7.754	7.05	7.57	0.394	0.432	0.026	0.101	0.016	0.05	0.01	0.009	0.19	0.056
ES3A_27.11	7.702	7.012	7.415	0.375	0.412	0.038	0.144	0.019	0.07	0.01	0.011	0.253	0.067

Sample	Zr	Nb	Ta	Mg	P	Mn	OH	Na	K	F	Total
ES3A_27.1	0.005	0.013	0	0.004	0.006	0.018	1.871	0.008	0.006	0.129	25.657
ES3A_27.2	0.003	0.008	0	0.09	0.007	0.048	1.734	0.008	0.007	0.266	25.768
ES3A_27.3	0.006	0.017	0	0.001	0.012	0.024	1.807	0.004	0.002	0.193	25.633
ES3A_27.4	0.011	0.043	0.004	0.004	0.019	0.023	1.969	0.006	0	0.031	25.511
ES3A_27.5	0.017	0.048	0.003	0.003	0.018	0.023	1.854	0.013	0	0.146	25.585
ES3A_27.6	0.011	0.042	0	0.003	0.02	0.022	1.942	0.012	0	0.058	25.519
ES3A_27.7	0.01	0.067	0.002	0.007	0.019	0.053	1.924	0.013	0	0.076	25.536
ES3A_27.8	0.01	0.066	0.002	0.004	0.022	0.052	1.931	0.014	0	0.069	25.556
ES3A_27.9	0.009	0.05	0.002	0.003	0.013	0.051	1.886	0.012	0	0.114	25.567
ES3A_27.10	0.018	0.047	0.003	0.006	0.013	0.051	1.828	0.009	0.001	0.172	25.625
ES3A_27.11	0.018	0.103	0.005	0.003	0.027	0.053	1.997	0.015	0	0.003	25.503

ES3A-49

Sample	Si	Ti	Ca	Al	Fe	La	Ce	Pr	Nd	Sm	Gd	ΣREE	Y
ES3A_49.1	7.713	7.184	7.616	0.326	0.323	0.026	0.102	0.01	0.05	0.01	0.007	0.179	0.057
ES3A_49.2	7.696	6.805	7.191	0.424	0.509	0.045	0.219	0.041	0.17	0.04	0.025	0.493	0.09
ES3A_49.3	7.707	6.983	7.614	0.433	0.49	0.029	0.117	0.021	0.07	0.02	0.015	0.243	0.071
ES3A_49.4	7.679	7.197	7.474	0.329	0.343	0.026	0.13	0.02	0.1	0.02	0.014	0.28	0.068
ES3A_49.5	7.739	7.268	7.741	0.315	0.295	0.026	0.078	0.01	0.03	0.01	0.002	0.129	0.015
ES3A_49.6	7.625	7.351	7.692	0.306	0.284	0.035	0.097	0.014	0.04	0.01	0.004	0.162	0.018
ES3A_49.7	7.831	7.195	7.902	0.365	0.325	0.006	0.015	0	0	0	0.003	0.018	0

Sample	Zr	Nb	Ta	Mg	P	Mn	OH	Na	K	F	Total
ES3A_49.1	0.009	0.051	0.003	0.002	0.011	0.042	1.975	0.013	0	0.025	25.559
ES3A_49.2	0.081	0.072	0.003	0.008	0.027	0.029	2	0.012	0	0	25.491
ES3A_49.3	0.015	0.026	0.002	0.005	0.014	0.034	1.858	0.004	0	0.142	25.671
ES3A_49.4	0.011	0.039	0.003	0.004	0.017	0.021	2	0.006	0	0	25.502
ES3A_49.5	0.007	0.019	0.002	0.002	0.017	0.024	1.868	0.006	0	0.132	25.607
ES3A_49.6	0.01	0.029	0.003	0.001	0.015	0.024	1.961	0.008	0.001	0.039	25.566
ES3A_49.7	0.001	0.005	0.001	0.002	0.005	0.014	1.837	0.004	0.015	0.163	25.69

ES3A-59

Sample	Si	Ti	Ca	Al	Fe	La	Ce	Pr	Nd	Sm	Gd	ΣREE	Y
ES3A_59.1	7.76	7.375	7.768	0.271	0.212	0.018	0.053	0.009	0.02	0	0.002	0.087	0.017
ES3A_59.2	7.766	7.362	7.576	0.264	0.233	0.019	0.08	0.012	0.05	0.01	0.004	0.152	0.036
ES3A_59.3	7.659	7.036	7.231	0.393	0.426	0.04	0.175	0.033	0.13	0.03	0.025	0.39	0.125
ES3A_59.4	7.7	7.04	7.432	0.408	0.447	0.026	0.13	0.023	0.1	0.02	0.019	0.287	0.108
ES3A_59.5	7.756	7.024	7.468	0.418	0.453	0.026	0.118	0.02	0.08	0.02	0.016	0.252	0.098
ES3A_59.6	7.741	7.29	7.624	0.326	0.297	0.029	0.089	0.013	0.04	0.01	0.003	0.147	0.019
ES3A_59.7	7.727	7.026	7.468	0.428	0.479	0.024	0.091	0.017	0.05	0.01	0.01	0.185	0.104

Sample	Zr	Nb	Ta	Mg	P	Mn	OH	Na	K	F	Total
ES3A_59.1	0.002	0.018	0.002	0.002	0.008	0.016	1.916	0.006	0	0.084	25.564
ES3A_59.2	0.007	0.029	0.001	0.001	0.017	0.021	1.91	0.004	0	0.09	25.49
ES3A_59.3	0.015	0.058	0.006	0.006	0.028	0.044	1.993	0.012	0	0.007	25.474
ES3A_59.4	0.013	0.034	0.001	0.004	0.017	0.044	1.933	0.009	0	0.067	25.571
ES3A_59.5	0.01	0.036	0.002	0.007	0.014	0.049	1.777	0.007	0.001	0.223	25.624
ES3A_59.6	0.009	0.022	0	0.003	0.014	0.024	1.891	0.006	0.006	0.109	25.557
ES3A_59.7	0.008	0.06	0.003	0.01	0.01	0.072	1.809	0.014	0	0.191	25.623

ES5-30

Sample	Si	Ti	Ca	Al	Fe	La	Ce	Pr	Nd	Sm	Gd	ΣREE	Y
ES5_30.1	7.852	6.859	7.492	0.467	0.482	0.023	0.105	0.019	0.09	0.02	0.021	0.254	0.102
ES5_30.2	7.874	6.827	7.552	0.471	0.478	0.023	0.103	0.02	0.09	0.02	0.021	0.257	0.103
ES5_30.3	7.811	7.007	7.335	0.359	0.379	0.04	0.164	0.025	0.11	0.02	0.019	0.341	0.094
ES5_30.4	7.803	6.956	7.357	0.367	0.389	0.043	0.165	0.026	0.11	0.02	0.016	0.34	0.095
ES5_30.5	7.878	7.131	7.611	0.326	0.314	0.022	0.086	0.012	0.04	0.01	0.007	0.154	0.031

ES5_30.6	7.878	7.148	7.633	0.33	0.3	0.021	0.075	0.015	0.04	0.01	0.006	0.138	0.028

Sample	Zr	Nb	Ta	Mg	P	Mn	OH	Na	K	F	Total
ES5_30.1	0.011	0.023	0.003	0.006	0.015	0.035	1.843	0.001	0	0.157	25.63
ES5_30.2	0.011	0.023	0.002	0.002	0.016	0.033	1.769	0.005	0	0.231	25.679
ES5_30.3	0.01	0.04	0.004	0	0.028	0.035	1.934	0.005	0.001	0.066	25.494
ES5_30.4	0.012	0.05	0.003	0.004	0.029	0.035	2	0.008	0	0	25.494
ES5_30.5	0.008	0.031	0.001	0	0.015	0.029	1.859	0.01	0.001	0.141	25.564
ES5_30.6	0.007	0.028	0.001	0.003	0.013	0.027	1.866	0.007	0.001	0.134	25.564

ES5-66

Sample	Si	Ti	Ca	Al	Fe	La	Ce	Pr	Nd	Sm	Gd	ΣREE	Y
ES5_66.1	7.833	7.207	7.652	0.292	0.294	0.026	0.085	0.008	0.04	0.01	0.005	0.14	0.023
ES5_66.2	7.821	7.217	7.663	0.271	0.27	0.025	0.086	0.013	0.04	0.01	0.006	0.151	0.025
ES5_66.3	7.835	7.183	7.953	0.359	0.311	0.001	0.013	0.006	0.01	0	0.001	0.027	0.012
ES5_66.4	7.848	7.183	7.912	0.372	0.312	0.003	0.015	0	0.01	0	0	0.025	0.012
ES5_66.5	7.788	6.897	7.324	0.443	0.394	0.036	0.165	0.031	0.13	0.03	0.028	0.382	0.119
ES5_66.6	7.846	6.943	7.528	0.398	0.446	0.024	0.109	0.021	0.08	0.02	0.016	0.236	0.079
ES5_66.7	7.833	6.991	7.456	0.391	0.389	0.032	0.135	0.022	0.09	0.01	0.014	0.275	0.078
ES5_66.8	7.885	7.033	7.539	0.36	0.351	0.033	0.121	0.019	0.07	0.01	0.005	0.22	0.042
ES5_66.9	7.947	7.226	7.846	0.31	0.23	0	0.012	0.002	0	0	0.002	0.022	0.006
ES5_66.10	7.964	7.285	7.849	0.257	0.173	0.002	0.011	0.002	0.01	0	0.001	0.02	0.007
ES5_66.11	7.767	7.342	7.843	0.251	0.238	0.008	0.043	0.006	0.02	0	0.001	0.068	0.015
ES5_66.12	7.813	7.212	7.855	0.348	0.331	0.012	0.035	0.005	0.01	0	0.005	0.057	0.014

Sample	Zr	Nb	Ta	Mg	P	Mn	OH	Na	K	F	Total
ES5_66.1	0.008	0.03	0.001	0.001	0.016	0.025	1.889	0.005	0	0.111	25.554
ES5_66.2	0.009	0.036	0.002	0	0.015	0.028	1.927	0.004	0	0.073	25.54
ES5_66.3	0.003	0.01	0.001	0	0.004	0.018	1.749	0.003	0.015	0.251	25.737
ES5_66.4	0.002	0.012	0.002	0	0.006	0.021	1.713	0.008	0.002	0.287	25.723
ES5_66.5	0.012	0.05	0	0.003	0.024	0.037	1.984	0.006	0	0.016	25.516
ES5_66.6	0.01	0.029	0	0.004	0.014	0.037	1.885	0.007	0	0.115	25.605
ES5_66.7	0.009	0.03	0.001	0	0.016	0.035	1.942	0.007	0	0.058	25.546
ES5_66.8	0.01	0.03	0.002	0.004	0.016	0.028	1.889	0.003	0	0.111	25.556
ES5_66.9	0.001	0.012	0	0.003	0.006	0.02	1.725	0.007	0.03	0.275	25.671
ES5_66.10	0.001	0.01	0	0	0.006	0.015	1.802	0.004	0.013	0.198	25.605
ES5_66.11	0.003	0.033	0.001	0	0.01	0.025	1.834	0.009	0.01	0.166	25.625
ES5_66.12	0.005	0.021	0	0	0.007	0.027	1.679	0.008	0.006	0.321	25.716

ES5-8

Sample	Si	Ti	Ca	Al	Fe	La	Ce	Pr	Nd	Sm	Gd	ΣREE	Y
ES5_8.1	7.898	7.085	7.68	0.37	0.352	0.02	0.07	0.014	0.04	0.01	0.008	0.134	0.029
ES5_8.2	7.894	7.052	7.696	0.373	0.359	0.023	0.074	0.009	0.04	0.01	0.004	0.131	0.029
ES5_8.3	7.858	7.12	7.576	0.319	0.285	0.029	0.101	0.016	0.06	0.01	0.008	0.189	0.043
ES5_8.4	7.92	7.006	7.682	0.373	0.369	0.024	0.082	0.014	0.05	0.01	0.007	0.158	0.033
ES5_8.5	7.907	7.036	7.616	0.368	0.376	0.023	0.077	0.013	0.04	0.01	0.004	0.149	0.038
ES5_8.6	7.926	6.998	7.693	0.398	0.382	0.022	0.073	0.012	0.04	0.01	0.003	0.137	0.035
ES5_8.7	8.077	6.99	7.483	0.38	0.353	0.021	0.069	0.01	0.04	0.01	0.006	0.127	0.028
ES5_8.8	7.918	6.989	7.669	0.394	0.399	0.02	0.07	0.009	0.04	0.01	0.004	0.126	0.025
ES5_8.9	7.796	7.195	7.536	0.293	0.279	0.034	0.118	0.013	0.06	0.01	0.01	0.21	0.045

ES5_8.10	7.813	7.092	7.72	0.371	0.414	0.022	0.077	0.011	0.04	0.01	0.004	0.141	0.035

Sample	Zr	Nb	Ta	Mg	P	Mn	OH	Na	K	F	Total
ES5_8.1	0.008	0.02	0	0.002	0.014	0.025	1.732	0.006	0	0.268	25.643
ES5_8.2	0.006	0.024	0	0.001	0.015	0.026	1.806	0.007	0	0.194	25.635
ES5_8.3	0.008	0.034	0.002	0	0.015	0.026	1.987	0.011	0.001	0.013	25.517
ES5_8.4	0.007	0.024	0.001	0.003	0.012	0.025	1.78	0.006	0.001	0.22	25.647
ES5_8.5	0.007	0.024	0.002	0.002	0.013	0.024	1.847	0.006	0	0.153	25.594
ES5_8.6	0.008	0.018	0	0.002	0.011	0.024	1.76	0.008	0	0.24	25.662
ES5_8.7	0.005	0.02	0	0.006	0.012	0.022	1.769	0.018	0.003	0.231	25.55
ES5_8.8	0.006	0.019	0.002	0.007	0.009	0.025	1.886	0.011	0.005	0.114	25.626
ES5_8.9	0.007	0.038	0.003	0.003	0.019	0.024	1.986	0.012	0.003	0.014	25.497
ES5_8.10	0.007	0.024	0	0.001	0.011	0.027	1.712	0.009	0.002	0.288	25.692

ESd1-15

Sample	Si	Ti	Ca	Al	Fe	La	Ce	Pr	Nd	Sm	Gd	ΣREE	Y
ESd1_15.1	7.821	7.07	7.576	0.296	0.367	0.029	0.086	0.008	0.04	0.01	0.007	0.144	0.023
ESd1_15.2	7.749	7.096	7.706	0.298	0.34	0.032	0.09	0.011	0.04	0.01	0.005	0.147	0.024
ESd1_15.3	7.734	7.432	7.752	0.247	0.213	0.024	0.052	0.005	0.02	0	0.002	0.082	0.013
ESd1_15.4	7.725	7.462	7.744	0.237	0.214	0.022	0.054	0.005	0.02	0	0.004	0.083	0.011

Sample	Zr	Nb	Ta	Mg	P	Mn	OH	Na	K	F	Total
ESd1_15.1	0.159	0.031	0	0.001	0.015	0.029	1.759	0.018	0.002	0.241	25.582
ESd1_15.2	0.134	0.037	0.001	0.001	0.021	0.032	1.765	0.017	0.007	0.235	25.642
ESd1_15.3	0.008	0.013	0.001	0.002	0.015	0.023	1.85	0.007	0.008	0.15	25.577
ESd1_15.4	0.007	0.013	0	0	0.016	0.023	1.834	0.009	0.004	0.166	25.57

ESd1-32

Sample	Si	Ti	Ca	Al	Fe	La	Ce	Pr	Nd	Sm	Gd	ΣREE	Y
ESd1_32.1	7.832	7.349	7.719	0.252	0.233	0.019	0.049	0.006	0.02	0	0.001	0.076	0.011
ESd1_32.2	7.752	7.414	7.752	0.254	0.226	0.021	0.047	0.005	0.02	0	0.004	0.078	0.011
ESd1_32.3	7.869	6.995	7.798	0.44	0.435	0.012	0.033	0.005	0.01	0	0.002	0.053	0.008
ESd1_32.4	7.826	7.042	7.802	0.422	0.424	0.013	0.03	0.002	0.01	0	0.001	0.046	0.01
ESd1_32.5	7.758	7.143	7.711	0.311	0.332	0.03	0.066	0.008	0.02	0	0.004	0.104	0.011
ESd1_32.6	7.818	7.156	7.718	0.295	0.3	0.027	0.063	0.007	0.02	0	0.003	0.096	0.011

Sample	Zr	Nb	Ta	Mg	P	Mn	OH	Na	K	F	Total
ESd1_32.1	0.007	0.014	0.002	0.003	0.017	0.023	1.809	0.01	0.002	0.191	25.569
ESd1_32.2	0.006	0.012	0.001	0.003	0.015	0.025	1.829	0.011	0.003	0.171	25.584
ESd1_32.3	0.041	0.009	0	0.003	0.015	0.026	1.75	0.008	0.001	0.25	25.715
ESd1_32.4	0.044	0.009	0.001	0.005	0.014	0.026	1.812	0.009	0.001	0.188	25.694
ESd1_32.5	0.052	0.033	0	0.004	0.06	0.029	1.861	0.011	0.001	0.139	25.589
ESd1_32.6	0.051	0.031	0.001	0.006	0.044	0.025	1.822	0.011	0	0.178	25.591

ESd1-36

Sample	Si	Ti	Ca	Al	Fe	La	Ce	Pr	Nd	Sm	Gd	ΣREE	Y
ESd1_36.1	7.762	6.732	7.628	0.252	0.418	0.034	0.093	0.016	0.04	0.01	0.004	0.16	0.023
ESd1_36.2	7.79	6.709	7.594	0.247	0.415	0.035	0.098	0.015	0.04	0.01	0.007	0.163	0.024
ESd1_36.3	7.796	6.779	7.62	0.25	0.401	0.035	0.091	0.01	0.04	0	0.006	0.148	0.02
ESd1_36.4	7.761	7.373	7.709	0.251	0.255	0.018	0.046	0.002	0.02	0	0.003	0.077	0.014
ESd1_36.5	7.799	7.328	7.746	0.246	0.276	0.02	0.05	0.007	0.02	0	0.002	0.084	0.012
ESd1_36.6	7.736	7.421	7.641	0.245	0.238	0.027	0.063	0.006	0.02	0.01	0.003	0.1	0.015
ESd1_36.7	7.77	7.369	7.673	0.247	0.243	0.027	0.06	0.004	0.02	0	0.006	0.096	0.016
ESd1_36.8	7.833	7.33	7.739	0.249	0.231	0.014	0.038	0.007	0.02	0	0.002	0.065	0.011

Sample	Zr	Nb	Ta	Mg	P	Mn	OH	Na	K	F	Total
ESd1_36.1	0.478	0.031	0.005	0.005	0.015	0.031	1.84	0.023	0	0.16	25.599
ESd1_36.2	0.498	0.035	0.006	0.003	0.016	0.031	1.786	0.021	0.001	0.214	25.592
ESd1_36.3	0.45	0.028	0.005	0.003	0.014	0.028	1.773	0.018	0.001	0.227	25.601
ESd1_36.4	0.02	0.017	0.004	0.003	0.016	0.023	1.87	0.009	0	0.13	25.551
ESd1_36.5	0.01	0.014	0.003	0.003	0.019	0.022	1.801	0.012	0	0.199	25.596
ESd1_36.6	0.009	0.018	0.002	0.003	0.026	0.022	1.883	0.007	0.011	0.117	25.521
ESd1_36.7	0.009	0.016	0.002	0.002	0.026	0.024	1.884	0.009	0.009	0.116	25.539
ESd1_36.8	0.022	0.017	0.003	0	0.015	0.024	1.835	0.007	0.001	0.165	25.564

RM1-7

Sample	Si	Ti	Ca	Al	Fe	La	Ce	Pr	Nd	Sm	Gd	ΣREE	Y
RM1_7.1	7.701	7.276	7.705	0.322	0.361	0.021	0.072	0.009	0.02	0	0.001	0.102	0.028
RM1_7.2	7.688	6.67	7.673	0.357	0.463	0.025	0.068	0.007	0.01	0	0	0.091	0.024
RM1_7.3	7.752	7.181	7.733	0.333	0.341	0.023	0.074	0.007	0.03	0	0.003	0.112	0.03
RM1_7.4	7.719	7.248	7.784	0.344	0.338	0.019	0.063	0.009	0.02	0	0.001	0.095	0.028
RM1_7.5	7.656	6.525	7.615	0.43	0.593	0.015	0.068	0.012	0.02	0	0.005	0.11	0.06
RM1_7.6	7.658	7.211	7.615	0.32	0.345	0.035	0.122	0.018	0.05	0	0.004	0.194	0.052
RM1_7.7	7.655	7.041	7.417	0.443	0.482	0.026	0.13	0.021	0.11	0.02	0.027	0.308	0.122
RM1_7.8	7.671	6.997	7.26	0.393	0.441	0.036	0.172	0.03	0.14	0.03	0.025	0.389	0.137
RM1_7.9	7.637	7.273	7.546	0.34	0.294	0.041	0.14	0.014	0.05	0	0.009	0.218	0.042
RM1_7.10	7.822	6.724	7.645	0.398	0.522	0.015	0.055	0.002	0.02	0	0.005	0.082	0.046

Sample	Zr	Nb	Ta	Mg	P	Mn	OH	Na	K	F	Total
RM1_7.1	0.007	0.048	0	0.005	0.011	0.045	1.715	0.015	0	0.285	25.659
RM1_7.2	0.008	0.421	0.013	0.007	0.013	0.064	1.862	0.045	0	0.138	25.573
RM1_7.3	0.008	0.061	0.002	0.003	0.012	0.047	1.749	0.015	0	0.251	25.66
RM1_7.4	0.009	0.045	0.001	0.003	0.009	0.046	1.665	0.011	0	0.335	25.703
RM1_7.5	0.01	0.448	0.016	0.009	0.008	0.087	1.76	0.048	0.001	0.24	25.642
RM1_7.6	0.009	0.048	0.002	0.005	0.024	0.044	1.915	0.018	0	0.085	25.588
RM1_7.7	0.01	0.028	0.001	0.004	0.015	0.041	1.877	0.008	0	0.123	25.603
RM1_7.8	0.013	0.057	0.006	0.006	0.028	0.041	2	0.012	0	0	25.491
RM1_7.9	0.009	0.058	0.003	0.005	0.021	0.044	1.903	0.007	0	0.097	25.543
RM1_7.10	0.008	0.245	0.013	0.008	0.008	0.078	1.747	0.037	0	0.253	25.66

RM1-3

Sample	Si	Ti	Ca	Al	Fe	La	Ce	Pr	Nd	Sm	Gd	ΣREE	Y
RM1-3.1	7.745	7.081	7.618	0.403	0.42	0.029	0.108	0.015	0.055	0.009	0.01	0.226	0.061

Sample	Si	Ti	Ca	Al	Fe	La	Ce	Pr	Nd	Sm	Gd	ΣREE	Y
RM1-3.2	7.719	7.139	7.57	0.391	0.415	0.027	0.115	0.016	0.062	0.01	0.008	0.238	0.067
RM1-3.3	7.757	6.925	7.434	0.462	0.503	0.026	0.123	0.023	0.108	0.023	0.023	0.326	0.123
RM1-3.4	7.696	6.956	7.3	0.391	0.438	0.036	0.169	0.028	0.131	0.024	0.025	0.413	0.13
RM1-3.5	7.714	7.022	7.296	0.376	0.434	0.027	0.14	0.029	0.119	0.03	0.028	0.373	0.134
RM1-3.6	7.756	6.945	7.227	0.394	0.458	0.027	0.145	0.027	0.138	0.037	0.035	0.409	0.153
RM1-3.7	7.745	6.897	7.312	0.478	0.553	0.026	0.134	0.027	0.122	0.034	0.032	0.375	0.14
RM1-3.8	7.75	6.882	7.137	0.419	0.485	0.037	0.174	0.036	0.162	0.04	0.036	0.485	0.155

Sample	Zr	Nb	Ta	Mg	P	Mn	OH	Na	K	F	Total
RM1-3.1	0.012	0.027	0.001	0.004	0.011	0.043	1.772	0.01	0.01	0.228	25.673
RM1-3.2	0.01	0.026	0	0.005	0.013	0.041	1.755	0.006	0.001	0.245	25.643
RM1-3.3	0.011	0.024	0.003	0.007	0.014	0.044	1.814	0	0	0.186	25.634
RM1-3.4	0.013	0.067	0.004	0.006	0.029	0.042	2	0.017	0.002	0	25.509
RM1-3.5	0.013	0.051	0.004	0.005	0.018	0.045	1.982	0.005	0	0.018	25.494
RM1-3.6	0.017	0.054	0.005	0.006	0.021	0.042	1.929	0.01	0	0.071	25.498
RM1-3.7	0.011	0.023	0.003	0.009	0.014	0.04	1.817	0.004	0.001	0.183	25.608
RM1-3.8	0.01	0.05	0.004	0.006	0.028	0.042	2	0.012	0	0	25.468

ROM1-21

Sample	Si	Ti	Ca	Al	Fe	La	Ce	Pr	Nd	Sm	Gd	ΣREE	Y
ROM1_21.1	7.579	7.048	6.911	0.318	1.187	0.043	0.135	0.02	0.07	0.01	0.007	0.238	0.039
ROM1_21.2	7.875	7.113	7.401	0.343	0.335	0.039	0.149	0.02	0.08	0.01	0.009	0.266	0.045
ROM1_21.3	7.872	7.135	7.682	0.318	0.371	0.024	0.06	0.008	0.02	0	0.002	0.087	0.018
ROM1_21.4	7.884	7.202	7.585	0.294	0.327	0.035	0.078	0.008	0.02	0	0	0.105	0.016
ROM1_21.5	7.854	6.639	7.025	0.53	0.638	0.01	0.073	0.019	0.08	0.04	0.048	0.261	0.295
ROM1_21.6	7.88	6.612	7.059	0.526	0.614	0.011	0.074	0.015	0.08	0.04	0.049	0.255	0.298
ROM1_21.7	7.856	7.032	7.313	0.361	0.376	0.03	0.134	0.021	0.1	0.02	0.017	0.291	0.109
ROM1_21.8	7.841	7.048	7.423	0.351	0.405	0.025	0.107	0.014	0.07	0.01	0.011	0.211	0.089

Sample	Zr	Nb	Ta	Mg	P	Mn	OH	Na	K	F	Total
ROM1_21.1	0.013	0.033	0.003	0.003	0.014	0.025	1.802	0.008	0.022	0.198	25.487
ROM1_21.2	0.014	0.032	0.001	0.002	0.017	0.026	1.764	0.007	0.025	0.236	25.543
ROM1_21.3	0.019	0.04	0.004	0.005	0.01	0.032	1.703	0.008	0.009	0.297	25.641
ROM1_21.4	0.012	0.032	0.001	0.007	0.014	0.027	1.773	0.008	0.018	0.227	25.569
ROM1_21.5	0.007	0.109	0.003	0.022	0.009	0.155	1.733	0.034	0	0.267	25.602
ROM1_21.6	0.009	0.11	0.005	0.019	0.009	0.153	1.74	0.032	0.002	0.26	25.608
ROM1_21.7	0.008	0.042	0.004	0.005	0.016	0.05	1.837	0.01	0.005	0.163	25.515
ROM1_21.8	0.009	0.062	0.004	0.009	0.011	0.058	1.767	0.014	0.011	0.233	25.575

ROM1-31

Sample	Si	Ti	Ca	Al	Fe	La	Ce	Pr	Nd	Sm	Gd	ΣREE	Y

ROM1_31.1	7.796	7.274	7.809	0.364	0.286	0.027	0.053	0.007	0.01	0	0	0.071	0.007
ROM1_31.2	7.883	7.198	7.783	0.367	0.279	0.023	0.052	0.002	0.01	0	0	0.065	0.008
ROM1_31.3	7.824	7.298	7.733	0.317	0.311	0.021	0.035	0.002	0.01	0	0.001	0.044	0.005
ROM1_31.4	7.853	7.241	7.735	0.311	0.334	0.021	0.034	0.002	0.01	0	0.001	0.046	0.003
ROM1_31.5	7.805	7.229	7.536	0.301	0.319	0.051	0.128	0.016	0.04	0	0.001	0.185	0.013
ROM1_31.6	7.799	7.198	7.582	0.3	0.318	0.051	0.129	0.011	0.04	0	0.002	0.184	0.015
ROM1_31.7	7.778	7.2	7.519	0.291	0.306	0.058	0.143	0.015	0.04	0.01	0.003	0.209	0.017
ROM1_31.8	7.82	7.152	7.529	0.298	0.317	0.057	0.145	0.014	0.04	0.01	0.004	0.21	0.016
ROM1_31.9	7.827	7.171	7.605	0.337	0.323	0.039	0.112	0.008	0.05	0.01	0.005	0.179	0.024
ROM1_31.10	7.812	7.193	7.572	0.346	0.33	0.039	0.111	0.012	0.05	0.01	0.002	0.176	0.024
ROM1_31.11	7.83	7.356	7.752	0.289	0.196	0.019	0.056	0.006	0.02	0	0.002	0.09	0.011
ROM1_31.12	7.814	7.335	7.759	0.296	0.196	0.022	0.055	0.008	0.03	0.01	0	0.093	0.013
ROM1_31.13	7.9	7.312	7.743	0.271	0.188	0.016	0.047	0.01	0.02	0	0.003	0.08	0.011
ROM1_31.14	7.821	7.395	7.741	0.266	0.186	0.017	0.043	0.004	0.02	0	0.003	0.068	0.01
ROM1_31.15	7.837	6.964	7.498	0.364	0.473	0.037	0.14	0.017	0.07	0.01	0.004	0.237	0.033
ROM1_31.16	7.814	6.984	7.47	0.36	0.46	0.043	0.133	0.017	0.06	0.01	0.008	0.229	0.029
ROM1_31.17	7.83	6.967	7.235	0.362	0.41	0.063	0.22	0.032	0.12	0.02	0.013	0.406	0.06
ROM1_31.18	7.798	7.015	7.298	0.383	0.342	0.068	0.23	0.033	0.12	0.02	0.013	0.409	0.046
ROM1_31.19	7.871	7.187	7.642	0.358	0.19	0.026	0.116	0.011	0.04	0	0	0.197	0.03
ROM1_31.20	7.791	7.317	7.615	0.262	0.243	0.034	0.099	0.011	0.05	0	0.002	0.161	0.021

Sample	Zr	Nb	Ta	Mg	P	Mn	OH	Na	K	F	Total
ROM1_31.1	0.008	0.005	0.001	0.001	0.01	0.023	1.666	0.005	0	0.334	25.688
ROM1_31.2	0.007	0.007	0	0.004	0.01	0.023	1.707	0.008	0	0.293	25.666
ROM1_31.3	0.007	0.003	0.001	0.002	0.012	0.026	1.759	0.011	0	0.241	25.623
ROM1_31.4	0.008	0.004	0	0.005	0.014	0.028	1.822	0.006	0	0.178	25.608
ROM1_31.5	0.01	0.018	0	0.003	0.042	0.025	1.775	0.009	0	0.225	25.549
ROM1_31.6	0.01	0.019	0	0.007	0.042	0.028	1.816	0.011	0	0.184	25.565
ROM1_31.7	0.017	0.038	0	0.007	0.038	0.025	1.867	0.011	0	0.133	25.52
ROM1_31.8	0.019	0.042	0.001	0.003	0.039	0.029	1.801	0.006	0	0.199	25.539
ROM1_31.9	0.01	0.024	0	0.005	0.018	0.024	1.776	0.006	0	0.224	25.593
ROM1_31.10	0.01	0.023	0	0.007	0.018	0.026	1.767	0.007	0	0.233	25.585
ROM1_31.11	0.006	0.011	0	0.001	0.011	0.017	1.751	0.008	0	0.249	25.601
ROM1_31.12	0.004	0.011	0.002	0	0.012	0.016	1.844	0.005	0	0.156	25.581
ROM1_31.13	0.004	0.009	0	0.003	0.009	0.017	1.816	0.007	0	0.184	25.57
ROM1_31.14	0.004	0.008	0	0.003	0.011	0.017	1.85	0.011	0	0.15	25.56
ROM1_31.15	0.086	0.021	0	0.004	0.018	0.022	1.746	0.013	0.001	0.254	25.614
ROM1_31.16	0.081	0.024	0	0.003	0.02	0.026	1.888	0.012	0	0.112	25.558
ROM1_31.17	0.016	0.052	0.003	0.005	0.033	0.019	1.878	0.006	0	0.122	25.469
ROM1_31.18	0.013	0.043	0.001	0.004	0.028	0.022	1.922	0.012	0	0.078	25.486
ROM1_31.19	0.018	0.018	0	0	0.003	0.019	1.877	0	0	0.123	25.557
ROM1_31.20	0.015	0.022	0.001	0.002	0.018	0.023	1.841	0.007	0.001	0.159	25.537

ROM1-40

Sample	Si	Ti	Ca	Al	Fe	La	Ce	Pr	Nd	Sm	Gd	ΣREE	Y

Sample												
ROM1_40.1	7.82	7.15	7.598	0.351	0.338	0.039	0.116	0.016	0.05	0.01	0.004	0.188	0.025
ROM1_40.2	7.826	7.142	7.602	0.349	0.327	0.036	0.118	0.013	0.04	0.01	0.003	0.185	0.022
ROM1_40.3	7.801	6.974	7.442	0.402	0.449	0.044	0.167	0.02	0.1	0.01	0.013	0.314	0.058
ROM1_40.4	7.866	7.04	7.516	0.397	0.414	0.023	0.092	0.014	0.05	0.01	0.007	0.174	0.065
ROM1_40.5	7.804	7.064	7.433	0.348	0.396	0.021	0.1	0.015	0.06	0.01	0.013	0.197	0.085
ROM1_40.6	7.811	7.042	7.446	0.348	0.402	0.023	0.104	0.017	0.06	0.01	0.013	0.207	0.087
ROM1_40.7	7.826	6.988	7.506	0.407	0.455	0.023	0.102	0.016	0.06	0.01	0.012	0.205	0.082
ROM1_40.8	7.856	6.975	7.512	0.407	0.436	0.025	0.102	0.017	0.06	0.01	0.012	0.203	0.087
ROM1_40.9	7.87	6.931	7.388	0.42	0.422	0.039	0.138	0.019	0.06	0.01	0.007	0.231	0.065
ROM1_40.10	7.857	6.977	7.417	0.352	0.408	0.036	0.134	0.018	0.06	0.01	0.007	0.231	0.078
ROM1_40.11	7.864	7.264	7.897	0.412	0.198	0.001	0.003	0.001	0	0	0.001	0.006	0.001
ROM1_40.12	7.821	7.322	7.897	0.363	0.166	0	0.006	0	0.01	0	0.004	0.019	0.018
ROM1_40.13	7.863	7.007	7.538	0.409	0.479	0.022	0.09	0.015	0.04	0.01	0.008	0.163	0.061
ROM1_40.14	7.84	6.986	7.588	0.431	0.492	0.021	0.084	0.011	0.04	0.01	0.007	0.151	0.065
ROM1_40.15	7.866	6.928	7.385	0.387	0.441	0.049	0.172	0.025	0.11	0.02	0.013	0.332	0.066
ROM1_40.16	7.867	6.941	7.388	0.403	0.447	0.042	0.155	0.022	0.1	0.02	0.011	0.309	0.058
ROM1_40.17	7.82	7.157	7.414	0.303	0.349	0.049	0.162	0.019	0.07	0.01	0.008	0.266	0.036
ROM1_40.18	7.797	7.164	7.539	0.293	0.329	0.047	0.141	0.015	0.05	0.01	0.005	0.222	0.026
ROM1_40.19	7.872	7.103	7.622	0.326	0.367	0.043	0.107	0.012	0.03	0	0.004	0.156	0.019
ROM1_40.20	7.849	6.96	7.349	0.374	0.413	0.034	0.133	0.02	0.07	0.01	0.012	0.243	0.09

Sample	Zr	Nb	Ta	Mg	P	Mn	OH	Na	K	F	Total
ROM1_40.1	0.01	0.025	0.002	0.005	0.019	0.027	1.749	0.003	0.009	0.251	25.612
ROM1_40.2	0.009	0.025	0.002	0.004	0.018	0.026	1.82	0.003	0.012	0.18	25.592
ROM1_40.3	0.037	0.032	0.001	0.002	0.018	0.021	1.757	0.002	0.002	0.243	25.601
ROM1_40.4	0.01	0.045	0.002	0.007	0.01	0.053	1.666	0.009	0	0.334	25.634
ROM1_40.5	0.007	0.086	0.002	0.006	0.016	0.07	1.793	0.015	0	0.207	25.556
ROM1_40.6	0.009	0.077	0.004	0.006	0.013	0.067	1.815	0.015	0	0.185	25.563
ROM1_40.7	0.009	0.054	0.003	0.006	0.01	0.055	1.699	0.013	0	0.301	25.647
ROM1_40.8	0.007	0.055	0.003	0.008	0.008	0.046	1.691	0.01	0	0.309	25.643
ROM1_40.9	0.013	0.07	0.001	0.008	0.02	0.07	1.806	0.016	0	0.194	25.567
ROM1_40.10	0.01	0.07	0.002	0.005	0.019	0.069	1.844	0.016	0.001	0.156	25.553
ROM1_40.11	0	0.01	0	0.002	0.014	0.012	1.685	0.005	0	0.315	25.687
ROM1_40.12	0.001	0.018	0	0.001	0.009	0.012	1.767	0.002	0	0.233	25.65
ROM1_40.13	0.009	0.039	0.001	0.009	0.009	0.069	1.585	0.01	0	0.415	25.692
ROM1_40.14	0.009	0.039	0.001	0.008	0.011	0.071	1.569	0.013	0	0.431	25.73
ROM1_40.15	0.041	0.036	0.001	0.007	0.015	0.021	1.758	0.004	0.001	0.242	25.577
ROM1_40.16	0.032	0.03	0.003	0.006	0.018	0.021	1.766	0.002	0.004	0.234	25.573
ROM1_40.17	0.016	0.042	0.003	0.004	0.013	0.024	1.839	0.007	0.002	0.161	25.505
ROM1_40.18	0.024	0.036	0.001	0.004	0.023	0.022	1.838	0.007	0.021	0.162	25.559
ROM1_40.19	0.03	0.034	0.002	0.007	0.01	0.023	1.689	0.011	0.01	0.311	25.637
ROM1_40.20	0.009	0.102	0.004	0.006	0.019	0.071	1.757	0.015	0	0.243	25.545

A.2 Ross of Mull Granite titanite EMPA data (wt% oxide)

A-13

Sample	P2O5	Nb2O5	Ta2O5	SiO2	TiO2	ZrO2	Al2O3	Fe2O3	Y2O3	La2O3
A13.1	0.1133	0.641	0.1206	28.5404	34.1373	0.1074	1.2211	2.2601	0.8151	0.4336
A13.2	0.0775	0.2393	0.0468	29.3766	35.883	0.073	1.2055	1.7131	0.4028	0.3309
A13.3	0.0683	0.2365	0.0539	28.7933	34.3761	0.0761	1.4057	2.2523	0.8706	0.286
A13.4	0.0558	0.2053	0.0346	28.9051	34.859	0.0716	1.4183	2.2063	0.801	0.239
A13.5	0.0615	0.2393	0.0416	29.7009	35.8373	0.0709	1.1991	1.8451	0.2754	0.2851
A13.6	0.0639	0.2339	0.062	29.1893	36.6711	0.0643	1.1654	1.4554	0.3057	0.3245
A13.7	0.0587	0.3193	0.0692	29.2458	34.5947	0.0636	1.3277	2.5042	0.679	0.2281

Sample	Ce2O3	Pr2O3	Nd2O3	Sm2O3	Gd2O3	MgO	CaO	MnO	ZnO	SrO
A13.1	1.753	0.3284	1.1171	0.2141	0.2146	0.0119	25.2817	0.235	0.0115	0.0837
A13.2	1.3192	0.2031	0.7516	0.1099	0.1265	0.0189	26.4749	0.1397	0.0031	-0.064
A13.3	1.3286	0.2431	1.2245	0.2996	0.3194	0.0115	25.5397	0.1495	0.0118	0.0579
A13.4	1.2579	0.2411	1.0315	0.2679	0.2624	0.0035	25.801	0.1615	-0.001	0.0599
A13.5	1.0208	0.1634	0.4701	0.092	0.0682	0.0128	26.7622	0.1293	0.0115	0.0357
A13.6	1.1154	0.1392	0.5647	0.0748	0.0995	0.0159	26.7606	0.123	0.0036	0.0241
A13.7	1.2097	0.1973	0.7507	0.1739	0.1751	0.0073	26.209	0.2513	0.0078	0.0521

Sample	SnO	H2O	Na2O	K2O	F	Total	O=F	Total
A13.1	0.0383	1.1024	0.0525	0.0016	0.0176	98.7583	0.0074	98.7509
A13.2	0.0056	1.0985	0.0126	-0.0017	0.0763	99.6852	0.0321	99.6531
A13.3	0.0223	1.0234	0.0153	0.0008	0.1887	98.785	0.0795	98.7055
A13.4	0.0113	1.0164	0.0148	0	0.2165	99.0819	0.0911	98.9907
A13.5	0.0153	1.0596	0.006	0.0087	0.1638	99.5402	0.069	99.4712
A13.6	0.0096	1.0549	0.0238	-0.0023	0.1716	99.692	0.0723	99.6197
A13.7	0.0232	1.0104	0.0245	-0.0001	0.2408	99.3714	0.1014	99.27

A-57

Sample	P2O5	Nb2O5	Ta2O5	SiO2	TiO2	ZrO2	Al2O3	Fe2O3	Y2O3	La2O3
A57.1	0.074	0.244	0.016	28.862	35.996	0.069	1.174	1.750	0.303	0.346
A57.2	0.066	0.265	0.021	29.205	35.984	0.074	1.185	1.738	0.307	0.349
A57.3	0.060	0.563	0.064	28.914	34.746	0.109	1.317	2.260	0.547	0.283
A57.4	0.072	0.350	0.014	28.768	35.254	0.151	1.215	2.029	0.445	0.406
A57.5	0.067	0.363	0.033	28.845	35.394	0.122	1.249	2.029	0.430	0.429
A57.6	0.102	0.723	0.070	29.083	35.069	0.107	1.172	2.044	0.592	0.419
A57.7	0.074	0.244	0.016	28.862	35.996	0.069	1.174	1.750	0.303	0.346

Sample	Ce2O3	Pr2O3	Nd2O3	Sm2O3	Gd2O3	MgO	CaO	MnO	ZnO	SrO
A57.1	1.33	0.2003	0.7229	0.1383	0.0934	0.0103	26.4563	0.1251	0.0045	0.0118
A57.2	1.314	0.2188	0.7241	0.1146	0.0761	0.0118	26.4196	0.1297	0.0057	0.0212
A57.3	1.1088	0.1481	0.6226	0.1043	0.1019	0.0233	26.2882	0.3249	0.0028	0.0412
A57.4	1.5782	0.2416	0.9426	0.1546	0.1655	0.026	25.9948	0.1672	0.0052	0.0344
A57.5	1.529	0.2425	0.9312	0.1808	0.0988	0.0154	25.8686	0.1518	0.0073	0.0459
A57.6	1.5689	0.2218	0.8743	0.1373	0.102	0.0132	25.9606	0.2513	0.0012	0.0678
A57.7	1.33	0.2003	0.7229	0.1383	0.0934	0.0103	26.4563	0.1251	0.0045	0.0118

Sample	SnO	H2O	Na2O	K2O	F	Total	O=F	Total
A57.1	0.0004	1.0054	0.008	0.0606	0.2521	99.2416	0.1061	99.1354
A57.2	0.0116	1.0282	0.0116	0.0642	0.2154	99.5328	0.0907	99.4421
A57.3	0.0404	0.9801	0.039	0.0057	0.295	98.9443	0.1242	98.8201
A57.4	0.0238	1.0042	0.0107	0.003	0.2432	99.2642	0.1024	99.1618
A57.5	0.0108	1.0087	0.0208	0.005	0.2372	99.26	0.0999	99.1602
A57.6	0.0243	1.0337	0.032	-0.0014	0.1957	99.797	0.0824	99.7145
A57.7	-0.0004	1.0054	0.008	0.0606	0.2521	99.2416	0.1061	99.1354

ES16-7

Sample	P2O5	Nb2O5	Ta2O5	SiO2	TiO2	ZrO2	Al2O3	Fe2O3	Y2O3	La2O3
ES16_7.1	0.0712	0.2284	0.0006	29.6004	35.3922	0.0764	1.2328	1.7493	0.3593	0.3068
ES16_7.2	0.0656	0.2496	0.0168	29.5151	35.9309	0.0834	1.2492	1.7444	0.3469	0.2884
ES16_7.3	0.0364	0.3382	0.0398	29.4053	34.9294	0.0486	1.3844	2.4003	0.5836	0.2142
ES16_7.4	0.0528	0.3976	0.0204	29.1138	34.5107	0.0653	1.3015	2.177	0.6046	0.253
ES16_7.5	0.0569	0.2135	0.0301	29.5863	35.5055	0.0704	1.2634	1.7995	0.3841	0.3332
ES16_7.6	0.0681	0.2151	0.0192	29.5771	35.6188	0.0815	1.26	1.8407	0.3909	0.3297

Sample	Ce2O3	Pr2O3	Nd2O3	Sm2O3	Gd2O3	MgO	CaO	MnO	ZnO	SrO
ES16_7.1	1.0935	0.1667	0.5585	0.0945	0.1001	0.0095	26.6731	0.1388	0.0086	0.0367
ES16_7.2	1.0656	0.1752	0.5739	0.1043	0.0811	0.0117	26.8023	0.1297	0.0068	0.0297
ES16_7.3	0.9361	0.1814	0.5248	0.129	0.1081	0.017	26.3122	0.2625	0.0008	0.0476
ES16_7.4	1.0172	0.1396	0.6415	0.1174	0.1519	0.0081	26.2997	0.2708	0.0003	0.029
ES16_7.5	1.174	0.1782	0.6911	0.1134	0.11	0.014	26.4693	0.1394	0.0144	0.0181
ES16_7.6	1.1943	0.1907	0.6619	0.1561	0.0885	0.0142	26.5427	0.1389	0.0088	0.0264

Sample	SnO	H2O	Na2O	K2O	F	Total	O=F	Total
ES16_7.1	0.0076	0.9842	0.0183	0.0117	0.3058	99.179	0.1288	99.0502
ES16_7.2	0.0128	0.977	0.0105	0.0115	0.3332	99.7858	0.1403	99.6455
ES16_7.3	0.0309	0.9256	0.0444	0.0028	0.4227	99.2778	0.178	99.0998
ES16_7.4	0.0196	0.9601	0.0562	0.0054	0.3299	98.5141	0.1389	98.3752
ES16_7.5	0.0132	1.0095	0.0185	0	0.2564	99.4299	0.108	99.3219
ES16_7.6	0.0061	1.0016	0.0145	0.0005	0.2775	99.6881	0.1169	99.5712

ES3A-27

Sample	P2O5	Nb2O5	Ta2O5	SiO2	TiO2	ZrO2	Al2O3	Fe2O3	Y2O3	La2O3
ES3A_27.1	0.014	0.0405	0.0019	30.1473	36.4066	0.015	1.2865	1.8781	0.0116	0.0244
ES3A_27.2	0.0263	0.1068	0.0008	29.8005	36.4878	0.0424	1.1157	1.6227	0.0419	0.0991
ES3A_27.3	0.0324	0.0698	0.0014	29.5601	36.4843	0.0249	1.6632	1.5908	0.0242	0.0885
ES3A_27.4	0.0523	0.1389	0.0075	29.262	36.6932	0.0429	1.0894	1.5278	0.0961	0.1517
ES3A_27.5	0.0851	0.3493	0.0548	28.4501	35.4435	0.0801	1.0897	1.6729	0.5352	0.2817
ES3A_27.6	0.078	0.4002	0.0429	28.8524	36.2022	0.1318	0.9122	1.6028	0.347	0.2871
ES3A_27.7	0.0907	0.3471	0.0053	28.7775	36.8832	0.0887	0.8711	1.362	0.3483	0.2958
ES3A_27.8	0.0838	0.5511	0.0284	28.7181	35.4965	0.0769	1.2634	1.6794	0.3554	0.4197
ES3A_27.9	0.0971	0.5418	0.0335	28.4593	35.5423	0.0744	1.0577	1.7528	0.4485	0.3577
ES3A_27.10	0.0583	0.4139	0.0225	29.0737	35.8039	0.0712	0.9942	1.6533	0.3367	0.3066
ES3A_27.11	0.0595	0.3901	0.038	29.0472	35.1173	0.1399	1.2527	2.1484	0.3951	0.2621

Sample	Ce2O3	Pr2O3	Nd2O3	Sm2O3	Gd2O3	MgO	CaO	MnO	ZnO	SrO
ES3A_27.1	0.0718	-0.018	0.0175	0.0204	0.0208	0.0178	27.861	0.0815	0.0041	0.0416
ES3A_27.2	0.3513	0.0338	0.1024	0.0351	0.0123	0.0094	27.9347	0.0824	0.0046	0.0068
ES3A_27.3	0.2724	0.0023	0.088	0.0253	0.0027	0.2309	27.8654	0.2182	0.0091	0.0081
ES3A_27.4	0.5444	0.0763	0.2398	0.0432	0.0148	0.002	27.4179	0.1072	0.0008	0.0122
ES3A_27.5	1.2384	0.2282	1.0881	0.2638	0.1909	0.0108	25.8305	0.1007	0.0048	0.0512
ES3A_27.6	0.9528	0.1162	0.4748	0.0639	0.0732	0.0065	26.8095	0.1024	0.0004	0.0214
ES3A_27.7	1.0407	0.1527	0.5467	0.1216	0.0425	0.0063	26.6769	0.0998	0.0015	0.0336
ES3A_27.8	1.4098	0.2082	0.6768	0.0992	0.0945	0.0168	26.0257	0.2328	0.0001	0.0392
ES3A_27.9	1.2924	0.1734	0.6253	0.1013	0.1033	0.0109	26.1665	0.2292	0.0016	0.0274
ES3A_27.10	1.1183	0.135	0.5466	0.0781	0.0907	0.0082	26.5164	0.2278	0.0054	0.0447
ES3A_27.11	1.0371	0.1685	0.5351	0.1372	0.097	0.0146	26.4658	0.2274	0.0043	0.0059

Sample	SnO	H2O	Na2O	K2O	F	Total	O=F	Total
ES3A_27.1	0.0085	0.9433	0.0061	0.2053	0.4275	99.5385	0.18	99.3585
ES3A_27.2	0.0018	1.0695	0.0151	0.0185	0.1552	99.1654	0.0653	99.1
ES3A_27.3	0.0088	0.9939	0.0164	0.0206	0.3214	99.6204	0.1354	99.485
ES3A_27.4	0.018	1.0242	0.0076	0.0046	0.2308	98.7679	0.0972	98.6707
ES3A_27.5	0.0053	1.095	0.0106	0.0006	0.0359	98.1405	0.0151	98.1254
ES3A_27.6	0.0283	1.0425	0.026	0.0003	0.1733	98.7261	0.073	98.6531
ES3A_27.7	0.0169	1.0962	0.0235	0.0002	0.0691	98.9587	0.0291	98.9296
ES3A_27.8	0.0202	1.0778	0.0241	0.0036	0.0895	98.6482	0.0377	98.6106
ES3A_27.9	0.0251	1.0769	0.0271	0.0018	0.0814	98.2794	0.0343	98.2451
ES3A_27.10	0.0342	1.0601	0.0224	0.0004	0.1355	98.7131	0.057	98.656
ES3A_27.11	0.0296	1.0266	0.017	0.0027	0.2037	98.8226	0.0858	98.7368

ES3A-49

Sample	P2O5	Nb2O5	Ta2O5	SiO2	TiO2	ZrO2	Al2O3	Fe2O3	Y2O3	La2O3
ES3A_49.1	0.0488	0.422	0.0475	28.8863	35.7804	0.0703	1.0375	1.6052	0.4041	0.2648
ES3A_49.2	0.117	0.5847	0.0411	28.3501	33.3336	0.6099	1.3256	2.4909	0.62	0.4472
ES3A_49.3	0.0611	0.2142	0.0293	28.5839	34.4384	0.116	1.361	2.4129	0.4945	0.2948
ES3A_49.4	0.0771	0.3234	0.0456	28.653	35.71	0.0825	1.0408	1.7016	0.478	0.2644
ES3A_49.5	0.0771	0.1583	0.0334	29.1422	36.391	0.0539	1.0055	1.4746	0.1051	0.265
ES3A_49.6	0.0647	0.2379	0.0345	28.5834	36.6437	0.0751	0.9722	1.415	0.1237	0.3579
ES3A_49.7	0.022	0.0444	0.0209	29.853	36.4763	0.0064	1.18	1.6447	0.0018	0.0618

Sample	Ce2O3	Pr2O3	Nd2O3	Sm2O3	Gd2O3	MgO	CaO	MnO	ZnO	SrO
ES3A_49.1	1.0386	0.0984	0.529	0.111	0.0833	0.0044	26.6217	0.1851	0.002	0.0577
ES3A_49.2	2.2059	0.4172	1.7848	0.3723	0.2788	0.0207	24.7244	0.1282	0.01	0.0655
ES3A_49.3	1.1811	0.2093	0.7663	0.1742	0.1646	0.0123	26.3547	0.1483	0.0115	0.0135
ES3A_49.4	1.3282	0.2073	1.0348	0.1855	0.1585	0.0111	26.0265	0.0919	0.0032	0.0505
ES3A_49.5	0.8062	0.1072	0.3289	0.0898	0.0212	0.0062	27.2037	0.1057	0.0014	0.015
ES3A_49.6	0.9909	0.1472	0.4206	0.0766	0.0502	0.0036	26.9098	0.1055	0.0086	0.0124
ES3A_49.7	0.1524	0.0039	0.0004	0.0078	0.0384	0.006	28.1149	0.063	0.0043	0.0188

Sample	SnO	H2O	Na2O	K2O	F	Total	O=F	Total
ES3A_49.1	0.0262	1.1086	0.0245	0.0004	0.0302	98.43	0.0127	98.4173
ES3A_49.2	0.0414	1.1045	0.022	0.0011	0.0841	99.0201	0	99.0201
ES3A_49.3	0.0205	1.0331	0.0072	0.0027	0.1664	98.244	0.0701	98.1739
ES3A_49.4	0.021	1.1187	0.0112	0.0016	0.0479	98.5741	0	98.5741
ES3A_49.5	0.0071	1.0543	0.0122	0.0002	0.1575	98.6008	0.0663	98.5345
ES3A_49.6	0.0075	1.1023	0.016	0.0025	0.0457	98.3989	0.0193	98.3797
ES3A_49.7	0.0039	1.0498	0.0082	0.0434	0.1968	98.9922	0.0829	98.9094

ES3A-59

Sample	P2O5	Nb2O5	Ta2O5	SiO2	TiO2	ZrO2	Al2O3	Fe2O3	Y2O3	La2O3
ES3A_59.1	0.0374	0.1477	0.0281	29.541	37.3329	0.014	0.8758	1.0736	0.119	0.1881
ES3A_59.2	0.0776	0.2423	0.011	29.5636	37.2696	0.0551	0.8531	1.1764	0.259	0.1947
ES3A_59.3	0.1206	0.4773	0.0873	28.3972	34.6873	0.1115	1.2369	2.0998	0.8711	0.3974
ES3A_59.4	0.0723	0.2801	0.0074	28.4588	34.5964	0.1018	1.2791	2.1962	0.7473	0.259
ES3A_59.5	0.0612	0.2987	0.0323	28.9815	34.8993	0.0776	1.3264	2.2499	0.6868	0.2647
ES3A_59.6	0.0639	0.1855	0.0013	29.4062	36.8235	0.0682	1.0522	1.4997	0.1359	0.3011
ES3A_59.7	0.0443	0.5	0.0394	29.0251	35.0925	0.0603	1.363	2.389	0.7342	0.2466

Sample	Ce2O3	Pr2O3	Nd2O3	Sm2O3	Gd2O3	MgO	CaO	MnO	ZnO	SrO
ES3A_59.1	0.5517	0.0941	0.2281	0.0264	0.022	0.0043	27.6015	0.073	0.0118	0.0161
ES3A_59.2	0.8312	0.1204	0.5157	0.0845	0.0498	0.0034	26.92	0.0928	0.0085	0.0216
ES3A_59.3	1.7717	0.3334	1.3622	0.2807	0.2818	0.0141	25.0199	0.1945	0.0073	0.0725
ES3A_59.4	1.3073	0.2307	0.9798	0.2093	0.2083	0.0103	25.6375	0.1922	0.0112	0.0618
ES3A_59.5	1.2036	0.2033	0.8713	0.1588	0.1818	0.0171	26.0457	0.2167	0.0012	0.043
ES3A_59.6	0.9264	0.1358	0.3932	0.0517	0.0393	0.0074	27.0316	0.107	0.001	0.0296
ES3A_59.7	0.9337	0.1717	0.5686	0.1455	0.1151	0.0246	26.183	0.3176	0.0065	0.0688

Sample	SnO	H2O	Na2O	K2O	F	Total	O=F	Total
ES3A_59.1	0.0055	1.0935	0.0109	0.0004	0.1011	99.1803	0.0426	99.1377

ES3A_59.2	0.0072	1.0901	0.0075	0.0033	0.1082	99.5419	0.0456	99.4963
ES3A_59.3	0.0453	1.1078	0.0222	0.0004	0.0081	98.9281	0.0034	98.9247
ES3A_59.4	0.0245	1.0708	0.0162	0.0032	0.0787	97.964	0.0332	97.9309
ES3A_59.5	0.0183	0.9954	0.0143	0.0039	0.2635	99.0723	0.111	98.9613
ES3A_59.6	0.0007	1.0769	0.012	0.0166	0.1311	99.4659	0.0552	99.4107
ES3A_59.7	0.0328	1.0186	0.028	0.0045	0.227	99.2674	0.0956	99.1718

ES5-30

Sample	P2O5	Nb2O5	Ta2O5	SiO2	TiO2	ZrO2	Al2O3	Y2O3	La2O3	Ce2O3
ES5_30.1	0.0678	0.1903	0.0402	29.2741	34.0052	0.0851	1.4759	0.7174	0.2344	1.0703
ES5_30.2	0.0711	0.1854	0.0275	29.2706	33.7498	0.0821	1.4855	0.7182	0.2364	1.0488
ES5_30.3	0.1231	0.3294	0.0531	29.0867	34.6968	0.0777	1.1341	0.66	0.4087	1.6661
ES5_30.4	0.1275	0.407	0.0375	28.995	34.3727	0.0946	1.1569	0.6599	0.429	1.6769
ES5_30.5	0.0686	0.2564	0.0141	29.691	35.7393	0.0621	1.042	0.2163	0.2262	0.8893
ES5_30.6	0.0603	0.2392	0.0168	29.892	36.0663	0.0556	1.0633	0.2001	0.2191	0.7737

Sample	Pr2O3	Nd2O3	Sm2O3	Gd2O3	MgO	CaO	MnO	FeO	ZnO	SrO
ES5_30.1	0.1963	0.9513	0.198	0.2324	0.015	26.0708	0.1557	2.3883	0.0067	0.0984
ES5_30.2	0.2065	0.9333	0.2458	0.2376	0.0053	26.2018	0.1469	2.3611	0.0081	0.0409
ES5_30.3	0.2596	1.1726	0.2267	0.2162	0.0082	25.495	0.1533	1.876	0.001	0.0695
ES5_30.4	0.2649	1.157	0.2392	0.1755	0.0105	25.5171	0.1555	1.9206	0.0053	0.0631
ES5_30.5	0.1199	0.4522	0.0706	0.0828	0.0033	26.7726	0.1299	1.5739	0.0114	0.0221
ES5_30.6	0.1571	0.3691	0.0792	0.0714	0.0071	27.031	0.1189	1.5112	0.0004	0.0195

Sample	SnO	H2O	Na2O	K2O	F	Total	O=F	Total
ES5_30.1	0.0245	1.0303	0.0016	0.0042	0.1846	98.6097	0.0777	98.532
ES5_30.2	0.0076	0.9859	0.0095	0.0008	0.2715	98.4882	0.1143	98.3738
ES5_30.3	0.0237	1.0797	0.0103	0.0032	0.0777	98.8307	0.0327	98.7979
ES5_30.4	0.0222	1.1142	0.015	0.0005	0.0562	98.5544	0	98.5544
ES5_30.5	0.0148	1.0506	0.0185	0.0044	0.1676	98.6631	0.0706	98.5926
ES5_30.6	0.0025	1.0613	0.0135	0.0033	0.161	99.173	0.0678	99.1052

ES5-66

Sample	P2O5	Nb2O5	Ta2O5	SiO2	TiO2	ZrO2	Al2O3	Y2O3	La2O3	Ce2O3
ES5_66.1	0.07	0.2497	0.0119	29.7609	36.4122	0.0601	0.94	0.1673	0.2727	0.885
ES5_66.2	0.0673	0.3006	0.0243	29.5787	36.2937	0.0736	0.8706	0.1793	0.261	0.8907
ES5_66.3	0.0174	0.0808	0.0165	29.5437	36.0201	0.0263	1.1476	0.0837	0.006	0.1306
ES5_66.4	0.028	0.102	0.0292	29.831	36.3073	0.0183	1.2012	0.0887	0.0319	0.1542
ES5_66.5	0.105	0.408	0.0023	28.7246	33.8242	0.0888	1.3855	0.8226	0.3601	1.6582
ES5_66.6	0.0618	0.2377	0.0058	29.2603	34.4322	0.0772	1.2599	0.5549	0.2451	1.1089
ES5_66.7	0.0723	0.2485	0.0147	29.211	34.6648	0.0691	1.2363	0.548	0.3238	1.3741
ES5_66.8	0.0701	0.2489	0.0242	29.7138	35.2434	0.0753	1.1517	0.3005	0.335	1.2435
ES5_66.9	0.0256	0.1038	0	30.372	36.7218	0.0098	1.0066	0.0441	0.0042	0.1234
ES5_66.10	0.026	0.0883	0	30.7422	37.3938	0.0092	0.841	0.051	0.0182	0.1189
ES5_66.11	0.046	0.2787	0.009	29.4484	37.0196	0.0242	0.808	0.1041	0.0823	0.4467
ES5_66.12	0.0313	0.1744	0.0313	29.707	36.4617	0.036	1.1216	0.1001	0.1211	0.3641

Sample	Pr2O3	Nd2O3	Sm2O3	Gd2O3	MgO	CaO	MnO	FeO	ZnO	SrO
ES5_66.1	0.0807	0.3985	0.0555	0.0609	0.0013	27.1343	0.111	1.4826	0.0097	0.016
ES5_66.2	0.1321	0.4287	0.0651	0.0718	-0.0263	27.0478	0.1244	1.3554	0.004	0.0269
ES5_66.3	0.0577	0.0614	0.0065	0.0094	-0.0109	27.9907	0.0821	1.5578	0.0063	0.0066
ES5_66.4	0.0067	0.0615	0.0462	0.002	0.0005	28.0697	0.0958	1.574	0.0053	0.0078
ES5_66.5	0.3113	1.3498	0.2899	0.3061	0.0083	25.21	0.1598	1.9294	0.0175	0.0623
ES5_66.6	0.2113	0.7855	0.1652	0.1754	0.011	26.2034	0.1641	2.2096	0.0037	0.0537
ES5_66.7	0.2255	0.9362	0.1514	0.1551	0.0057	25.9519	0.1527	1.9277	0.0017	0.048
ES5_66.8	0.1915	0.7041	0.0909	0.059	0.0097	26.5156	0.1268	1.7559	0.0013	0.038
ES5_66.9	0.0173	0.0328	0.0369	0.0181	0.0082	27.9863	0.0887	1.168	0.0138	0.0567
ES5_66.10	0.0226	0.0691	0.0116	0.0083	0.0072	28.2792	0.0675	0.8854	0.0021	0.0149
ES5_66.11	0.0611	0.1672	0.0175	0.0154	0.0003	27.7566	0.1118	1.1973	0.0116	0.022
ES5_66.12	0.0556	0.116	0.0138	0.0575	0.021	27.8753	0.1192	1.6699	0.01	0.0169

Sample	SnO	H2O	Na2O	K2O	F	Total	O=F	Total
ES5_66.1	0.0146	1.0758	0.0102	0.0004	0.1338	99.3895	0.0564	99.3332
ES5_66.2	0.018	1.0927	0.0069	0.0047	0.087	98.9737	0.0366	98.937
ES5_66.3	0.0099	0.9889	0.0064	0.0441	0.2989	98.1993	0.1259	98.0734
ES5_66.4	0.0093	0.9759	0.0165	0.0057	0.3455	98.9942	0.1455	98.8488
ES5_66.5	0.0318	1.0972	0.0107	-0.001	0.0183	98.1018	0.0077	98.0941
ES5_66.6	0.0183	1.0536	0.0131	0.0026	0.1362	98.3903	0.0573	98.333
ES5_66.7	0.02	1.0856	0.0132	0.0008	0.0685	98.4531	0.0289	98.4242
ES5_66.8	0.0164	1.0671	0.0059	-0.0005	0.1325	99.0817	0.0558	99.0259
ES5_66.9	0.0102	0.988	0.0147	0.0905	0.3329	99.2175	0.1402	99.0774
ES5_66.10	0.0073	1.0429	0.0076	0.0388	0.2417	99.9519	0.1018	99.8501
ES5_66.11	0.0184	1.0428	0.0181	0.0299	0.1985	98.9018	0.0836	98.8183
ES5_66.12	0.013	0.9569	0.0153	0.018	0.3863	99.414	0.1627	99.2513

ES5-8

Sample	P2O5	Nb2O5	Ta2O5	SiO2	TiO2	ZrO2	Al2O3	Y2O3	La2O3	Ce2O3
ES5_8.1	0.0612	0.1678	0.0055	30.0233	35.8126	0.0643	1.1918	0.2079	0.2013	0.7245
ES5_8.2	0.0666	0.1998	0.01	29.9175	35.5425	0.0432	1.2007	0.204	0.2342	0.7619
ES5_8.3	0.0688	0.2877	0.027	29.7649	35.8676	0.0593	1.0238	0.3038	0.3004	1.0402
ES5_8.4	0.0552	0.2041	0.0177	29.9654	35.2493	0.0507	1.1962	0.234	0.2477	0.8525
ES5_8.5	0.0587	0.2004	0.0297	30.0279	35.5331	0.0575	1.1851	0.2681	0.2354	0.7998
ES5_8.6	0.0508	0.1492	0.0031	30.0667	35.3027	0.0586	1.2824	0.249	0.2292	0.755
ES5_8.7	0.0562	0.1721	0.0033	31.0877	35.7768	0.042	1.2411	0.2036	0.214	0.7257
ES5_8.8	0.0399	0.1572	0.0257	30.1229	35.3574	0.0502	1.2716	0.1795	0.2114	0.7279
ES5_8.9	0.085	0.3152	0.0375	29.5152	36.2199	0.0522	0.9419	0.3171	0.3535	1.2178
ES5_8.10	0.0492	0.2039	0.0011	29.4426	35.5401	0.0532	1.1864	0.2505	0.226	0.7948

Sample	Pr2O3	Nd2O3	Sm2O3	Gd2O3	MgO	CaO	MnO	FeO	ZnO	SrO
ES5_8.1	0.1414	0.396	0.054	0.0956	0.005	27.2487	0.1131	1.7791	0.0072	0.0192
ES5_8.2	0.091	0.3703	0.0947	0.0459	0.0033	27.2254	0.1165	1.8066	0.0035	0.0339
ES5_8.3	0.1661	0.5906	0.0867	0.0933	-0.0137	26.7835	0.1142	1.4349	0.0043	0.0332
ES5_8.4	0.1483	0.4724	0.1096	0.0743	0.0073	27.1294	0.1127	1.8546	0.0001	0.0071
ES5_8.5	0.1392	0.468	0.1171	0.0408	0.0047	26.9952	0.1097	1.8993	0.0078	0.0146
ES5_8.6	0.1274	0.465	0.0524	0.036	0.0041	27.2365	0.107	1.9238	0.0025	0.0103
ES5_8.7	0.107	0.3785	0.0802	0.0677	0.0166	26.8809	0.0993	1.8042	0.0059	0.0275
ES5_8.8	0.0931	0.3832	0.0735	0.0489	0.0186	27.2318	0.1137	2.0166	0.01	0.0231
ES5_8.9	0.1372	0.6532	0.0798	0.1168	0.0069	26.6296	0.1065	1.406	0.0152	-0.046
ES5_8.10	0.1174	0.4386	0.0781	0.0486	0.0031	27.1514	0.1214	2.0738	0.0011	0.0515

Sample	SnO	H2O	Na2O	K2O	F	Total	O=F	Total
ES5_8.1	0.0117	0.9871	0.0111	0.0007	0.322	99.6203	0.1356	99.4847
ES5_8.2	0.0014	1.0263	0.0146	0.001	0.2322	99.1984	0.0978	99.1007
ES5_8.3	0.0242	1.1282	0.0211	0.0018	0.016	99.2086	0.0067	99.2019
ES5_8.4	0.0161	1.0094	0.0127	0.0034	0.2637	99.2868	0.111	99.1758
ES5_8.5	0.0131	1.0516	0.0119	0.0002	0.1836	99.4378	0.0773	99.3605
ES5_8.6	0.0044	1.0008	0.0164	0.0008	0.2881	99.4045	0.1213	99.2831
ES5_8.7	0.0208	1.021	0.0364	0.0091	0.2807	100.3274	0.1182	100.2093
ES5_8.8	0.0111	1.0754	0.0208	0.0151	0.1376	99.3831	0.058	99.3251
ES5_8.9	0.002	1.1273	0.0225	0.0103	0.0165	99.37	0.0069	99.363
ES5_8.10	0.0042	0.9672	0.0181	0.0053	0.3432	99.1179	0.1445	98.9734

ESd1-15

Sample	P2O5	Nb2O5	Ta2O5	SiO2	TiO2	ZrO2	Al2O3	Fe2O3	Y2O3	La2O3
ESd1_15.1	0.0659	0.2605	0.0047	29.7979	35.8193	1.2425	0.956	1.8581	0.1628	0.3024
ESd1_15.2	0.0952	0.3038	0.0153	29.1446	35.4869	1.0347	0.9504	1.6975	0.1679	0.3307
ESd1_15.3	0.0671	0.1092	0.0073	29.6143	37.8442	0.0613	0.8041	1.084	0.0912	0.2538
ESd1_15.4	0.0726	0.1061	0.0098	29.6289	38.0574	0.0542	0.7697	1.0893	0.0787	0.2239

Sample	Ce2O3	Pr2O3	Nd2O3	Sm2O3	Gd2O3	MgO	CaO	MnO	ZnO	SrO
ESd1_15.1	0.8932	0.0885	0.3959	0.0614	0.0774	0.0025	26.9397	0.1292	0.0029	0.0225
ESd1_15.2	0.9238	0.1114	0.3704	0.0611	0.0518	0.0025	27.0509	0.1414	0.0005	0.0151
ESd1_15.3	0.5463	0.0486	0.2053	0.0457	0.0246	0.0049	27.7056	0.1059	0.0051	0.0076
ESd1_15.4	0.2649	1.157	0.2392	0.1755	0.0105	25.5171	0.1555	1.9206	0.0053	0.0631

Sample	SnO	H2O	Na2O	K2O	F	Total	O=F	Total
ESd1_15.1	0.0126	1.0046	0.0347	0.0072	0.2904	100.4029	0.1223	100.2806
ESd1_15.2	0.0073	0.9953	0.0334	0.0205	0.2792	99.2758	0.1176	99.1582
ESd1_15.3	0.0114	1.062	0.0138	0.0252	0.1817	99.9251	0.0765	99.8486
ESd1_15.4	0.0015	1.0543	0.0177	0.0133	0.2017	100.0769	0.085	99.992

ESd1-32

Sample	P2O5	Nb2O5	Ta2O5	SiO2	TiO2	ZrO2	Al2O3	Fe2O3	Y2O3	La2O3
ESd1_32.1	0.0755	0.1193	0.0245	30.0885	37.5421	0.0521	0.8217	1.1918	0.0823	0.1942
ESd1_32.2	0.0694	0.0986	0.0085	29.8395	37.9489	0.0477	0.8294	1.1584	0.0788	0.217
ESd1_32.3	0.0698	0.0754	0.0223	30.1243	35.609	0.3186	1.43	2.2142	0.0603	0.1288
ESd1_32.4	0.0623	0.0756	0.008	30.1203	36.0431	0.3466	1.3793	2.1702	0.0747	0.132
ESd1_32.5	0.2695	0.2828	0.0066	29.6925	36.3542	0.4051	1.0103	1.6911	0.0771	0.3092
ESd1_32.6	0.197	0.2636	0.0147	29.8726	36.3575	0.3979	0.9566	1.5245	0.0803	0.283

Sample	Ce2O3	Pr2O3	Nd2O3	Sm2O3	Gd2O3	MgO	CaO	MnO	ZnO	SrO
ESd1_32.1	0.5189	0.0593	0.1905	0.0193	0.0168	0.0085	27.675	0.1028	0.001	0.0042
ESd1_32.2	0.4973	0.0482	0.2022	0.0286	0.0429	0.0081	27.8491	0.1143	0.0046	0.0129
ESd1_32.3	0.3403	0.0505	0.1212	0.0221	0.0208	0.007	27.8639	0.1172	0.0078	0.0271
ESd1_32.4	0.3155	0.0231	0.1406	-0.0046	0.0091	0.0123	28.027	0.117	0.0044	0.0054
ESd1_32.5	0.6878	0.0855	0.2346	0.0436	0.0476	0.009	27.5448	0.1322	0.0019	0.0156
ESd1_32.6	0.6595	0.0692	0.2341	0.0148	0.0312	0.0145	27.5219	0.1133	0.004	0.0237

Sample	SnO	H2O	Na2O	K2O	F	Total	O=F	Total
ESd1_32.1	0.0007	1.0416	0.0202	0.0056	0.2324	100.0846	0.0979	99.9867
ESd1_32.2	0.0022	1.0552	0.0218	0.0078	0.2085	100.3873	0.0878	100.2995
ESd1_32.3	0.0001	1.0043	0.0158	0.0031	0.3029	99.9075	0.1275	99.7799
ESd1_32.4	0.0026	1.0457	0.0169	0.0028	0.2285	100.3533	0.0962	100.257
ESd1_32.5	0.0027	1.0679	0.0213	0.0036	0.1682	100.1491	0.0708	100.0783
ESd1_32.6	0.0053	1.0439	0.0223	0.0009	0.2145	99.8918	0.0903	99.8015

ESd1-36

Sample	P2O5	Nb2O5	Ta2O5	SiO2	TiO2	ZrO2	Al2O3	Fe2O3	Y2O3	La2O3
ESd1_36.1	0.0661	0.2558	0.0668	29.0266	33.4771	3.665	0.7984	2.0792	0.16	0.3426
ESd1_36.2	0.0707	0.2917	0.0864	29.0989	33.3234	3.8181	0.7838	2.061	0.1715	0.3531
ESd1_36.3	0.0615	0.2301	0.0639	29.1095	33.6582	3.4452	0.7923	1.9892	0.1406	0.3503
ESd1_36.4	0.0727	0.1437	0.0619	29.6321	37.4305	0.1554	0.8134	1.2956	0.1035	0.1889
ESd1_36.5	0.0836	0.118	0.0484	29.6826	37.0843	0.0767	0.7957	1.3969	0.0878	0.2018
ESd1_36.6	0.1175	0.1496	0.0286	29.5909	37.7454	0.0736	0.7967	1.2075	0.1053	0.2766
ESd1_36.7	0.1159	0.1334	0.0315	29.6458	37.3885	0.0714	0.8007	1.2297	0.1121	0.2825
ESd1_36.8	0.0704	0.1421	0.0398	30.2882	37.6869	0.1766	0.8172	1.1884	0.0769	0.151

Sample	Ce2O3	Pr2O3	Nd2O3	Sm2O3	Gd2O3	MgO	CaO	MnO	ZnO	SrO
ESd1_36.1	0.9502	0.1644	0.4236	0.0743	0.0495	0.0129	26.6219	0.1373	0.0022	0.0133
ESd1_36.2	0.999	0.1521	0.402	0.0501	0.0837	0.0079	26.476	0.1361	0.0016	0.0086
ESd1_36.3	0.9308	0.105	0.3962	0.0358	0.07	0.0085	26.5564	0.1243	0.0105	0.0171
ESd1_36.4	0.475	0.0239	0.2482	0.0313	0.0333	0.0068	27.4685	0.1054	0.0005	0.0106
ESd1_36.5	0.516	0.0693	0.2198	0.0411	0.0191	0.0089	27.5156	0.099	0.0085	0.0248
ESd1_36.6	0.6619	0.0617	0.235	0.0665	0.0299	0.0082	27.2794	0.0971	0.0002	0.0085
ESd1_36.7	0.6291	0.0455	0.2475	0.0308	0.0695	0.0048	27.3261	0.1087	0.0011	0.0134
ESd1_36.8	0.4031	0.0774	0.1653	0.031	0.0221	0.0037	27.929	0.1083	0.0126	0.0029

Sample	SnO	H2O	Na2O	K2O	F	Total	O=F	Total
ESd1_36.1	0.0111	1.0318	0.0445	0.002	0.1887	99.65	0.0795	99.5705
ESd1_36.2	0.0111	0.9999	0.0408	0.0022	0.2533	99.6812	0.1067	99.5746
ESd1_36.3	0.018	0.9926	0.0345	0.004	0.2677	99.3949	0.1127	99.2822
ESd1_36.4	0.0071	1.0705	0.0175	0.0001	0.1565	99.5347	0.0659	99.4688
ESd1_36.5	0.0065	1.0274	0.0236	0.0006	0.2398	99.3708	0.101	99.2698
ESd1_36.6	0.0073	1.0799	0.014	0.0321	0.1414	99.8061	0.0595	99.7466
ESd1_36.7	0.007	1.0778	0.0185	0.0264	0.1398	99.5431	0.0589	99.4843

ESd1_36.8	0.006	1.0637	0.0134	0.0024	0.2017	100.6734	0.0849	100.5885

RM1-7

Sample	P2O5	Nb2O5	Ta2O5	SiO2	TiO2	ZrO2	Al2O3	Fe2O3	Y2O3	La2O3
RM1_7.1	0.0504	0.3985	0.0052	28.903	36.3155	0.0568	1.0244	1.8023	0.2001	0.2177
RM1_7.2	0.0577	3.4838	0.1832	28.7336	33.1507	0.0639	1.1336	2.2973	0.1698	0.2549
RM1_7.3	0.0527	0.501	0.0299	29.0195	35.7502	0.062	1.0592	1.6956	0.214	0.2363
RM1_7.4	0.0382	0.3684	0.0166	28.7824	35.9384	0.0673	1.0897	1.6731	0.1981	0.1902
RM1_7.5	0.0353	3.6722	0.2247	28.3695	32.1517	0.0777	1.3518	2.9194	0.4147	0.1554
RM1_7.6	0.1066	0.389	0.0338	28.3488	35.4996	0.0696	1.0065	1.6953	0.3635	0.3545
RM1_7.7	0.0657	0.2296	0.0124	28.1265	34.4036	0.0757	1.3804	2.3517	0.8394	0.2573
RM1_7.8	0.1234	0.4628	0.0745	28.1481	34.1435	0.1	1.2227	2.1522	0.9435	0.3595
RM1_7.9	0.0925	0.4803	0.0355	28.4543	36.0369	0.0676	1.0761	1.4555	0.2973	0.4167
RM1_7.10	0.0356	2.0125	0.1729	29.0141	33.168	0.062	1.2532	2.5746	0.3193	0.1516

Sample	Ce2O3	Pr2O3	Nd2O3	Sm2O3	Gd2O3	MgO	CaO	MnO	ZnO	SrO
RM1_7.1	0.7375	0.0932	0.1955	0.0084	0.0151	0.0119	26.9913	0.2001	0.0067	0.0288
RM1_7.2	0.6925	0.0684	0.1451	0.0247	0.0009	0.0167	26.7649	0.2836	0.0031	0.1271
RM1_7.3	0.7563	0.068	0.2656	0.0305	0.0374	0.0082	27.0198	0.2092	0.006	0.007
RM1_7.4	0.6453	0.0877	0.2001	0.0321	0.0114	0.0085	27.0891	0.2005	0.0019	0.0253
RM1_7.5	0.6881	0.1181	0.2235	0.0359	0.0533	0.0213	26.3394	0.3797	0.0012	0.1113
RM1_7.6	1.2376	0.1805	0.4741	0.0453	0.0486	0.0112	26.3131	0.1904	0.0037	0.0225
RM1_7.7	1.3065	0.2139	1.1006	0.2436	0.2995	0.0104	25.4376	0.1799	0.007	0.0467
RM1_7.8	1.7222	0.2978	1.3828	0.2924	0.275	0.0154	24.8642	0.1777	0.0097	0.0914
RM1_7.9	1.4262	0.1393	0.5274	0.0401	0.0975	0.0126	26.24	0.1929	0.0041	0.0189
RM1_7.10	0.5606	0.0177	0.1633	0.046	0.0612	0.0195	26.4675	0.3401	0.0008	0.0746

Sample	SnO	H2O	Na2O	K2O	F	Total	O=F	Total
RM1_7.1	0.0388	0.9648	0.0294	-0.0044	0.3386	98.6271	0.1426	98.4845
RM1_7.2	0.0691	1.0433	0.0877	-0.0028	0.163	98.8883	0.0686	98.8197
RM1_7.3	0.0357	0.9817	0.0298	-0.0002	0.2969	98.3656	0.125	98.2406
RM1_7.4	0.0248	0.9306	0.0215	-0.0004	0.3952	98.0091	0.1664	97.8427
RM1_7.5	0.1029	0.978	0.0915	0.0021	0.2809	98.6869	0.1183	98.5686
RM1_7.6	0.0299	1.0629	0.0346	-0.0019	0.0993	97.6171	0.0418	97.5753
RM1_7.7	0.0122	1.034	0.0155	0.0001	0.1429	97.7389	0.0602	97.6788
RM1_7.8	0.0292	1.1002	0.0233	-0.0024	-0.0136	97.9103	0	97.9103
RM1_7.9	0.0392	1.063	0.0139	-0.0007	0.1143	98.323	0.0481	98.2749
RM1_7.10	0.0607	0.9717	0.0715	0.0012	0.2963	97.841	0.1248	97.7162

RM1-3

Sample	P2O5	Nb2O5	Ta2O5	SiO2	TiO2	ZrO2	Al2O3	Fe2O3	Y2O3	La2O3
RM1-3.1	0.0465	0.2249	0.0102	28.9006	35.1401	0.0913	1.2762	2.0822	0.429	0.2941
RM1-3.2	0.0591	0.2201	0.0047	29.047	35.7241	0.0779	1.2472	2.0768	0.4757	0.2756
RM1-3.3	0.0612	0.1949	0.0373	28.8065	34.1956	0.0821	1.4548	2.4816	0.8549	0.2612
RM1-3.4	0.1253	0.5446	0.0532	28.4458	34.1916	0.0991	1.2266	2.1493	0.9052	0.3649
RM1-3.5	0.0803	0.4196	0.0539	28.6582	34.6914	0.1028	1.1848	2.1405	0.9359	0.2718
RM1-3.6	0.091	0.4393	0.0633	28.7394	34.2205	0.1268	1.2379	2.255	1.0641	0.2684
RM1-3.7	0.0631	0.1868	0.0401	28.7564	34.0527	0.0874	1.5053	2.7299	0.9745	0.2613
RM1-3.8	0.1223	0.408	0.0582	28.5947	33.7663	0.0767	1.3125	2.3793	1.0745	0.3671

Sample	Ce2O3	Pr2O3	Nd2O3	Sm2O3	Gd2O3	MgO	CaO	MnO	ZnO	SrO
RM1-3.1	1.0977	0.1573	0.5702	0.1001	0.1084	0.0111	26.5324	0.1905	0.0046	0.0253
RM1-3.2	1.1794	0.1625	0.658	0.1039	0.0885	0.0114	26.5889	0.1826	0.0036	0.0526
RM1-3.3	1.2523	0.2336	1.1191	0.2441	0.2534	0.0166	25.7678	0.1915	0.0017	0.0643
RM1-3.4	1.7053	0.2858	1.3562	0.2623	0.2828	0.0157	25.1829	0.1822	0.0163	0.0623
RM1-3.5	1.4201	0.2917	1.2354	0.3245	0.3178	0.0124	25.2981	0.198	0.0036	0.0694
RM1-3.6	1.4711	0.2756	1.4306	0.3991	0.391	0.0156	24.995	0.1816	0.0075	0.0386
RM1-3.7	1.3596	0.2764	1.2692	0.3641	0.358	0.0231	25.3405	0.1771	0.0029	0.0439
RM1-3.8	1.7577	0.3637	1.6728	0.425	0.4056	0.0143	24.5769	0.1809	0.0224	0.0679

Sample	SnO	H2O	Na2O	K2O	F	Total	O=F	Total

RM1-3.1	0.0207	0.9912	0.0192	0.028	0.2694	98.5914	0.1134	98.4779
RM1-3.2	0.0076	0.9902	0.0116	0.0033	0.2912	99.4873	0.1226	99.3647
RM1-3.3	0.0273	1.01	-0.004	0.0001	0.2182	98.7659	0.0919	98.674
RM1-3.4	0.0408	1.1083	0.0315	0.0063	0.0351	98.5656	0	98.5656
RM1-3.5	0.0306	1.1037	0.0091	0.0048	0.0215	98.8022	0.009	98.7932
RM1-3.6	0.0335	1.0718	0.0191	0	0.0828	98.8727	0.0349	98.8378
RM1-3.7	0.0155	1.0114	0.0079	0.0019	0.2148	99.08	0.0905	98.9895
RM1-3.8	0.0235	1.1063	0.0232	0.0042	0.0261	98.7096	0	98.7096

ROM1-21

Sample	P2O5	Nb2O5	Ta2O5	SiO2	TiO2	ZrO2	Al2O3	Fe2O3	Y2O3	La2O3
ROM1_21.1	0.0631	0.2774	0.0426	28.5727	35.3304	0.1035	1.0174	5.945	0.276	0.4373
ROM1_21.2	0.0782	0.271	0.0073	29.9656	35.9905	0.1077	1.1081	1.6961	0.3246	0.4043
ROM1_21.3	0.047	0.3359	0.0503	30.0573	36.2275	0.1456	1.0311	1.882	0.1286	0.2523
ROM1_21.4	0.0649	0.2691	0.015	30.2309	36.7198	0.0947	0.9559	1.6675	0.1177	0.3635
ROM1_21.5	0.0409	0.8908	0.0401	29.1175	32.7264	0.0537	1.6663	3.1417	2.0549	0.102
ROM1_21.6	0.0391	0.897	0.0717	29.1127	32.4822	0.0691	1.6494	3.013	2.0656	0.1124
ROM1_21.7	0.0718	0.3526	0.0603	29.6175	35.2516	0.0642	1.1539	1.8861	0.7749	0.3053
ROM1_21.8	0.05	0.5187	0.0562	29.4851	35.2452	0.0675	1.1186	2.0259	0.6323	0.2576

Sample	Ce2O3	Pr2O3	Nd2O3	Sm2O3	Gd2O3	MgO	CaO	MnO	ZnO	SrO
ROM1_21.1	1.3913	0.2079	0.6826	0.1176	0.0839	0.0064	24.3187	0.1121	0.0009	0.0326
ROM1_21.2	1.5506	0.2265	0.8079	0.1061	0.1056	0.0062	26.2829	0.1186	0.0107	0.0317
ROM1_21.3	0.6264	0.0873	0.1597	0.0194	0.0231	0.0116	27.376	0.1441	0.0042	0.0363
ROM1_21.4	0.8138	0.0794	0.2002	0.0039	-0.0098	0.0176	27.143	0.1236	0.0095	0.0254
ROM1_21.5	0.7413	0.189	0.8702	0.402	0.5396	0.0535	24.3086	0.6795	0.0091	0.1262
ROM1_21.6	0.751	0.1525	0.8082	0.4183	0.5448	0.0462	24.339	0.6682	0.0053	0.1183
ROM1_21.7	1.3824	0.2203	1.0387	0.2331	0.1974	0.0133	25.7317	0.224	0.0133	0.0399
ROM1_21.8	1.0992	0.1474	0.7113	0.1197	0.1248	0.0216	26.0527	0.256	0.0048	0.0557

Sample	SnO	H2O	Na2O	K2O	F	Total	O=F	Total
ROM1_21.1	0.0132	1.0183	0.0163	0.0662	0.2364	100.3362	0.0995	100.2367
ROM1_21.2	0.0098	1.0063	0.0137	0.0732	0.284	100.5449	0.1196	100.4254
ROM1_21.3	0.014	0.9746	0.0149	0.027	0.359	100.0352	0.1512	99.8841
ROM1_21.4	0.0078	1.0193	0.0151	0.053	0.2749	100.2601	0.1158	100.1443
ROM1_21.5	0.0999	0.963	0.0642	0.0009	0.3134	99.0582	0.132	98.9262
ROM1_21.6	0.1071	0.9639	0.0618	0.0057	0.3034	98.6823	0.1277	98.5545
ROM1_21.7	0.0257	1.0383	0.0201	0.0162	0.1942	99.8734	0.0818	99.7917
ROM1_21.8	0.0357	0.9961	0.027	0.0326	0.2772	99.3582	0.1167	99.2415

ROM1-31

Sample	P2O5	Nb2O5	Ta2O5	SiO2	TiO2	ZrO2	Al2O3	Fe2O3	Y2O3	La2O3
ROM1_31.1	0.047	0.0455	0.0136	29.8513	37.0361	0.0613	1.1841	1.4571	0.053	0.2783
ROM1_31.2	0.044	0.0563	-0.0115	30.3553	36.8576	0.0585	1.1975	1.4273	0.0552	0.2423
ROM1_31.3	0.0562	0.0268	0.0206	30.4096	37.72	0.0579	1.0452	1.6053	0.0337	0.2176
ROM1_31.4	0.0624	0.032	0.0056	30.4755	37.3665	0.0611	1.0228	1.7221	0.0249	0.2164
ROM1_31.5	0.1914	0.1515	0.0125	29.9357	36.8678	0.0822	0.98	1.6275	0.0937	0.5332
ROM1_31.6	0.1908	0.1571	0.0134	29.7885	36.5575	0.0772	0.9709	1.6136	0.1055	0.5247
ROM1_31.7	0.1717	0.3227	0.0046	29.6232	36.4681	0.135	0.9409	1.5511	0.1199	0.5974
ROM1_31.8	0.1776	0.3529	0.0119	29.8953	36.3582	0.1511	0.9661	1.6108	0.1182	0.5872
ROM1_31.9	0.0802	0.1989	0.0042	29.9222	36.4574	0.0808	1.0943	1.6432	0.1696	0.402
ROM1_31.10	0.0816	0.1985	0.0109	29.8543	36.5568	0.0785	1.1216	1.6754	0.1712	0.4021
ROM1_31.11	0.0499	0.0897	0.0014	30.1849	37.7107	0.05	0.9448	1.0042	0.0824	0.2034
ROM1_31.12	0.0527	0.0941	0.0233	30.2047	37.6998	0.0308	0.9701	1.009	0.0938	0.2327
ROM1_31.13	0.0404	0.0773	0.0042	30.2123	37.1851	0.0339	0.88	0.9542	0.0789	0.1698
ROM1_31.14	0.0497	0.0653	0.0055	30.1209	37.8731	0.0328	0.868	0.9497	0.072	0.1772
ROM1_31.15	0.0809	0.1776	0.0042	29.3221	34.6457	0.6595	1.1561	2.3537	0.2355	0.3789
ROM1_31.16	0.0881	0.2039	0.0011	29.4317	34.9816	0.6238	1.1498	2.3013	0.2033	0.4426
ROM1_31.17	0.1424	0.4266	0.042	29.0375	34.3594	0.1186	1.1395	2.0226	0.4159	0.6349
ROM1_31.18	0.1227	0.3555	0.0142	29.011	34.7065	0.1019	1.2098	1.6912	0.3222	0.6853
ROM1_31.19	0.0142	0.151	0.0048	29.9259	36.3338	0.1442	1.1553	0.9618	0.2126	0.2029
ROM1_31.20	0.082	0.1878	0.0181	29.704	37.0974	0.1143	0.8459	1.2331	0.1497	0.3521

Sample	Ce2O3	Pr2O3	Nd2O3	Sm2O3	Gd2O3	MgO	CaO	MnO	ZnO	SrO
ROM1_31.1	0.5577	0.0719	0.1023	0.0139	0.002	0.0021	27.9062	0.1038	0.0002	0.0163
ROM1_31.2	0.5457	0.0227	0.1209	0.0052	-0.0151	0.0093	27.9696	0.1065	0.0061	0.0099
ROM1_31.3	0.375	0.0166	0.0624	-0.0015	0.0145	0.0052	28.0514	0.1211	0.008	0.0442
ROM1_31.4	0.3588	0.0232	0.0709	0.0217	0.0131	0.0119	28.0175	0.1279	-0.013	0.0023
ROM1_31.5	1.3363	0.1647	0.3889	0.042	0.0122	0.0072	26.9761	0.1128	0.0087	0.0328
ROM1_31.6	1.351	0.1124	0.4105	0.0471	0.0235	0.0186	27.0293	0.1255	0.0001	0.0192
ROM1_31.7	1.49	0.1584	0.4614	0.0588	0.0322	0.018	26.7299	0.1119	0.011	0.0122
ROM1_31.8	1.5096	0.1437	0.4488	0.0581	0.0451	0.0079	26.8654	0.1324	0.0005	0.0247
ROM1_31.9	1.1694	0.0881	0.4872	0.0846	0.0575	0.0126	27.137	0.1077	0.0008	0.0167
ROM1_31.10	1.1561	0.1297	0.4845	0.0661	0.027	0.0186	27.0078	0.1155	0.0027	0.0253
ROM1_31.11	0.593	0.0677	0.2606	0.0274	0.0223	0.0031	27.8938	0.0774	0.0056	0.0102
ROM1_31.12	0.5828	0.0848	0.2661	0.0554	0.0038	0.0009	27.991	0.0735	0.0106	0.0154
ROM1_31.13	0.4929	0.1004	0.1879	0.026	0.0349	0.0073	27.639	0.0746	0.0036	0.001
ROM1_31.14	0.4534	0.0395	0.1624	0.0303	0.0344	0.0083	27.8261	0.0792	0.0131	0.0109
ROM1_31.15	1.4309	0.1705	0.6947	0.1124	0.0472	0.0111	26.1828	0.096	0.0018	0.0513
ROM1_31.16	1.3666	0.174	0.6613	0.0825	0.0856	0.0077	26.2609	0.1136	0.0058	0.0262
ROM1_31.17	2.2305	0.3292	1.2708	0.2061	0.1439	0.0134	25.0417	0.0835	0.0013	0.0605
ROM1_31.18	2.3399	0.3391	1.1972	0.1903	0.1431	0.0095	25.34	0.0967	0.0131	0.0368
ROM1_31.19	1.1427	0.165	0.603	0.1098	0.0439	0.0108	27.1166	0.0833	0.0153	0.0388
ROM1_31.20	1.0284	0.1138	0.4932	0.0325	0.0283	0.0048	27.0973	0.1051	0.0123	0.0204

Sample	SnO	H2O	Na2O	K2O	F	Total	O=F	Total
ROM1_31.1	0.0035	0.9566	0.0092	-0.0018	0.4039	100.1603	0.1701	99.9902
ROM1_31.2	0.0015	0.9853	0.0164	-0.0035	0.3569	100.4387	0.1503	100.2885
ROM1_31.3	0.005	1.025	0.0223	0.0003	0.2962	101.2351	0.1247	101.1104
ROM1_31.4	0.0063	1.0601	0.0127	0.0008	0.2184	100.9348	0.092	100.8429
ROM1_31.5	0.0069	1.0204	0.0185	-0.0021	0.2734	100.8311	0.1151	100.716
ROM1_31.6	0.0014	1.04	0.0218	-0.001	0.2219	100.3888	0.0934	100.2953
ROM1_31.7	0.0163	1.0662	0.0214	-0.0038	0.1599	100.2699	0.0673	100.2026
ROM1_31.8	0.0039	1.0323	0.012	0.0002	0.2402	100.7292	0.1011	100.628
ROM1_31.9	0.0052	1.0181	0.0109	0.0007	0.2704	100.503	0.1139	100.3892
ROM1_31.10	0.0065	1.0126	0.0145	-0.0021	0.2811	100.46	0.1183	100.3417
ROM1_31.11	0.0046	1.0119	0.0152	0.0012	0.3038	100.6091	0.1279	100.4811
ROM1_31.12	0.0085	1.0686	0.0101	0.002	0.1906	100.7576	0.0803	100.6773
ROM1_31.13	0.0018	1.0412	0.0132	0.0056	0.2226	99.4773	0.0937	99.3835
ROM1_31.14	0.01	1.0682	0.0209	0.0053	0.1827	100.1428	0.0769	100.0658
ROM1_31.15	0.0247	0.9796	0.0257	0.0024	0.3	99.0923	0.1263	98.966
ROM1_31.16	0.0305	1.0659	0.0233	0.0004	0.1339	99.438	0.0564	99.3817
ROM1_31.17	0.0091	1.0439	0.0121	0.0019	0.1436	98.8671	0.0605	98.8066
ROM1_31.18	0.0097	1.0722	0.0221	0.0002	0.0914	99.0847	0.0385	99.0462
ROM1_31.19	0.017	1.0697	0.0024	0	0.1483	99.6163	0.0624	99.5539
ROM1_31.20	0.0202	1.0525	0.0134	0.0023	0.1911	99.9673	0.0805	99.8869

ROM1-40

Sample	P2O5	Nb2O5	Ta2O5	SiO2	TiO2	ZrO2	Al2O3	Fe2O3	Y2O3	La2O3
ROM1_40.1	0.0864	0.2073	0.0335	29.6576	36.0622	0.0749	1.1283	1.7052	0.1773	0.3978
ROM1_40.2	0.0811	0.2092	0.025	29.6071	35.9299	0.073	1.1216	1.6429	0.1599	0.3735
ROM1_40.3	0.0779	0.2646	0.0194	29.1175	34.6155	0.2818	1.2724	2.2273	0.4069	0.4425
ROM1_40.4	0.0457	0.3778	0.0223	29.8841	35.5663	0.0813	1.2794	2.0896	0.4614	0.2395
ROM1_40.5	0.0717	0.7257	0.0279	29.7397	35.7931	0.0532	1.1258	2.0059	0.606	0.2158
ROM1_40.6	0.0567	0.6501	0.0564	29.6206	35.5102	0.0735	1.1185	2.0261	0.623	0.2353
ROM1_40.7	0.044	0.4452	0.0462	29.4256	34.9395	0.0668	1.2991	2.271	0.5824	0.2387
ROM1_40.8	0.0378	0.457	0.0405	29.6175	34.9663	0.0578	1.3008	2.1839	0.6148	0.257
ROM1_40.9	0.0895	0.5858	0.0162	29.9334	35.0545	0.0983	1.357	2.1304	0.4653	0.398
ROM1_40.10	0.0848	0.5889	0.0219	29.7981	35.1885	0.0766	1.1321	2.054	0.5594	0.372
ROM1_40.11	0.0628	0.0864	0.0222	30.3311	37.2584	0.0032	1.3477	1.0173	0.0059	0.0105
ROM1_40.12	0.0388	0.1504	0.005	30.109	37.4821	0.0112	1.1863	0.8516	0.1312	-0.0145
ROM1_40.13	0.0423	0.3301	0.0166	29.8578	35.3822	0.0696	1.3182	2.4168	0.4357	0.2296
ROM1_40.14	0.0506	0.3237	0.0152	29.621	35.0993	0.0726	1.3809	2.4725	0.4601	0.2187
ROM1_40.15	0.0652	0.2974	0.0079	29.5072	34.5592	0.3125	1.2314	2.1986	0.4257	0.4949
ROM1_40.16	0.0789	0.2535	0.0455	29.6305	34.7653	0.2502	1.2888	2.2381	0.4136	0.4289
ROM1_40.17	0.0568	0.3561	0.0385	29.7909	36.2529	0.1218	0.9789	1.7658	0.258	0.5037
ROM1_40.18	0.1043	0.2996	0.0209	29.5238	36.0706	0.1863	0.9422	1.6552	0.1858	0.4856
ROM1_40.19	0.0428	0.2824	0.0327	29.9549	35.9461	0.2344	1.0523	1.8574	0.1326	0.4388

| ROM1_40.20 | 0.0853 | 0.853 | 0.0622 | 29.5922 | 34.8926 | 0.0728 | 1.1962 | 2.0708 | 0.6404 | 0.348 |

Sample	Ce2O3	Pr2O3	Nd2O3	Sm2O3	Gd2O3	MgO	CaO	MnO	ZnO	SrO
ROM1_40.1	1.2032	0.17	0.4988	0.0538	0.0429	0.0136	26.8945	0.1217	0.0072	0.0304
ROM1_40.2	1.218	0.1363	0.4639	0.0757	0.0354	0.011	26.8419	0.1158	0.0088	0.0071
ROM1_40.3	1.7002	0.2031	1.0442	0.1523	0.1499	0.0061	25.9239	0.0926	0.0054	0.0506
ROM1_40.4	0.9547	0.1478	0.5285	0.1219	0.0832	0.0181	26.6528	0.2384	0.0042	0.0726
ROM1_40.5	1.0402	0.1607	0.6025	0.1406	0.1502	0.0149	26.437	0.3152	0.0034	0.0521
ROM1_40.6	1.0805	0.173	0.6727	0.1098	0.1512	0.015	26.3534	0.2987	0.0034	0.0535
ROM1_40.7	1.0519	0.1633	0.6721	0.1233	0.1389	0.0146	26.3403	0.2442	0.001	0.0302
ROM1_40.8	1.0518	0.1779	0.6556	0.1134	0.1397	0.0196	26.434	0.2031	0.0013	0.0602
ROM1_40.9	1.4294	0.1973	0.6129	0.0942	0.0824	0.0198	26.2259	0.313	0.0081	0.0313
ROM1_40.10	1.3907	0.1923	0.6579	0.1085	0.0779	0.0138	26.2549	0.3095	0.007	0.0543
ROM1_40.11	0.0338	0.0156	-0.0325	0.0083	0.0065	0.0057	28.4296	0.0557	0.0133	0.002
ROM1_40.12	0.0601	0.0023	0.0577	0.0434	0.0407	0.0022	28.3749	0.0548	0.0023	0.0078
ROM1_40.13	0.9303	0.1525	0.4612	0.0734	0.0954	0.0237	26.7161	0.3075	0.0006	0.0423
ROM1_40.14	0.869	0.1124	0.4455	0.0744	0.0781	0.0198	26.7577	0.3156	0.0106	0.0366
ROM1_40.15	1.7656	0.2594	1.1015	0.1893	0.1491	0.017	25.8564	0.092	0.0091	0.0415
ROM1_40.16	1.5985	0.2275	1.0706	0.2044	0.1241	0.0154	25.9742	0.0934	0.0175	0.0298
ROM1_40.17	1.6876	0.1945	0.713	0.1051	0.0916	0.0109	26.3623	0.1071	0.0081	0.0382
ROM1_40.18	1.4603	0.1571	0.5725	0.0768	0.054	0.0107	26.6421	0.099	0.0017	0.024
ROM1_40.19	1.1173	0.1238	0.3104	0.0482	0.0484	0.0172	27.072	0.1025	0.0084	0.0192
ROM1_31.20	1.366	0.208	0.7185	0.1078	0.1339	0.0145	25.8606	0.3162	0.0062	0.061

Sample	SnO	H2O	Na2O	K2O	F	Total	O=F	Total
ROM1_40.1	0.0103	0.9944	0.005	0.0275	0.3012	99.8745	0.1268	99.7477
ROM1_40.2	0.0006	1.0324	0.0063	0.0347	0.215	99.419	0.0905	99.3285
ROM1_40.3	0.0106	0.983	0.0042	0.0058	0.2871	99.294	0.1209	99.1731
ROM1_40.4	0.0224	0.9486	0.018	0.0036	0.4018	100.1834	0.1692	100.0142
ROM1_40.5	0.0434	1.0243	0.0297	0.0003	0.2494	100.5766	0.105	100.4716
ROM1_40.6	0.0449	1.0317	0.0299	0.0012	0.2222	100.1532	0.0936	100.0597
ROM1_40.7	0.0365	0.9575	0.0252	0.0025	0.3583	99.4853	0.1509	99.3344
ROM1_40.8	0.0305	0.9555	0.0196	0.0019	0.3688	99.7044	0.1553	99.549
ROM1_40.9	0.0445	1.0295	0.031	0.0009	0.2339	100.4429	0.0985	100.3445
ROM1_40.10	0.0452	1.0487	0.0309	0.0015	0.1866	100.1945	0.0786	100.1159
ROM1_40.11	0.0009	0.9744	0.0102	0.0013	0.3841	100.0512	0.1617	99.8895
ROM1_40.12	0.0062	1.0199	0.0048	0.0004	0.2835	99.9161	0.1194	99.7967
ROM1_40.13	0.0281	0.9023	0.0194	0.0005	0.4984	100.3077	0.2099	100.0978
ROM1_40.14	0.0424	0.8889	0.0246	0.0011	0.5147	99.8587	0.2167	99.6419
ROM1_40.15	0.0169	0.9889	0.0079	0.0022	0.2865	99.8418	0.1206	99.7212
ROM1_40.16	0.0077	0.9975	0.0043	0.0109	0.2782	99.9999	0.1172	99.8827
ROM1_40.17	0.0054	1.0505	0.0135	0.0062	0.1935	100.6727	0.0815	100.5912
ROM1_40.18	0.0247	1.0433	0.0127	0.062	0.194	99.8834	0.0817	99.8017
ROM1_40.19	0.0105	0.9637	0.0211	0.0286	0.3741	100.2204	0.1575	100.0629
ROM1_40.20	0.0494	0.993	0.0284	-0.0023	0.2899	99.8996	0.1221	99.7775

B

B.1 Fish Canyon Tuff and Pagosa Peak Dacite EMPA data (cpfu)

The data is presented as atoms per formula unit (most as cations, plus anions per formula unit for OH and F). The unit cell for titanite in this case is based on having 24 cations, 38 oxygen anions, plus an additional 2 anions of water/volatiles (OH, F).

BFC-124-1

Sample	Si	Ti	Ca	Al	Fe	La	Ce	Pr	Nd	Sm	Gd	ΣREE
BFC124_1.2	7.753	7.098	7.571	0.41	0.399	0.033	0.11	0.014	0.058	0.011	0.011	0.201
BFC124_1.1	7.758	7.121	7.516	0.402	0.386	0.036	0.11	0.017	0.051	0.007	0.009	0.194

Sample	Y	Zr	Nb	Ta	Mg	P	Mn	OH	Na	K	F	Total
BFC124_1.2	0.061	0.013	0.03	0	0.008	0.013	0.047	1.76	0.006	0.002	0.24	25.645
BFC124_1.1	0.054	0.012	0.032	0.002	0.008	0.013	0.044	1.835	0.01	0.003	0.165	25.592

BFC-124-7

Sample	Si	Ti	Ca	Al	Fe	La	Ce	Pr	Nd	Sm	Gd	ΣREE
BFC124_7.1	7.739	6.917	7.081	0.426	0.559	0.037	0.17	0.028	0.135	0.032	0.036	0.396
BFC124_7.2	7.772	6.86	7.276	0.471	0.571	0.032	0.14	0.025	0.104	0.025	0.025	0.319
BFC124_7.3	7.792	7.052	7.366	0.425	0.441	0.04	0.14	0.019	0.059	0.012	0.011	0.236
BFC124_7.4	7.764	7.03	7.546	0.451	0.437	0.038	0.12	0.018	0.058	0.01	0.009	0.218
BFC124_7.5	7.762	7.083	7.497	0.421	0.414	0.036	0.12	0.014	0.061	0.009	0.012	0.22
BFC124_7.6	7.782	6.876	7.241	0.465	0.551	0.029	0.14	0.026	0.11	0.025	0.029	0.331

Sample	Y	Zr	Nb	Ta	Mg	P	Mn	OH	Na	K	F	Total
BFC124_7.1	0.171	0.016	0.047	0.002	0.015	0.018	0.068	1.856	0.016	0.006	0.144	25.517
BFC124_7.2	0.156	0.013	0.034	0.002	0.017	0.01	0.075	1.778	0.012	0	0.222	25.626
BFC124_7.3	0.064	0.015	0.036	0.001	0.011	0.014	0.065	1.784	0.011	0	0.216	25.573
BFC124_7.4	0.059	0.013	0.031	0	0.01	0.012	0.057	1.71	0.007	0	0.29	25.675
BFC124_7.5	0.06	0.012	0.033	0.003	0.01	0.014	0.05	1.743	0.005	0.001	0.257	25.623
BFC124_7.6	0.173	0.011	0.035	0.003	0.02	0.01	0.073	1.741	0.015	0	0.259	25.621

BFC-124-5

Sample	Si	Ti	Ca	Al	Fe	La	Ce	Pr	Nd	Sm	Gd	ΣREE
BFC124_5.1	7.797	7.093	7.471	0.412	0.387	0.033	0.11	0.011	0.057	0.011	0.01	0.2
BFC124_5.2	7.815	7.022	7.481	0.446	0.45	0.039	0.12	0.014	0.053	0.007	0.009	0.202
BFC124_5.3	7.732	6.948	7.314	0.425	0.451	0.049	0.18	0.025	0.1	0.018	0.018	0.345
BFC124_5.4	7.599	7.088	7.435	0.444	0.471	0.036	0.15	0.017	0.083	0.017	0.012	0.277
BFC124_5.5	7.804	7.068	7.444	0.383	0.373	0.039	0.13	0.018	0.062	0.011	0.009	0.229

Sample	Y	Zr	Nb	Ta	Mg	P	Mn	OH	Na	K	F	Total
BFC124_5.1	0.064	0.011	0.03	0	0.01	0.013	0.045	1.822	0.008	0.005	0.178	25.581
BFC124_5.2	0.053	0.012	0.029	0	0.011	0.014	0.052	1.709	0.013	0	0.291	25.642
BFC124_5.3	0.105	0.011	0.059	0.004	0.014	0.017	0.078	1.872	0.02	0	0.128	25.575
BFC124_5.4	0.104	0.015	0.039	0.002	0.013	0.016	0.069	1.864	0.004	0	0.136	25.616
BFC124_5.5	0.058	0.013	0.041	0.002	0.01	0.017	0.051	1.884	0.01	0.002	0.116	25.547

BFC-104b-5

Sample	Si	Ti	Ca	Al	Fe	La	Ce	Pr	Nd	Sm	Gd	ΣREE
BFC104_5.1	7.816	7.100	7.467	0.379	0.369	0.034	0.112	0.016	0.060	0.010	0.011	0.209
BFC104_5.2	7.779	7.008	7.387	0.424	0.473	0.042	0.149	0.019	0.076	0.013	0.010	0.266
BFC104_5.3	7.745	7.003	7.407	0.421	0.486	0.043	0.152	0.021	0.075	0.013	0.011	0.272
BFC104_5.4	7.795	7.110	7.495	0.361	0.394	0.036	0.110	0.017	0.056	0.010	0.009	0.202
BFC104_5.5	7.760	6.997	7.319	0.383	0.431	0.052	0.183	0.024	0.092	0.014	0.012	0.325

Sample	Y	Zr	Nb	Ta	Mg	P	Mn	OH	Na	K	F	Total
BFC104_5.1	0.061	0.014	0.033	0.003	0.008	0.017	0.045	1.826	0.008	0.003	0.174	25.562
BFC104_5.2	0.079	0.012	0.039	0.002	0.011	0.010	0.069	1.808	0.011	0.010	0.192	25.618
BFC104_5.3	0.079	0.012	0.039	0.001	0.011	0.014	0.067	1.794	0.003	0.000	0.206	25.603
BFC104_5.4	0.056	0.016	0.035	0.001	0.008	0.018	0.047	1.729	0.006	0.000	0.271	25.580
BFC104_5.5	0.087	0.013	0.052	0.004	0.013	0.018	0.057	1.812	0.010	0.000	0.188	25.521

BFC-129-10

Sample	Si	Ti	Ca	Al	Fe	La	Ce	Pr	Nd	Sm	Gd	ΣREE
BFC_129_10.1	7.788	6.898	7.425	0.431	0.506	0.037	0.145	0.022	0.091	0.016	0.017	0.290
BFC_129_10.2	7.730	7.229	7.717	0.347	0.337	0.028	0.068	0.007	0.021	0.002	0.002	0.100
BFC_129_10.3	7.796	7.156	7.613	0.339	0.312	0.030	0.099	0.013	0.042	0.004	0.003	0.160
BFC_129_10.4	7.833	6.950	7.601	0.462	0.453	0.028	0.103	0.016	0.066	0.012	0.011	0.209
BFC_129_10.5	7.890	6.968	7.550	0.440	0.422	0.027	0.102	0.015	0.056	0.010	0.010	0.193
BFC_129_10.6	7.805	7.023	7.569	0.427	0.413	0.035	0.116	0.016	0.061	0.010	0.012	0.214

Sample	Y	Zr	Nb	Ta	P	Mg	Mn	OH	Na	K	F	Total
BFC_129_10.1	0.112	0.013	0.043	0.002	0.013	0.012	0.074	1.764	0.011	0	0.236	25.649
BFC_129_10.2	0.016	0.017	0.045	0.002	0.011	0.000	0.058	1.739	0.007	0	0.261	25.644
BFC_129_10.3	0.033	0.018	0.051	0.003	0.015	0.006	0.052	1.878	0.011	0	0.122	25.593
BFC_129_10.4	0.060	0.017	0.022	0.001	0.012	0.008	0.047	1.693	0.001	0	0.307	25.703
BFC_129_10.5	0.058	0.016	0.019	0.002	0.014	0.006	0.049	1.662	0	0	0.338	25.654
BFC_129_10.6	0.060	0.013	0.029	0.003	0.012	0.007	0.047	1.672	0.002	0	0.328	25.656

BFC-55-18

Sample	Si	Ti	Ca	Al	Fe	La	Ce	Pr	Nd	Sm	Gd	ΣREE
BFC55_18.1	7.696	7.012	7.479	0.437	0.488	0.042	0.15	0.019	0.075	0.01	0.013	0.263
BFC55_18.2	7.716	7.027	7.389	0.398	0.44	0.043	0.16	0.023	0.087	0.012	0.015	0.3
BFC55_18.3	7.708	6.982	7.279	0.399	0.471	0.054	0.19	0.027	0.098	0.015	0.014	0.342
BFC55_18.4	7.725	6.994	7.476	0.433	0.465	0.043	0.15	0.022	0.072	0.01	0.009	0.266
BFC55_18.5	7.701	7.058	7.428	0.427	0.482	0.043	0.15	0.018	0.071	0.009	0.011	0.258
BFC55_18.6	7.693	7.047	7.523	0.427	0.453	0.04	0.14	0.017	0.068	0.006	0.01	0.242
BFC55_18.7	7.764	7.107	7.456	0.41	0.409	0.036	0.12	0.014	0.065	0.012	0.01	0.222

Sample	Y	Zr	P	Nb	Ta	Mg	Mn	OH	Na	K	F	Total
BFC55_18.1	0.096	0.013	0.01	0.043	0.001	0.013	0.074	1.717	0.014	0	0.283	25.683
BFC55_18.2	0.097	0.012	0.016	0.051	0.002	0.007	0.071	1.836	0.017	0	0.164	25.592
BFC55_18.3	0.105	0.014	0.019	0.061	0.003	0.011	0.073	1.904	0.02	0	0.096	25.545
BFC55_18.4	0.075	0.01	0.013	0.04	0.002	0.01	0.062	1.852	0.011	0.001	0.148	25.628
BFC55_18.5	0.073	0.013	0.013	0.041	0.001	0.015	0.065	1.75	0.011	0	0.25	25.634
BFC55_18.6	0.07	0.014	0.011	0.044	0.002	0.01	0.062	1.793	0.013	0	0.207	25.654
BFC55_18.7	0.062	0.013	0.012	0.028	0.002	0.007	0.047	1.791	0.012	0.011	0.209	25.6

B.2 Fish Canyon Tuff and Pagosa Peak Dacite EMPA data (wt% oxides)

BFC-124-1

Sample	P2O5	Nb2O5	Ta2O5	SiO2	TiO2	ZrO2	Al2O3	Fe2O3	Y2O3	La2O3
BFC124_1.1	0.0605	0.2663	0.0241	29.5884	36.115	0.09	1.3008	1.9538	0.3855	0.3741
BFC124_1.2	0.0565	0.2488	0.0019	29.3714	35.759	0.0973	1.3182	2.0073	0.4337	0.3366

Sample	Ce2O3	Pr2O3	Nd2O3	Sm2O3	Gd2O3	MgO	CaO	MnO	ZnO	SrO
BFC124_1.1	1.1421	0.1763	0.5477	0.0791	0.1044	0.0207	26.7522	0.1962	0.0039	0.0426
BFC124_1.2	1.106	0.1471	0.6188	0.1158	0.1291	0.0205	26.77	0.2088	0.0043	0.0491

Sample	SnO	H2O	Na2O	K2O	F	Total	O=F	Total
BFC124_1.1	0.0191	1.049	0.0205	0.0076	0.1992	100.4727	0.0839	100.3888
BFC124_1.2	0.0031	0.9997	0.0114	0.0059	0.2873	100.0565	0.121	99.9355

BFC-124-7

Sample	P2O5	Nb2O5	Ta2O5	SiO2	TiO2	ZrO2	Al2O3	Fe2O3	Y2O3	La2O3
BFC124_7.1	0.0768	0.3856	0.0205	28.6355	34.0346	0.1223	1.3387	2.7512	1.1881	0.3717
BFC124_7.2	0.046	0.2835	0.0322	28.8954	33.9162	0.0977	1.4846	2.8207	1.0923	0.3217
BFC124_7.3	0.062	0.3	0.0172	29.3971	35.3829	0.1169	1.3618	2.2131	0.4571	0.4106
BFC124_7.4	0.0537	0.2569	0.0046	29.0544	34.9868	0.1017	1.4312	2.1732	0.4124	0.3867
BFC124_7.5	0.0632	0.2722	0.0419	29.164	35.3928	0.0921	1.343	2.0665	0.4257	0.3682
BFC124_7.6	0.0426	0.2859	0.0419	28.7448	33.772	0.081	1.4581	2.7046	1.1982	0.2952

Sample	Ce2O3	Pr2O3	Nd2O3	Sm2O3	Gd2O3	MgO	CaO	MnO	ZnO	SrO
BFC124_7.1	1.6657	0.2869	1.4023	0.3441	0.4027	0.037	24.4549	0.2977	0.0024	0.0932
BFC124_7.2	1.4211	0.2568	1.083	0.2747	0.2785	0.0435	25.2478	0.3285	0.0042	0.0943
BFC124_7.3	1.3964	0.2005	0.6285	0.1349	0.1253	0.0284	25.9383	0.2882	0.0079	0.0587
BFC124_7.4	1.2533	0.1826	0.6105	0.1101	0.1052	0.0261	26.3569	0.2526	0.0035	0.035

Sample									
BFC124_7.5	1.2745	0.1493	0.6404	0.1012	0.1326	0.0264	26.2907	0.2217	0.0026	0.0295
BFC124_7.6	1.4257	0.2675	1.1426	0.2724	0.3258	0.0491	24.9636	0.318	0.0166	0.096

Sample	SnO	H2O	Na2O	K2O	F	Total	O=F	Total
BFC124_7.1	0.0262	1.0294	0.0301	0.018	0.169	99.0913	0.0711	99.0202
BFC124_7.2	0.0229	0.991	0.0234	0.0028	0.2609	99.2267	0.1099	99.1168
BFC124_7.3	0.0122	1.009	0.0214	0.0001	0.2579	99.7597	0.1086	99.6511
BFC124_7.4	0.0107	0.9594	0.0141	0.001	0.3431	99.0862	0.1445	98.9417
BFC124_7.5	0.0093	0.9818	0.01	0.0022	0.3054	99.3752	0.1286	99.2466
BFC124_7.6	0.029	0.9641	0.0285	0.0018	0.3024	98.7129	0.1273	98.5856

BFC-124-5

Sample	P2O5	Nb2O5	Ta2O5	SiO2	TiO2	ZrO2	Al2O3	Fe2O3	Y2O3	La2O3
BFC124_5.1	0.0584	0.2498	0.0009	29.2916	35.434	0.086	1.3144	1.9339	0.4498	0.3397
BFC124_5.2	0.0614	0.2426	0.0067	29.2954	35.0029	0.0902	1.4192	2.2403	0.3763	0.3963
BFC124_5.3	0.0721	0.4831	0.0529	28.5633	34.1314	0.0828	1.3319	2.2133	0.73	0.4935
BFC124_5.4	0.0685	0.3162	0.0316	27.9813	34.7079	0.1117	1.3866	2.3048	0.7198	0.3638
BFC124_5.5	0.0766	0.3464	0.0247	29.5444	35.578	0.1029	1.2306	1.874	0.4141	0.4029

Sample	Ce2O3	Pr2O3	Nd2O3	Sm2O3	Gd2O3	MgO	CaO	MnO	ZnO	SrO
BFC124_5.1	1.1383	0.1122	0.595	0.1159	0.1153	0.0246	26.1956	0.2002	0.0051	0.0356
BFC124_5.2	1.2182	0.1436	0.5581	0.0794	0.0988	0.0266	26.1707	0.2321	0.0017	0.0216
BFC124_5.3	1.8588	0.257	1.0381	0.1983	0.2015	0.0345	25.2182	0.3409	0.0067	0.0694
BFC124_5.4	1.49	0.1767	0.86	0.1781	0.1321	0.033	25.5523	0.3008	0.0071	0.0645
BFC124_5.5	1.3336	0.1909	0.6588	0.1192	0.1005	0.0246	26.303	0.2261	0.0124	0.0454

Sample	SnO	H2O	Na2O	K2O	F	Total	O=F	Total
BFC124_5.1	0.0129	1.0259	0.0147	0.0142	0.2119	98.9351	0.0892	98.8459
BFC124_5.2	0.0082	0.9605	0.0246	0.0007	0.3447	98.9993	0.1451	98.8542
BFC124_5.3	0.0231	1.037	0.0375	0.0006	0.1491	98.5486	0.0628	98.4859
BFC124_5.4	0.0107	1.029	0.0076	0.0006	0.1584	97.9277	0.0667	97.861
BFC124_5.5	0.0072	1.0693	0.0186	0.0047	0.1386	99.8021	0.0584	99.7437

BFC-104b-5

Sample	P2O5	Nb2O5	Ta2O5	SiO2	TiO2	ZrO2	Al2O3	Y2O3	La2O3	Ce2O3
BFC104_5.1	0.0767	0.3052	0.0182	29.704	35.951	0.1072	1.175	0.4402	0.3546	1.1886
BFC104_5.2	0.0441	0.3234	0.0256	29.2922	35.141	0.0933	1.3729	0.6153	0.3894	1.5263
BFC104_5.3	0.0612	0.3296	0.0096	29.3265	35.2643	0.0936	1.352	0.5655	0.443	1.5706
BFC104_5.4	0.0814	0.2922	0.0188	29.7081	36.0333	0.1247	1.1689	0.401	0.3672	1.1459
BFC104_5.5	0.072	0.3189	0.0563	29.6244	35.5576	0.1034	1.195	0.4405	0.4025	1.339

Sample	Pr2O3	Nd2O3	Sm2O3	Gd2O3	MgO	CaO	MnO	FeO	ZnO	SrO
BFC104_5.1	0.1623	0.6447	0.1353	0.1166	0.0211	26.5325	0.1936	1.7724	0.0066	0.0635
BFC104_5.2	0.1837	0.7996	0.1388	0.0908	0.0404	25.9929	0.3201	2.4019	0.0155	0.065
BFC104_5.3	0.2133	0.7974	0.1381	0.1233	0.0283	26.1773	0.2984	2.4474	0.0018	0.0449
BFC104_5.4	0.1735	0.601	0.1055	0.1041	0.0201	26.6606	0.2131	1.9969	0.0155	0.0505
BFC104_5.5	0.1753	0.7231	0.1448	0.1186	0.0136	26.529	0.2117	1.9589	0.0011	0.0398

Sample	SnO	H2O	Na2O	K2O	F	Total	O=F	Total
BFC104_5.1	0.0221	1.0409	0.0132	0.008	0.2086	100.1919	0.0879	100.104
BFC104_5.2	0.0102	0.9774	0.0222	0.0009	0.3227	100.125	0.1359	99.9891
BFC104_5.3	0.0156	1.0287	0.0068	-0.0026	0.2249	100.5173	0.0947	100.4225
BFC104_5.4	0.0074	1.0208	0.012	0.0103	0.2571	100.5237	0.1082	100.4155
BFC104_5.5	0.0184	1.0259	0.012	0.0037	0.2346	100.279	0.0988	100.1802

BFC-129-10

Sample	P2O5	Nb2O5	Ta2O5	SiO2	TiO2	ZrO2	Al2O3	Y2O3	La2O3	Ce2O3
BFC129_10.1	0.0602	0.3439	0.0417	29.0182	34.0553	0.0881	1.3456	0.7608	0.3685	1.5047
BFC129_10.2	0.0517	0.3804	0.0237	29.6165	36.8302	0.1339	1.1271	0.1127	0.2893	0.7123
BFC129_10.3	0.0773	0.4756	0.0575	29.455	36.1541	0.1396	1.0558	0.225	0.3176	0.9821
BFC129_10.4	0.0513	0.205	0.0086	29.4118	34.5229	0.1375	1.471	0.4457	0.2983	1.0951
BFC129_10.5	0.0635	0.1588	0.0325	29.6658	34.8381	0.1231	1.4041	0.4132	0.278	1.0436
BFC129_10.6	0.0587	0.2482	0.043	29.5618	35.6689	0.1063	1.3796	0.3997	0.3746	1.1707

Sample	Pr2O3	Nd2O3	Sm2O3	Gd2O3	MgO	CaO	MnO	FeO	ZnO	SrO
BFC129_10.1	0.2182	0.9585	0.1755	0.1953	0.0282	25.7616	0.3153	2.4071	0.0059	0.0759
BFC129_10.2	0.0703	0.2226	0.0261	0.0262	0.0003	27.5965	0.2609	1.7154	0.0002	0.0218
BFC129_10.3	0.1245	0.4308	0.0194	0.0207	0.0154	26.9371	0.2318	1.5421	0.0027	0.0463
BFC129_10.4	0.1783	0.7561	0.1716	0.1371	0.0197	26.5026	0.2338	2.398	0.0017	0.0294
BFC129_10.5	0.1496	0.5928	0.1108	0.1116	0.0145	26.495	0.2188	2.106	0.0124	0.0318
BFC129_10.6	0.1462	0.6333	0.0839	0.1306	0.0149	26.5791	0.2095	2.0421	0.0103	0.0363

Sample	SnO	H2O	Na2O	K2O	F	Total	O=F	Total
BFC129_10.1	0.0196	1.0253	0.0191	0.0007	0.1901	98.9067	0.08	98.8267
BFC129_10.2	0.007	1.0134	0.021	0.002	0.2855	100.5236	0.1202	100.4033
BFC129_10.3	0.0179	1.0672	0.0207	0.0001	0.1468	99.5166	0.0618	99.4548
BFC129_10.4	0.0157	0.9526	0.0021	0.001	0.3642	99.3818	0.1534	99.2285
BFC129_10.5	0.0086	0.9525	0.004	0.0003	0.3687	99.154	0.1553	98.9987
BFC129_10.6	0.0131	0.9791	0.0061	0.0008	0.3334	100.1832	0.1404	100.0428

BFC-55-18

Sample	P2O5	Nb2O5	Ta2O5	SiO2	TiO2	ZrO2	Al2O3	Fe2O3	Y2O3	La2O3
BFC55_18.1	0.0449	0.3549	0.0089	28.4029	34.4137	0.0952	1.369	2.3931	0.6685	0.4209
BFC55_18.2	0.0693	0.4171	0.0249	28.5562	34.5826	0.0944	1.2505	2.1656	0.6777	0.4272
BFC55_18.3	0.0831	0.4999	0.0402	28.5179	34.3504	0.1084	1.2517	2.3155	0.7276	0.5441
BFC55_18.4	0.0549	0.3274	0.0241	28.6922	34.5427	0.0776	1.363	2.2961	0.5222	0.4349
BFC55_18.5	0.0556	0.3382	0.0159	28.7369	35.0237	0.1009	1.3519	2.3886	0.5118	0.4326
BFC55_18.6	0.0486	0.3622	0.0279	28.6275	34.8691	0.1102	1.3477	2.2413	0.4865	0.407
BFC55_18.7	0.0517	0.2292	0.029	29.074	35.39	0.0985	1.3014	2.0364	0.4376	0.3613

Sample	Ce2O3	Pr2O3	Nd2O3	Sm2O3	Gd2O3	MgO	CaO	MnO	ZnO	SrO
BFC55_18.1	1.4695	0.1908	0.7735	0.112	0.1464	0.0313	25.7621	0.3214	0.0029	0.0603
BFC55_18.2	1.6509	0.2292	0.8999	0.1292	0.1645	0.0178	25.5215	0.3111	0.011	0.0521
BFC55_18.3	1.9019	0.2724	1.013	0.1569	0.1601	0.028	25.1376	0.3181	0.0021	0.0502
BFC55_18.4	1.5516	0.2252	0.7486	0.1126	0.1018	0.0247	25.9162	0.2728	0.0066	0.0526
BFC55_18.5	1.5168	0.1872	0.7447	0.1029	0.1291	0.0363	25.8701	0.2865	0.0126	0.04
BFC55_18.6	1.4281	0.1744	0.7034	0.0681	0.1177	0.0244	26.1269	0.2723	0.0076	0.0332
BFC55_18.7	1.2424	0.1467	0.6811	0.1334	0.115	0.0186	26.0598	0.2069	0.0076	0.0434

Sample	SnO	H2O	Na2O	K2O	F	Total	O=F	Total
BFC55_18.1	0.0096	0.9502	0.0275	-0.002	0.3298	98.299	0.1389	98.1601
BFC55_18.2	0.0269	1.0189	0.0327	-0.0012	0.1914	98.4705	0.0806	98.3899
BFC55_18.3	0.0254	1.0562	0.0383	0.0012	0.1122	98.662	0.0473	98.6148
BFC55_18.4	0.0089	1.0312	0.022	0.0024	0.1739	98.527	0.0732	98.4538
BFC55_18.5	0.0212	0.9789	0.0205	0.0012	0.2952	99.1594	0.1243	99.0351
BFC55_18.6	0.019	1.0001	0.024	-0.004	0.244	98.7379	0.1027	98.6352
BFC55_18.7	0.0113	1.0057	0.0223	0.0308	0.247	98.9377	0.104	98.8337

C

EMPA operating conditions/detection limits

2sig detection limit calculation — Calibration and unknown values as measured late May–June 2007

Element	Standard info K cps/nA	conc std (wt%)	Matrix/ mineral	meas conc (wt%)	Pk cps	Unknown info Bgd cps	BC (nA)	total count time	dl (2sig) (ppm)	Simon's lld (wt%)	%error (rel) on conc	error (2sig) (on conc) (wt%)
F	184.43	21.67	titanite	0.15	10.63	5.40	15	40	86	0.109	16.88	0.051
Na	356.64	11.34	titanite	0.02	420.00	392.40	80	60	30	0.016	18.85	0.008
Mg	283.72	17.08	titanite	0.01	63.60	54.80	80	60	22	0.010	22.56	0.005
Al	724.23	37.93	titanite	0.63	1120.10	145.00	80	60	31	0.018	0.60	0.008
Si	635.23	24	titanite	13.57	5096.00	45.60	15	40	81	0.183	0.24	0.086
P	311.77	22.14	titanite	0.03	54.10	24.50	80	40	21	0.009	6.57	0.004
K	344.82	12.6	titanite	0.00	172.10	163.50	80	40	28	0.002	47.63	0.001
Ca	1074.21	34.32	titanite	18.93	9747.10	151.90	15	40	125	0.186	0.18	0.088
Ti	361.11	59.34	titanite	21.50	1758.90	20.40	15	40	235	0.495	0.42	0.233
Mn	1123.01	100	titanite	0.13	183.00	88.00	80	40	50	0.021	3.81	0.010
Fe	827.59	69.94	titanite	1.30	229.50	23.30	15	40	129	0.095	1.53	0.045
Zn	623.9	58.68	titanite	0.00	249.40	249.30	80	60	72	0.173	4077.17	0.082
Sr	460.76	47.7	titanite	0.00	303.70	319.20	80	60	90	-0.001	-29.40	-0.001
Y	344.91	78.74	titanite	0.31	96.40	19.90	80	60	49	0.034	2.41	0.016
Zr	180.06	49.76	titanite	0.07	41.20	23.50	80	60	65	0.025	8.22	0.012
Nb	470.46	100	titanite	0.26	102.50	32.20	80	60	58	0.033	2.90	0.016
Sn	1138.46	100	titanite	0.01	196.00	186.00	80	40	71	0.019	43.70	0.009
La	135.45	58.71	titanite	0.27	76.30	34.10	80	60	123	0.052	4.46	0.025
Ce	150.11	58.06	titanite	0.97	220.80	47.60	80	60	129	0.071	1.62	0.034
Pr	118.79	58.71	titanite	0.14	80.50	61.30	80	60	187	0.067	11.30	0.032
Nd	140.82	59.3	titanite	0.56	165.40	76.80	80	60	179	0.076	3.15	0.036
Sm	161.98	60.64	titanite	0.11	124.40	105.70	80	60	186	0.069	14.80	0.033
Gd	178.03	61.18	titanite	0.10	156.40	137.00	80	60	195	0.068	16.11	0.032
Ta	607.05	100	titanite	0.03	230.60	222.40	80	60	119	0.060	47.39	0.028

References

Aleinikoff, J. N., R. P. Wintsch, et al. (2002). "U-Pb geochronology of zircon and polygenetic titanite from the Glastonbury Complex, Connecticut, USA: an integrated SEM, EMPA, TIMS, and SHRIMP study." Chemical Geology **188**(1-2): 125-147.

Arima, M. and A. D. Edgar (1983). "A High-Pressure Experimental-Study on a Magnesian-Rich Leucite-Lamproite from the West Kimberley Area, Australia - Petrogenetic Implications." Contributions to Mineralogy and Petrology **84**(2-3): 228-234.

Bachmann, O. and G. W. Bergantz (2003). "Rejuvenation of the Fish Canyon magma body: A window into the evolution of large-volume silicic magma systems." Geology **31**(9): 789-792.

Bachmann, O. and M. A. Dungan (2002). "Temperature-induced Al-zoning in hornblendes of the Fish Canyon magma, Colorado." American Mineralogist **87**(8-9): 1062-1076.

Bachmann, O., M. A. Dungan, et al. (2005). "Insights into shallow magmatic processes in large silicic magma bodies: the trace element record in the Fish Canyon magma body, Colorado." Contributions to Mineralogy and Petrology **149**(3): 338-349.

Bachmann, O., M. A. Dungan, et al. (2000). "Voluminous lava-like precursor to a major ash-flow tuff: low-column pyroclastic eruption of the Pagosa Peak Dacite, San Juan volcanic field, Colorado." Journal of Volcanology and Geothermal Research **98**(1-4): 153-171.

Bachmann, O., M. A. Dungan, et al. (2002). "The Fish Canyon magma body, San Juan volcanic field, Colorado: Rejuvenation and eruption of an upper-crustal batholith." Journal of Petrology **43**(8): 1469-1503.

Bachmann, O., F. Oberli, et al. (2007). "Ar-40/Ar-39 and U-Pb dating of the Fish Canyon magmatic system, San Juan Volcanic field, Colorado: Evidence for an extended crystallization history (vol 236, pg 134, 2007)." Chemical Geology **240**(1-2): 193-193.

Bailey, E. B. a. A., E.M. (1925). The Geology of Staffa, Iona and western Mull, Geologocal Survey of Great Britain.

Barbarin, B. (1990). "Granitoids - Main Petrogenetic Classifications in Relation to Origin and Tectonic Setting." Geological Journal **25**(3-4): 227-238.

Barthelmy, D. (2005). Titanite Mineral Data.

Beckinsale, R. D. a. O., J. (1973). "Potassium-argon ages for minerals from the Ross of Mull, Argyllshire." Scottish Journal of Geology **9**: 147-156.

Bernau, R. and G. Franz (1987). "Crystal-Chemistry and Genesis of Nb-Rich, V-Rich, and Ai-Rich Metamorphic Titanite from Egypt and Greece." Canadian Mineralogist **25**: 695-705.

Bluck, B. J. (2001). Caledonian and related events in Scotland**: 375-404.

Broska, I., D. Harlov, et al. (2007). "Formation of magmatic titanite and titanite-ilmenite phase relations during granite alteration in the Tribec Mountains, Western Carpathians, Slovakia." Lithos **95**(1-2): 58-71.

Browne, B. L., J. C. Eichelberger, et al. (2006). "Magma mingling as indicated by texture and Sr/Ba ratios of plagioclase phenocrysts from Unzen volcano, SW Japan." Journal of Volcanology and Geothermal Research **154**(1-2): 103-116.

Cerny, P., M. Novak, et al. (1995). "The Al(Nb, Ta)Ti-2 Substitution in Titanite - the Emergence of a New Species." Mineralogy and Petrology **52**(1-2): 61-73.

Cerny, P. and Rivadisa.L (1972). "Comments on Crystal-Chemistry of Titanite." Acta Crystallographica Section A **28**: S67-S67.

Chakhmouradian, A. R. (2004). "Crystal chemistry and paragenesis of compositionally unique (Al-, Fe-, Nb-, and Zr-rich) titanite from Afrikanda, Russia." American Mineralogist **89**(11-12): 1752-1762.

Charlier, B. L. A., O. Bachmann, et al. (2007). "The upper crustal evolution of a large silicic magma body: Evidence from crystal-scale rb-sr isotopic Heterogeneities in the fish canyon magmatic system, Colorado." Journal of Petrology **48**(10): 1875-1894.

Cherniak, D. J. (1995). "Sr and Nd Diffusion in Titanite." Chemical Geology **125**(3-4): 219-232.

Cherniak, D. J. (2006). "Zr diffusion in titanite." Contributions to Mineralogy and Petrology **152**(5): 639-647.

Clarke, B. (1992). Granitoid Rocks. London, Chapman & Hall.

Cunningham-Craig, E. H. (1911). The Geology of Colonsay and Oronsay with Part of the Ross of Mull. Memoir of the Geological Survey of Scotland,, Geologocal Survey of Scotland.

Davis, W. J. and V. J. McNicoll (2005). "U-Pb discordance in titanite and the interpretation of the thermal history of metamorphic rocks." Geochimica Et Cosmochimica Acta **69**(10): A26-A26.

Deer W.A., H. R. A., Zussman J. (1992). An Introduction To The Rock Forming Minerals. London, Pearson Education Ltd. .

Della Ventura, G., F. Bellatreccia, et al. (1999). "Zr- and LREE-rich titanite from Tre Croci, Vico Volcanic complex (Latium, Italy)." Mineralogical Magazine **63**(1): 123-130.

Dempster, T. J. H., D.C.; Bluck, B.J. (2004). "Zircon growth in slate." Geology **32**: 221-224.

Dickin, A. P. and R. A. Exley (1981). "Isotopic and Geochemical Evidence for Magma Mixing in the Petrogenesis of the Coire Uaigneich Granophyre, Isle of Skye, Nw Scotland." Contributions to Mineralogy and Petrology **76**(1): 98-108.

Didier, J. and B. Barbarin (1991). Enclaves and Granite Petrology. Amsterdam, Elsevier.

Ellwood, B. B., J. C. Stormer, et al. (1989). "Fish Canyon Tuff, Colorado - the Problem of 2 Magnetic Polarities in a Single Tuff." Physics of the Earth and Planetary Interiors **56**(3-4): 329-336.

Enami, M., K. Suzuki, et al. (1993). "Al-Fe3+ and F-Oh Substitutions in Titanite and Constraints on Their P-T Dependence." European Journal of Mineralogy **5**(2): 219-231.

Exley, R. A. (1980). "Micro-Probe Studies of Ree-Rich Accessory Minerals - Implications for Skye Granite Petrogenesis and Ree Mobility in Hydrothermal Systems." Earth and Planetary Science Letters **48**(1): 97-110.

Franz, G. and F. S. Spear (1985). "Aluminous Titanite (Sphene) from the Eclogite Zone, South-Central Tauern Window, Austria." Chemical Geology **50**: 33-46.

Frost, B. R., K. R. Chamberlain, et al. (2001). "Sphene (titanite): phase relations and role as a geochronometer." Chemical Geology **172**(1-2): 131-148.

Green, T. H. and N. J. Pearson (1986). "Rare-Earth Element Partitioning between Sphene and Coexisting Silicate Liquid at High-Pressure and Temperature." Chemical Geology **55**(1-2): 105-119.

Groat, L. A., R. T. Carter, et al. (1985). "Tantalian Niobian Titanite from the Irgon Claim, Southeastern Manitoba." Canadian Mineralogist **23**: 569-571.

Gromet, L. P. and L. T. Silver (1983). "Rare-Earth Element Distributions among Minerals in a Granodiorite and Their Petrogenetic Implications." Geochimica Et Cosmochimica Acta **47**(5): 925-939.

Grunder, A. L. and D. R. Boden (1987). "Magmatic Conditions of the Fish Canyon Tuff, Central San-Juan Volcanic Field, Colorado - Comment." Journal of Petrology **28**(4): 737-746.

Gupta, L. N. and S. Marwaha (1989). "Zoning in Plagioclase (Normal and Oscillatory) in the Feldspar Porphyries of Karsog Area, Lesser Himalaya, Himachal-Pradesh, India." Journal of the Geological Society of India **33**(3): 223-227.

Halliday, A. N., Aftalion, M., Van Breemen, O. & Jocelyn, J. (1979). Petrogenetic significance of Rb–Sr and U–Pb isotope systems in the 400 Ma old British Isles granitoids and their hosts. Caledonides of the British Isles— Reviewed. A. L. Harris, Holland, H. D. & Leake, B. E. London, Geological Society. **8:** 653–661.

Harlov, D., P. Tropper, et al. (2006). "Formation of Al-rich titanite (CaTiSiO4O-CaAlSiO4OH) reaction rims on ilmenite in metamorphic rocks as a function of fH(2)O and fO(2)." Lithos **88**(1-4): 72-84.

Harris, A. L. a. H., A.J. (1999). Ross of Mull. Sheet 43S. Solid and Drift. 1:50,000 provisional series. Keyworth, Notingham, British Geological Survey

Higgins, J. B. and P. H. Ribbe (1976). "Crystal-Chemistry and Space Groups of Natural and Synthetic Titanites." American Mineralogist **61**(9-10): 878-888.

Higgins, J. B. and P. H. Ribbe (1977). "Structure of Malayaite, Casnosio4, a Tin Analog of Titanite." <u>American Mineralogist</u> **62**(7-8): 801-806.

Highton, A. (2001). Knockvologan to Eilan A'Chalmin. <u>Caledonian Igneous Rocks of Great Britain</u> D. Stephenson. London, NHBS. **GCR Volume No. 17:** 648.

Hildreth, W. (1981). "Gradients in Silicic Magma Chambers - Implications for Lithospheric Magmatism." <u>Journal of Geophysical Research</u> **86**(NB11): 153-192.

Holdsworth, R. E., A. L. Harris, et al. (1987). "The Stratigraphy, Structure and Regional Significance of the Moine Rocks of Mull, Argyllshire, Western Scotland." <u>Geological Journal</u> **22**(2): 83-107.

Holten, T., B. Jamtveit, et al. (2000). "Noise and oscillatory zoning of minerals." <u>Geochimica Et Cosmochimica Acta</u> **64**(11): 1893-1904.

Hughes, J. M., E. S. Bloodaxe, et al. (1997). "Incorporation of rare earth elements in titanite: Stabilization of the A2/a dimorph by creation of antiphase boundaries." <u>American Mineralogist</u> **82**(5-6): 512-516.

Imonetti, A. S., L. M. Heaman, et al. (2007). "In situ petrographic thin section U-Pb dating of zircon, monazite, and titanite using laser ablation-MC-ICP-MS (vol 253, pg 87, 2006)." <u>International Journal of Mass Spectrometry</u> **261**(2-3): 239-239.

Jacques, J. M. and R. J. Reavy (1994). "Caledonian Plutonism and Major Lineaments in the Sw Scottish Highlands." <u>Journal of the Geological Society</u> **151**: 955-969.

Janeczek, J. (1996). "Nb-, Ta- and Sn-rich titanite and its alteration in pegmatites from Zolkiewka, Poland." <u>Neues Jahrbuch Fur Mineralogie-Monatshefte</u>(10): 459-469.

Johnson, M. C. and M. J. Rutherford (1989). "Experimentally Determined Conditions in the Fish Canyon Tuff, Colorado, Magma Chamber." <u>Journal of Petrology</u> **30**(3): 711-737.

Kalischewski, F., I. Lubashevsky, et al. (2007). "Boundary-reaction-diffusion model for oscillatory zoning in binary crystals grown from solution." <u>Physical Review E</u> **75**(2).

Karsli, O., F. Aydin, et al. (2004). "Magma interaction recorded in plagioclase zoning in granitoid systems, Zigana Granitoid, Eastern Pontides, Turkey." <u>Turkish Journal of Earth Sciences</u> **13**(3): 287-305.

Kowallis, B. J., E. H. Christiansen, et al. (2005). "Titanite as a tool in tephra provenance studies: An example from the Late Jurassic." <u>Geochimica Et Cosmochimica Acta</u> **69**(10): A15-A15.

Kuscu, G. G. and P. A. Floyd (2001). "Mineral compositional and textural evidence for magma mingling in the Saraykent volcanics." <u>Lithos</u> **56**(2-3): 207-230.

Lehmann, B., C. Storey, et al. (2007). "In-situ U-Pb dating of titanite in the Tokapal-Bhejripadar kimberlite system, central India." <u>Journal of the Geological Society of India</u> **69**(3): 553-556.

Lheureux, I. (1993). "Oscillatory Zoning in Crystal-Growth - a Constitutional Undercooling Mechanism." Physical Review E **48**(6): 4460-4469.

Liferovich, R. P. and R. H. Mitchell (2005). "Composition and paragenesis of Na-, Nb- and Zr-bearing titanite from Khibina, Russia, and crystal-structure data for synthetic analogues." Canadian Mineralogist **43**: 795-812.

Liferovich, R. P. and R. H. Mitchell (2006). "Crystal structure of a synthetic aluminoan tantalian titanite: a reconnaissance study." Mineralogical Magazine **70**(1): 115-121.

Liferovich, R. P. and R. H. Mitchell (2006). "Tantalum-bearing titanite: synthesis and crystal structure data." Physics and Chemistry of Minerals **33**(2): 73-83.

Lipman, P., M. Dungan, et al. (1997). "Comagmatic granophyric granite in the Fish Canyon Tuff, Colorado: Implications for magma-chamber processes during a large ash-flow eruption." Geology **25**(10): 915-918.

Lipman, P. W., B. R. Doe, et al. (1978). "Petrologic Evolution of San-Juan Volcanic Field, Southwestern Colorado - Pb and Sr Isotope Evidence." Geological Society of America Bulletin **89**(1): 59-82.

Lipman, P. W., M. A. Dungan, et al. (1996). "Recurrent eruption and subsidence at the Platoro caldera complex, southeastern San Juan volcanic field, Colorado: New tales from old tuffs (vol 108, pg 1039, 1996)." Geological Society of America Bulletin **108**(11): 1514-1514.

Lloyd, F. E., A. D. Edgar, et al. (1996). "LREE distribution in perovskite, apatite and titanite from South West Ugandan xenoliths and kamafugite lavas." Mineralogy and Petrology **57**(3-4): 205-228.

Malcherek, T., A. Bosenick, et al. (2004). "Isomorphy of structural phase transitions in LiTaOSiO4, LiTaOGeO4 and titanite, CaTiOSiO4." Journal of Solid State Chemistry **177**(10): 3254-3262.

Malcherek, T., C. M. Domeneghetti, et al. (1999). "A high temperature diffraction study of synthetic titanite CaTiOSiO4." Phase Transitions **69**(1): 119-131.

Malcherek, T., C. Paulmann, et al. (2001). "Diffuse scattering anisotropy and the P2(1)/a <-> A2/a phase transition in titanite, CaTiOSiO4." Journal of Applied Crystallography **34**: 108-113.

Naeser, C. W. (1967). "Use of Apatite and Sphene for Fission Track Age Determinations." Geological Society of America Bulletin **78**(12): 1523-&.

Nakada, S. (1991). "Magmatic Processes in Titanite-Bearing Dacites, Central Andes of Chile and Bolivia." American Mineralogist **76**(3-4): 548-560.

Oberli, F., O. Bachmann, et al. (2002). "The fish canyon Tuff: Ar-Ar versus U-Pb age discrepancy re-assessed." Geochimica Et Cosmochimica Acta **66**(15A): A565-A565.

Oberti, R., D. C. Smith, et al. (1991). "The Crystal-Chemistry of High-Aluminum Titanites." European Journal of Mineralogy **3**(5): 777-792.

Odegard, M., O. Skar, et al. (2005). "Preparation of a synthetic titanite glass calibration material for in situ microanalysis by direct fusion in graphite electrodes: A preliminary characterisation by EPMA and LA-ICP-MS." Geostandards and Geoanalytical Research **29**(2): 197-209.

Orsini, J., C. Cocirta, et al. (1991). Genesis of mafic-microgranular enclaves through dfferentiation of basic magmas, mingling and chemical exchanges with their host granitoid magmas. . Enclaves and Granite Petrology. J. Didier and B. Barbarin. Amsterdam, Elsevier. **13:** 445-464.

Panov, E. N. and Tarnovsk.An (1973). "Rare-Earth Elements in Accessory Sphene of Granitoids of Northeastern Transbaikal Region." Geokhimiya(1): 135-139.

Paterson, B. A. and W. E. Stephens (1992). "Kinetically Induced Compositional Zoning in Titanite - Implications for Accessory-Phase Melt Partitioning of Trace-Elements." Contributions to Mineralogy and Petrology **109**(3): 373-385.

Paul, B. J., P. Cerny, et al. (1981). "Niobian Titanite from the Huron Claim Pegmatite, Southeastern Manitoba." Canadian Mineralogist **19**(4): 549-552.

Perseil, E. A. and D. C. Smith (1995). "Sb-rich titanite in the manganese concentrations at St Marcel-Praborna, Aosta Valley, Italy: Petrography and crystal-chemistry." Mineralogical Magazine **59**(397): 717-734.

Petford, N., B. Paterson, et al. (1996). "Melt infiltration and advection in microdioritic enclaves." European Journal of Mineralogy **8**(2): 405-412.

Piccoli, P., P. Candela, et al. (2000). Interpreting magmatic processes from accessory phases: titanite - a small-scale recorder of large-scale processes**:** 257-267.

Piccoli, P., P. Candela, et al. (2000). "Interpreting magmatic processes from accessory phases: titanite - a small-scale recorder of large-scale processes." TRANSACTIONS OF THE ROYAL SOCIETY OF EDINBURGH-EARTH SCIENCES

 91(1-2): 257-267.

Piper, J. D. A. (1998). "Palaeomagnetism of the Ross of Mull granite complex, western Scotland: lower Palaeozoic apparent polar wander of the Orthotectonic Caledonides." Geophysical Journal International **132**(1): 133-148.

Pitcher, W. S. (1995). The Nature and Origin of Granite. Glasgow, Chapman & Hall.

Potts, G. J., R. H. Hunter, et al. (1995). "Late-Orogenic Extensional Tectonics at the Nw Margin of the Caledonides in Scotland." Journal of the Geological Society **152**: 907-910.

Preston, R. J., B. R. Bell, et al. (1998). "The Loch Scridain Xenolithic sill complex, Isle of Mull, Scotland: Fractional crystallization, assimilation, Magma-Mixing and crustal anatexis in subvolcanic conduits." Journal of Petrology **39**(3): 519-550.

Prince, A. T. (1943). "The system albite-anorthite-sphene." Journal of Geology **51**(1): 1-16.

Prowatke, S. and S. Klemme (2003). "Melt compositional controls on trace element partitioning: An experimental study of titanite/melt partitioning." Geochimica Et Cosmochimica Acta **67**(18): A385-A385.

Prowatke, S. and S. Klemme (2005). "Effect of melt composition on the partitioning of trace elements between titanite and silicate melt." Geochimica Et Cosmochimica Acta **69**(3): 695-709.

Prowatke, S. and S. Klemme (2006). "Rare earth element partitioning between titanite and silicate melts: Henry's law revisited." Geochimica Et Cosmochimica Acta **70**(19): 4997-5012.

Pugliese, S. a. P., N. (2001). "Reconstruction and visualisation of melt topology in veined microdioritic enlcaves." Electronic Geosciences **6**(2): 1-23.

Reavy, R. J. (2001). "Caledonian Granites - emplacement." Open University Geological Society Journal **22**(2).

Reiners, P. W. and K. A. Farley (1999). "Helium diffusion and (U-Th)/He thermochronometry of titanite." Geochimica Et Cosmochimica Acta **63**(22): 3845-3859.

Ribbe, P. H. (1982). Orthosilicates, Mineralogocal Society of America.

Rock, N. M. S. and R. H. Hunter (1987). "Late Caledonian Dyke-Swarms of Northern Britain - Spatial and Temporal Intimacy between Lamprophyric and Granitic Magmatism around the Ross of Mull Pluton, Inner Hebrides." Geologische Rundschau **76**(3): 805-826.

Russell, J. K., L. A. Groat, et al. (1994). "Lree-Rich Niobian Titanite from Mount Bisson, British-Columbia - Chemistry and Exchange Mechanisms." Canadian Mineralogist **32**: 575-587.

Sawka, W. N., B. W. Chappell, et al. (1984). "Light-Rare-Earth-Element Zoning in Sphene and Allanite During Granitoid Fractionation." Geology **12**(3): 131-134.

Seifert, W. (2005). "REE-, Zr-, and Th-rich titanite and associated accessory minerals from a kersantite in the Frankenwald, Germany." Mineralogy and Petrology **84**(3-4): 129-146.

Seifert, W. and W. Kramer (2003). "Accessory titanite: an important carrier of zirconium in lamprophyres." Lithos **71**(1): 81-98.

Shaw, N. (2003). The origin of mafic segragations in the Ross of Mull Granite, Division of Earth Sciences, University of Glasgow

Shelley, D. (1993). Igneous and Metamorphic Rocks Under the Microscope. London, Chapman & Hall.

Sparks, R. S. J. and L. A. Marshall (1986). "Thermal and Mechanical Constraints on Mixing between Mafic and Silicic Magmas." Journal of Volcanology and Geothermal Research **29**(1-4): 99-124.

Speer, J. A. and G. V. Gibbs (1974). "Crystal-Structure of Synthetic Titanite, Catiosio4, and Domain Texture of Natural Titanites." Transactions-American Geophysical Union **55**(4): 462-462.

Staatz, M. H., N. M. Conklin, et al. (1977). "Rare-Earths, Thorium, and Other Minor Elements in Sphene from Some Plutonic Rocks in West-Central Alaska." Journal of Research of the Us Geological Survey **5**(5): 623-628.

Stephens, W. E. (2001). "Polycrystalline amphibole (clots) in granites as potential I-type restite: an ion microprobe study of rare-earth distributions " Australian Journal of Earth Sciences **48**: 591-601.

Taylor, M. and G. E. Brown (1976). "High-Temperature Structural Study of P21-Areversiblea2-a Phase-Transition in Synthetic Titanite, Catisio5." American Mineralogist **61**(5-6): 435-447.

Tiepolo, M., R. Oberti, et al. (2002). "Trace-element incorporation in titanite: constraints from experimentally determined solid/liquid partition coefficients." Chemical Geology **191**(1-3): 105-119.

Tindle, A. G. (1991). Trace element behaviour in microgranular enclaves from granitic rocks. Enclaves and Granite Petrology. J. Didier and B. Barbarin. Amsterdam, Elsevier. **13:** 313-331.

Vuorinen, J. H. and U. Halenius (2005). "Nb-, Zr- and LREE-rich titanite from the Alno alkaline complex: Crystal chemistry and its importance as a petrogenetic indicator." Lithos **83**(1-2): 128-142.

Whitney, J. A. and J. C. Stormer (1985). "Mineralogy, Petrology, and Magmatic Conditions from the Fish-Canyon Tuff, Central San-Juan Volcanic Field, Colorado." Journal of Petrology **26**(3): 726-762.

Wones, D. R. (1989). "Significance of the Assemblage Titanite + Magnetite + Quartz in Granitic-Rocks." American Mineralogist **74**(7-8): 744-749.

Woolley, A. R., R. G. Platt, et al. (1992). "Niobian Titanite and Eudialyte from the Ilomba Nepheline Syenite Complex, North Malawi." Mineralogical Magazine **56**(384): 428-430.

Xirouchakis, D. and D. H. Lindsley (1998). "Equilibria among titanite, hedenbergite, fayalite, quartz, ilmenite, and magnetite: Experiments and internally consistent thermodynamic data for titanite." American Mineralogist **83**(7-8): 712-725.

Zachariasen, W. H. (1930). "The crystal structure of Titanite." Zeitschrift Fur Kristallographie **73**(1): 7-16.

Zaniewski, A., R. J. Reavy, et al. (2006). "Field relationships and emplacement of the Caledonian Ross of Mull Granite, Argyllshire." Scottish Journal of Geology **42**: 179-189.